THE IMMUNOGENICITY OF CHOLANGIOCYTE CELLULAR THERAPIES

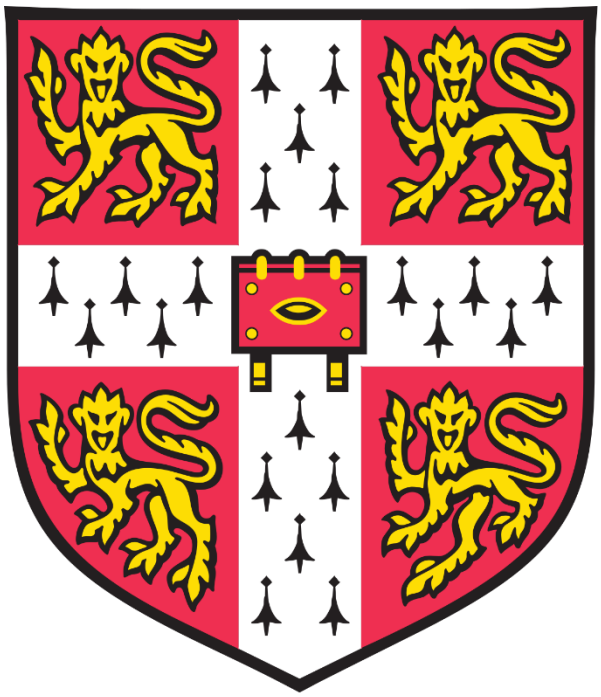

Olivia Catherine Tysoe

Gonville and Caius College

Department of Surgery

University of Cambridge

Supervisors

Mr Kourosh Saeb-Parsy & Prof Ludovic Vallier

This dissertation is submitted for the degree of Doctor of Philosophy

October 2019

DECLARATION

This dissertation is the result of my own work and includes nothing which is the outcome of work done in collaboration except as specified in the text. This dissertation is not substantially the same as any that I have submitted, or, is being concurrently submitted for a degree or diploma or other qualification at the University of Cambridge or any other University or similar institution. I further state that no substantial part of my dissertation has already been submitted, or, is being concurrently submitted for any such degree, diploma or other qualification at the University of Cambridge or any other University or similar institution. In accordance with the guidelines of the degree committee of Clinical Medicine this dissertation does not exceed 60,000 words and it contains less than 150 figures.

SUMMARY

The immunogenicity of cholangiocyte cellular therapies

Olivia Catherine Tysoe

Cholangiocytes are the epithelial cells of the biliary system, responsible for the transport and modification of bile. Cholangiocyte disorders, known as cholangiopathies, are a diverse group of life-threatening conditions characterised by cholestasis, ductopenia and eventual liver failure. There are currently no curative treatments for cholangiopathies aside from liver transplantation and while individual cholangiopathies are rare, together they account for a third of adult and 70% of paediatric liver transplants. There is a scarcity of suitable organs for transplantation, however, so development of cholangiocyte cellular therapies capable of replacing or repairing damaged bile ducts would have significant therapeutic value. The safety of such therapies must be assessed before they are suitable for clinical translation and an essential component of that is an evaluation of immunogenicity.

In this dissertation I investigated the immunogenicity of cholangiocyte organoids (COs) from an established system developed within the Vallier lab. I first assessed the survival of COs *in vivo* and generate CO lines expressing luciferase to allow for real-time bioluminescent imaging *in vivo*. I characterised the expression of HLA molecules on COs compared to primary cholangiocytes and after exposure to a series of pro-inflammatory environments and demonstrated that expression of HLA molecules is reduced in COs compared to primary cholangiocytes but that exposure to pro-inflammatory cytokines restored high levels of HLA expression. I also showed that physiologically-relevant concentrations of pro-inflammatory cytokines were sufficient to upregulate HLA class II expression on COs.

To assess the immunogenicity of COs in a transplant environment I used two humanised mouse models. I demonstrated that these models can induce an immune response against allogeneic COs and compared the response to allogeneic and autologous COs in both models. I identified HLA-matched CO lines and immune cell donors and investigated the impact of HLA-matching on the immunogenicity of CO allografts in a humanised mouse model. Overall, the work presented in this dissertation advances the understanding of the immunogenicity of cholangiocyte organoids, both in terms of their expression of immunogenic antigens and the response towards COs within both an allogeneic and autologous transplantation setting.

ACKNOWLEDGEMENTS

This work would not have been possible without all of the help and support I have received over these four years from my friends, family, mentors, supervisors and colleagues. I am incredibly grateful to all of you.

I first want to thank my supervisors, Kourosh Saeb-Parsy and Ludovic Vallier, for choosing me for this project and for all their support and guidance throughout. Kourosh, you have been the most amazing PhD supervisor I could ever have asked for. I can't really articulate just how much of a difference you have made and how much your support has meant to me throughout these last four years. Thank you for all your generosity with your time and attention, for caring about my wellbeing as much as my success and for believing in me even in the times when I didn't believe in myself. Most of all, thank you for cultivating such a fantastic, caring environment in the group and for inspiring us all to believe in the work we're doing and our capacity to achieve it. Ludovic, thank you for all your insight and advice throughout this project. Thank you for welcoming me into your lab, for giving me experience and resources I never would have had otherwise. I have learnt so much from you and I know I am a better scientist because of it.

Fotis, you are a fantastic mentor and a wonderful friend. Thank you for always encouraging me, for pushing me when I needed it, for being honest with me when I needed it, and for never letting me settle for anything less than my best. Thank you for all the amazing opportunities you have given me and for all the time you've taken to help me succeed. I can't imagine how I would have made it through this PhD without your help, your guidance, but most of all your friendship. You have been my greatest support through the most difficult times and my most enthusiastic champion in my successes. Thank you.

Nikola, Nikitas, I'm so glad I had you guys with me since the beginning of this whole thing. Thank you for keeping me sane and for putting up with me all this time. Thank you for all your help in the lab, but most of all your support through the ups and downs of this PhD. Krish, thank you for being so fantastic and for doing so much, for me but also for the whole lab. Thank you for keeping everything afloat, for helping me with so many things in the lab (those donor details are just the tip of the iceberg of everything you've done) and for always being there with helpful advice and a sympathetic ear. Tim, Alba, Beth, thank you for always helping me with my animal work when I asked, and for being generally great people to work with. Anja, Michelle, Abbie, Natasha and John, thank you for helping to make the KSP group such a wonderful group to work in. The KSP group really is something special and everyone in it is a part of that.

Kath, thank you for teaching me all those basic techniques back in first year and for helping me get started with this project. Silvia, thank you for all your help with sectioning and with things in the lab,

everything you taught me has been invaluable. Jackie, thank you for all the work you've done in CBS for me and everyone in the group.

Teresa, you are an absolute delight to work with and having you around this last year and a half has made everything just so much more fun. I couldn't have asked for a better co-first author, thank you for all the hard work you've done and continued to do and for always cheering me up. Brandon, thank you for all your help with the viral transduction work, I really couldn't have done it without you. Thanks for being so generous with your time and for being such a fun person to work with. Imbisaat, thank you for teaching me all the basics of TC back in first year. Steph, thank you for helping me with so many things, small and big, over the years, your help has been invaluable. Anna, Daniel, Loukia, Rute, Carola, Giovanni, everyone in the Vallier lab now and throughout my PhD, thank you for making the Vallier lab such a great group to be a part of and for filling those hours of TC with loads of fun memories.

Frances, thank you for being such an amazing summer student and for working so hard. I hope your PhD is going amazingly. Negar, thank you for all your help back in first year, you helped me with some very key experiments that might not have worked out so well without you.

Thank you to everyone involved in CBTM for your amazing work in collecting, processing and storing tissue from deceased donors. This project really wouldn't have been possible without all of you. Thank you to all the animal technicians in CBS, in particular the surgical technicians, for your help with the animal experiments.

Kieran, thank you for being there for me throughout so much of this PhD, first as a friend and now as my amazing boyfriend. These last two years have been so much better thanks to your constant support.

Steve, thank you for all your encouragement and for all the ways you've helped me out. Thank you for always being interested in what I'm doing and letting me ramble on about it for ages.

Thank you to all my family for supporting me and putting up with me for these last four years. To my grandparents, M&G, thank you for encouraging me to apply to Cambridge, and for always offering me a place to stay in London and for spoiling me whenever I'm around. Dad, reading Carl Sagan with you and chatting about stem cells when I was younger was part of what made me fall in love with science in the first place; thank you for inspiring me to pursue it as a career. Mum, thank you so much for your constant support and for always looking after me and making sure I'm doing well, not just this las month but always. And my amazing brothers, Barnaby, Henry and Teddy- thank you for always supporting me, encouraging me and keeping me sane. You three are the best brothers I could hope for.

Finally, I would like to extend my sincerest gratitude to all the tissue donors and their families, without whom none of this work would have been possible.

LIST OF ABBREVIATIONS AND ACRONYMS

2D – 2 dimensional

3D – 3 dimensional

AE2 – Anion Exchanger 2

AFP – Alpha Fetoprotein

ALP – Alkaline Phosphatase

AMA - of autoantibodies to inner mitochondrial antigens

APC – Antigen Presenting Cell

B_2M – Beta2 Microglobulin

BA – Biliary Atresia

BD – Bile Duct

BLI – Bioluminescence Imaging

BLT – Bone marrow, Liver, Thymus

BMP4 – Bone Morphogenic Protein 4

BSA – Bovine Serum Albumin

Ca^{2+} - Calcium

cAMP – cyclic Adenosine Monophosphate

CBD – Common Bile Duct

CCL - chemokine ligand

CD- Cluster of Differentiation

CK- Cytokeratin

Cl- chlorine

CLC – Cholangiocyte-Like Cell

cm - centimetres

CO – Cholangiocyte Organoid

CTL – Cytotoxic T Lymphocyte

DAMP – Damage-Associated Molecular Patterns

DKK - Dickkopf-related protein 1

DMEM – Dulbecco's Modified Eagle Medium

DNA – Deoxyribonucleic acid

ECO – Extrahepatic Cholangiocyte Organoid

EGF – Epithelial Growth Factor

ESC – Embryonic Stem Cell

FACS - Fluorescence-Activated Cell Sorting

FBS – Foetal Bovine Serum

FGF – Fibroblast Growth Factor

FOXF1 – Forkhead box protein F1

g – Gravity

G- Gauge

GC – Germinal Centre

GFP – Green Fluorescent Protein

GGT - Gamma-glutamyl transferase

GMP- Good Manufacturing Practice

GVHD – Graft vs Host Disease

HCO_3 – Bicarbonate

HEK – Human Embryonic Kidney

HHEX - Hematopoietically-Expressed Homeobox Protein

HLA – Human Leukocyte Antigen

HNF – Hepatocyte Nuclear Factor

hPSCs – human Pluripotent Stem Cell

HSC – Haematopoietic Stem Cell

IBD – Irritable Bowel Syndrome

ICO – Intrahepatic Cholangiocyte Organoid

IFN-γ – Interferon Gamma

IHD – Intrahepatic Duct

IL – Interleukin

iPSC- induced Pluripotent Stem Cell

JAG - Jagged

KLF4 - Kruppel-like factor 4

LGR5 - Leucine Rich Repeat Containing G Protein-Coupled Receptor 5

Luc – Luciferase

MACS – Magnetic-Activated Cell Sorting

MAPK - mitogen-activated protein kinase

MEF – Mouse Endothelial Fibroblast

MHC – Major Histocompatibility Complex

ml – millilitre

mm – millimetre

mRNA – messenger RNA

NF-κB - Nuclear Factor kappa-light-chain-enhancer of activated B cells

NK – Natural Killer

NOD- Non-Obese Diabetic

NOG - NOD/Shi-scid/IL-2Rγ^{null}

NSG – NOD/SCID/Gamma

OCT3/4 - octamer-binding transcription factor 3/4

PAMP – Pathogen-Associated Molecular Pattern

PBC – Primary Biliary Cirrhosis

PBL – Peripheral Blood Lymphocyte

PBMC – Peripheral Blood Mononuclear Cell

PBS – Phosphate Buffered Saline

PD1 - Programmed cell death protein 1

PDL1 – Programmed cell death ligand 1

PDX1 - Pancreatic and Duodenal homeobox 1

PRR – Pattern Recognition Receptors

PSC - Primary Sclerosing Cholangitis

RAG – Recombination Activating Gene

RFP – Red Fluorescent Protein

RNA – Ribonucleic acid

RPM – Revolutions Per Minute

RPMI – Roswell Park Memorial Institute media

SCID – Severe Combined Immunodeficiency

SOX – SRY-box

SpMC – Splenocyte Mononuclear Cell

SRC – SCID-Repopulating Cell

SSEA1 - Stage specific embryonic antigen-1

TGFβ – Transforming Growth Factor β

Th1 – T-helper 1

TLR – Toll-like Receptor

TNFα – Tumour Necrosis Factor

Treg – T regulatory cell

UDCA - Ursodeoxycholic acid

VEGF - Vascular Endothelial Growth Factor

WE – William's E

µl - microlitre

µm - micrometre

µM – micromole

CONTENTS

LIST OF FIGURES

LIST OF TABLES

CHAPTER 1. INTRODUCTION

1.1 Cholangiocytes and cholangiopathies

1.1.1 Cholangiocyte physiology and development

Biliary anatomy

Cholangiocytes are the epithelial cells of the intra- and extrahepatic bile ducts and are responsible for the modification of bile through the transport of water and soluble molecules into the bile duct lumen [1]. The primary function of the biliary tree is to transport bile from the liver to the gallbladder, where it is stored and released into the duodenum to aid emulsification and absorption of fats. Bile is secreted from hepatocytes, which are arranged in hexagonal structures known as hepatic lobules, into the bile canalicular, narrow (0.5-2 μm) channels between hepatocytes that emerge into the canals of Hering, the connecting space between the hepatic lobules and the intreahepatic bile ducts[2]. The canals of Hering are lined with cuboid, immature cholangiocytes and are thought to contain a niche of bipotent hepatic progenitor cells[3]. The canals of Hering merge into the biliary ductules which then continue into the intralobular intrahepatic bile ducts, which are between 15-100 μm in diameter. The intrahepatic biliary ducts grow progressively larger in diameter until they merge into two large ducts, the right and left intrahepatic ducts (both >800 μm in diameter). These two large intrahepatic ducts drain into the extrahepatic common hepatic duct, then the cystic duct, which transports bile to the gallbladder (figure 1.1). When bile is required for digestion, the gallbladder is stimulated to contract and release the bile into the common bile duct, where it is transported to the duodenum.

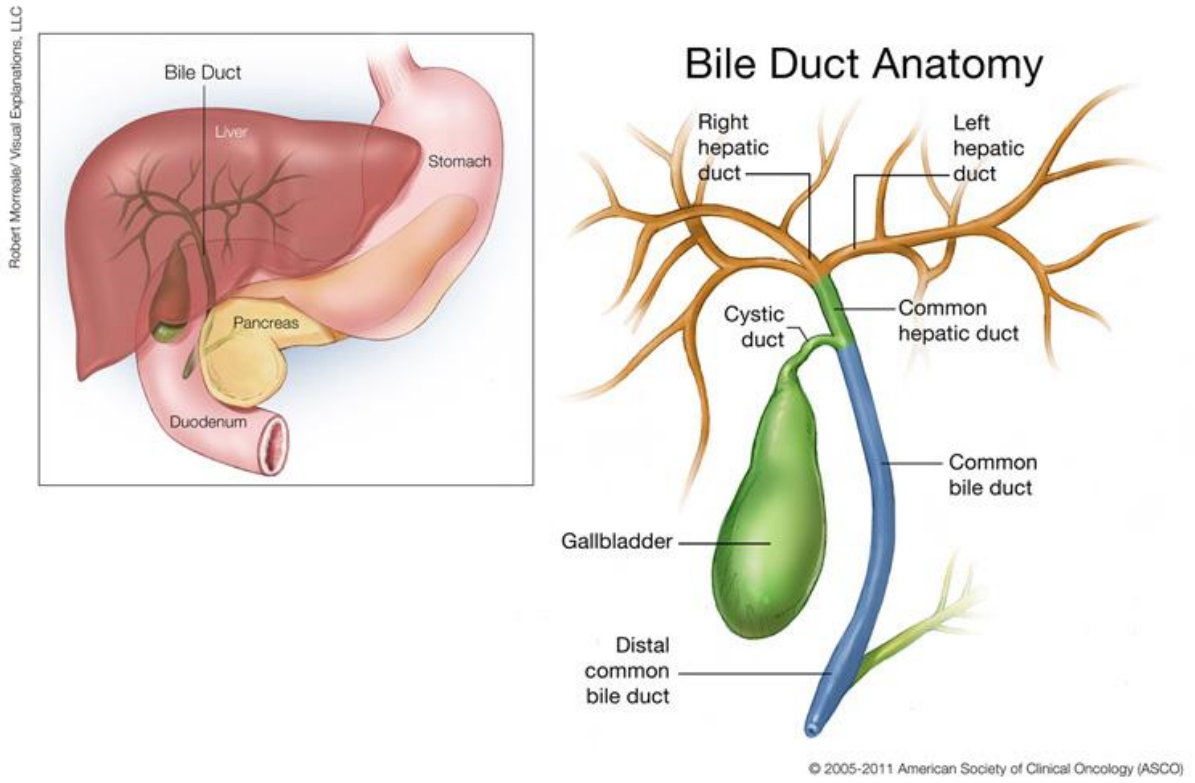

Figure 1.1: Schematic demonstrating the anatomy of the biliary tree
Schematic adapted from www.cancer.net.

Biliary physiology

Cholangiocytes vary in size according to their location in the biliary tree and can be divided into two types- small cholangiocytes, located within the intrahepatic bile ductules (diameter <15 µm), and large cholangiocytes, located within the gallbladder, extrahepatic bile duct and the larger intrahepatic ducts (diameter >15 µm)[2,4]. Small and large cholangiocytes also differ in their morphology, physiological role and gene expression. Small cholangiocytes are cuboidal in shape with a high nucleus-to-cytoplasm ratio while large cholangiocytes have a columnar morphology and a small nucleus-to-cytoplasm ratio. Additionally, small cholangiocytes are less specialised; large cholangiocytes are more polarised and possess cilia on their apical membranes for chemo- and mechanosensing within the bile duct lumen[2,4]. Large cholangiocytes are responsible for cAMP-dependent bile modification in response to the hormone secretin[5], while small cholangiocytes contribute to bile modification through a Ca^{2+}-mediated pathway. Small cholangiocytes are less sensitive to liver injury than large cholangiocytes and are responsible for repopulating the biliary epithelium in cases of damage[6].

The primary function of cholangiocytes is to transport and modify bile, primarily in response to secretin, which is produced in the small intestine after food consumption[2,4,7]. This is mostly achieved through the cAMP-mediated secretin-dependent bicarbonate (HCO_3^-) secretion pathway. Secretin is produced

within the duodenum in response to chyme (food remnants after digestion in the stomach) entering the small intestine. Secretin then binds to the basolateral membrane of large cholangiocytes within the intrahepatic and extrahepatic bile ducts, prompting the phosphorylation of the cystic fibrosis transmembrane conductance regulator (CFTR). This results in the release of chloride ions (Cl^-) into the bile duct lumen, activating the apical Cl^-/HCO_3^- anion exchanger 2 (AE2) and causing an influx of bicarbonate into the bile duct lumen. This serves two purposes, to form a layer protect the cholangiocytes from the harmful effects of concentrated bile acids and to increase the osmotic flow of water from the cholangiocytes to the bile duct lumen[8,9]. This bicarbonate-mediated influx of water is responsible for up to 40% of the bile flow volume. Damage to cholangiocytes, for instance through cholangiopathies such as primary schlerosing cholangitis and primary biliary cirrhosis, can lead to cholestasis (disruption or blockage of bile flow) due to the loss of this secretin-dependent bicarbonate-mediated pathway resulting in inadequately dilute bile.

Cholangiocyte development

Intrahepatic and extrahepatic cholangiocytes develop independently, from two different origins. Intrahepatic cholangiocytes develop from hepatoblasts[10], a liver progenitor cell type shared with hepatocytes, while extrahepatic cholangiocytes develop at an earlier stage from a common progenitor with pancreatic cells.

The liver develops from definitive endoderm, one of the three initial germ layer cell types in the embryo following gastrulation. Definitive endoderm develops into the primitive gut tube[10-13], with hepatic endoderm emerging specifically from the foregut region of this primitive gut tube. Following paracrine signalling of factors such as bone morphogenetic protein 4 (BMP4) and fibroblast growth factor (FGF) from cardiac mesoderm, foregut endoderm transitions into hepatoblasts[10,12,13], bipotent progenitor cells expressing markers of both hepatic lineage (such as hepatic nuclear factor 4a (HNF4a) and alpha fetoprotein (AFP)) and biliary lineage (such as cytokeratin 19 (CK19))[10]. Cholangiocyte differentiation from hepatoblasts begins around 8 weeks post gestation and starts in the hilum of the liver, near the portal vein. Portal hepatoblasts, co-ordinated by a wide variety of signalling pathways such as TGFβ/Activin/BMP, FGF, Wnt, and JAG/Notch, organise into a ductal plate[10,14] and undergo commitment to a biliary identity through the expression of biliary markers such as CK19 and Sox9. Initially the ductal plate forms as a single layer of cells, then develops into a double layer and forms small tubular structures[14-16], a process that is regulated through the Notch signalling pathway[15]. These tubules migrate into the surrounding mesenchyme and develops into individual bile ducts, branching out from the hilum into the parenchymal tissue. Non-canonical Wnt signalling through the planar cell polarity pathway is essential to keep the cholangiocytes of the developing bile ducts in a uniform orientation within the ductal plane[17,18]. This is necessary to maintains tubular architecture when bile

ducts are maturing and branching into the liver, and deficiencies in this pathway can lead to fibropolycystic liver diseases[18].

The developmental origins of extrahepatic cholangiocytes is less well understood, however they are known to originate in the ventral foregut, between the liver and the ventral pancreas. Extrahepatic cholangiocytes develop from a common progenitor with pancreatic cells, which expresses both the SRY-Related HMG-Box Transcription Factor Sox17 and the Pancreatic and Duodenal Homeobox 1 (PDX1) transcription factor[10,14,19]. Through the influence of Notch signalling, this progenitor cell type then differentiates into a cholangiocyte-like cell type, expressing Sox17 but not PDX1 and a pancreatic-like cell type, expressing PDX1 but not Sox17[10,14,19]. Other signalling factors affecting the development of the extrahepatic biliary tree are Hhex, a factor required for the suppression of a duodenal lineage, and HNF6, HNF1a and FoxF1, which are all associated with gallbladder development[10,14]. Once the extrahepatic bile ducts begin to form, they emerge from the ventral pancreas towards the liver, where they merge with the intrahepatic biliary system at the liver hilum.

1.1.2 Immunobiology of cholangiocytes

Cholangiocytes, as the epithelial cells of the biliary tree, are exposed to a wide range of microbial antigens from the gastrointestinal tract and the portal vein. Under healthy conditions, cholangiocytes secrete IgA and antimicrobial peptides such as β-defensin 2, lactoferrin and cathelicidin into the bile duct lumen to protect against potential pathogens from the small intestine and to clear antigens from the bile[20]. Secretion of these antimicrobial molecules is upregulated during infection. Cholangiocytes also constitutively express a range of Pattern Recognition Receptors (PRRs), such as Toll-like receptors (TLRs), which are expressed on their luminal membrane and respond to Pathogen-Associated Molecular Patterns (PAMPs) such as lipopolysaccharide (LPS), a bacterial macromolecule[20-22]. Upon activation by PAMPs, TLRs stimulate a range of immune responses through the NF-κB and MAPK pathways, including the upregulation of adhesion molecules, secretion of pro-inflammatory cytokines such as TNF-α, upregulation of HLA molecules and secretion of antimicrobial peptides[20-22].

Cholangiocytes, like all nucleated cell types[23], constitutively express HLA class I and are capable of presenting antigen to CD8+ cytotoxic T cells. Cholangiocytes do not express HLA class II within a normal, healthy environment, however, exposure to pro-inflammatory conditions, including cholangiopathies such as Primary Biliary Cholangitis (PBC) and Primary Schlerosing Cholangitis (PSC), and post-transplant conditions such as GVHD and allograft rejection can lead to *de novo* expression of HLA class II molecules[24,25]. This has also been reported in *in vitro* cultured cholangiocytes stimulated with inflammatory cytokines such as IFN-γ and TNF-α[26].

Cholangiocytes can become "activated" in response to a wide variety of insults, such as infection, xenobiotics, ischaemia and injury[20,22]. This activated state is characterised by increased cholangiocyte proliferation and a pro-inflammatory and pro-fibrotic environment, through which the cholangiocytes attempt to repair the injury. Autocrine stimulation with regenerative factors such as IL-6 and VEGF promote cholangiocyte proliferation, while secretion of cytokines and chemokines such as CCL20 and IL-8 attract a range of immune cells such as T-cells and macrophages which in turn secrete pro-inflammatory factors to aid in biliary repair[20-22].

Suboptimal repair or persistent biliary damage can result in a pathological state of continual increased inflammation and fibrosis, ultimately leading to biliary cirrhosis. This pathological activated state, and the corresponding influx of immune and mesenchymal cells, is known as ductular reaction and plays an important role in the progression of many cholangiopathies such as PBC and PSC[20].

1.1.3 Cholangiopathies

Biliary conditions, typically referred to as cholangiopathies, are a diverse group of conditions affecting cholangiocytes. Cholangiopathies are typically progressive diseases characterised by bile duct inflammation, cholestasis, fibrosis and eventual ductopenia (destruction of the bile ducts). This can often result in end-stage liver failure or cholangiocarcinoma, with no current curative pharmacological interventions[1,21,27]. While individual cholangiopathies tend to be rare, the lack of effective long-term treatment other than liver transplantation for many conditions means that their collective impact on morbidity and mortality is significant. The aetiology of different cholangiopathies are wide-ranging and often complex or unclear, with causes ranging from single genetic mutations (e.g. cystic fibrosis), idiopathic (often with a suspected autoimmune component, such as primary biliary cholangitis) or malignant (e.g. cholangiocarcinoma). Some of the most prevalent cholangiopathies that can potentially be impacted by the development of intrahepatic or extrahepatic cholangiocyte cellular therapies are described below.

Primary Schlerosing Cholangitis

PSC is a cholangiopathy primarily affecting adult men, with a median age of approximately 40 years at presentation[28]. It is characterised by cholestasis and obliterative fibrosis of large and medium bile ducts, leading to stricture formation within the intra- and extrahepatic bile ducts resulting in eventual ductopenia and liver cirrhosis[29,30]. The pathogenesis of PSC is unknown and likely multifactorial, although it is strongly associated with inflammatory bowel disease (IBD), with between 65-90% of PSC patients also presenting with IBD[28]. One proposed aetiology of PSC is an immune response caused by exposure to intestinal pathogens such as lipopolysaccharide through the portal circulation, or aberrant

expression of adhesion molecules on cholangiocytes leading to homing of memory T-cells, resulting in portal inflammation[29]. PSC is a progressive disease with no current curative pharmacological therapeutic options[31]. Surgical endoscopic management can be used to treat biliary strictures, although liver transplantation is the only effective long-term treatment, with PSC currently being the fifth most common indication for liver transplant in the United States[32].

Primary Biliary Cholangitis

PBC is an adult cholangiopathy, mostly affecting older women. The condition primarily affects the small bile ducts within the intrahepatic biliary system and is characterised by inflammation, damage to cholangiocytes and ductopenia, and infiltration of immune cells such as lymphocytes, macrophages, eosinophils and NK cells into the portal tract. PBC has an unclear aetiology but is considered an autoimmune condition, caused by development of autoantibodies to inner mitochondrial antigens (AMAs)[33-35]. AMAs primarily attack the pyruvate dehydrogenase complex, leading to an influx of immune cells to the affected cholangiocytes[33,34]. This results in cholangiocyte cell killing by cytotoxic T cells and NK cells, as well as the production of a pro-inflammatory environment due to the release of inflammatory cytokines by CD4+ T cells. Two therapeutic options currently exist for the treatment of PBC, Ursodeoxycholic Acid (UDCA), which can slow disease progression[36,37] but is not curative, and liver transplantation[38-40].

Biliary Atresia

Biliary atresia (BA) is a progressive, inflammatory cholangiopathy affecting neonatal infants. While BA is a rare condition, affecting 0.5-0.8 per 100,000 live births in developed nations, it is the most common cause of liver transplantation in infants[39,41] and typically results in death within two years due to progressive liver cirrhosis if left untreated[41-44]. Biliary atresia is an idiopathic cholangiopathy[44,45] characterised by obstruction and fibrosing obliteration of the extrahepatic bile ducts. This leads to cholestasis, resulting in end-stage liver cirrhosis[42,45]. Intrahepatic bile ducts can also undergo fibrosis, inflammation and cholestasis- this is most commonly seen when the extrahepatic biliary system is obstructed at the level of the porta hepatis, which occurs in over 90% of all cases. The current preferred treatment for biliary atresia is Kasai portoenterostomy[44], a surgical procedure whereby the duodenum is directly anastomosed to the porta hepatis, allowing for drainage of bile into the small intestine[46]. This procedure alone allows up to 15% of recipients to live predominantly symptom-free lives[47], while 50-60% of all BA patients will require a liver transplant at some point in their life, even after a successful Kasai portoenterostomy[44,45].

Alagille's Syndrome

Alagille's syndrome is a genetic condition caused by mutations in the Notch signalling pathway[48,49]. It is an autosomal dominance disorder affecting many areas of the body, although the severity of the disease varies between patients[50]. Approximately 97% of Alagille's syndrome cases are caused by mutations in Jagged 1, a Notch signalling ligand, although mutations of the NOTCH2 gene can also be responsible. The prevalence of Alagille's syndrome is estimated to be 1 in 70,000[51], although this figure is considered to be an underestimate due to the variable penetrance of the condition[50]. Alagille's syndrome can affect the cardiovascular system, kidney function, physical and mental development and cause abnormalities in the skeleton and facial features[52], but the most common clinical feature is defects of the biliary tree, in particular ductopenia and chronic cholestasis[50,52-54]. Alagille's syndrome is progressive, with 15% of patients developing cirrhosis and liver failure requiring a liver transplant[50,54].

1.1.4 Treatment of cholangiopathies

The available treatments for cholangiopathies are limited. There are surgical options to treat some cholangiopathies, such as portoenterostomy for biliary atresia[44], a procedure that involves anastomosing the jejunum to the liver above the portal vein to allow drainage of bile directly into the small intestine, and some pharmacological therapies such as Ursodeoxycholic Acid (UDCA) for PBC can slow disease progression[36,37].

Currently, however, the only curative treatment for end-stage cholangiopathies is liver transplantation, either whole-organ transplantation from a deceased donor or partial liver transplantation from a living or deceased donor. The number of people requiring liver transplantation, however, is greater than the number of available organs[55]. The high demand for donor organs has led to increased use of organs donated after circulatory death (DCD donors) in the UK and elsewhere, resulting in a modest increase in overall donations[56]. However the number of organ transplants performed annually still only accounts for approximately 10% of the global demand[57]. Additionally, there are considerable practical concerns with the use of solid organ transplants as the organ must undergo a period of ischaemia between removal from the donor and implantation into the recipient. This can result in cell death and reduce the quality of the organ, increasingly the likelihood of graft failure.

The risk of rejection further complicates solid organ transplantation. While liver grafts are less likely to be rejected than other organs[58], the risk is still present and recipients of liver transplants still require immunosuppression, in most cases for the rest of their lives[59]. Long-term immunosuppressive treatment is associated with an increased risk of cancer, approximately double that of the general population[60], as well as cardiovascular disorders[61] and opportunistic infections[62]. One potential solution to the problems of solid organ transplantation is cellular therapies. It is hoped that cellular therapies will be able to provide a cost-effective, safe alternative to solid organ transplantation while reducing or

altogether avoiding the challenges of limited supply, graft failure and immune rejection that can occur in conventional organ transplantation. .

1.2 Regenerative Cellular Therapies

1.2.1 Overview

Cellular therapies are a promising alternative to solid organ transplantation, either as a temporary 'bridging' treatment until an organ transplant can be carried out, or, eventually, as a curative treatment. In order to become an effective and realistic alternative to organ transplantation, cellular therapies must meet several important criteria. They must be safe (non-tumorigenic and remain localised to only the intended anatomical site) and effective (able to perform all the necessary functions and significantly improve the clinical outcome for the patient). They should ideally also have low immunogenicity, requiring minimal or no immunosuppression. They should certainly not be more immunogenic than existing solid organ therapies. Lastly, cellular therapies must utilise cells that are abundant, readily available when required and result in therapies that are cost effective on a large scale. Currently there are two leading options for cellular therapies: those derived from stem cells and those derived from primary cells. Stem cell-based therapies can be further divided into those derived from adult stem cells, embryonic stem cells (ESCs) and induced pluripotent stem cells (iPSCs).

1.2.2 Embryonic stem cells

Embryonic stem cells are derived from the inner cell mass of blastocysts and are pluripotent; i.e., they able to differentiate into any of the three primary germ layers (mesoderm, ectoderm and endoderm) from which all adult cell types are derived. ESCs are capable of indefinite propagation as they express high levels of telomerase, allowing for continual repair of telomeres after cell division[63]. ESCs have a round shape, high nucleus-to-cytoplasm ratio and form tightly packed colonies in culture. ESCs were first isolated from mice in 1981[64], using techniques adapted from culturing teratocarcinoma lines, and subsequently from humans in 1998[65]. Since then, progress has been made towards potential therapeutic use of ESCs for a range of diseases, such as age-related macular degeneration[66], heart failure[67,68], spinal cord injury[69] and Parkinson's disease[70]. ESCs were initially seen as a highly promising source for cellular therapies because of their pluripotency, their ability to be rapidly expanded from a small number of cells and their potentially reduced immunogenicity when compared to primary cells or solid organ transplants (due to a lower level of human leukocyte antigen (HLA) expression[71]). More recent studies, however, have suggested that ESCs and ESC-derived differentiated cells may be more immunogenic

than previously recognised, possibly on a level comparable with solid-organ transplants[72]. Additionally, research into and therapeutic use of ESCs has been complicated by ethical concerns, prompting many researchers to focus on iPCS, which do not require the use of human embryos.

1.2.3 Induced Pluripotent Stem Cells

Induced pluripotent stem cells (iPSCs) are pluripotent cells that are generated from adult somatic cells but are genetically, morphologically and functionally highly similar to ESCs. iPSCs were first generated from mouse embryonic and adult fibroblasts in 2006[73] and then from adult human fibroblasts in 2007[74]. Since then iPSCs have attracted a great deal of attention, as they offer the same clinical and scientific potential as ESCs while avoiding the ethical controversy of deriving cells from human embryos. iPSCs are generated through "reprogramming" adult somatic cells by inducing the overexpression of four pluripotency transcription factors - Oct3/4, Sox2, Klf4 and c-Myc, which alter the cell's epigenome and induces expression of pluripotency associated genes such as Nanog, SSEA1 and Oct4, reverting it to a pluripotent state. The c-Myc transgene was found to increase the risk of tumour formation in iPSC-derived chimeric mice[75] and has since been shown to be dispensable in the reprogramming process[76]. This has resulted in many researchers no longer using c-Myc as a reprogramming factor when generating iPSCs for translational research[77,78]. The expression of reprogramming factors can be induced by a variety of different methods - initially a retroviral vector was used by the Yamanaka group to integrate the transgenes into the genome[73] but due to the low efficiency and concerns over accidental integration of viral genes, other methods have been developed. These include the use of lentivirus vectors, which can integrate into non-dividing cell types and can be edited to include a Cre-recombinase cassette capable of excising any viral DNA integrated into the genome[79], and Sendai virus vectors, which are RNA viruses and therefore incapable of genome integration[80]. Additionally, transgene-free methods of reprogramming have been investigated, including transfecting cells with mRNA[81] for the reprogramming factors or introducing the reprogramming factors as protein into the cells directly[82]. Disadvantages of iPSCs as cellular therapies include the continued lack of an ideal reprogramming vector, uncertainty over the immunogenicity of iPSCs[72,83], including from autologous donors[83], and the current inability of iPSCs to fully differentiate into all cell types *in vitro*. Additionally, there are concerns that incomplete epigenetic reprogramming and a lingering "epigenetic memory"[84] may prevent iPSCs from being truly pluripotent and limit their ability to differentiate into all cell types, as well as safety concerns about the potential for iPSCs and iPSC-derived therapies to be tumourigenic, in particular the risk of teratoma formation[85].

1.2.4 Primary Cells

Primary cells are adult somatic cells isolated from tissues. Human primary cells can be derived either from living donors though biopsies or blood donation or from deceased donors. A clear advantage of primary cell lines for cellular therapy is that the cells are already fully differentiated and functional and, as they do not undergo reprogramming, are free from many of the safety concerns associated with iPSCs. Additionally, some cell types have already been used for primary cell therapy for several years, such as the transplantation of pancreatic islets to treat type 1 diabetes mellitus[86,87]. A major limitation of primary cell therapy is the inability to culture many primary cell types for any significant length of time. While some cell types, such as fibroblasts, can be maintained and expanded *in vitro* for prolonged periods[88], most complex cell types cannot be cultured for more than a few weeks[89,90]. Primary cells commonly dedifferentiate in culture[91-93], although advances in co-culture and 3D culture systems can mitigate this to some degree[94,95]. As the majority of cell therapies are likely to involve transplantation of cells from allogeneic donors, many primary cellular therapies are likely to induce an immune response and require immunosuppression, in a similar manner to solid organ allografts.

1.2.5 Organoids

The development of the organoid culture system over the last decade has had a major impact on the *in vitro* culture of both primary cells and cells derived from pluripotent stem cells, with significant implications for the study of tissue and cell development, disease modelling, drug screening and regenerative cellular therapies. While the term "organoid" can be broad in its meaning[96], it is typically used to refer to an *in vitro* culture of 3D cellular structures suspended within an artificial extracellular matrix, capable of self-organisation and long-term self-renewal[96-98]. Organoids can be derived either from primary tissue or from pluripotent stem cells after differentiation towards a particular lineage. In the case of primary-derived organoids, another important requirement is that the organoids retain key characteristics of their original tissue in terms of their gene expression, functionality and genetic stability.

The first example of an organoid culture system was developed in 2009 from intestinal stem cells found in the intestinal crypts of adult mice[99]. These stem cells expressed the marker leucine-rich repeat-containing G-protein-coupled receptor 5 (LGR5), allowing for their isolation and *in vitro* expansion. This original organoid system was developed after a series of key discoveries: firstly, the importance of the Wnt signalling pathway[100] - a key signalling pathway regulating cell proliferation, cell fate determination and cell polarity in both embryonic and adult tissue[101]- in propagating adult intestinal stem cells[102]. Secondly, the identification of LGR5 as an intestinal stem cell marker[103] and, lastly, the discovery that the Wnt agonist R-spondin could bind to LGR5 to induce intestinal stem cell hyperplasia *in vivo* in mice[104].

These discoveries allowed the development of a 3D culture system relying on Matrigel - a laminin-rich hydrogel derived from a murine sarcoma[105]- to suspend the organoids within a 3D structure, and Wnt signalling, provided by the Wnt agonist Rspondin-1, to promote cell proliferation through the Wnt/β-catenin pathway. In addition, two final growth factors that had previously been demonstrated to play a role in intestinal cell proliferation, epidermal growth factor[106] (EGF) and Noggin[107] (a BMP inhibitor), were shown to be necessary for organoid proliferation and culture expansion.

Importantly, these organoids contained all cell types of the intestinal epithelium and recapitulated the crypt and villus structure of the native intestinal tissue. These crypt and villus-like structures surrounded a central lumen in each organoid, with fully-differentiated epithelium comprising the villus-like areas and LGR5+ stem cells remaining in the crypt-like areas, as seen in native intestinal tissue.

Since this initial work, many other organoid culture systems have been developed for a wide variety of different cell and tissue types, modifying the specific culture conditions and growth factors to promote the survival and proliferation of particular lineages [108-113]. Furthermore, the organoid culture system has been applied to the culture of cells derived from pluripotent stem cells[114-119] , with the aim of increasing the maturity of these differentiated cell types and compensating for the difficulty in accessing primary tissue[120].

The development of organoid culture technology has great potential for regenerative cellular therapies as it allows for the long-term culture of many primary cell types previously difficult to maintain *in vitro*, as well as improving the differentiation and expansion potential of many iPSC-derived cellular therapies. Due to the highly proliferative nature of most organoid systems, only a small amount of starting tissue is required to establish and expand primary-derived organoids, while many terminally differentiated iPSC-derived organoids can be passaged and expanded long-term, which is not typically the case for 2D differentiation systems. Furthermore, many organoid systems are increasing the potential of the technology through co-culture with other cell types, such as mesenchymal or endothelial cells[121-123]. Additionally, cells generated through organoid technology can be seeded on artificial scaffolds or decellularised tissue to produce bioengineered tissue for use in regenerative medicine.

A limitation of organoid culture systems is the continued requirement for an extracellular matrix derived from xenogenic material in order to maintain the 3D structure and allow for optimal cell proliferation. Matrigel and other basement membrane matrices are derived from murine tissue and are not chemically defined, making them non-compliant with good manufacturing practice (GMP) standards, a requirement for any product developed for clinical use. Chemically defined, non-xenogenic artificial extracellular matrices are being developed to replace Matrigel, although this technology is not yet optimised and Matrigel remains in widespread use. Additionally, in the case of

primary-derived organoids, access to human tissue can be a logistical challenge, with many tissue types only available from deceased donors or through a biopsy. While iPSC-derived organoids can be generated from more readily available cells, the maturity of the resulting organoids is not always optimal.

Within the Vallier lab, we have developed a novel organoid culture system for the derivation and long-term expansion of cholangiocyte organoids (COs) [124,125]. COs can be derived from both extrahepatic and intrahepatic biliary tissue[125] and represent a population of mature, adult large cholangiocytes capable of survival and expansion for up to six months. COs display typical cholangiocyte morphology, including cilia, and express key cholangiocyte markers at levels consistent with primary tissue, even after long-term culture. They maintain standard cholangiocyte functionality such as alkaline phosphatase activity, gamma glutamyl transferase activity and ion transfer in response to hormones such as secretin. Importantly, we have demonstrated COs' capacity to successfully generate artificial biliary tissue through seeding on tubular collagen scaffolds. These artificial bile ducts were able to rescue a model of murine extrahepatic biliary injury[124] and work is ongoing to develop artificial bile ducts of a size appropriate for human transplantation. Additionally, assessment of the potential of COs to repopulate and repair damage to the intrahepatic biliary system is in progress. Given the potential for COs to be used as a regenerative therapy for cholangiopathies of both the extrahepatic and intrahepatic biliary system, it is important to fully characterise the immunogenicity of these organoids. This will determine the best strategy for translating this cellular therapy to the clinic, as well as potentially discovering methods of reducing or eliminating the alloimmune response to any CO cellular therapy or artificial tissue.

1.3 The immune response

1.2.2 Allograft rejection

In solid-organ transplantation, there are three recognised pathways that mediate the alloimmune response to donor tissue - the direct, indirect and semi-direct allorecognition pathways [126]. The indirect allorecognition pathway is the typical pathway of (allo)antigen recognition - recipient antigen presenting cells (APCs) endocytose HLA and other molecules from donor cells and process them into antigenic peptides which are then presented via HLA class II molecules on recipient APCs. Recipient CD4+ effector T helper cells (Th cells) then bind to recipient APC HLA class II molecules expressing donor alloantigen and to B7 (CD80/CD86; costimulatory molecules expressed on the APC) and undergo activation and clonal expansion. In a manner similar to the immune response to infections, the activated

Th cells produce pro-inflammatory cytokines and provide help to naïve B cells in the lymphoid tissue. This results in B-cell activation and the formation of germinal centres (GCs) within the secondary lymphoid tissue (spleen and lymph nodes)[127]. B-cells undergo maturation and antibody class-switching in GCs through somatic hypermutation, resulting in the production on highly specific IgG antibody. Activated recipient APCs can also activate CD8+ T cells, resulting in their maturation into cytotoxic T lymphocytes (CTLs) which then kill target cells, a process that is aided by Th cells.

The direct allorecognition pathway involves the activation of recipient Th cells by intact donor HLA class II molecules, presented by donor APCs present in the graft. This pathway typically dominates during the early, acute response to organ transplantation and becomes less prominent with time as donor APCs are lost [128]. The putative semi-direct allorecognition pathway was discovered relatively recently and involves the transfer of intact HLA molecules from donor APCs to recipient APCs, which then present antigen to recipient T cells [129].

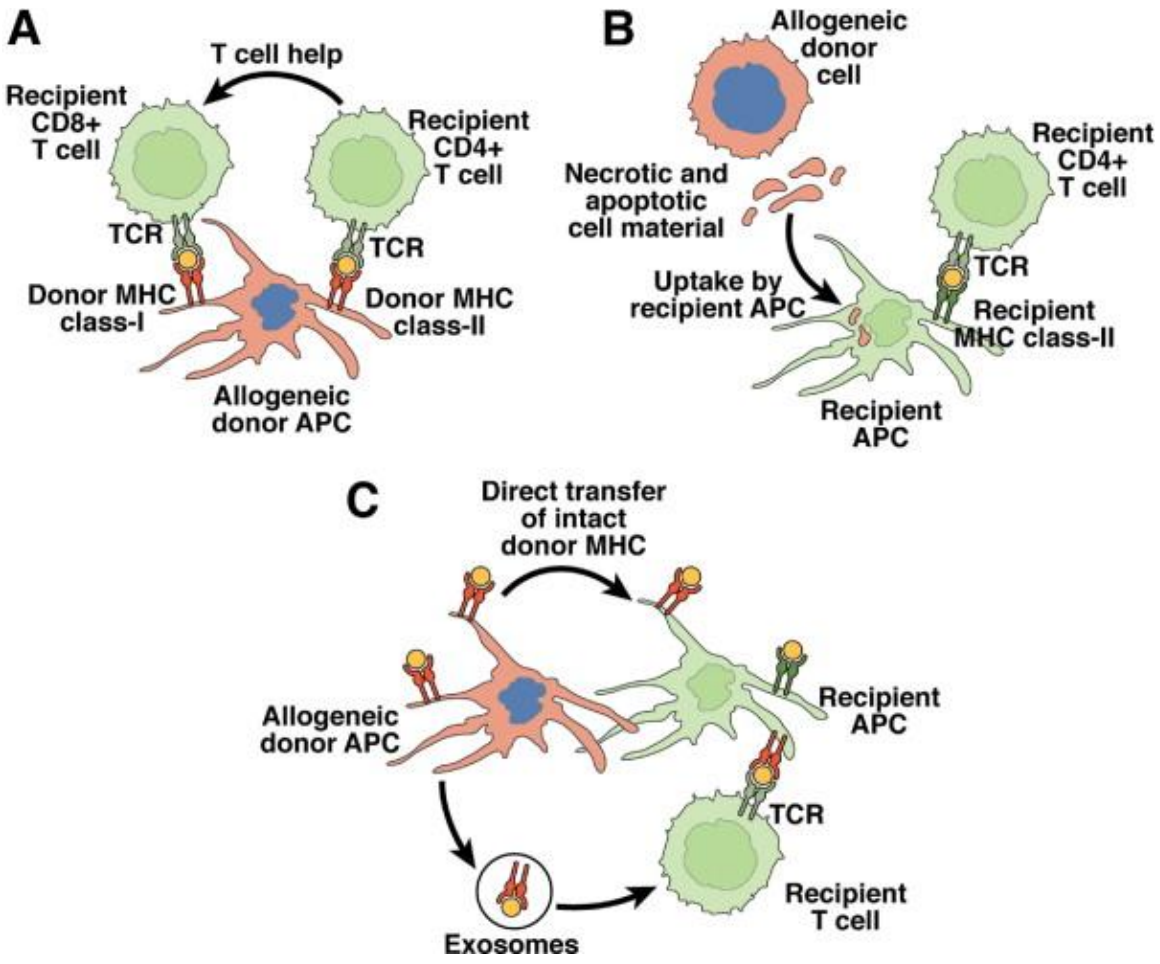

Figure 1.2: Schematic demonstrating the three alloimmune recognition pathways
Schematic representation of the three pathways of alloimmune recognition: the direct pathway (A), the indirect pathway (B) and the semidirect pathway (C). Schematic adapted from Sánchez–Fueyo and Strom (2011)[130].

In all allorecognition pathways, successful activation of effector T cells by APCs requires not only the interaction of HLA molecules with the T cell receptor (known as Signal 1) but also the interaction of costimulatory molecules (Signal 2). Signal 2 involves, amongst others, the interaction of CD80/CD86 on the APC with CD28 on the Th cell. This results in production of IL-2, a pro-inflammatory cytokine which stimulates proliferation in T cells [131]. If a T cell binds to HLA class I or II on an APC but does not receive signal 2 then the cell will undergo anergy [132,133]. Under normal conditions, CD86 is expressed at low levels on APCs and both CD86 and CD80 are upregulated after exposure to pathogen-associated molecular patterns (PAMPs) or, in the context of transplant, damage-associated molecular patterns (DAMPs). DAMPs bind to pattern recognition receptors (PRRs) [134] and induce a signalling

cascade resulting in the activation of the transcription factor NF-kB. This upregulates expression of HLA class II, CD80 and CD86.

Allograft rejection can be divided into acute and chronic responses. Although these categories are based on the timeframe of rejection rather than the underlying mechanisms, acute rejection is typically mediated by T cells [135], although antibody-mediated hyperacute rejection and acute antibody-mediated rejection can also occur. Both CD4+ and CD8+ T cells contribute to acute rejection, although CD4+ T cells can be sufficient to induce acute rejection [136,137]. Chronic rejection is often antibody-mediated; the recipient generates *de novo* antibodies against donor HLA class I and II molecules, resulting in fixation of complement and recruitment of macrophages and neutrophils to the graft [138,139]. Memory T cells also contribute to chronic allograft rejection [140,141], including by direct-pathway interaction with graft endothelial cells [142].

The optimal desired outcome in any allogeneic transplant setting is operational transplant tolerance. This is defined as the survival of a functioning graft within an immunocompetent recipient, without the need for immunosuppressive therapy and with no functional or histological signs of rejection [130]. As alloantigens are not presented to immature T cells in the thymus during embryonic development, central tolerance towards allografts cannot be attained, although it is possible to develop peripheral tolerance through a two-step mechanism of deletion of alloreactive effector T cells and the proliferation of graft-protective regulatory T cells (Tregs) [143]. Initial deletion of effector T cells can be induced by costimulation blockade of CD28-B7 and CD40L-CD40 interaction, resulting in apoptosis of the alloreactive T cells [143 144]. Deletion of effector T cells is followed by an increase in the proportion of Tregs, which in turn can further decrease the number of active effector T cells through mechanisms such as downregulating expression of costimulatory molecules on APCs through direct cell-cell interaction [145], interacting directly with effector T cells to induce anergy or apoptosis [146], secreting IL-10 and TGF-β to downregulate APC function and IL-2 production by effector T cells [147] or to convert effector T cells into Tregs [148].

1.2.3 Methods of preventing allograft rejection

HLA matching is when donor organs are assigned to recipients based on a match between their HLA molecules. This matching is optimally performed at the level of specific HLA alleles, but before the advent of DNA-typing, HLA-matching was performed according to serotype, a much lower level of resolution[149]. There are six classical HLA molecules: HLA-A, HLA-B, HLA-C (HLA class I) and HLA-DR, HLA-DP and HLA-DQ (HLA class II). HLA genes are all located on chromosome 6 and are highly polymorphic, with over 2550 HLA class I and II alleles currently identified[150]. HLA matching has been demonstrated to be highly effective at improving long-term graft survival and patient survival in solid organ transplantation[151,152] and is highly important in HSC transplantation[153]. The extent to which HLA-

matching improves transplant outcomes varies according to organs, with the allograft survival of organs such as kidneys and hearts clearly linked to the degree of HLA compatibility between donor and recipient[152], while the benefit of HLA matching in liver allografts remains unclear, with the majority of evidence suggesting it is has no impact on either graft or patient survival[154,155]. While HLA matching has been demonstrated to be effective for most organs, in cases of solid organ transplantation it is typically only performed for kidney grafts, as other organs have too few available grafts and too high a susceptibility to ischaemia for HLA matching to be practical[152].

The most common and effective method of preventing allograft rejection is administration of immunosuppressive agents to the transplant recipient. Immunosuppressive treatments can be broadly divided into three categories, induction immunosuppression, maintenance immunosuppression and treatment of acute rejection[156]. Immunosuppressive treatments can be either pharmacological agents such as calcineurin inhibitors such as (for example, cyclosporine A and tacrolimus) or biological agents such as monoclonal antibodies[157].

Immunosuppression is highly effective at stopping immune rejection in the early stages post-transplantation but long-term use often has negative side-effects such as nephrotoxicity[158], increased likelihood of cancer due to reduced ability of the immune system to detect and destroy transformed cells[159] and an increased susceptibility to pulmonary infections[160]. Long-term immunosuppression is often essential, as it is unusual for a transplant recipient to ever gain full tolerance to their graft and low-level immunosuppression often needs to be maintained life-long[157]. Due to the harmful side effects of long-term immunosuppression, identifying an alternative method of ameliorating immunogenicity in cellular therapies would have a significant benefit to the health of patients receiving such therapies.

1.2.4 Immunogenicity of cellular therapies

While autologous cellular therapies is considered the ideal therapeutic option for many conditions requiring cellular therapies[161], generating autologous cellular therapies and bioengineered tissue for every patient would be highly time consuming and unlikely to be logistically or economically viable for the foreseeable future. Additionally, if generating primary-derived cellular therapies, such as COs, deriving autologous cell lines may not always be possible in cases where the native biliary system is significantly damaged (e.g., late stage primary biliary cirrhosis) or missing altogether (e.g., biliary atresia).

Allogeneic primary derived cellular therapies are expected to have similar immunogenicity to their tissue of origin but may be less immunogenic than a solid organ transplantation. This is because cellular therapies would typically be a purified population of one cell type (for example, cholangiocytes, hepatocytes) and so would lack passenger lymphocytes, including APCs. In solid organ transplants, these passenger APCs would interact with the recipient's immune system via the direct alloimmune pathway due to their expression of HLA class II and costimulatory molecules, as well as via the

semidirect and indirect alloimmune pathways. Cellular therapies, in contrast, would not be able to interact with the recipient immune system through the direct pathway as non-professional APCs lack co-stimulatory molecules and express HLA class II only under heightened pro-inflammatory conditions. Despite this, it is highly unlikely that allogeneic cellular therapies would be able to be transplanted without some form of immunosuppression or other attempts to ameliorate their immunogenicity.

Aside from standard immunosuppressive treatment, one method for reducing immunogenicity of cellular therapies that is under investigation is HLA matching of donors and recipients. This has been discussed in the context of generating banks of pluripotent stem cell therapies from a wide range of donors of varying HLA types, particularly homozygous donors, in order to provide allogeneic, HLA-matched cells for as many patients as possible[162-166]. The impact of HLA matching has been investigated in the context of iPSC and ESC-derived cellular therapies, with reports indicating so far the HLA matching is able to significantly reduce, although not entirely prevent, the immune response to allogeneic cellular therapies[167-170]. While the generation of banks of homozygous cell lines is likely to be challenging[149], particularly in multi-ethnic populations, genetic engineering strategies can be used to knock out heterozygous HLA types, reducing immunogenicity and improving the likelihood of finding an HLA match[171].

Another promising option is genetic modification of cellular therapies to remove HLA expression completely, particularly HLA class I, which is expressed on all nucleated cell types. This has been shown to reduce immunogenicity by preventing or limiting CD8+ T cell mediated cytotoxic killing[172,173], however HLA I KO cells remain vulnerable to cell killing from natural killer (NK) cells[174]. The impact of NK cells can be ameliorated by the concurrent overexpression of a non-classical HLA class I molecule, such as HLA E or G, on HLA class I KO cells[175].

1.4. Humanised mouse models

1.4.1 Immunodeficient mice

Clinical translation of cellular therapies is critically dependent upon the ability to assess the *human* immune response they induce. While mouse models are essential for investigating the safety and functionality of cellular therapies, as well as contributing towards immunological research in general, the differences between mouse and human immune systems and the need to test human-specific cellular therapies require the "humanisation" of the mouse immune compartment. Generation of these models requires the use of severely immunocompromised mouse strains, onto which human leukocytes can be engrafted through a variety of methods outlined below. The first steps towards generation of humanised

mice was the discovery of the severe combined immunodeficiency (SCID) mouse strain, which contain almost no mature B or T lymphocytes and are unable to reject skin xenografts[176]. This phenotype is due to a mutation of the *prkdc* gene (encoding protein kinase C) on chromosome 16 which affects the DNA repair mechanism essential for VDJ recombination during maturation of B and T cells[177]. Subsequently, $RAG1^{-/-}$ and $RAG2^{-/-}$ strains were generated[178,179] – these strains are homozygous for a mutation in the RAG1 and RAG2 genes respectively, preventing VDJ recombination and T and B lymphocyte maturation in a similar manner to SCID mice. Backcrossing the non-obese diabetic NOD/ShiLtj (NOD) strain with the SCID or $RAG1/2^{-/-}$ strains was an important advance in humanised mouse research as NOD/SCID mice had reduced NK cells, reduced macrophage functionality and lacked complement as well as the near-complete lack of T and B cells typical of SCID mice[180].

It was not until the development of the NOD/shi-SCID/γ (NOG) strain, however, that engraftment of immunodeficient mice with human leukocytes became efficient enough to allow for effective humanised mice research. NOG mice lack T, B and NK cells, have reduced macrophage, complement and dendritic cell activity and engrafted human haematopoietic stem cells (HSCs) more effectively than other immunocompromised strains. NOG mice were generated by crossing NOD/shi-SCID mice with $\gamma_c^{-/-}$ mice, which have a mutation in the γ chain of the common cytokine receptor[181] (formerly known as the IL-2 receptor)[182] resulting in an abrogated, non-functional form of the molecule. The common cytokine receptor γ-chain (γc) is found within the receptors for the cytokines IL-2, IL-4, IL-7, IL-9, IL-15 and IL-21. The lack of IL-15 and IL-2 signalling results in an inability to form NK cells[183,184], while the lack of signalling from IL-2 and multiple other cytokines (e.g. IL-4, IL-7) contributes further to the deficiency in B and T cells[182]. Around the same time, a similar strain, the NOD/LtSz-*Prkdc*^{scid} *Il2rg*^{tm1Wjl}/J (NSG) strain, was developed. NSG mice are similar to NOG mice, with the principle difference that their IL-2Rγ chain is completely lacking, rather than simply non-functional [185]. NSG mice are commonly used for the generation of humanised mice as they provides highly effective engraftment of human leukocytes[186].

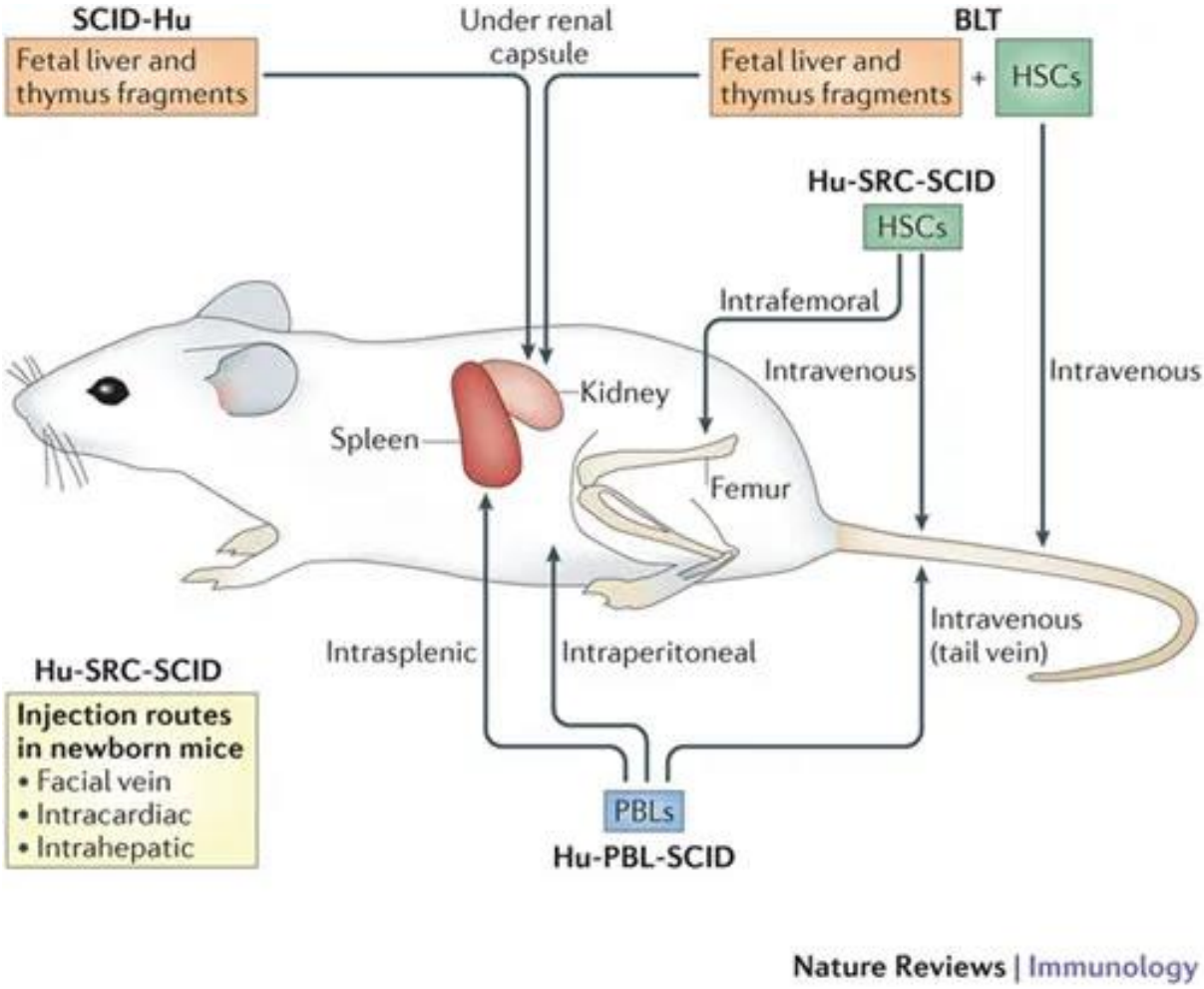

Figure 1.3: Schematic of the different humanised mouse models
Figure adapted from Schultz et al. (2012)[186]

1.4.2 The Hu-SRC-SCID model

The human SCID repopulating cell (Hu-SRC-SCID) method of reconstitution of the human immune compartment involves the engraftment of immunodeficient mice with human haematopoietic stem cells (HSCs) after gamma irradiation. Gamma irradiation is necessary to ensure that any residual murine leukocytes are eradicated and to provide an adequate biological niche within the bone marrow for the engraftment of human HSCs[187]. Irradiation and engraftment with human HSCs can be carried out either on newborn[188] or adult[189] mice. Following injection of HSCs, multiple lineages of human lymphoid and myeloid cells develop over a period of one to three months and can be found in the spleen and bone marrow, including B cell, T cells, NK cells dendritic cells and platelets[185,188,190] . The level of engraftment and the success of multilineage differentiation of human cells is highly variable and is dependent on a range of factors such as the route of HSC delivery, the age of the recipient mice, the origin of the HSCs and the strain of mice used[191]. Human B cells at multiple stages of development have been found in the spleen and BM of Hu-SRC-SCID mice, including pre-B cells, pro-B cells and

early B cells[192], however fully mature B-cells are rare[192]. While these B cells have been shown to produce high levels of IgM and IgD antibody, very little IgG production has been demonstrated[192,193] and class switching has been difficult to demonstrate[135,194]. This is likely due in large part to the lack of properly developed germinal centres in the spleen and other secondary lymphoid tissues[195], resulting in a suboptimal antigen-specific B-cell response. Additionally, the proportions of CD3+ T cells is often very low[192,196]. While mature CD3+ T cells can be found in Hu-SCR-SCID mice and are able to proliferate after stimulation, the degree of proliferation and the survival of the T cells is significantly lower than that of normal human PBMCs, due to inadequate maturation in the murine thymus[135].

1.4.3 The Hu-PBL-SCID model

This model involves the reconstitution of immunodeficient mice with adult peripheral blood mononuclear cells (PBMCs) [lymphocytes], typically by intravenous[197] or intraperitoneal[198] injection. This method of engraftment provides a rapid immune response, resulting in infiltration or rejection of engrafted human tissue in as little as seven days[197]. The Hu-PBL-SCID model has been used to demonstrate acute, cell-mediated rejection of multiple cell types, such as islets[199], endothelial cells[200] and skin grafts [200,201] and to test the efficacy of Treg treatment for allograft rejection and dysfunction [202,203].

If left for longer than a few weeks, mice reconstituted through the Hu-PBL method will develop xenogenic graft-versus-host disease (GVHD) - wherein the allogeneic donor (human) lymphocytes are activated by recipient (mouse) antigen and attack the recipient tissue, often fatally[204]. This occurs in response to mouse MHC molecules[197,205], a development that can be useful for modelling GVHD but acts as a confounding factor for the study of transplant rejection more generally. This limitation can be reduced by ensuring that adequate positive and negative controls are used within each experiment, to ensure that any rejection seen is above the baseline GVHD response. In contrast to the Hu-SRC model, PBMC reconstitution typically results in a significant predominance of CD3+ T cells, with very little engraftment of B cells and an approximately even ratio of CD4+ and CD8+ T cells[199,206,207]. Antigen-specific activation of T cells has not been adequately demonstrated, likely due to the lack of APCs in this model.

1.4.4 Advances in humanised mice

Current humanised mouse models have significant limitations in their ability to adequately recapitulate the human immune system. Multiple solutions to these remaining limitations are under exploration, mostly through the development of additional transgenic strains better capable of supporting human haematopoiesis and immune cell engraftment.

For the Hu-PBL model, one of the most significant drawbacks is the inevitable development of a strong xenogenic GVHD response. Transgenic strains have been developed which lack murine MHC, significantly reducing this effect. The first strain to be developed was the NOG-Iab^{null}B2m^{null} strain[208] - NOG immunodeficient mice lacking murine MHC class I and II through the knock-out of the Beta-2 Microglobulin (B2M) molecule essential for MHC class I expression and the I-Ab isoform of murine MHC class II. This double KO strain still allows for the engraftment of human PBMCs capable of allogeneic rejection of human grafts but levels of GVHD are significantly reduced compared to the standard NOG strain. Additionally, these mice are capable of developing antigen-specific human B and T cells when challenged with antigen.

A similar advance was the development of NSG-*B2M*^{null}*(IA IE)*^{null} and NSG-*(K*^{b}*D*^{b}*)*^{null}*(IA)*^{null} mice[209], two NSG strains lacking both MHC class I and II through different knockout mutations. Both strains permit engraftment of adult human leukocytes capable of rejecting allogeneic grafts with minimal GVHD[209]. Due to the lack of the B2M molecule, the NSG-*B2M*^{null}*(IA IE)*^{null} mice cannot maintain IgG antibody at expected levels within the peripheral blood. This is due to the requirement for the neonatal Fc receptor to maintain IgG levels within the blood, and expression of the neonatal Fc receptor is dependent upon B2M[210]. This issue does not arise with the NSG-*B2M*^{null}*(IA IE)*^{null} variant, however.

For Hu-SRC model there have been several recent developments, including the development of an NSG strain expressing human HLA DR1 or HLA DR4 molecules, potentially allowing for a more physiologically relevant T cell education within the mouse thymus, with the aim of improving the overall T cell response in the Hu-SRC model. Additionally, a variety of transgenic strains expressing human cytokines have been developed to promote better differentiation of specific myeloid or lymphocyte populations. To promote myeloid cell and macrophage development, NOG mice expressing GM-CSF and IL3 were developed[211], along with NSG-SGM3 mice which showed increased engraftment of both myeloid and Treg populations[212], while IL-15 expressing transgenic mice are able to improve the development of NK cells[213,214].

1.4.5 Assessment of immunogenicity using humanised mice

Humanised mice can be used to assess the degree of alloimmune or autoimmune response to human cellular or tissue grafts. This assessment can be made through several methods, one of the most common being the histological examination of the graft area for signs of graft damage and lymphocytic infiltration[215,216], often accompanied by a quantitative assessment of the degree of lymphocyte infiltration between different experimental groups[206,217]. In instances where the graft expresses factors or causes physiological effects that can be detected or measured in the serum of peripheral blood, such as blood sugar levels for islet transplantation in diabetic mice, this is a common method of assessing graft survival and function in live mice[215,218]. In instances where such functional readouts are not

available, it is becoming increasingly common to track the survival of grafts *in vivo* using some form of live imaging, often bioluminescent imaging (BLI)[175,219-221]. This requires the generation of graft cells expressing the gene luciferase, typically firefly luciferase. Luciferase constructs can be introduced into the cells in a variety of ways, such as electroporation, lipofection and viral transduction, although primary-derived cells typically require transduction with lentiviral vectors for efficient construct integration[222]. The luciferase enzyme, when exposed to its substrate, luciferin, catalyses a reaction resulting in the emission of visible light. When small animals transplanted with cells containing a luciferase construct are given an intraperitoneal injection of 100-200 µl of luciferin, typically at a concentration of 20-50µg/ml, the graft cells emit light that can be detected through the skin and muscle using a bioluminescent *in vivo* imager. The light signal can be detected qualitatively, to produce an image showing the graft location within the animal's body, and also quantitatively, to give a measurement of photon intensity in a selected region of interest, making this technique useful for tracking graft survival in humanised mouse models.

1.5 Aims and objectives

The overarching aim of this dissertation was to explore the immunogenicity of cholangiocyte organoids, with the view towards eventual clinical translation. I aimed to assess the extent to which COs would be rejected within a transplantation setting to determine the necessity of ameliorative measures such as immunosuppression, HLA matching or HLA knock-out. I then aimed to explore the viability of using HLA matching to reduce the immunogenicity of COs in an alloimmune setting. To characterise the immunogenicity of COs I relied on a combination of *in vitro* and *in vivo* assessment of antigenicity and humanised mouse models.

Chapter 3: Characterisation and refinement of cholangiocyte organoid culture systems

The overall aims of the experiments presented in this chapter were to demonstrate the efficacy of the CO system for interrogating questions of cholangiocyte cellular therapy immunogenicity, to refine the system to improve its suitability for generating cellular therapies and to develop CO lines capable of real-time *in vivo* monitoring. Specifically, the objectives of this chapter were to:

- Characterise the CO system previously developed by our lab and assess its suitability for humanised mouse studies
- Refine the CO system to allow for generation of CO lines from intrahepatic tissue- to expand the available pool of donors for CO lines and to allow sampling of biliary tissue from patients with intrahepatic biliary conditions
- Improve method for generating bioengineered biliary tissue to advance the translation of CO therapies closer towards clinical application- this will also allow for assessment of more physiologically relevant graft structures in humanised mice
- Generate CO lines expressing luciferase to allow for tracking of CO grafts *in vivo* and quantitative assessment of graft rejection in humanised mice

Chapter 4: Assessment of the antigenicity of cholangiocyte cellular therapies

The aim of this chapter was to characterise the expression of immunogenic markers on COs, specifically the expression of HLA class I and II molecules. I aimed to assess how HLA expression changed in response to the move from primary cholangiocytes to cultured organoids and the extent to which these changes could be reversed by pro-inflammatory stimulation, with the understanding that HLA expression would affect CO immunogenicity in an allogeneic transplant setting. To this end, I also aimed to characterise CO upregulation of HLA, particularly HLA class II, in a series of physiologically relevant models of pro-inflammatory environments, both *in vivo* and *in vitro*. This information would also help us to assess the necessity for either full or partial HLA-matching for CO cellular therapies.

- Assess the expression of HLA molecules on COs compared to primary cholangiocytes
- Assess the expression of HLA molecules on COs after exposure to IFN-γ
- Assess the expression of HLA molecules on COs in a range of physiologically relevant pro-inflammatory environments through co-culture with activated lymphocytes and transplant into immunocompetent or humanised mice

Chapter 5: Assessment of the immunogenicity of cholangiocyte cellular therapies

In this chapter I aimed to establish two complementary humanised mouse models, a model of splenocyte (SpMC) reconstitution and one of haematopoietic stem cell (HSC) reconstitution. I assessed the immune response of these two models to allogeneic and autologous CO grafts and established a system of bioluminescent imaging (BLI) in live mice to monitor and quantify the rejection of CO grafts. I also aimed to compare the immunogenicity of HLA matched and HLA mismatched CO grafts using a humanised mouse model. The specific aims of this chapter were to:

- Establish the SpMC-reconstituted and HSC-reconstituted humanised mouse models
- Assess the capacity of SpMC-reconstituted and HSC-reconstituted humanised mice to reject allogeneic CO grafts
- Compare the immune response to allogeneic and autologous CO grafts in humanised mice
- Compare the immunogenicity of HLA-matched and HLA-mismatched allogeneic CO grafts in an HSC-reconstituted humanised mouse model

CHAPTER 2. METHODS

2.1 Cell culture methods

2.1.1 Cholangiocyte organoid culture

Isolation of primary cells

All primary cells and tissues (biliary tissue, liver biopsies, splenocytes, blood and bone marrow) were isolated from deceased organ donors within Addenbrooke's Hospital and obtained with full ethical approval (Ethical approval reference number: 15/EE/0152) or from human pancreases retrieved for transplantation but subsequently declined (ethical approval reference number: 12/EE/0253 and 16/EE/00227- since 29/07/2016). Tissue from both donation after circulatory death (DCD) and donation after brainstem death (DBD) donors were used, although peripheral blood could only be taken from DBD donors. All samples were processed in a type 2 laminar flow cabinet in an appropriate category two tissue culture facility using sterile instruments.

2.1.1.1 Isolation of cholangiocytes from extrahepatic biliary tissue

Cholangiocytes were isolated from the common bile duct or gallbladder of deceased organ donors. The biliary tissue was excised from either DBD or DCD deceased donors by a transplant surgeon after the retrieval of organs for transplantation, and transferred to a sterile 50 ml centrifuge tube containing University of Wisconsin (UW) cold storage solution. Alternatively, bile duct tissue was isolated from declined pancreases unsuitable for transplant that had been accepted for research. The tissue was kept at 4 °C until it could be transferred to the category 2 facility within the Laboratory of Regenerative Medicine for processing. Processing of tissue occurred as soon after excision as possible, with a maximum cold storage time of approximately ten hours.

All tissue processing took place in a category 2 biosafety cabinet within a category 2 tissue culture facility. The bile duct or gallbladder was incised longitudinally in a 10 cm petri dish filled with William's E+ medium. The tissue was washed gently three times in 50 ml centrifuge tubes of sterile PBS to remove any bile. The tissue was returned to the 10 cm petri dish and the lumen was carefully scraped using a sterile scalpel to remove the epithelial cells. The tissue was washed repeatedly with William's E+ during this process until it was judged that as many cells as possible had been transferred into the media. The presence of biliary cells was confirmed using an Olympus CKX41 microscope. The cell suspension was then transferred into a 50 ml centrifuge tube and centrifuged at 444 g for 4 minutes at room temperature. The pellet was then washed in 10 ml of William's E+ medium and any fibrous tissue removed using a p1000 pipette before a further centrifugation step. If the cell suspension

contained a high number of erythrocytes, an additional red blood cell lysis step was included. The pellet was resuspended in 10 ml of ice-cold red blood cell lysis buffer and incubated at 4 ℃ for 10 minutes. The cells were then centrifuged for 4 minutes at 444 g and resuspended in 5 ml of William's E+ to wash. The cell suspension was centrifuged at 444 g for 4 minutes and the cholangiocytes were plated in 50 µl droplets in the method described in Section 2.1.6.

2.1.1.2 Isolation of cholangiocytes from intrahepatic biliary tissue

Intrahepatic cholangiocytes were isolated from liver tissue from deceased organ donors. A fine needle biopsy of liver tissue was taken from either DBD or DCD deceased donors by a transplant surgeon after the retrieval of organs for transplantation, and transferred to a sterile 15 ml centrifuge tube containing William's E+. The tissue was kept at 4 °C until it could be transferred to the category 2 facility within the Laboratory of Regenerative Medicine for processing. Processing occurred as soon after excision as possible, with a maximum cold storage time of six hours.

All tissue processing took place in a category 2 biosafety cabinet within a category 2 tissue culture facility. The biopsy was transferred to a sterile, dry 10 cm tissue culture dish using sterile forceps. The tissue was dissected into as small pieces as possible (<1 mm^3) using a sterile scalpel. The tissue was then washed with 1 ml of William's E+ media with 50 ng/ml of EGF and 10 µM (1 µl/ml) of Y27632 and collected using a p1000 pipette. The tissue pieces were transferred to a 15 ml centrifuge tube and centrifuged at 200g for 3 minutes. The media was removed using a p1000 pipette and the tissue was washed with 1 ml of William's E+ media with 50 ng/ml of EGF and 10 µM (1 µl/ml) of Y27632 and centrifuged for a further 3 minutes at 200g. The tissue pieces were then plated in 50 µl droplets in the method described in Section 2.1.1.3.

2.1.1.3 Plating of primary-derived cholangiocyte organoids

Before plating of COs, the required number of 24-well tissue culture plates were pre-heated at 37 °C for at least one hour prior to plating- ideally overnight whenever possible. Matrigel was thawed on ice for two hours to overnight prior to starting the plating procedure. The CO pellet (or pellet of primary cholangiocytes/primary liver pieces) was resuspended in William's E+ medium supplemented with EGF, R-spondin-1, Dickkopf-related protein 1 (DKK-1) and Y27632 at triple the concentration required for organoid maintenance. This was done to ensure that the concentration of cytokines was correct after the addition of Matrigel. The pellet was resuspended in a volume of this 3X William's E+ medium appropriate for the number of wells being plated. For example, if plating 9 wells, the pellet was resuspended in 150 µl of William's E+ media with 1.5 µg/ml R-spondin, 150 ng/ml EGF, 30 µM (3 µl/ml) Y27632 and 300 ng/ml DKK-1.

The thawed Matrigel stock was mixed thoroughly with a p1000 pipette. The Matrigel was kept on ice throughout the entire procedure and was mixed with care to avoid bubbles. Matrigel was added to the cell suspension in a 2:1 ratio (66.7% vol/vol) and mixed well. A pre-warmed 24 well cell culture plate was transferred to the plate heater and the organoids were plated in 50 µl Matrigel/media domes using a p1000 pipette, each in a well of the 24 well plate. The cell suspension was mixed thoroughly before plating each dome, to ensure equal distribution of cells between each dome. The Matrigel domes were allowed to solidify for 1-2 minutes in the plate heater. Once the domes were confirmed to have solidified, the plate was gently inverted and kept in the 37 °C incubator for 30 minutes. This step was required to ensure the cell clumps did not attach to the bottom of the plate and was omitted when plating dissected liver tissue or EpCAM+ sorted single cells. The 3X William's E+ media solution was made up to a final concentration of 500 ng/ml Rspondin, 50 ng/ml EGF, 10 µM (1 µl/ml) Y27632 and 100 ng/ml DKK-1 (+/- 50 ng/ml HGF) and 1 ml of this supplemented media was added per organoid dome using a 5 ml or 10 ml pipette. Media was added slowly to avoid disrupting the Matrigel domes. The organoids were then cultured at 37 °C in a cell culture incubator.

2.1.1.4 Maintenance of primary-derived cholangiocyte organoids

Media for the COs was changed approximately every 48 hours. William's E+ medium supplemented with 500 ng/ml Rspondin, 50 ng/ml EGF and 100 ng/ml DKK-1 was used for organoid maintenance and 1 ml was added to each well of a 24 well plate. In cases of slow-growing or suboptimal CO lines, 2 µM of FSK was added to the maintenance media. COs were passaged approximately every 5 days. Visual inspection of organoids was used to determine when plates were ready for passage, as premature passage could lead to a suboptimal number of cells while a delay in passaging could lead to the collapse of larger organoids, potentially causing permanent damage to the CO culture.

2.1.1.5. Passaging of cholangiocyte organoids

Media was aspirated and 500 µl of cell recovery solution was added to each well. The pipette was aimed at the centre of the Matrigel dome and the cell recovery solution was ejected forcefully to disrupt the surface of the dome. The Matrigel domes were then mechanically dissociated by scraping with a p1000 pipette. The cells were transferred from each well to a 15 ml centrifuge tube after dissociation. Each well was then washed with 500 µl of cell recovery solution- the same 500 µl was carried across to each of the wells to minimize the volume of cell recovery solution required for the washes. This final 500 µl was then added to the centrifuge tube. The cells were incubated on ice at 4 °C for 30 minutes to fully dissolve the Matrigel and then centrifuged at 444 g for 4 minutes at room temperature. The supernatant was aspirated and the cells were washed in 1 -7 ml of William's E+ medium, depending on the size of

the pellet. If necessary, the cell suspension was divided at this stage, typically into 4-6 15 ml centrifuge tubes and the organoids were plated as described in section 2.1.1.3.

2.1.1.6 Cryopreservation and thawing

COs were cryopreserved after removal from organoid culture as described in section 2.1.1.5. The resulting organoid pellet was washed once in 1 ml of William's E+ medium and then centrifuged at 444g for 4 minutes. The pellet was resuspended in 1-6 ml of CellBanker2 depending on the size of the pellet. The CO suspension was transferred to 2 ml cryovials at 1 ml per cryovial and the cryovials were frozen immediately at -80°C. For long-term cryopreservation, COs were transferred to a liquid nitrogen tank.

When thawing COs, cryovials were removed from the liquid nitrogen tank/-80 °C freezer and transferred immediately to dry ice to prevent uncontrolled thawing. CO cryovials were thawed in a 37 °C water bath and the cells transferred immediately to pre-warmed WE+ medium supplemented with 10 µM Y27632 and centrifuged at 444 g for 4 minutes. Thawed cells were washed once in 5 ml of pre-warmed William's E+ medium and then plated as described in section 2.1.1.3.

2.1.2 LX2 cell culture

LX2 cells were cultured in 25 cm^2 (T25) uncoated tissue culture flasks with 4ml of LX2 medium (see the lists of media in appendix table 1). LX2 medium was changed every 48 hours. The cells were passaged when the flask reached confluency, approximately every five days. The medium was aspirated and the cells were washed in PBS. The PBS was aspirated and 500 µl of trypsin-EDTA (0.05%) was added. The cells were incubated at 37°C for approximately 5 minutes, until the cells had lifted from the flask surface. The cells were collected in a 15 ml centrifuge tube and washed with 4 ml of LX2 medium. The cells were centrifuged for five minutes at 300g and the medium was aspirated. The pellet was resuspended in 1 ml of LX2 medium and approximately 100 µl of the cell suspension was added to a fresh T25 flask containing 4 ml of LX2 medium.

2.1.3 PBMC/SpMC culture

2.1.3.1 Isolation of mononuclear cells from primary spleen tissue

Original method (2015-2016)

5 cm^3 spleen sections were obtained from deceased organ donors and transferred to University of Wisconsin (UW) organ preservation solution before processing. The spleen was stored at 4 °C for up to 24 hours before processing. The tissue was mechanically dissociated using a 100 µm steel sieve and

washed with Dulbecco's Modified Eagle Medium (DMEM) (Gibco Life Technologies) and 10% foetal calf serum (FCS) (Sigma Life Sciences). After dissociation the cells were filtered through a 70 µm filter into a 50 ml centrifuge tube. 50 ml Centrifuge tubes were prepared with 17 ml of Lymphoprep™ gradient (StemCell Technologies) and 20 ml of the cell suspension was layered on top in each tube. The tubes were then centrifuged at 300 g for 20 minutes with the centrifuge brake off. The mononuclear cell fraction was isolated and washed in DMEM + 10% FCS. After centrifugation at 300 g for 20 minutes with the centrifuge brake on, the cells were resuspended in 10 ml of DMEM+10% FCS and counted using a haemocytometer. After a second similar centrifugation step, the cells were cryopreserved in FCS + 10% DMSO at a concentration of approximately 1.0 x 10^8 cells/ml and placed in a Mr. Frosty™ Freezing Container (ThermoFischer Scientific) for 24h before being transferred for long-term storage in a liquid nitrogen Dewar (at -196 °C).

Updated method (2017 onwards)

5 cm^3 spleen sections were obtained from deceased organ donors and transferred to University of Wisconsin (UW) organ preservation solution before processing. The spleen was stored at 4 °C for up to 24 hours before processing. Spleen tissue was cut into small pieces (approximately 5mm^3) with a scalpel on a sterile, dry 10 cm tissue culture dish. A gentleMACS™ dissociator (Miltenyi Biotec) was used to dissociate the tissue to a single cell suspension. Spleen tissue was placed into gentleMACS™ "C" Tubes with PBS + 2% FCS and dissociated using a pre-set programme B-0. The resulting cell suspension was filtered through a 70 µm cell strainer to remove any fibrous debris and diluted at a 1:1 ratio with PBS + 2% FCS. Lymphoprep™ was used to isolate the lymphocytes from the cell suspension. 50 ml centrifuge tubes were prepared with 15 ml room-temperature Lymphoprep™ in each tube and 20 ml of the filtered suspension was carefully layered on top. Tubes were centrifuged at 800 g for 25 min at 20 °C with no brake. The mononuclear cell layer was collected from each tube using a Pasteur pipette and the mononuclear cell fraction from all tubes were combined into one 50 ml centrifuge tube. The tube was topped up to 50 ml with PBS + 2% FCS and centrifuged at 300 g for 7 minutes with the break on. The supernatant was aspirated and the pellet was resuspended in 10 ml of Red Blood Cell Lysis (RBCL) 1x buffer for 10 minutes at 4°C. Cells were then washed and counted using an automated cell counter. Based on the cell count, the appropriate volume of cryopreservation medium to resuspend the pellet in to obtain a concentration of 5.0 x 10^7 cells/ml was calculated. The cell suspension was centrifuged at 300 g for 7 minutes and then resuspended in the appropriate volume of cryopreservation media (FCS + 10% DMSO). The cell suspension was aliquoted into pre-labelled cryovials (1 ml per cryovial) and the cryovials were placed into a pre-cooled Nalgene Mr. Frosty™ freezing container. The Mr. Frosty™ container was stored at -80°C for a minimum of 24 hours (a maximum of seven days) before the cryovials were transferred to a liquid nitrogen dewar for long-term storage.

2.1.3.2 Isolation of PBMCs from primary peripheral blood

Peripheral blood was collected in heparinised 50 ml syringes from DBD donors during surgery with the assistance of the anaesthetist. The peripheral blood was then stored at room temperature on a benchtop orbital shaker at 150 rpm for up to 12 hours before processing. The peripheral blood was filtered through a 70 µm cell strainer and diluted in a 1:1 ratio with PBS + 2% FCS. Mononuclear cells were then isolated using Lymphoprep^{TM}, processed and cryopreserved as described in section 2.1.3.1.

2.1.3.3 Isolation of mononuclear cells from primary bone marrow

Bone marrow was collected using a Jamshidi needle from the vertebral bodies of DBD or DCD donors and transferred into heparinised 50 ml syringes. The bone marrow was stored at room temperature on a benchtop orbital shaker at 150 rpm for up to 12 hours before processing. Bone marrow was filtered through a 70 µm filter and then diluted in a 6:1 ratio with PBS + 2% FCS (6 parts bone marrow to 1 part PBS + 2% FCS). Mononuclear cells were then isolated using Lymphoprep^{TM}, processed and cryopreserved as described in section 2.1.3.1.

2.1.3.4 Thawing of mononuclear cells

Thawing media (50% DMEM and 50% FCS) was prepared in advance and warmed to 37 °C in a water bath. The required cryovial was removed from liquid nitrogen storage and kept on dry ice before being transferred to a 37 °C water bath. The cryovial was held in the water bath and monitored closely until almost all of the cell suspension had thawed. The vial was quickly transferred to a pre-prepared category 2 tissue culture cabinet. The cell suspension was gently added to a 15 ml centrifuge tube containing 10 ml of pre-warmed thawing media (if more than one cryovial was being thawed at a time, then each vial was added to a separate 15 ml centrifuge tube containing 10 ml of thawing media) and the tube was centrifuged at 300 g for 7 minutes. The supernatant was aspirated and the pellet resuspended by gently flicking. The cell suspension was washed in 5 ml of thawing media to remove any traces of DMSO and centrifuged at 300 g for 7 minutes. The pellet was then resuspended in 10 ml of DMEM + 10% FCS and 60 µg/ml DNase I. The cell suspension was incubated at 37 °C for 20 minutes, or until all clumping was gone. The cell suspension was centrifuged at 300 g for 7 minutes and resuspended in 10 ml of DMEM + 10% FCS (without DNase I). The cells were counted using an automated cell counter with trypan blue as a live/dead stain.

2.1.3.5 PBMC activation

PBMCs prepared as described in 2.1.3.4 and resuspended in an appropriate volume of complete RPMI media to give a concentration of 1.0 x 10^6 cells/ml. The cell suspension was aliquoted into wells of a 24 well plate at a volume of 100 µl (1.0 x 10^5 cells) per well. CD3/CD28 Dynabeads were resuspended

and the required volume (0.5 µl per 10^5 cells) was transferred to a 1.5 ml Eppendorf. The beads were washed in 1 ml of sterile PBS with 0.1% BSA and pelleted using a DynaMag-2 magnet. The PBS 0.1% BSA was removed and the beads were resuspended in a volume of RPMI equal to the initial volume removed from the Dynabead vial. 0.5 µl of beads were added to each well requiring activation and the plate was gently agitated to mix the beads with the cells. The plate was transferred to a humidified incubator with 5% CO_2 at 37 °C for 24 hours. The beads were removed from the cells using the DynaMag magnet 24 hours after activation and the cells were returned to the plate without changing the media.

2.2 Humanised mouse methods

2.2.1 Engraftment with HSCs

Irradiation of NSG mice

Female NSG mice between the ages of 5-6 weeks were exclusively used for the HSC-reconstitution humanised mouse model. The required cages of NSG mice were transferred to the irradiator room. The animals were transferred from their cage to the irradiator box in a category 2 biosafety cabinet. The time required to produce 2.5 Gy of irradiation was calculated and the animals were placed in the irradiator at the second shelf level. The door was shut and the required time was input into the irradiator. Irradiation was initiated and, when complete, the animals were removed from the irradiator and transferred back to their cage. They were returned to their usual location in the animal facility. The animals were reconstituted with SpMCs or CD3-depleted bone marrow no later than 24 hours after irradiation. Any animals that had been irradiated but could not be reconstituted (for example, due to a lack of available cells) were culled.

Thawing and CD3-depletion of cryopreserved bone marrow lymphocytes

Cells were thawed as described in section 2.1.3.4 and counted using an automated cell counter. The required volume of MACS beads and MACS buffer necessary for MACS cell sorting was calculated based on the cell number. Cells were resuspended in 80 µl of MACS buffer per 10^7 cells and 20 µl of MACS beads per 10^7 cells. The suspension was mixed well and incubated on ice for 15 minutes. During the incubation time, the MACS cell sorter was turned on and a column exchange was run to ensure a new, sterile set of columns was used. The storage buffer was exchanged for a new bottle of MACS running buffer. At the end of the 15 minute incubation, 10 ml of MACS buffer was added to the cell suspension to wash and the cells were centrifuged at 300g for 7 minutes. The supernatant was aspirated

and the cell suspension was resuspended in 5 ml of MACS buffer and transferred to a 15 ml centrifuge tube. The cell suspension was CD3-depleted using an AutoMACS cell sorter on the "depleteS" programme. The cells were counted using an automated cell counter and centrifuged at 300g for 7 minutes at room temperature. The cells were resuspended in an appropriate volume of sterile saline for a concentration of 1.0 x 10^7 cells per 100 µl.

Tail vein injection of CD3-depleted BM leukocytes

CD3-depleted bone marrow leukocytes were transported to the animal facility on ice. The controlled heating unit was cleaned, transferred to a category 2 biosafety cabinet and set to 37°C for two hours. The irradiated NSG mice were transferred to the heating unit while the rest of the equipment was prepared (minimum of ten minutes). Individual 1 ml syringes with 30G needles were prepared for each animal, to prevent contamination and needle damage from multiple usage. The cell suspension was mixed with a 1 ml syringe with a 30G needle to break up any cell clumps and then the required number of syringes were loaded with 100 µl of cell suspension each. All air bubbles were removed from the needles and syringes and the syringes were placed on a sterile surface in the biosafety cabinet. A supply of sterile tissues was prepared and the tail vein restraint was cleaned and set in the biosafety cabinet. The first mouse was transferred to the tail vein restraint and secured in place, with the tail hanging outside the restraint and held in place. The 100 µl of cell suspension was injected intravenously into the tail vein and the bleeding was stopped using a sterile tissue. The mouse was then transferred back to the cage and the process was repeated until all animals were injected.

2.2.2 Engraftment with PBMCs/SpMCs

IP injection of PBMCs/SpMCs

PBMCs/SpMCs were thawed and counted as described in section 2.1.3.4. The cells were centrifuged at 300g for 7 minutes and resuspended in a volume of RPMI media to give a concentration of 1.0 x 10^7 cells per 100 µl. The cells were transferred to a small universal tube and transported on ice to the animal facility. The required cage of mice were transferred to a category 2 biosafety cabinet. The mice were scruffed and injected with 100 µl of the cell suspension though an intraperitoneal injection. The mice were then returned to their cage.

2.2.3 Tail vein bleeds

The controlled heating unit was cleaned using Trigene and the Category 2 biosafety cabinet cleaned using Trigene and ethanol. The controlled heating unit was placed in the biosafety cabinet and turned

on- set to 37°C for two hours. The mice were transferred into the controlled heating unit from their cages and left for 10 minutes. Bleeding tubes were primed with heparin and the required number of 27G needles were opened and sterile tissues were prepared. The bleeding stand was cleaned with Trigene and placed in the biosafety cabinet. After the ten minutes incubation, mice were removed individually from the heating unit by their tail and placed in the bleeding stand with their tail hanging out of the tube. One of the two tail veins was located and briefly pierced with the needle. The needle was withdrawn and 2-6 drops of blood was collected using a heparinised bleeding tube. Sterile tissue was applied to the wound. The mouse was removed from the bleeding stand and pressure was maintained with the tissue until bleeding had stopped. The mouse was transferred back to the cage. The bleeding tube was capped and the blood mixed with the heparin.

2.2.4 Transplantation of cells under the kidney capsule

A cell suspension in 100% Matrigel was prepared as described in section 2.1.1.5 and transported to the animal facility on ice. The cages of mice for transplantation were transferred to the surgery room and the surgical space and equipment was prepared. The cell suspension was loaded into an autoclaved Hamilton syringe with a blunt 27 gauge needle and kept on ice, with a layer of autoclaved foil between the syringe and the ice to maintain sterility. The surgical technician anaesthetised the first mouse using isoflurane at a flow rate of 2% and shaved the area directly above the left kidney (if both kidneys were being transplanted then the area above the right kidney was also shaved). The shaved area was cleaned and the mouse was given a subcutaneous injection of Temgesic analgesic by the technician and transferred to the surgery room where it was placed on the heat mat.

The animal was turned onto its left side, with the kidney facing directly up, and secured to the isoflurane nose cone and the heat mat with surgical tape. The isoflurane was set to 2% and the oxygen flow rate was set to 2 L/minute. A 2 ml syringe was placed under the mouse to elevate the kidney and the mouse was covered in a sterile drape, leaving the left side exposed. The heat mat was set to 37 °C and the internal temperature of the animal was monitored using a rectal probe.

The magnification of the surgical microscope was set to 6x and the location of the kidney was identified through the skin. An incision was made in the skin directly above this area. The incision was made no larger than was judged to be necessary for the kidney to fit through, typically approximately 5 mm. The magnification was increased to 10x and a second incision was made in the muscle directly above the kidney, taking care to avoid nerves and blood vessels. If not immediately obvious, the kidney was located using a sterile cotton bud and then gently pushed out through the incision in the muscle and skin using a pincer movement with the thumbs and forefingers of both hands. Sterile saline was immediately applied to the kidney to prevent it drying.

The magnification of the surgical microscope was increased to 16x and a small incision was made in the side of the kidney using a 30G needle. This needle was then set aside. The syringe containing the cell suspension was taken from the ice box and the blunt Hamilton needle was inserted into the kidney through the incision made with the 30G needle. Once the end of the needle was at the kidney capsule, approximately 30 µl of the cell suspension was injected into the kidney- great care was taken to ensure the suspension was injected directly below the kidney capsule and not into the parenchyma, as this would risk causing a pulmonary embolism if the cell suspension entered the bloodstream. The needle was withdrawn and placed directly back on ice to prevent the Matrigel from solidifying. Simultaneously, a sterile cotton bud was placed onto the exit wound where the needle was withdrawn and pressure was applied to stop any bleeding. Once the bleeding had stopped, the kidney was placed back into the abdominal cavity using a sterile cotton bud.

The muscle was sutured using Novosyn 3/0 sutures with uninterrupted sutures (approximately 3 sutures, depending on the size of the incision). The skin was closed using interrupted sutures, typically three to five sutures depending on the size of the incision. Two skin clips were applied to the skin using an automated clip applicator and the surgical technician transferred the mouse to the recovery room. The animals were monitored by the technicians every ten minutes after the procedure for an hour, to ensure there were no health effects of the procedure or anaesthetic. The animals were then monitored and weighed daily for a week after the procedure and the skin clips were removed by the technicians seven days after the surgical procedure.

2.2.5 Non-recovery removal of organs/tissue under general anaesthetic

The surgical bench area was prepared as if for a normal surgical procedure (see section 2.2.4). Animals were anaesthetised by the surgical technician using isoflurane at flow rate 2.5% and the abdomen was shaved. The animal was placed on its back on the heat mat by the surgical technician and secured to the nose cone using surgical tape. A laparotomy was performed and the abdomen was opened using an Alm self-retaining retractor. The surgical microscope was set to 16x magnification and the organs were gently moved using a sterile cotton bud until the inferior vena cava (IVC) was located. A 1 ml syringe with a 27G needle was inserted into the IVC and as much blood as possible was taken, typically between 800-1000 µl, depending on the size of the mouse. This blood was then shared between one heparinised and one non-heparinised Eppendorf tubes- for flow cytometry and serum samples, respectively. The kidneys, spleen and any other required organs were carefully excised using fine surgical scissors and transferred to individual labelled universal tubes filled with Hank's balanced salt solution (HBSS) for further processing later. If required for the experiment, the femurs were also removed and transferred to individual labelled universal tubes filled with HBSS for further processing later.

2.2.6 Bioluminescent live imaging of transplanted mice

Luciferin was reconstituted with sterile deionised water at a concentration of 20 mg/ml and aliquoted into 1 ml aliquots and stored at -20°C until required.

The animals were transferred to the imaging room and the IVIS imager was initialised using the Living Image programme. The IVIS imager stage area was cleaned using ethanol wipes and the anaesthetic box was cleaned using Trigene. The waste scavenger, oxygen and anaesthetic systems were set up and the oxygen flow rate (pre-set to 2 L/min) was checked.

The nose cones and dividers were cleaned using ethanol and set up in the IVIS imager. 1 ml syringes with 30G needles were set up with the required amount of luciferin for the number of mice to be injected- no more than three mice were injected with the same syringe in order to reduce the risk of damage to the needle from reuse. Each mouse was injected intraperitoneally with 150 µl of luciferin and transferred immediately to the anaesthetic chamber. In instances where more than one cage of mice required imaging, each cage was injected and imaged separately.

A timer was set for ten minutes and the anaesthetic flow rate was set to 2%. Once the animals were anaesthetised they were transferred to the anaesthetic nose cones in the IVIS imager and placed with their left side facing upwards, making note of the order of the animals by ear notch in cases where repeat imaging at another time was required. During the ten minute wait, the Living Image programme was set up with the required imaging sequence. Typically, one image was taken using the automatic exposure setting and then a series of images were taken at defined exposure times according to the requirements of the specific experiment (e.g. 120 seconds, 60 seconds and 30 seconds). The use of an automatic exposure time allowed high-quality images to be taken, while setting pre-set exposure times allowed images to be comparable across multiple animals and imaging sessions, a requirement of quantification. Once the ten minute waiting step was finished, the imager was initialised and the series of images obtained. Once this was completed, the animals were immediately transferred back to their cages and the anaesthetic flow turned off.

2.3 In vitro characterisation methods

2.3.1 RNA isolation and qPCR

2.3.1.1 Extraction of RNA from cultured cells

Cells were lysed using 250 µl of RNA lysis buffer (Sigma) and snap-frozen in dry ice. Samples were stored at -80°C until use. RNA extraction was performed with a Sigma GenElute™ Mammalian Total

RNA Miniprep Kit and the yield of RNA was measured by measuring 1.0 µl of the RNA extract on a Nanodrop spectrophotometer.

2.3.1.2 Reverse Transcription of RNA samples

The volume of RNA solution containing 500 ng of RNA was calculated and mixed nuclease-free water to a total volume of 11.8 µl. This was added to a 1.5 ml Eppendorf along with 0.5µl of Random Primer (Promega, C1181) and 1.0 µl of dNTP mix (Promega, U1511). The tube was briefly centrifuged and incubated at 65°C for five minutes and then snap cooled on ice. A master mix was made up for the reverse transcription reaction, the volumes for one RNA sample were: 4.0 µl of 5x 1st strand buffer (Invitrogen), 2.0 µl DTT (Invitrogen), 0.5 µl of RNase OUT (Invitrogen) and 0.2 µl of Superscript II (Invitrogen 18064071). 6.625 µl of this master mix was added per sample and the tube was briefly centrifuged. The tube was incubated at room temperature for 10 minutes, then at 42°C for 50 minutes and finally at 70°C for 15 minutes. At the end of the reaction, 580 µl of nuclease free water was added to make the cDNA solution to a final volume of 600 µl and then stored in the -80°C freezer.

2.3.1.3 Quantitative PCR

Reagents were thawed on ice and a master mix was made up for each primer pair. HydroxyMethylBilane Synthase (HMBS) was used as the housekeeping gene and run on every plate to allow for normalisation between plates. The volumes of each reagent per reaction were: 7.5 µl Sensi mix (Bioline); 0.6 µl forward primer; 0.6 µl reverse primer and 1.3 µl nuclease free water. Master mixes were kept on ice. 10 µl of each primer master mix was pippetted into a 96 well non-skirted PCR plate and then 5 µl of the appropriate cDNA samples were added, changing pipette tip between each well to avoid cross-contamination. The plate was briefly centrifuged and then run on the Stratagene Mx-3005P (Agilent) with the following programme: first cycle at 95°C for 10 minutes, 40 cycles of 95°C for 30 seconds, 60°C for 30 seconds and 72°C for 30 seconds and then one cycle at 95°C for one minute. All primers were generated by Sigma and are listed in appendix table 2.

2.3.2 Immunofluorescence

2.3.2.1 Immunofluorescence of cholangiocyte organoids

William's E+ culture medium was aspirated and 1 ml of 4 % PFA (vol/vol) was added per well. PFA was added gently to the side of the well to not disrupt the Matrigel dome and the plate was incubated at 4 °C for 20 minutes to fix the cells. The PFA was aspirated with a p1000 pipette to avoid disruption to

the Matrigel dome and each well was washed twice for ten minutes per wash using PBS. If required, the plate was sealed and kept at 4 °C for up to four weeks until ready for immunofluorescence staining.

A solution of 10% (vol/vol) donkey serum and 0.1% (vol/vol) TritonX-100 in PBS was prepared and 1 ml of this solution was added to each organoid well. The plate was incubated at room temperature for one hour to block and permeabilise the COs. The primary antibodies were diluted in a solution of 1% (vol/vol) donkey serum and 0.1% (vol/vol) TritonX-100 in PBS (see appendix table 4 for the dilutions of all antibodies used). 500 µl of primary antibody solution was added per CO well and the COs were stained overnight at 4 °C. The COs were washed three times with 1% donkey serum and 0.1% TritonX-100 in PBS. Each wash was 45 minutes. The secondary antibodies were diluted in a solution of 1% (vol/vol) donkey serum and 0.1% (vol/vol) TritonX-100 in PBS (see appendix table 4 for dilutions). 500 µl of secondary antibody solution was added per CO well and the organoids were stained overnight at 4 °C. CO plates were wrapped in foil to prevent exposure of the secondary antibody to light. Hoechst 33258 was diluted 1:10,000 (vol/vol) in PBS, the secondary antibody solution was aspirated from the CO wells and 1 ml of the Hoecscht 33258 solution was added per well. COs were incubated in this Hoecscht 33258 solution for 10 minutes at room temperature. The organoids were then washed three times in PBS, each wash for 45 minutes at room temperature. A final 1 ml of PBS was added per CO well. The COs were either imaged immediately or the plate was sealed, wrapped in foil and stored at 4 °C (for no more than three months) until ready for analysis.

2.3.2.2 Immunofluorescence of OCT-embedded cryosections

Cryosection slides were thawed and during thawing, a barrier pen was used to draw a square around each cryosection (typically two or three sections per slide). Approximately 100 µl of 4% paraformaldehyde was added to each section and the slides were incubated at 4°C for 20 minutes. The slides were transferred back to room temperature and washed twice for five minutes per wash using PBS. The sections were blocked for 30 minutes at room temperature using PBS + 0.1% Triton X + 10% donkey serum. The primary antibodies were diluted in a solution of 1% (vol/vol) donkey serum and 0.1% (vol/vol) TritonX-100 in PBS (see appendix table 4 for the dilutions of all antibodies used). 200 µl of primary antibody solution was added per section and the slides were stained overnight at 4 °C. The sections were returned to room temperature and washed three times with 1% donkey serum and 0.1% TritonX-100 in PBS. Each wash was 5 minutes. The secondary antibodies were diluted in a solution of 1% (vol/vol) donkey serum and 0.1% (vol/vol) TritonX-100 in PBS (see appendix table 4 for dilutions). 200 µl of secondary antibody solution was added per section and the sections were stained for one hour at room temperature. Hoechst 33258 was diluted 1:10,000 (vol/vol) in PBS, the secondary antibody solution was discarded and 200 µl of the Hoecscht 33258 solution was added per section. Sections were incubated in this Hoecscht 33258 solution for 5 minutes at room temperature. Three five

minute washes with PBS were then performed. The PBS was discarded and one drop of Fluoromount G mounting solution was added per section. The slides were carefully mounted with a coverslip, making sure there were no air bubbles on or near the tissue.

2.3.2.3 Imaging and analysis

Imaging was performed using a Zeiss LSM 700 confocal microscope. ImageJ 1.51h software (Wayne Rasband, NIHR, USA, http://Imagej.nih.gov/ij) was used for image processing such as merging of different channels, addition of scale bars and analysis such as lymphocyte counting.

2.3.3 Flow cytometry

2.3.3.1 Flow cytometry of cholangiocyte organoids

COs were removed from organoid culture as described in section 2.1.1.5. The pellet was resuspended in 1 ml of William's E+ media and centrifuged at 444g for 4 minutes. A solution of Accutase (pre-warmed to 37 °C) with 4 mg/ml of DNase I and 10 μM Y27632 was prepared. Addition of DNase I was necessary to prevent cell clumping and Y27632 was important to reduce cell death during dissociation. The supernatant was aspirated and the pellet was resuspend in 1 ml of the Accutase solution. The cells were incubated at 37 °C for up to five minutes to produce a single-cell suspension. The cells were inspected under a microscope halfway through to check the progress of the dissociation and once a single-cell suspension had been obtained, 1 ml of William's E+ media or PBS 1% BSA (wt/vol) with 4 mg/ml of DNase I and 10 μM Y27632 was added to the cell suspension with a p1000 pipette. The single cell suspension was centrifuged at 444 g for 4 minutes at room temperature and the pellet was resuspended in 1 ml of William's E+ media or PBS 1% BSA (wt/vol) with 4 mg/ml of DNase I and 10 μM Y27632. The cells were filtered through a 40 μm filter.

2.3.3.2 Staining for cell-surface markers

A 1 in 20 dilution of FcR block in PBS 1% BSA was prepared. The cells were centrifuged at 444 g for 4 minutes at room temperature and resuspended in 200 μl ml of diluted FcR block. The cells were incubated at room temperature for 30 minutes. A master mix of all conjugated antibodies was prepared in PBS 1% BSA (see appendix table 4 for antibody dilutions). An aliquot of the cell suspension (typically at least 1 x 10^5 cells) was set aside as an unstained control. The cells were centrifuged at 444 g for 4 minutes at room temperature and the pellet was resuspended in 200 μl of master mix solution and incubated at 4 °C for half an hour. The cells were washed three times in PBS 1% BSA (5 minutes per wash) and filtered through a 40 μm filter into a FACS tube before analysis.

2.3.3.3 Staining for intracellular markers

The cells were centrifuged at 444 g for 4 minutes at room temperature and the pellet resuspended in 1 ml of 4% PFA. The cells were incubated at 4 °C for 15 minutes to fix and then 1 ml of PBS 1% BSA was added to wash. The cells were centrifuged at 444 g for 4 minutes at room temperature and gently resuspended in 1 ml of PBS 1% BSA. This wash step was repeated three times, with each wash lasting 5 minutes. A 1 in 20 dilution of FcR block in PBS 1% BSA + 0.1% Triton X was prepared. The cells were centrifuged at 444 g for 4 minutes at room temperature and resuspended in 200 µl ml of diluted FcR block. The cells were incubated at room temperature for 30 minutes. After the blocking step, a small aliquot of cells was set aside as a secondary-only control and another as an unstained control. The cells were centrifuged at 444 g for 4 minutes at room temperature. A solution of primary antibodies was prepared in PBS 1% BSA + 0.1% Triton X and the cells were resuspended in 200 µl of primary antibody solution and incubated at room temperature for one hour. The cells were washed three times in PBS 1% BSA +0.1% Triton X (5 minutes per wash). A solution of secondary antibodies was prepared in PBS 1% BSA +0.1% Triton X and the cells (and secondary-only control) were resuspended in 200 µl of secondary antibody solution. The cells were incubated at room temperature for an hour and were kept in the dark to prevent exposure of the secondary antibody to light. The cells were washed three times in PBS 1% BSA +0.1% Triton X (5 minutes per wash) and then resuspended in 200 µl of PBS 1% BSA (wt/vol) and filtered through a 40 µm filter before analysing the sample on the flow cytometer. All flow cytometric analyses were performed on a FACS Cyan flow cytometer and analysed using FlowJo version 10.4.2.

2.3.4 GGT assay

GGT assays were performed using a MaxDiscovery gamma-Glutamyl Transferase (GGT) Enzymatic Assay Kit according to the manufacturer's instructions.

2.3.5 ALP assay

Alkaline phosphatase staining was carried out on 4% PFA-fixed CO wells using the BCIP/NBT color development substrate (5-bromo-4-chloro-3-indolyl-phosphate/nitro blue tetrazolium, Promega) according to the manufacturer's instructions.

2.3.6 ELISA

ELISAs for IFN-γ were performed using a Thermo Fisher IFN gamma Human Uncoated ELISA Kit and Thermo Fisher uncoated ELISA 96 well plates, according to the manufacturer's instructions.

2.4 Analysis of *in vivo* samples

2.4.1 Histology

2.4.1.1 Preparation of OCT-embedded samples

The tissue was washed in PBS and an OCT mould was filled with OCT solution. The tissue was gently placed in the mould using forceps and arranged in the desired orientation. The OCT mould was gently placed in a large box of dry ice until fully frozen and then transferred to -80°C storage until required. OCT tissue blocks were sectioned using a Bright OTF5000 cryostat. The tissue was sectioned at a thickness of 7.5 μm and collected onto Sigma PolyPrep slides.

2.4.1.2 Preparation of paraffin-embedded samples

The tissue was washed in PBS and then placed into a universal tube containing 10% formalin. The sample was fixed overnight at room temperature on a rocker and then washed twice in PBS for five minutes per wash. The tissue was then transferred to a solution of 80% ethanol and 20% deionised water and stored at 4°C for up to one week. An automatic tissue processor was used to prepare the sample for embedding in paraffin. The paraffin blocks were left at 4°C overnight before being transferred to room temperature storage. Paraffin-embedded samples were sectioned using a Leica RM2255 microtome. The tissue was sectioned at a thickness of 5 μm and collected onto VWR SuperFrost Plus slides.

2.4.1.3 IF staining of cryosections

When staining cryosections, unfixed slides were taken from -80 storage and the sections were outlined with a barrier pen while the slides were thawing. Immediately after thawing, 100-200 μl of 4% PFA was added to each section and the slides were incubated at 4°C for 20 minutes to fix the tissue. The slides were returned to room temperature and two five minute washes were performed with PBS. The slides were then stained as described in section 3.2.2.1, with each section receiving 200 μl of antibody master mix during staining. The slides were incubated overnight in a Sigma Aldrich StainTray to prevent drying. After staining, 1 drop of Fluoromount G mounting medium was added per section and the slides were mounted with a coverslip and stored at 4°C in the dark until required for imaging.

2.4.1.4 IF staining of paraffin-embedded sections

Paraffin-embedded sections were deparaffinised through a series of 5 minutes washes: 2 washes with xylene, 2 with 100% ethanol, 2 with 90% ethanol, 2 with 80% ethanol, 2 with 70% ethanol and 2 with 50% ethanol. The slides were then incubated in a beaker of citrate buffer and boiled for 15 - 20 minutes in a water bath. The beaker was removed from the water bath and left for ten minutes to cool at room

temperature. The slides were then transferred to room temperature PBS and then stained for immunofluorescence analysis as described in section 2.4.1.3, without any further fixation or wash steps.

2.4.2 Preparation of murine spleen/bone marrow/peripheral blood samples for flow cytometry

2.4.2.1 Preparation of murine spleen samples

Murine spleen samples were dissociated by filtering through a 40 µm filter into a 50 ml centrifuge tube and the filter washed multiple times with RPMI medium to collect as many cells as possible. The cells were centrifuged at 300g for 7 minutes at room temperature and the supernatant discarded. The pellet was resuspended in 1 ml of cold red cell lysis buffer and incubated at 4°C for ten minutes. 10 ml of RPMI medium was added to wash and the tube was centrifuged again at 300g for 7 minutes at room temperature. The supernatant was discarded and the pellet resuspended in 200 µl of FACS buffer. The cell suspension was transferred to a U-bottomed 96 well plate for further washes and staining as described in section 2.3.3.

2.4.2.2 Preparation of murine bone marrow samples

Bone marrow samples were extracted from the femur bones of culled humanised mice and the marrow cells were isolated by repeated flushing of RPMI media through the femur using a 27 gauge needle and a 1 ml syringe. The bone marrow was then dissociated into single cells using the 1 ml syringe and 27 gauge needle and the cell suspension was transferred to a centrifuge tube. The cells were treated with red cell lysis buffer as described in section 2.4.2.1 and then transferred to a U-bottomed 96 well plate for further processing.

2.4.2.3 Preparation of murine peripheral blood samples

Peripheral blood samples were transferred either directly to a 96 well plate (if < 200 µl in volume) or to a 15 ml centrifuge tube for larger volumes. The samples were centrifuged at 400g for 4 minutes at room temperature and the supernatant discarded. The pellets were resuspended in cold red cell lysis buffer- 150 µl for samples in a 96 well plate and 1 ml for samples in a centrifuge tube. Red cell lysis was performed as described in section 2.4.2.1. In the case of peripheral blood samples, it was often necessary to perform red cell lysis two or three times in order to ensure adequate removal of red blood cells.

2.5 Gene editing

2.5.1 Plasmid preparation

2.5.1.1 Plasmid expansion and extraction

Plasmids obtained from Addgene as agar stabs and inoculated into 100 ml of sterile LB broth with 100 µl of ampicillin. The broth was incubated overnight (approximately 16 hours) at 37°C in a shaking incubator at 150 rpm. The broth was aliquoted into two 50 ml centrifuge tubes and centrifuged at 1500g for 30 minutes. The supernatant was discarded and the plasmids were extracted using a QIAGEN® Plasmid Plus Midi Kit according to the manufacturer's instructions. The plasmid was resuspended in 200 µl of RNase-free water and the concentration of DNA was measured using a Nanodrop spectrophotometer.

2.5.2 Viral packaging

2.5.2.1 Maintenance and passaging of HEK 293T cells

HEK 293T cells were cultured on 10 cm^2 tissue culture dishes in MEF media. The media was changed every 48 hours and the cells were passaged approximately every five days, once a confluent monolayer had been reached. During passaging, the cells were washed in PBS and incubated in TryplE for approximately 3 minutes at 37°C to lift the cells from the plate. The cells were added to a centrifuge tube containing equal volume of MEF media to wash and centrifuged at 300g for 3 minutes at room temperature. The pellet was resuspended in 1 ml of MEF media. 10 ml of MEF media was added to an uncoated 10 cm^2 tissue culture dish and 100 µl of HEK 239T cells from the 1 ml suspension was added to the 10 cm plate. The plate was gently shaken to distribute the cells evenly, and this was confirmed by examination under the microscope. The cells were then returned to the 37°C incubator.

2.5.2.2 Plating of HEK 293T cells in flask

The cells were removed from the 10 cm plate using tryplE as described in 2.5.2.1 and resuspended in 1 ml of MEF media. The cells were counted using an automated cell counter (1 in 10 dilution in trypan blue) and the volume of the 1 ml suspension containing 1.8 x 10^7 cells was calculated. 25 ml of MEF media was added to an uncoated T175 flask and the calculated volume of HEK 293T cell suspension containing 1.8 x 10^7 cells was added to this flask using a p1000 pipette. The flask was shaken gently to ensure an even distribution of cells on the bottom of the flask and incubated overnight at 37° C. The T175 flask of HEK 293T cells was transferred to a category 2 tissue culture room in preparation for viral packaging.

2.5.2.3 Preparation of plasmid packaging components

1.5 ml of RPMI media was added to a 15 ml centrifuge tube and an appropriate volume of each plasmid was added to obtain the following amounts: 25 µg of the vector plasmid, 14 µg of the PAX2 helper plasmid and 6 µg of the MD2.G envelope plasmid. The tube was briefly vortexed and 68 µl of TurboFect reagent was added. The tube was vortexed again and left to sit at room temperature for 20-30 minutes. The transfection solution was added to the T175 flask of in a dropwise fashion and the flask gently rocked to ensure even distribution of the solution across the entire surface of the flask. The flask was returned to the 37°C incubator for 18-24 hours. The media was aspirated from the flask after the 18-24 hours and the cells were gently washed with 10 ml of sterile PBS. The PBS was aspirated and 25 ml of fresh MEF media was added. The flask was returned to the incubator for a further 24-36 hours.

2.5.2.4 Extraction and concentration of packaged virus

The media containing the viral particles was carefully transferred to a 50 ml centrifuged tube and filtered using a 0.45 µm filter. 5 U/ml of DNase I and 1 mM of $MgCl_2$ was added to the supernatant and mixed well. The tube was left at room temperature for 20 minutes. 8 ml of Lenti-X concentrator was added per 25 ml of supernatant and incubated at 4°C for 45 minutes. The samples was then centrifuged at 1500g for 45 minutes at 4°C. The supernatant was carefully aspirated and the pellet gently resuspended in 250 µl (1000^{th} the original volume of supernatant) of PBS. The viral suspension was quickly aliquoted into single-use 20 µl aliquots and stored at -80°C until required.

2.5.3 Viral transduction

COs were made into a single cell suspension as described in 2.3.3.1. The cells were counted using an automated cell counter and resuspended in 1 of WE+ media with EGF, Rspondin, DKK and Y at the usual concentrations (Section 2.1.1.3). The cells were transferred to the category 2 tissue culture room. A 20 µl aliquot of the required virus was thawed and the full viral aliquot was added to the cell suspension, along with 1:1000 of polybrene solution (1 µl). The CO suspension was gently mixed and transferred to a single well of a six well plate and incubated at 37°C overnight. The cell suspension was transferred to a 15 ml centrifuge tube, washed in 10 ml of WE+ media and centrifuged at 400g for 4 minutes at room temperature. The cells were then plated in organoid format (typically 6-9 wells) as described in section 2.1.1.3. After 24 hours, the CO wells were washed in PBS after 24 hours and provided with new media. The cells were washed and the media exchanged again 48 hours after plating, at which point the plate was taken out of the category 2 room and returned to the category 1 tissue culture room.

CHAPTER 3: CHARACTERISATION AND REFINEMENT OF CHOLANGIOCYTE ORGANOID CULTURE SYSTEMS

Statement of Source

Figures 3.1 - 3.4 and 3.6 – 3.10 and the text for the introduction presented in this chapter are based upon my first author publication referenced below[125] and has been taken verbatim or slightly modified from this source.

O. C. Tysoe, A. W. Justin, T. Brevini, S. E. Chen, K. T. Mahbubani, A. K. Frank, H. Zedira, E. Melum, K. Saeb-Parsy, A. E. Markaki, L. Vallier, F. Sampaziotis. Isolation and propagation of primary human cholangiocyte organoids for the generation of bioengineered biliary tissue. Nat Protoc. 2019;14:1884-1925.

3.1 Introduction

Cholangiopathies comprise a diverse group of disorders characterized by damage to the biliary tree and loss of bile ducts resulting in cholestasis, hepatic injury and ultimately liver failure[1,27]. However, treatment options are limited to liver transplantation. Indeed, biliary disease remains the leading indication for this intervention in children, with more than 70% of paediatric liver grafts being used to treat biliary atresia[39]. The generation of healthy biliary tissue suitable for replacing or reconstructing damaged bile ducts could address the clinical need for alternative therapeutic approaches and reduce pressure on the transplant waiting list.

Sampaziotis et al. developed a system for culturing cholangiocyte organoids derived from primary biliary tissue. To achieve expansion of the isolated cholangiocytes, the cells were embedded in Matrigel and treated with a combination of EGF, R-Spondin-1 and DKK-1. EGF has been well established to promote the proliferation of cells in organoid format[105] and had previously been demonstrated to be a required factor in the culture of iPSC-derived cholangiocyte organoids[223]. To support the long-term expansion of adult cholangiocytes we used R-spondin-1, a Wnt agonist reported to stimulate organoid derivation from multiple adult epithelia[110,113,224-227]. However, R-spondin promotes the propagation of adult stem cells rather than mature epithelial populations by enhancing canonical Wnt signalling[228]. To avoid the amplification of adult stem cells, we introduced DKK-1[229], a canonical Wnt/β-catenin pathway antagonist[230,231]. When used in combination with R-spondin, DKK-1 inhibits canonical and enhances non-canonical Wnt signalling though the planar cell polarity (PCP) pathway[124], which has been reported to play a role in cholangiocyte maturation[17,232]. The combination of EGF, R-Spondin-1 and DKK-1 allowed for long-term, large-scale expansion of functional, genetically stable, primary adult COs.

COs are capable of long-term expansion, retain expression of key cholangiocyte markers and functionality and, importantly are able to populate artificial collagen scaffolds and successfully rescue *in vivo* models of extrahepatic biliary injury. These properties demonstrate the system's potential as a source of cholangiocyte cellular therapies for the treatment of cholangiopathies. However, the immunogenicity of COs and CO-derived therapeutic products must be determined before CO cellular therapies can be used in a clinical setting.

In order to characterise the immune response to COs, it was first necessary to derive additional CO lines from donors for which autologous immune cells (PBMCs, SpMCs and/or bone marrow) could also be obtained. These lines were then characterised to ensure they had been derived and maintained effectively and were representative of the CO system. In this chapter we describe the characterisation of COs derived using our standard CO protocol.

Furthermore, in collaboration with Dr Fotios Sampaziotis and Teresa Brevini, several refinements were made to the CO protocol and to the protocol for developing artificial biliary tissue, in order to expand the available sources of CO lines and improve the generation of artificial biliary tissue. The original CO protocol developed by Sampaziotis et al. only allowed for derivation of COs from extrahepatic biliary tissue (common bile duct and gallbladder), but not intrahepatic tissue. This potential limitation would restrict the availability of CO lines, as it would not permit derivation of lines where the gall bladder or extrahepatic bile duct was is not available (including from deceased donors in a research setting and from potential live donors or explanted livers from transplant recipients, from which liver biopsies could be taken). In order to obtain tissue from these potential donors, I developed a method for the derivation of intrahepatic cholangiocyte organoids (ICOs) from liver biopsies, in collaboration with Fotios Sampaziotis, which I present in this chapter.

Additionally, one important application of the CO system in the development of cellular therapies is the generation of artificial bile ducts that can replace or repair bile ducts damaged by cholangiopathies or surgical complications. The original protocol for the generation of artificial biliary tissue required the CO cells to be mixed in with the collagen gel during the densification process, rather than seeded onto the lumen of the densified collagen tubular scaffold. As seeding the CO cells onto the scaffold surface represents a more physiological approach, we developed a protocol for seeding CO cells directly onto the surface of densified collagen scaffolds, including in the lumen of tubular scaffolds. This aspect of the project was done in collaboration with Teresa Brevini, under the supervision of Fotios Sampaziotis and utilising tubular scaffolds generated by Alexander Justin.

As a significant proportion of the work for this project requires transplantation of COs *in vivo* and the monitor graft survival, it was necessary to assess the capacity of COs to survive and proliferate *in vivo.* Additionally, it was important to develop a system to allow COs to be easily identified and tracked *in vivo*. I chose to use bioluminescence imaging (BLI) using a construct expressing luciferase and red

fluorescent protein (RFP) under an Ef1α promoter. BLI is commonly used for a wide variety of *in vivo* research applications[233-236], including assessment of graft survival in transplantation models[237-239] and has the major advantage of allowing for imaging of live animals on multiple occasions, as well as being relatively straightforward to perform compared to other types of imaging such as magnetic resonance imaging (MRI) and positron emission tomography (PET)[235]. In this chapter we characterise the ability of COs to survive *in vivo* and develop a bioluminescent imaging system to allow for live imaging and quantification of CO grafts *in vivo.*

3.2 Results

3.2.1 Cholangiocyte organoids express key cholangiocyte markers and functionality

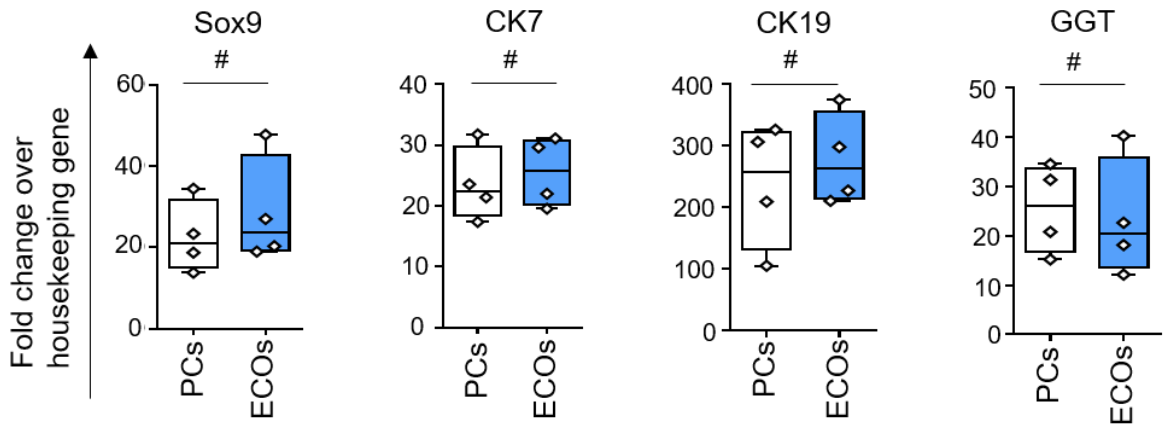

Figure 3.1: qRT–PCR of representative CO lines confirming the expression of the key biliary markers
Sox9, cytokeratin 7 (CK7), cytokeratin 19 (CK19) and gamma glutamyl transpeptidase (GGT) in COs compared to freshly isolated primary cholangiocytes (PC). COs express key cholangiocyte markers at comparable levels to primary cholangiocytes. n = 4 biological replicates. Centre line, median; box, interquartile range (IQR); whiskers, range (minimum to maximum). Values relative to the housekeeping gene HMBS. # P > 0.05 (two-tailed Student's t-test).

Using our established protocol for the derivation and maintenance of COs[124,125], I first focused on generating and validating new CO lines. Throughout the duration of this project, I generated 66 CO lines from 43 separate donors (appendix table 3) aged between 23 and 77. Neither donor age nor any other demographic factor was found to impact on the health of the CO line or success of line derivation. Derivation efficiency was typically close to 100%, although different methods of derivation resulted in different success rates and variation in the processing of the tissue before derivation could also impact derivation success. For example, common bile duct tissue that had not been adequately flushed of bile typically resulted in a much lower rate of derivation success (from 95% successful to 40%). I aimed to generate as many CO lines as possible with corresponding autologous immune cells available, as well as to potentially identify CO lines for which fully and/or partially HLA matched immune cell donors were available (see chapter 5 for more details).

In keeping with our previously reported results[124], these CO lines expressed the cholangiocyte markers Sox9, cytokeratin 7 (CK7), cytokeratin 19 (CK19) and gamma-glutamly transferase (GGT) at levels similar to primary cholangiocytes (no statistically significant difference), as determined by qRT-PCR (figure 3.1). Expression of these markers was confirmed via immunofluorescence (figure 3.2), as was the lack of the hepatocyte marker albumin.

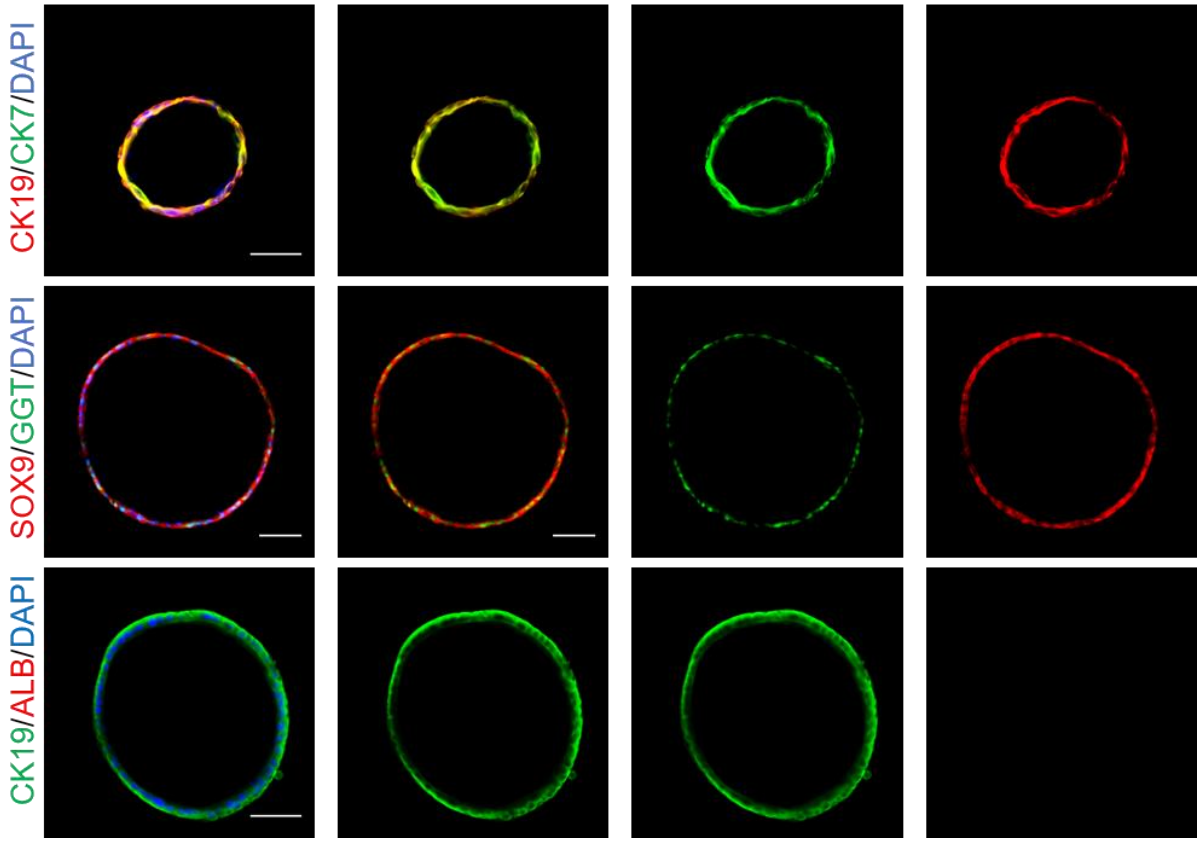

Figure 3.2: Representative immunofluorescence images demonstrating expression of key biliary markers in COs

Immunofluorescence images demonstrating CK7 (green) CK19 (red), Sox9 (red) and GGT (green) expression in COs and the lack of expression of the hepatic marker albumin (red). Scale bar, 50 μm. (See appendix table 1 for a detailed list of antibodies and concentrations used).

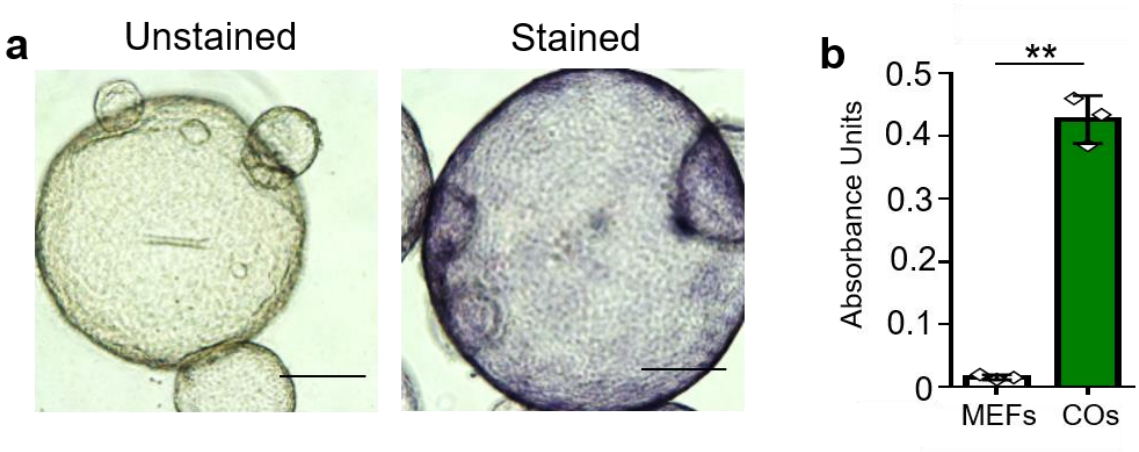

Figure 3.3: COs display typical cholangiocyte functional properties

(**a**) COs demonstrate ALP activity. Left- unstained CO control; right- COs stained with ALP assay substrate. Scale bars, 100 μm. (**b**) GGT activity of COs measured in absorbance units (a.u.); n = 3; MEFs: mouse embryonic feeders, used as a negative control. Error bars, s.d.; individual data points are demonstrated; **P < 0.01, two-tailed Student's t-test.

CO lines display the typical functional properties of large cholangiocytes, such as alkaline phosphatase and gamma-glutamly transferase activity (figure 3.3). COs represent a highly purified cholangiocyte population. Population purity increases after derivation and plating, with the isolation of primary cholangiocytes typically resulting in a purity of >90% (for isolation of extrahepatic cholangiocytes), which increases to >99% once in CO culture (figure 3.4). This level of purity remains stable throughout the duration of culture (up to 20 passages).

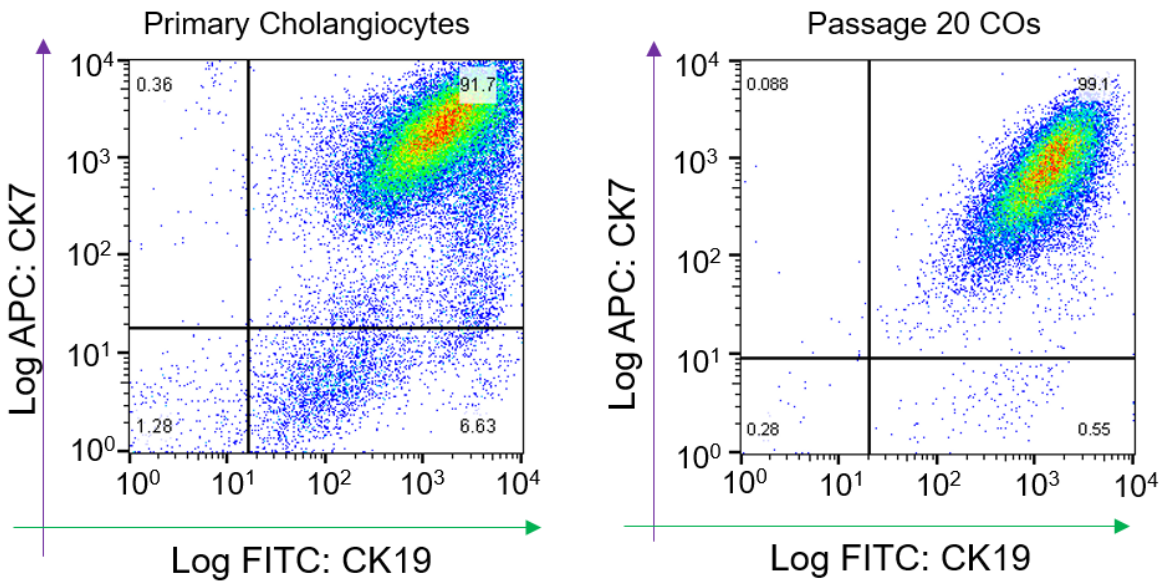

Figure 3.4: Flow cytometric quantification of CK7 and CK19 expression in primary cholangiocytes and COs
Representative flow cytometric analyses performed on isolated primary cholangiocytes (left) compared to COs after long term culture (20 passages) (right). The population of primary cholangiocytes is >90% CK7+/CK19+ while the population of passage 20 COs demonstrates >99% CK7+/CK19+ expression (gating strategy demonstrated in appendix figure 1).

3.2.2 Cholangiocyte organoids can be derived from intrahepatic biliary tissue

In order to capture all possible sources of CO lines, it was important to adapt the existing CO protocol to enable derivation of CO lines from intrahepatic as well as extrahepatic biliary tissue. As our main source of biliary tissue was from deceased organ donors, I initially attempted two methods of isolating cholangiocytes from pieces of whole liver tissue from livers deemed unsuitable for transplantation. The first method involved cutting a small piece of liver tissue (approximately 1 cm^3) and gently scraping it with a scalpel into a tissue culture dish filled with William's E+ media, with the aim of dissociating the tissue into small clumps of cells. These small clumps of cells were then collected, centrifuged and plated in organoid format as described in Section 2.1.1.3. The second method involved manual dissociation of the liver tissue by sieving through a 100 µm sieve and then collecting the cells and plating as described above. While both of these methods resulted in the generation of CO lines (figure 3.5), they were both inefficient. In typical CO lines derived from the gallbladder or bile duct, organoids emerge within 48 hours of initial plating and require passaging within five days, while lines derived by either of these two methods were not ready to be passaged until 8-10 days later. Additionally, far fewer organoids developed per well compared to extrahepatic CO lines, and several of the organoids showed signs of thickening and collapse. While passaging was successful for both methods, the low numbers of organoids in passage 0 resulted in a much slower expansion of the CO lines than typical and prevented the cryobanking of early passages of these CO lines.

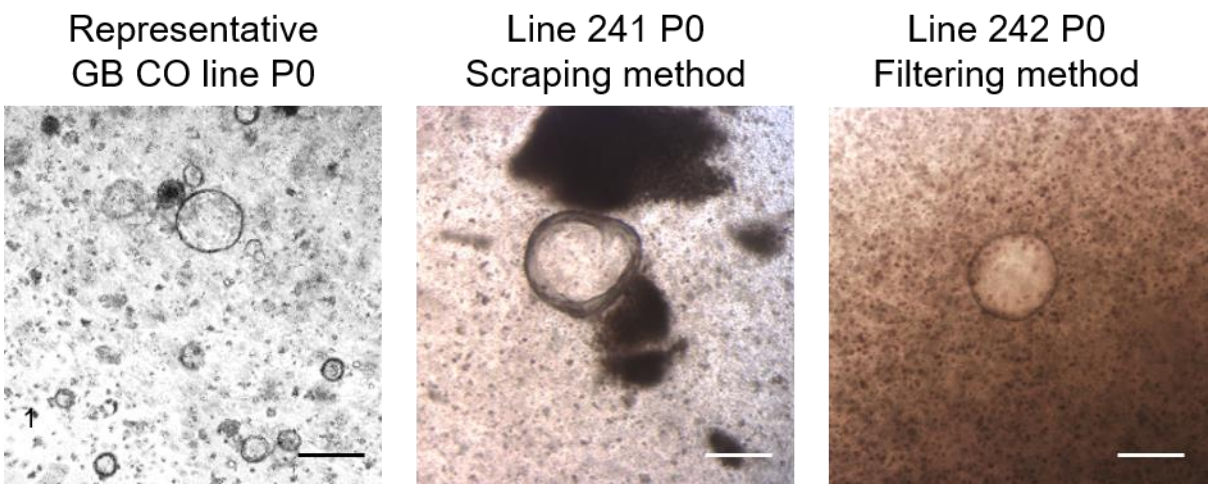

Figure 3.5: Comparison of initial organoid development in passage 0 CO lines using different derivation methods
Brightfield images comparing a representative gallbladder (GB) CO line at passage 0, 24 hours after derivation, with two intrahepatic bile duct (IHD) lines derived by either the scraping method or filtering method at passage 0, five days after derivation. Scale bar = 200 μm. Multiple organoids can be seen proliferating in the P0 GB line, while in the same spatial area, only one organoid has developed in each of the two IHD lines, despite a greater length of time elapsing since initial derivation.

Due to the limitations of these two derivation methods, I developed a new protocol for intrahepatic CO (ICO) derivation. This new method preferentially involved sampling the liver tissue as a needle biopsy rather than excising a whole piece of tissue (although whole tissue pieces could be used in instances where it was not possible to take biopsies). The tissue was then finely diced using a scalpel. The tissue pieces were collected, centrifuged and then plated as described in Section 2.1.1.3.

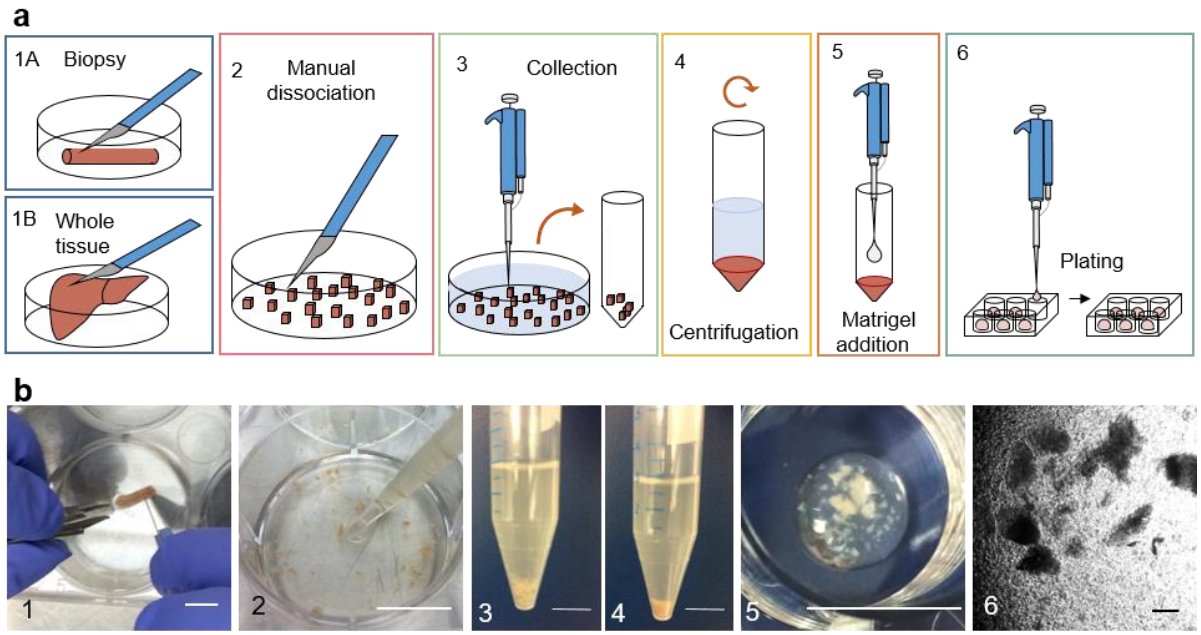

Figure 3.6: Development of a method for isolation intrahepatic cholangiocyte organoids (ICOs) from liver tissue
(a) Schematic representation of ICOs derivation (b) Representative images of key stages of ICO derivation. **1**: Dissection of liver tissue. **2**: Collection of dissected tissue. **3-4**: Dissected tissue before **(3)** and after **(4)** centrifugation. **5**: Representative image of liver tissue after embedding in Matrigel, prior to media addition. **1-5**: Scale bars, 1 cm. **6**: Representative brightfield images of liver tissue immediately after plating. Scale bar, 200 μm.

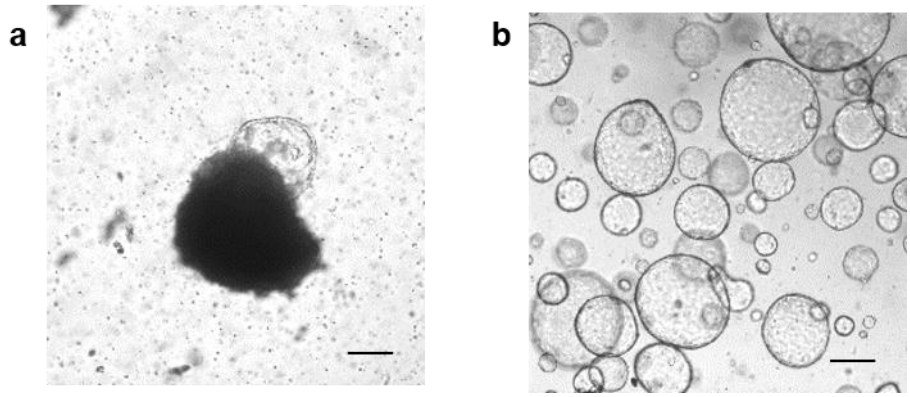

Figure 3.7: Brightfield images of intrahepatic cholangiocyte organoids
(a) An intrahepatic organoid emerging from liver tissue at passage 0 (scale bar = 200 μm) and (b) brightfield image of an established ICO line at passage 20 displaying typical healthy morphology (scale bar = 200 μm).

In this new method, I did not attempt to fully dissociate the liver tissue but instead plated the tissue as relatively large (0.5-1.0 mm^3) pieces in standard CO conditions (William's E+ media with EGF, Rspondin and DKK-1). After several days (typically between 3-5 days), cholangiocyte organoids began

to emerge from the tissue pieces, while all other cell types in the liver tissue did not proliferate (figure 3.7), as the WE+ media components and additional cytokines (EGF, Rspondin-1, DKK-1) promote the survival and proliferation of cholangiocytes while not supporting the survival of other cell types[124]. The ICO lines were typically ready for passaging at 7-10 days after derivation. While this method required a similar time to the previous two methods, it typically resulted in a much greater number of organoids at passage 0. This enabled the lines to be expanded more rapidly and early passages to be cryopreserved due to the greater cell number. Additionally, despite ICO lines deriving from intrahepatic biliary tissue rather than extrahepatic, ICOs could be derived and maintained in identical conditions to ECOs, without any other requirements. After initial derivation, all CO lines maintained similar characteristics and morphology, regardless of tissue of origin or derivation method (figure 3.8). Importantly, established ICO lines also expressed key cholangiocyte markers at levels comparable to both freshly isolated primary cholangiocytes and extrahepatic CO lines derived from the common bile duct or gallbladder (figure 3.9).

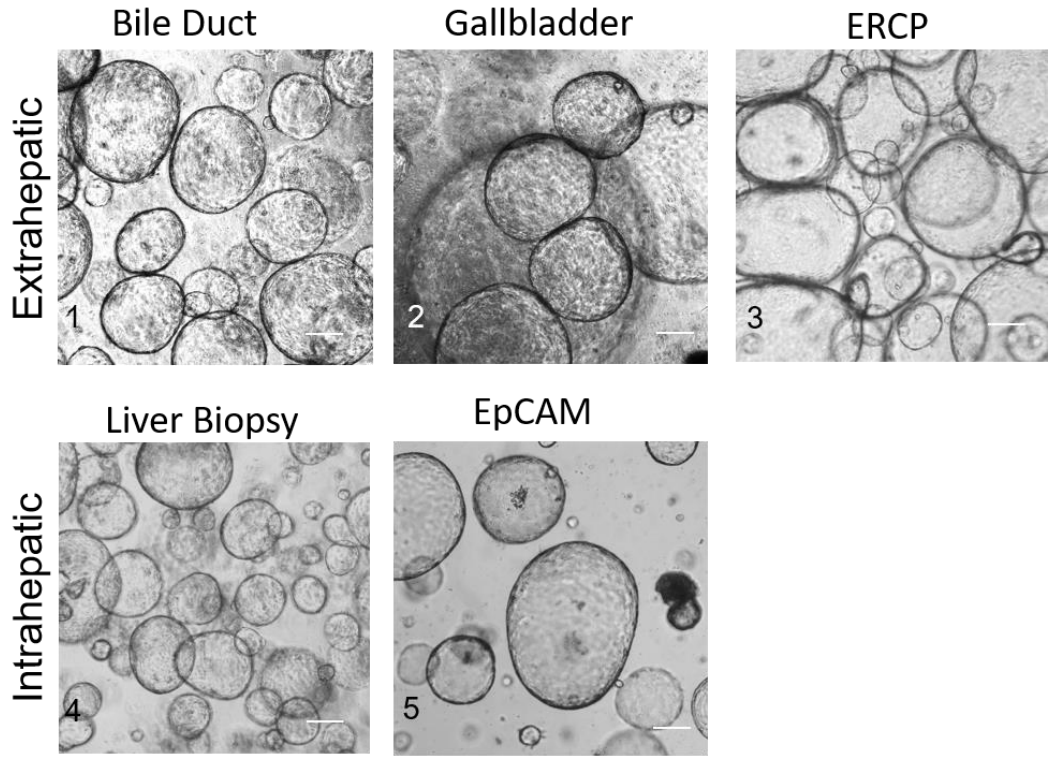

Figure 3.8: Representative brightfield images of healthy CO lines derived from all tissue types
1: bile duct, 2: gallbladder, 3: Endoscopic Retrograde Cholangio-Pancreatography (ERCP) brushings, 4: liver biopsy and 4: EpCAM+ sorted liver cells. Scale bars- 200 μm

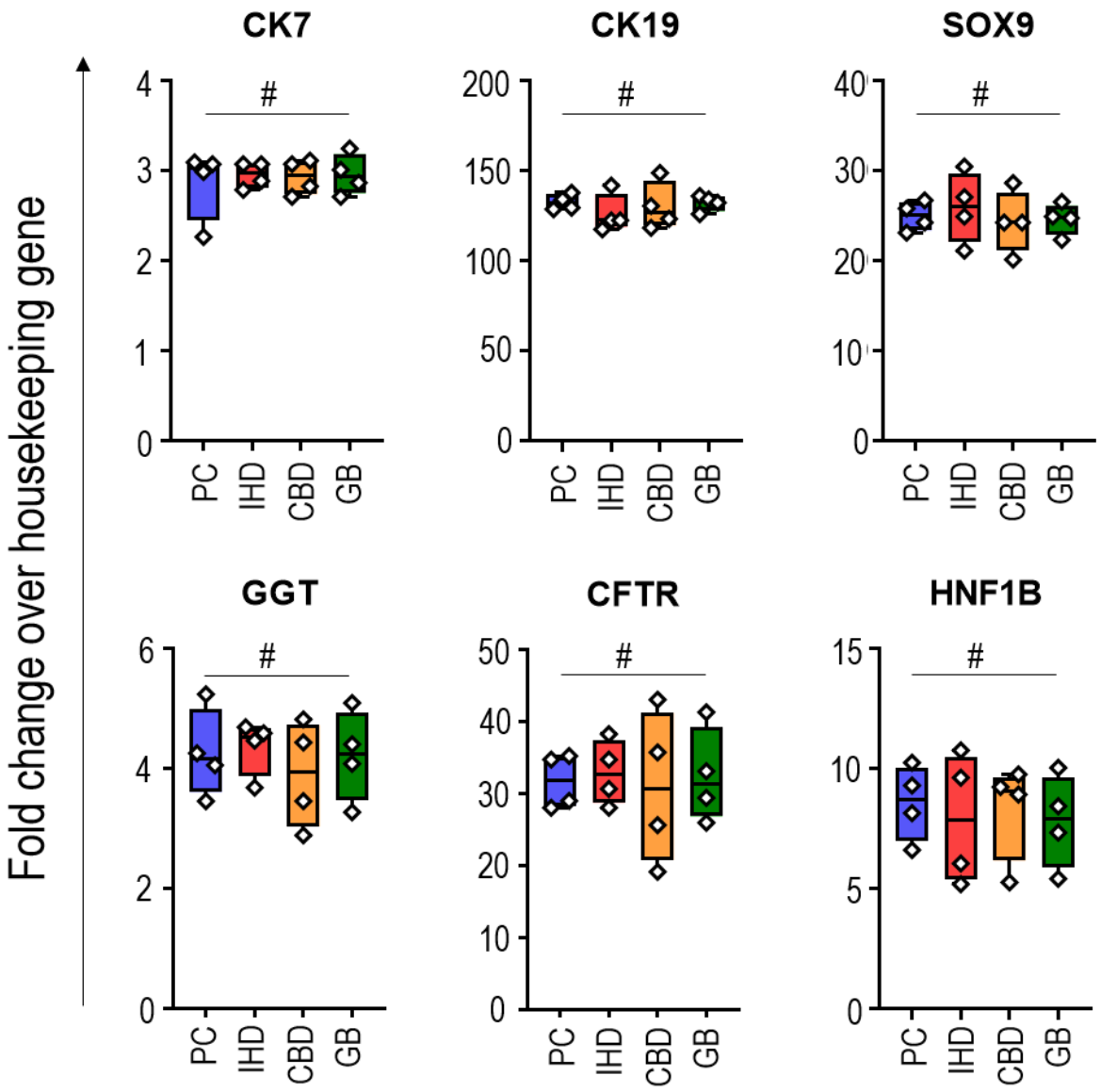

Figure 3.9: qRT–PCR comparison of representative CO lines derived from intrahepatic and extrahepatic biliary tissue

Sox9, cytokeratin 7 (CK7), cytokeratin 19 (CK19), gamma glutamyl transpeptidase (GGT), cystic fibrosis transmembrane conductance regulator (CFTR) and Hepatocyte Nuclear Factor-1 Beta (HNF1B) in freshly isolated primary cholangiocytes (PC) compared to established (passage 20) CO lines derived from intrahepatic ducts (IHD), the common bile duct (CBD) and the gallbladder (GB). IHD, CBD and GB CO lines express key cholangiocyte markers at comparable levels to primary cholangiocytes. n = 4 biological replicates. Centre line, median; box, interquartile range (IQR); whiskers, range (minimum to maximum). Values relative to the housekeeping gene HMBS. # $P > 0.05$ (One-way ANOVA with Dunnett's multiple comparisons).

qRT-PCR data provided by Fotios Sampaziotis.

3.2.3: Refinements to the generation of artificial biliary tissue

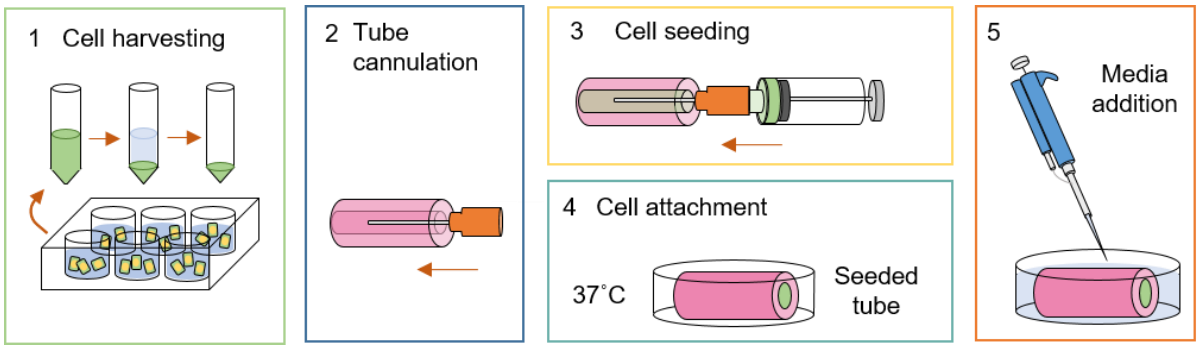

Figure 3.10: Schematic representation of densified collagen tube seeding.
1: COs are removed from Matrigel and manually dissociated to a single cell suspension. 2: The densified collagen tube is cannulated with a small-gauge needle. 3: The cell suspension is loaded into the syringe which is then attached to the needle and the cells are seeded in the lumen of the tube. 4: The tube is left at 37°C without media for approximately half an hour to ensure adequate attachment of the cells to the lumen wall. 5: William's E+ media is added to the plate to the point of covering the tube.

In our original protocol for generating bioengineered artificial biliary tissue, the CO cells were dissociated to small clumps and mixed into the collagen gel during the densification process. This ensured that cells were retained within the tubular scaffold but did not adequately reflect a physiological biliary system. We refined the protocol to allow for seeding of CO cells directly onto the surface of the scaffold (figures 3.10 and 3.11) by delivering the cells in a highly concentrated, low volume suspension into the lumen of the scaffold. The scaffold was dried for 30-60 minutes before seeding to encourage the cell suspension to adhere to the scaffold walls, and then left without media for a further 30-60 minutes to allow the cells to attach.

This refined method was successful in seeding small (200 μm lumen diameter) tubular scaffolds (figure 3.11) and work is ongoing by Fotios Sampaziotis and Teresa Brevini to adapt the protocol to scaffolds of appropriate size for human transplantation (0.5-1.0 cm lumen diameter).

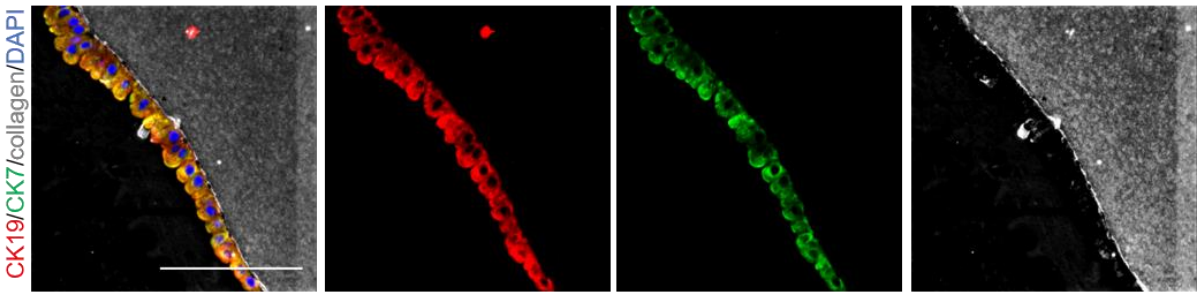

Figure 3.11: Successful seeding of CO cells on the luminal surface of a densified collagen tube
Immunofluorescence images showing expression of key biliary markers (CK19 and CK7) in CO-seeded densified collagen tubes. COs seeded on the luminal surface of densified collagen tubes retain expression of key cholangiocyte markers (CK19 and CK7) and form an uninterrupted monolayer. Scale bar, 100 μm.

3.2.4: COs survive *in vivo* when transplanted under the kidney capsule

COs were transplanted under the kidney capsule of immunodeficient NSG mice in order to assess the survival and proliferation of the cells *in vivo*. Approximately 1.0 x 10^6 cells were injected per animal, in a suspension of 100% Matrigel, containing the cytokines EGF and Y27632. EGF was chosen as it is a cytokine known to promote proliferation of epithelial cells[105,124,223] and Y27632 helps prevent apoptosis caused by disruption of cell-cell and cell-matrix contact[105,240]. COs typically survived *in vivo* and formed cystic, duct-like structures under the kidney capsule, often surrounded by a layer of fibrosis due to the transplantation. The rate of proliferation and degree of survival of CO lines was highly variable and some lines were not able to survive *in vivo* for even the minimum required time of two weeks (table 3.1), while others proliferated rapidly and were able to survive for at least 12 weeks *in vivo*. Eight lines in total were transplanted *in vivo* over the course of this project, with two lines failing to survive *in vivo* to any extent (appendix figure 2), resulting in a survival rate of 75%. All CO lines transplanted thus far have been derived from extrahepatic biliary tissue. CO survival and morphology was assessed at the point of culling (variable, according to the experiment) by immunofluorescence on cryosections. COs retained expression of key cholangiocyte markers (figure 3.12).

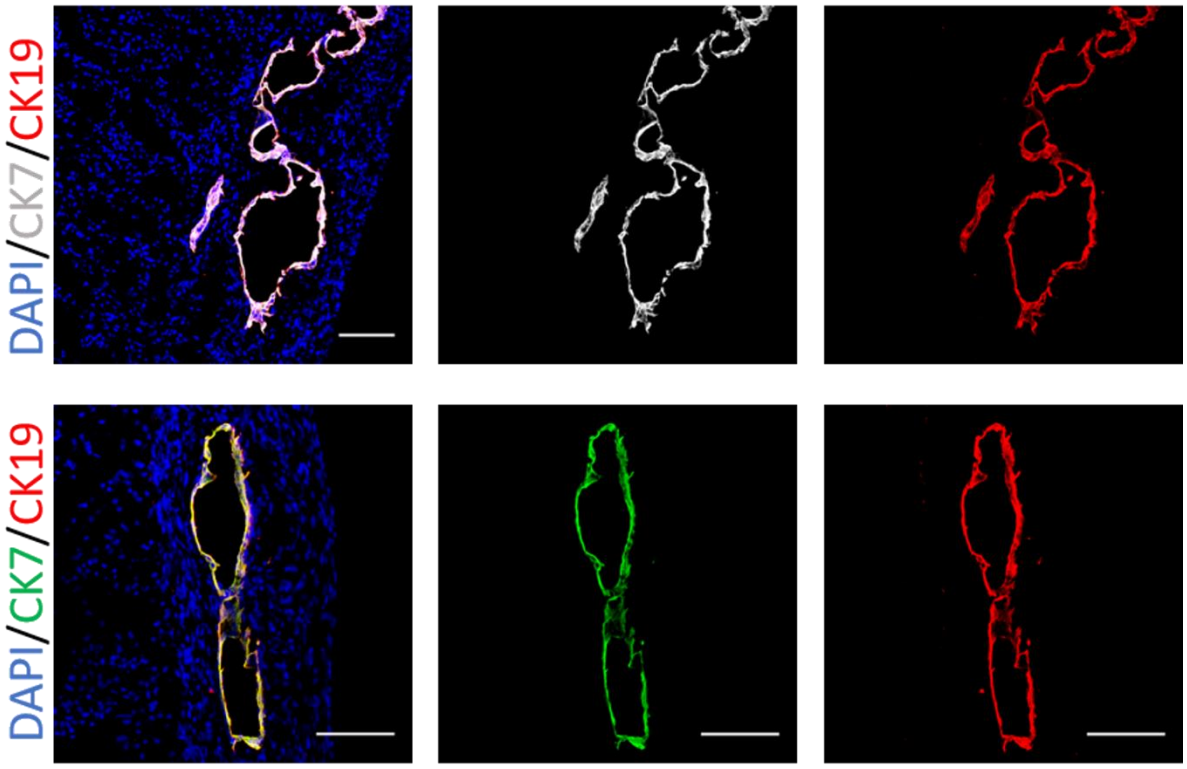

Figure 3.12: CO lines survive *in vivo* under the kidney capsule of NSG mice
Immunofluorescent images of two different CO lines four weeks after transplantation under the kidney capsule in immunodeficient NSG mice. CO lines form duct-like cystic structures and retain expression of key cholangiocyte markers such as CK7 and CK19. The degree of CO survival and the rate of proliferation is highly line-dependent (total of eight CO lines tested *in vivo*). Scale bar = 100 μm.

CO line	CO line passage at transplant	Line survival *in vivo*	Line quality *in vivo*	Weeks *in vivo*
200 (BD)	P6	Yes	Good	12
243 (BD)	Variable (P6-P10)	No	-	Variable (2-16)
256 (BD)	Variable (P7-P10)	Yes	Good	Variable (2-6)
261 (BD)	P10	No	-	4
286 (GB)	P6	Yes	Poor	4
299 (BD)	P7	Yes	Good	3
325 (BD)	P4	Yes	Good	4
378 (BD)	P6	Yes	Good	4

Table 3.1: Variation in survival and proliferation of CO lines in vivo
Table showing the eight CO lines transplanted *in vivo*. All lines were of extrahepatic origin, either bile duct (BD) or gallbladder (GB). The criterion for survival was set at the ability to locate living CO cells at the site of transplantation at least two weeks post-transplantation. "Good" quality lines are defined as lines surviving at least four weeks *in vivo*, with reliable survival across all transplanted animals and formation of duct-like structures. "Poor" quality lines are defined as lines unable to reliably survive over four weeks post-transplant, with survival varying between transplanted animals and abnormal graft structure.

3.2.5: bioluminescent imaging can be used to monitor CO survival *in vivo*

In order to enable CO grafts to be monitored in live animals and to quantify changes in graft size during experiments, we generated luciferase-expressing CO lines. I initially chose a commercially-available construct (available as pre-packaged lentiviral particles) with luciferase and GFP both controlled by a CMV promoter (figure 3.13).

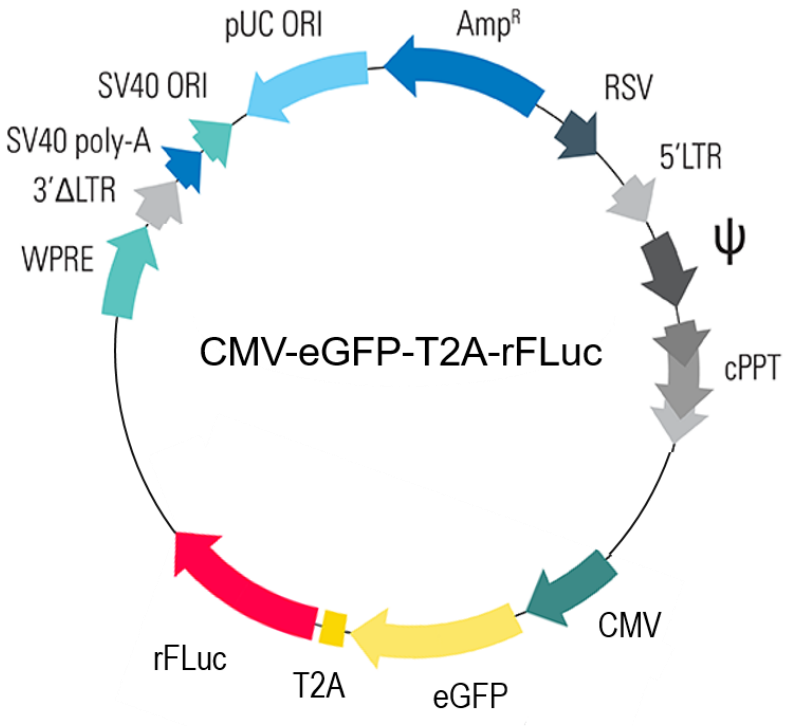

Figure 3.13: Plasmid map of the construct used to generate the initial GFP-Luciferase CO lines. The luciferase and GFP genes are both controlled by the CMV promoter and joined by a T2A linker.

This construct was transduced into two passage 2 BD lines, 378 and 312, at a multiplicity of infection (MOI) of 5 and 10, respectively. Both lines were successfully transduced (figure 3.14), and were sorted by flow cytometry on GFP expression at two passages after transduction. Only approximately 1% of the population of both CO lines were GFP+ at the time of sorting.

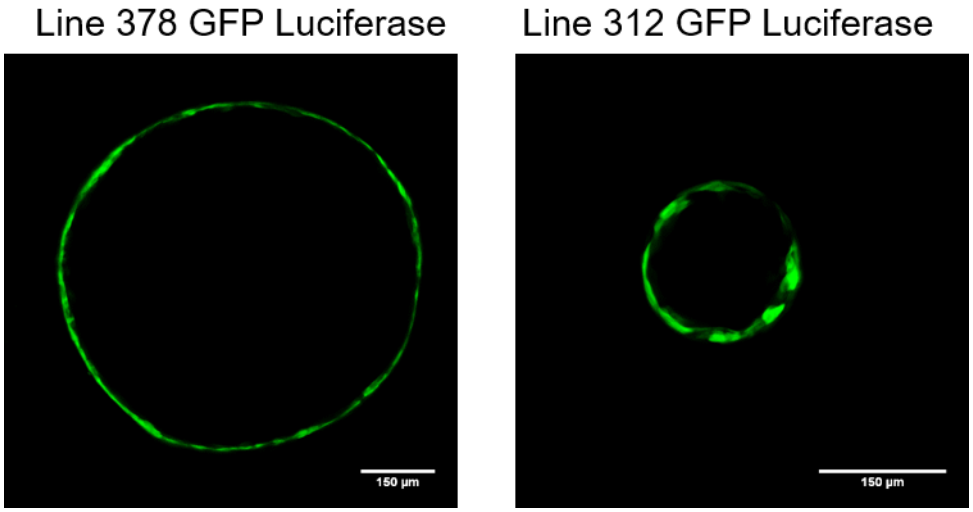

Figure 3.14: Generation of GFP luciferase CO lines
Fluorescent images of two CO lines (378 and 312) transduced with a GFP luciferase construct, at P0 after transduction (P3 in total). Scale bar = 150 µm.

These lines were transplanted under the kidney capsule of NSG mice (1.0×10^6 cells per mouse) and BLI was performed 24 hours after transplant (figures 3.15 and 3.16). Both lines expressed luciferase and were able to be detected *in vivo*. NSG mice were transplanted with the 312 GFP Luc line at different cell numbers to determine the sensitivity of the luciferase signal (figure 3.15). Luciferase signal showed a broadly linear dose-response curve to the number of cells transplanted. Luminescence was detectable at 1.0×10^5 cells, 10 times fewer than was typically transplanted in a standard *in vivo* experiment, but the signal was low, while injection of 1.5×10^6 cells resulted in significant over-saturation. From this I determined that the typical cell number of approximately 1.0×10^6 cells per mouse remained the optimal choice.

While both lines could be detected by BLI at 24 hours after transplant, when imaged again at four weeks post-transplant, no signal was detectable for either CO line (figure 3.16). Upon culling, the kidneys were sectioned and imaged by immunofluorescence and surviving grafts were found (figure 3.17). These grafts were proliferative and expressed typical cholangiocyte markers but did not express GFP, either as natural fluorescence or when stained with a GFP-specific antibody (figure 3.17). A lack of GFP signal was also seen in the two lines *in vitro* following flow cytometric sorting, with no detectable GFP signal seen after five passages (P11) (figure 3.18).

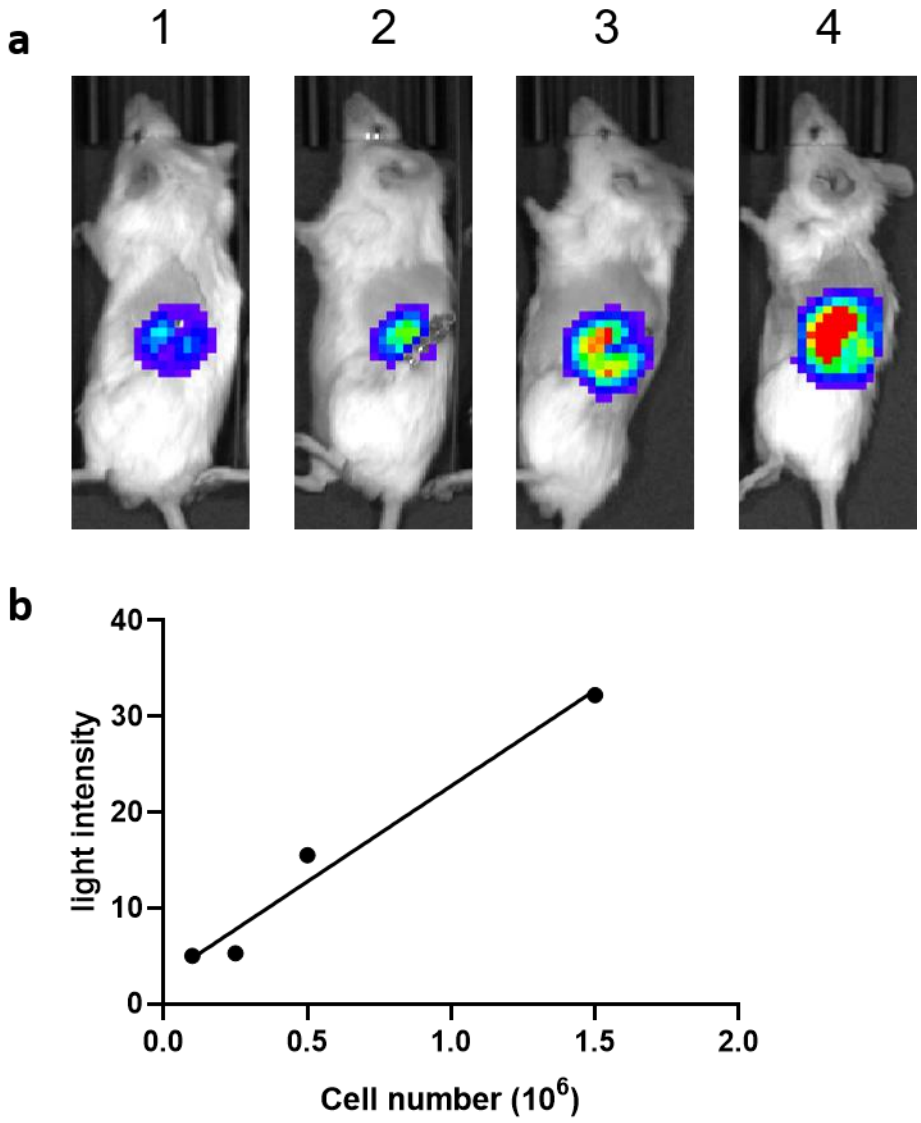

Figure 3.15: Assessment of luciferase sensitivity *in vivo*
Luminescence intensity at varying cell concentrations *in vivo*, one day after transplantation. (a) IVIS images of GFP-luciferase COs (line 312) under the kidney capsule at increasing cell numbers. 1: 1.0 x 10^5 cells; 2: 2.5 x 10^5 cells; 3: 5.0 x 10^5 cells; 4: 1.5 x 10^6 cells. Imaging exposure time- 120 seconds. (b) Dose-response curve of light intensity (10^5 photons) against CO cell number (10^6). Values based on luminescence readings from imaged mice shown in (a). Luminescent signal increases linearly with increasing cell number. Signal is clearly visible at 1.0 x 10^5 cells, 10 times fewer than typically injected, while 1.5 x 10^6 cells resulted in over-saturation at the typical exposure time of 120 seconds.

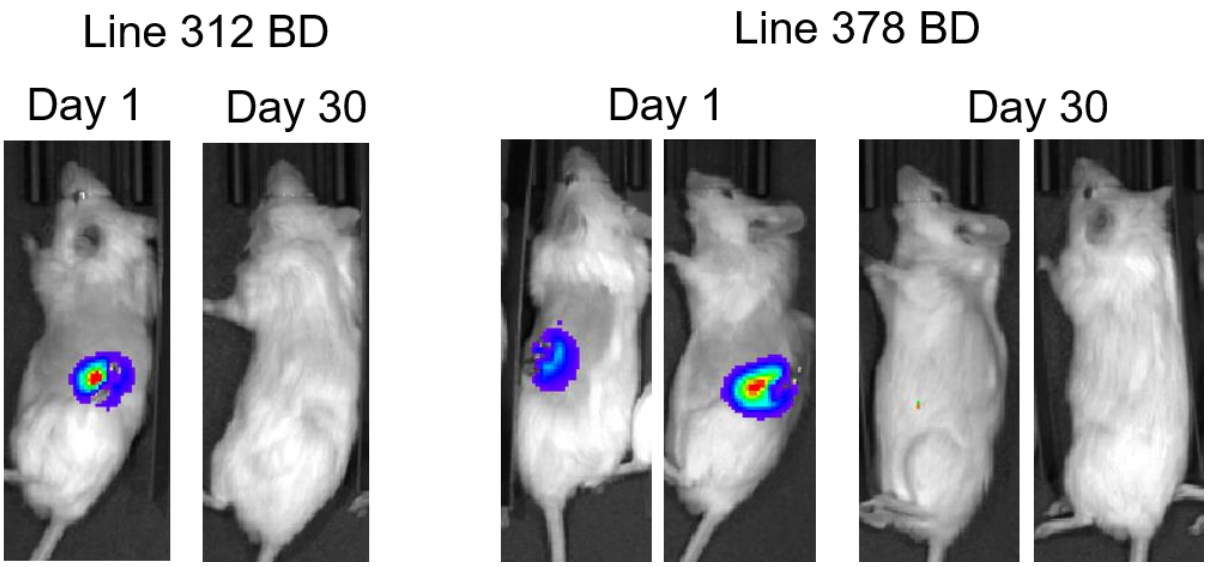

Figure 3.16: Assessment of the long-term expression of luciferase signal *in vivo*
NSG mice were transplanted with approximately 1.0 x 10^6 cells of either the 312 GFP Luciferase or 378 GFP luciferase line and imaged 24 hours post-transplantation (left) and 30 days post-transplantation (right) with automatic exposure. High levels of luminescence were seen at day 1 post-transplantation but luminescent signal was gone from all animals at day 30.

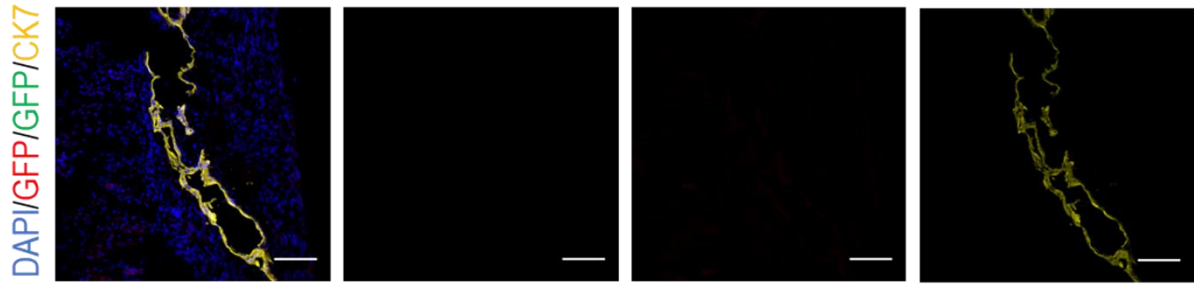

Figure 3.17: GFP-Luciferase COs survive in vivo at four weeks post-transplantation

Immunofluorescent images of 378 GFP-Luciferase COs (passage 6) under the kidney capsule at four weeks post-transplantation. 378 COs express the cholangiocyte markers CK7 (yellow) and CK19 (not shown here) but do not express GFP, either as natural fluorescent signal (green) or via anti-GFP antibody staining (red). Scale bar = 100 μm.

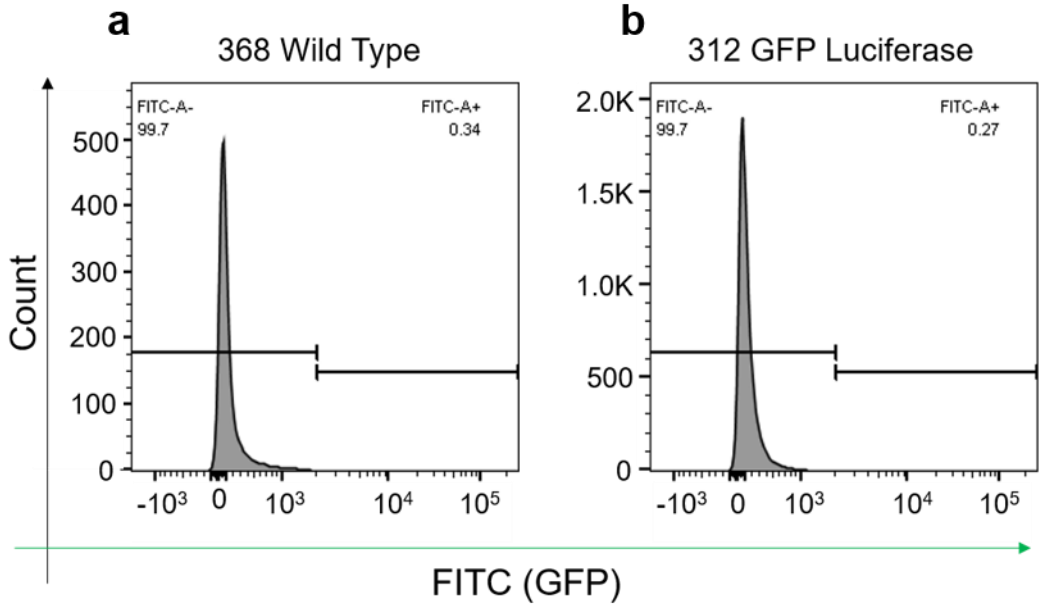

Figure 3.18: Flow cytometric analyses of GFP expression in 312 GFP-Luciferase COs compared to a wild-type CO control
(a) GFP expression in 368 wild-type control COs and (b) GFP expression in 312 GFP-luciferase COs. Flow cytometry gating: $>10^3$ = positive expression $< 10^3$ = no expression. No positive expression seen in either the WT control or 312 GFP-luciferase lines.

Due to loss of luminescence signal over time *in vivo* and the complete loss of GFP signal (preventing selection of transduced cells as GFP was the only selection marker), I discontinued using the established GFP-Luciferase lines and explored a new luciferase construct. Due to time constraints, I selected a commercially available plasmid, with two important new criteria for selection: a promoter less likely to be silenced in primary-derived cells (either Ef1α or CAG) and an antibiotic resistance gene, to ensure availability of two methods of selection. I investigated several constructs (data not shown) and eventually chose the LL420 plasmid from Systems Bioscience (figure 3.19). This plasmid contains luciferase and RFP under the Ef1α promoter, joined by a T2A linker and has a separate puromycin resistance gene under the mPGK promoter. I packaged this plasmid into viral particles in-house using HEK 293T cells and successfully transduced the 299 BD line at passage 2 (figure 3.20). The 299 RFP-Luciferase COs were transduced at an efficiency of 40% (according to RFP expression at P4, two passages after transduction). The cells were flow cytometrically sorted by RFP signal at P4 and treated with puromycin at 4 ng/ml for seven days at P6 (P1 after flow sorting) (figure 3.21). Due to time constraints and logistical challenges at the time, I was unable to assess the proportion of RFP+ cells post-sort, however work is ongoing to determine this and to assess the stability of RFP expression in the 299 BD line.

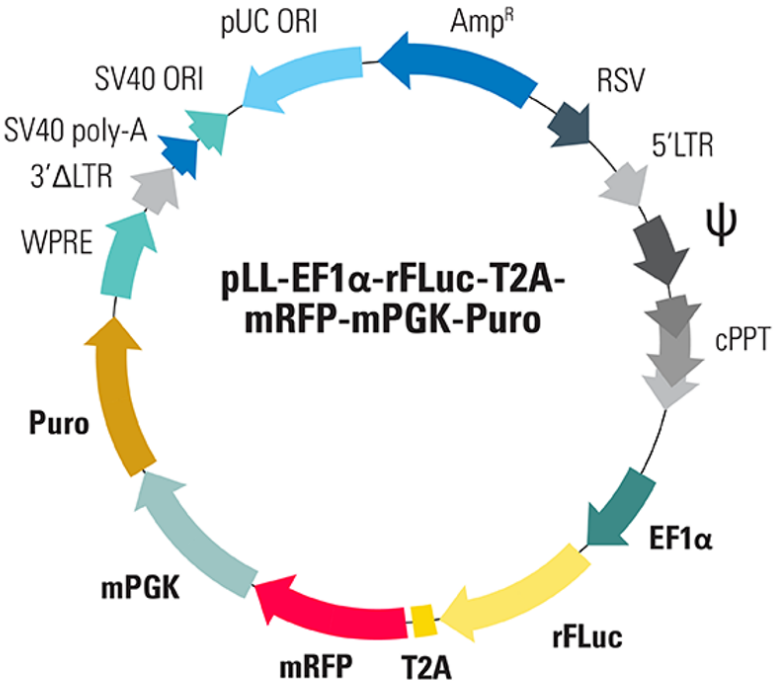

Figure 3.19: Plasmid map of the LL420 luciferase construct
This construct was used to generate the 299 BD Luc-RFP CO line. The luciferase and RFP genes are both controlled by the Ef1α promoter and joined by a T2A linker. A puromycin resistance gene is controlled separately by the mPGK promoter.

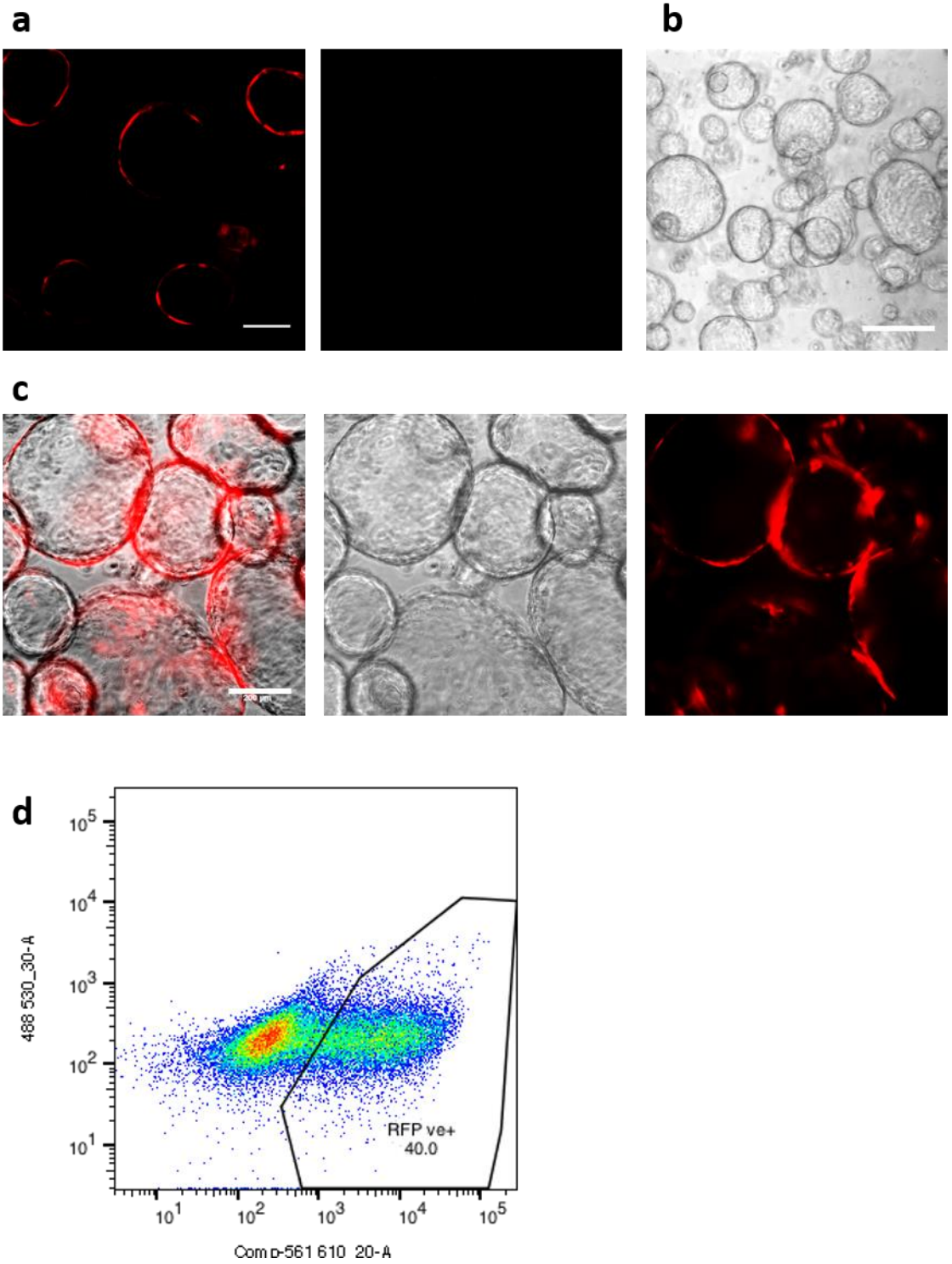

Figure 3.20: Transduction of 299 BD COs with the LL420 construct.
(a) Fluorescent image of 299 BD one passage after transduction (passage 3) showing RFP expression in the majority of cells. Lack of expression in the GFP channel confirms the RFP signal is at a level above background. (b) Brightfield image of 299 BD one passage after transduction (passage 3) demonstrating a healthy, normal morphology after transduction. (c) Overlay of RFP and brightfield images of 299 BD two passages after transduction (passage 4) displaying strong RFP expression in some cells but low or absent expression in others. (d) Flow cytometry diagram of 299 BD three passages after transduction (passage 5) (live single cells) showing 40% of cells as RFP+.

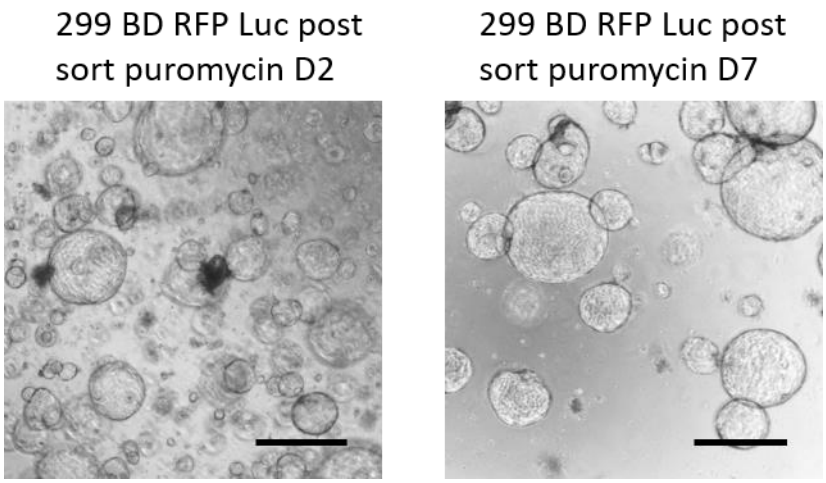

Figure 3.21: 299 BD RFP Luciferase COs treated with puromycin after cell sorting by flow cytometry
Brightfield images of 299 BD RFP Luciferase COs treated with 4 ng/ml puromycin at day two of puromycin treatment compared to day seven. Scale bar- 200 μm. Cell death (determined through morphological changes) can be seen at day two following puromycin treatment but the majority of cells remain healthy and proliferative.

Luciferase expression in 299 RFP Luciferase COs was tested *in vitro* and *in vivo* (figure 3.22). *In vitro* expression was compared against wild-type 299 COs and 299 COs transduced with a construct expressing GFP only. Each condition contained approximately 1.0×10^5 cells and the luciferin substrate was added at a concentration of 300 μg/ml, according to the recommendations of the plasmid manufacturer. 299 RFP Luciferase COs showed a strong luminescent signal while no signal was seen in wild-type or GFP control COs.

NSG mice were injected with approximately 5.0×10^5 299 RFP Luciferase COs and imaged 24 hours after transplantation. A clear luciferase signal was seen in one animal, while the CO graft was less visible in the other animal, possibly due to a technical error in the transplantation procedure preventing the full volume of cells from being delivered. Furthermore, luciferase activity was observed in 299 RFP Luciferase COs *in vitro* at passage 20, 18 passages after viral transduction (figure 3.23), demonstrating that the 299 RFP luciferase CO line is robust and viable long-term and that the luciferase construct is not silenced in vitro, even after several months. Work is currently ongoing to quantify the long-term luciferase expression in the 299 RFP luciferase CO line, to determine whether the luciferase signal intensity per cell decreases after long-term culture.

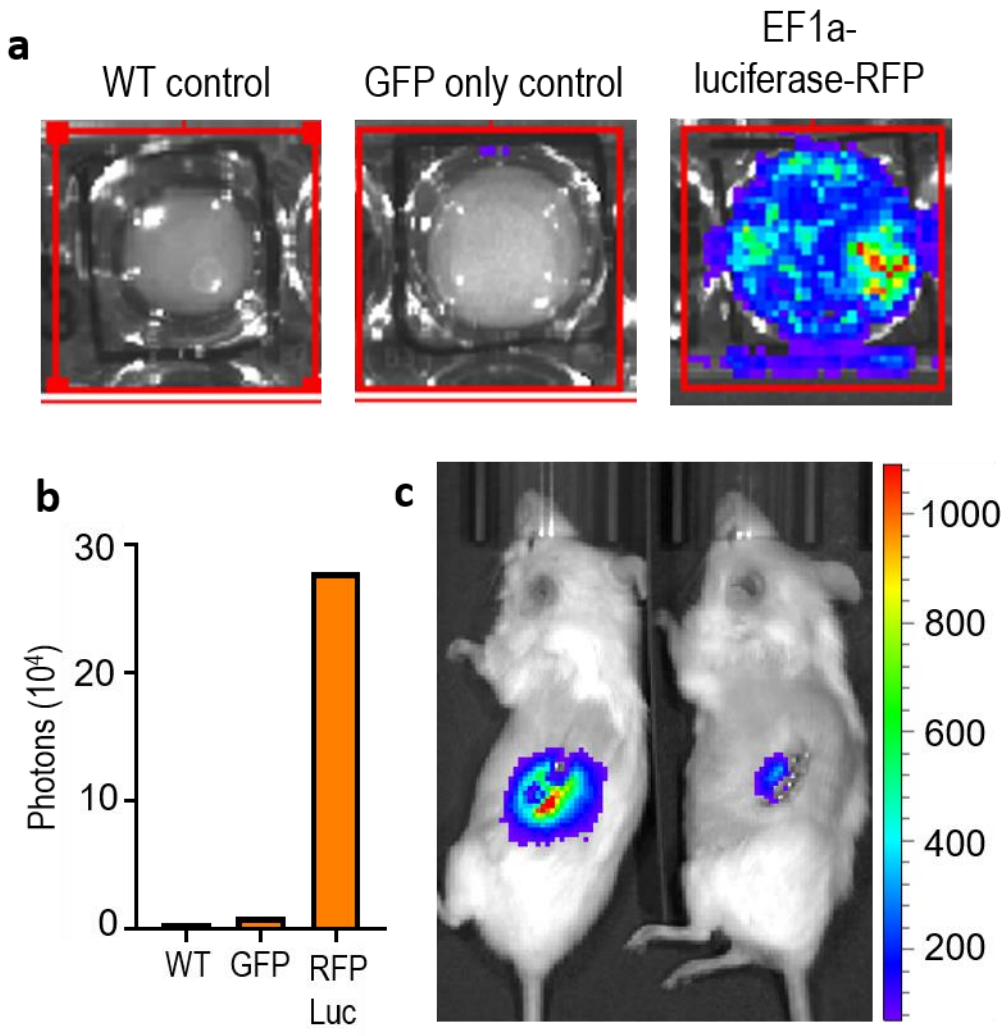

Figure 3.22: Luciferase activity in 299 BD RFP Luciferase COs *in vitro* and *in vivo*
(a) IVIS images of 299 BD COs transduced with the Ef1a-Luciferase-RFP LL420 construct compared to a 299 BD wild-type control and a 299 BD GFP-only control. (b) Luminescence intensity (photons) of the Ef1a-Luciferase-RFP LL420 construct compared to a 299 BD wild-type control and a 299 BD GFP-only control. (c) IVIS image of 5.0 x 10^5 299 BD RFP-Luc COs one day post-transplantation (automatic exposure time, measured in photons).

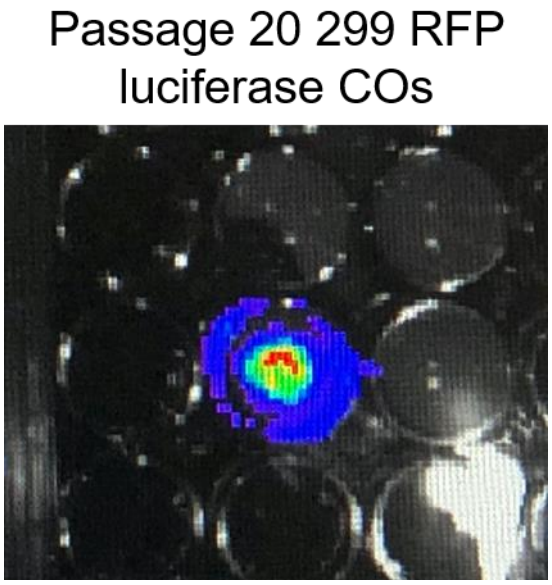

Figure 3.23: Luciferase activity persists long-term in vitro in 299 BD RFP Luciferase COs
IVIS image of 299 BD COs transduced with the Ef1a-Luciferase-RFP LL420 construct at passage 20, 18 passages after viral transduction, demonstrating persistent long-term expression of luciferase signal.

3.3 Discussion

Refinement of the cholangiocyte organoid protocol and establishment of new cholangiocyte organoid lines

In this chapter, the establishment of new CO lines and the refinements made to the CO protocol were described. I have demonstrated that I can successfully isolate and maintain new CO lines in accordance with our established extrahepatic CO protocol, with a derivation efficacy of 93% across all tissue types and methods of derivation. The most important factor in determining the success of a CO derivation appears to be the initial processing of the tissue, before CO derivation.

This was highlighted by the dramatic decrease in successful CO derivation in common bile ducts which have not been adequately flushed of bile compared to those which were thoroughly flushed. This is likely due to the toxicity of bile – cholangiocytes are normally protected against the toxic effects of bile, however due to the effects of ischaemia and lack of nutrients in an explanted bile duct, the metabolic activity of the explanted cholangiocytes is likely to be reduced, making them vulnerable to damage from bile. A similar loss of viable cholangiocytes was seen in gallbladders that had not been flushed, although due to the overall greater cell numbers in gallbladder compared to bile duct samples, this was much less likely to result in derivation failure. As my biliary tissue samples were primarily derived from deceased organ donors and were collected during an ongoing retrieval procedure by the transplant surgeons, there is a limit on how much control can be exerted over the tissue sampling process. As this is the case, it is important to ensure that CO lines are derived from biliary tissue as soon as possible after tissue collection.

I have also demonstrated that the extrahepatic CO protocol can be adapted for intrahepatic CO isolation and maintenance. My initial attempts at intrahepatic derivation, while able to produce CO lines, were not effective due to the low organoid numbers produced and the resulting slow expansion of the CO lines. This was likely due to the highly stressful processing methods required, particularly the filtration method, resulting in cholangiocyte cell death due to the disruption of cell-cell contact[240-242]. Additionally, as I initially tried ICO derivation from roughly cuboid pieces of liver, approximately $1cm^3$, there was likely a high amount of cell death within the tissue between the time of sampling and line derivation due to ischaemia, as the tissue was too large to allow oxygen and nutrients to adequately diffuse through it entirely. These factors likely greatly reduced the number of viable cholangiocytes within the tissue, meaning that a very small number of organoids were able to survive and proliferate, even from a relatively large amount of starting tissue. This highlights again the importance of collecting tissue samples for line derivation in the most optimal manner for cell survival, even when the tissue is processed as soon after collection as possible.

My final method resulted in much more effective CO line derivation, most likely due to two factors: a change in the tissue sampling method from whole tissue pieces to core needle biopsies (diameter 2.0 mm) and a less disruptive form of mechanical dissociation. Dicing the tissue with a scalpel resulted in tissue pieces <0.5 mm^3, small enough to be plated in organoid format and for media to diffuse through the tissue entirely, but large enough that many of the bile ducts within the tissue were left intact. Maintaining these tissue pieces in William's E+ media and our established CO cytokines allowed for the survival and proliferation of cholangiocytes while discouraging the survival of all other cell types within the tissue. As with our ECO derivation method, this results in a highly pure cholangiocyte population within a few passages.

A limitation of this method of ICO derivation is that it does not allow for the derivation of an ICO line from a single cell, which, while not necessary for this project, may be required for some experiments, such as tracking the development of mutations after the establishment of an organoid line. Hand-picking individual organoids, while possible with this method, is technically challenging and there is no guarantee that individual organoids were derived from a single cell, making them unsuitable for experiments requiring monoclonal lines. We have developed a separate protocol for isolating cholangiocytes as single cells from liver tissue through EpCAM+ sorting via MACS or FACS[125], however, this derivation method has a very low efficiency (appendix table 3) so we preferentially use the whole-tissue derivation method described in this chapter when single cell isolation is not required.

Refinement of the protocol for generating bioengineered biliary tissue

We have developed a protocol for generating bioengineered artificial bile ducts through seeding the luminal surface of a densified collagen construct with COs. The benefit of our new method for the generation of bioengineered biliary tissue is that it more accurately reflects the physiology of the native bile duct, with a monolayer of biliary epithelium lining the collagen tube rather than cholangiocyte organoids being embedded within the collagen walls. This is an improvement on previously published protocols for generating bioengineered biliary tissue, which relied either on the use of immortalised cell lines or on murine-derived organoids seeded on the outside of tubular scaffolds[243,244]

The main limit of the new seeding method is that it is technically challenging to perform and requires a high cell numbers due to the high proportion of cell death after the initial seeding. This typically happens due to the failure of a proportion of cells to attach to the scaffold combined with the effect of the prolonged drying time (30-60 minutes) required for cell adherence. Additionally, it is necessary to leave the seeded tube in culture for between 2-6 weeks (depending on the size of the tube and the initial number of cells) to allow for the formation of a complete monolayer. Work is ongoing by Teresa Brevini and Fotios Sampaziotis to further refine this technique and determine the optimum length of time for seeded tubes to remain in culture before transplantation.

Assessment of *in vivo* survival of CO lines

The survival of CO lines *in vivo* is essential for their clinical application, and failure to properly assess the *in vivo* survival capacity of particular CO lines can lead to significant experimental challenges (see chapter 5). I have demonstrated in this chapter that COs are able to survive and proliferate *in vivo* under the kidney capsule and retain expression of cholangiocyte markers. However, the extent of survival and proliferation is line-dependent and several CO lines did not survive after transplantation. There did not appear to be any correlation between the age (passage number) of the line and its ability to survive *in vivo*, nor was there any change in CO maintenance or transplantation technique between lines. Equally, donor-specific factors did not appear to be the cause, as lines showing poor or no survival (243, 261 and 286) were not from significantly older or younger donors than lines that engrafted well *in vivo*, nor were there any other noticeable differences between the two donor groups. There was not any notable difference in quality and proliferation rate *in vitro* of successful CO lines (*in vivo* survival) compared to unsuccessful CO lines. However, it is possible that there were differences in line quality which undetectable by morphological assessment alone. One strategy to address this would be to assess the quality of each CO line intended for transplantation through RT-qPCR assessment of expression of key cholangiocyte markers (e.g. CK19, CK7, Sox9, CFTR) compared to CO lines with high viability *in vivo*. Due to the unpredictable nature of CO survival *in vivo*, it is also important to test the survival of all CO lines *in vivo* in NSG mice before their use in immunogenicity experiments. Additionally, now that I have generated luciferase-expressing CO lines (figures 3.20 and 3.21), bioluminescent imaging can be used *in vivo* to track the survival and proliferation of CO grafts post-transplantation.

Generation of luciferase CO lines for *in vivo* imaging

In order to better monitor and quantify the survival of COs *in vivo*, I generated COs expressing the enzyme luciferase. This enabled me to perform bioluminescent imaging in live mice and to quantify CO graft growth or death during *in vivo* experiments, technique that is increasingly common in studies of allograft survival in humanised mice[175,221,239]. I used a lentiviral transduction system to introduce the luciferase construct into the cells. Lentiviral transduction has the limitations of requiring packaging of the transgene plasmid into viral particles and the risk of integration of viral DNA into the genome[245] and there has been recent developments in using other transfection methods such as lipofection and electroporation with primary-derived organoids[246-249]. However, as we had already established a method of lentiviral transduction in COs and have effectively generated GFP and RFP COs using this protocol, I felt it most efficient to continue using our established method of lentiviral transduction.

One limitation in the generation of luciferase CO lines is the requirement for the organoids to be dissociated into single cells before lentiviral transduction and again before FACS sorting to purify the

luciferase-positive population. As cholangiocytes are epithelial cells which naturally form a monolayer with tight junctions between cells, dissociation to single cells can result in a noticeable loss in cell viability. This is particularly true when the cells must remain in a single-cell suspension for a prolonged period of time, as is necessary during viral transduction and FACS sorting. Careful dissociation with an appropriate enzymatic dissociation solution (e.g. Accutase) and addition of DNase I during the dissociation process and ROCK inhibitor throughout dissociation and transduction/sorting can help improve viability but cannot prevent cell death entirely. For this reason, viral transduction and the generation of purified luciferase CO lines was limited to only very early passage CO lines (< P3) in order to maximise the chance of line survival and proliferation, both *in vitro* and *in vivo*.

An additional limitation of our current transduction method is the use of randomly integrated genetic constructs rather than targeting constructs to integrate into a safe genetic harbour such as the AAVS1 locus[250,251]. While this has the significant advantage of being quicker and less technically challenging than targeted integration, it risks disrupting the endogenous chromatin and potentially integrating into an existing gene, which could impact on cell behaviour or lead to malignant transformation[252,253]. Additionally, random integration into the genome increases the risk of the transgene(s) being silenced over time[254-256].

Taken together, these factors greatly increase the risk that expression of the transgene construct - in this case, luciferase and RFP - will eventually be lost, either due to out-competition of transduced cells by the wild-type population, or transgene silencing. It is likely that the loss of GFP expression and *in vivo* luciferase expression in our initial luciferase lines (378 and 312 GFP luciferase) was due to silencing of the CMV promoter, which is previously reported to be at risk of silencing when transduced into primary or primary-derived cells[257]. I attempted to mitigate this risk as much as possible in my second attempt at generating luciferase CO lines, through a stringent selection process of both FACS sorting and puromycin treatment and by choosing the Ef1a promoter, which is known to be stable and provide relatively strong expression in multiple cell types[258-261]. Work is ongoing to assess the stability of luciferase and RFP expression in my 299 RFP luciferase line, as well as to characterise the expression of typical CO markers in the 299 RFP luciferase line compared to the WT 299 line, to ensure the transduction has not negatively affected the health of the line.

Preliminary IVIS data demonstrates that the 299 RFP luciferase CO line retains luciferase activity at passage 20 (figure 3.23), however this activity has not been normalised to total cell number and so can only demonstrate that some degree of luciferase expression remains after long-term culture and cannot determine whether the level of luciferase activity has decreased compared to early passage 299 RFP luciferase COs. Additional experiments to assess the luciferase activity of 299 RFP luciferase CO line at multiple passages normalised to overall cell number is required to be confident that consistent luciferase expression is retained long-term. If the random integration strategy is demonstrated to have

negatively impacted cellular behaviour or survival, or if reliable long-term luciferase and RFP expression cannot be guaranteed, it may be necessary to develop luciferase CO lines using a targeted integration strategy for future experiments.

CHAPTER 4. ASSESSMENT OF THE ANTIGENICITY OF CHOLANGIOCYTE CELLULAR THERAPIES

4.1 Introduction

HLA class I and II are a group of highly polymorphic cell-surface molecules responsible for presenting antigen to cells of the immune system, primarily to T cells[262]. HLA class I molecules (HLA-A, HLA-B and HLA-C) are found on all nucleated cells and present endogenous antigen peptides to cytotoxic CD8+ T cells while HLA class II molecules (HLA-DR, HLA-DP and HLA-DQ) are found on the surface of antigen presenting cells (APCs) and present antigen from exogenous sources[262]. HLA class II is expressed constitutively on professional APCs- immune cells such as macrophages, dendritic cells and B cells- but can also be expressed on non-professional antigen presenting cells such as endothelial cells and many epithelial cell types[263,264], including cholangiocytes[26]. Transplantation of solid organs or cellular therapies can result in an inflammatory reaction[130], during which pro-inflammatory cytokines will be upregulated. Exposure of cholangiocyte cellular therapies to this inflammatory environment may result in the upregulation of immunogenic markers, including HLA molecules. As HLA is known to be the major determinant of immunogenicity in a transplantation setting[130], it is important to characterise the expression of HLA on COs in order to assess their likelihood of inducing an immune response in cases of allogeneic transplantation.

Interferon-γ (IFN-γ) is a pro-inflammatory cytokine produced by a range of immune cell types, most notably T cells and NK cells. IFN-γ is produced during a Th1 immune response, which is characterised by a highly pro-inflammatory environment and, in is involved in the clearance of bacterial and viral infections, as well as tumour cells[265]. In the case of transplantation, Th1 T cells are an important mediator of allograft rejection[130]. IFN-γ plays multiple roles during an immune response, most notably the activation of macrophages, however it is also responsible for upregulating expression of HLA class I and class II. IFN-γ is able to upregulate HLA class I on all nucleated cell types and HLA class II on antigen presenting cells and a variety of other cell types[266-268], including endothelial[269] and epithelial cells. HLA upregulation by IFN-γ is mediated by the JAK/STAT signalling pathway, which is initiated by the binding of IFN-γ to the dimeric IFN-γ receptor at the cell surface membrane. Phosphorylation of STAT1 results in the upregulation of the Interferon Regulatory Factor-1 (IRF-1) which induces HLA class I expression[270]. HLA class II expression is also mediated by the JAK/STAT pathway but requires the upregulation of the Class II Transactivator (CIITA)[271,272] which then activates HLA class II genes directly.

Exposure of primary cholangiocytes to the pro-inflammatory cytokines IFN-γ, IL-1 and TNF-α has been demonstrated to induce increased expression of adhesion molecules[273], as well as to increase expression of HLA class I and to induce *de novo* expression of HLA class II molecules[26]. Expression

of HLA class II on healthy intrahepatic cholangiocytes has also been reported[274]. While this effect has been primarily demonstrated *in vitro*, cholangiocytes from livers with PBC[274], PSC, GVHD and allograft rejection[25] have been shown to express HLA class II[275]. This has caused speculation that cholangiocytes may be able to act as APCs to CD4+ T cells - this may be unlikely, however, as it is still not clear whether cholangiocytes can express CD80 and CD86, even under inflammatory conditions. Cholangiocytes exposed to pro-inflammatory cytokines *in vitro* have not been shown to express CD80 or CD86[26,274], although cholangiocytes from patients with PBC have been found to express CD80 and CD86[24]. IFN-γ challenged intrahepatic cholangiocytes have been shown to be capable of presenting antigen to CD4+ T cells via HLA class II, however the cholangiocytes were incapable of inducing T-cell proliferation due to their lack of CD80/CD86[276]. Cholangiocytes have also been shown to constitutively express CD40 *in vitro*[26,277] and CD40 expression is upregulated by exposure to TNF-α and IFN-γ[26].

In this chapter I present the results of my assessment of the expression of HLA class I and II molecules in COs under both normal and pro-inflammatory conditions. I first investigated the expression of HLA in COs compared to primary cholangiocytes through *in vitro* challenge with IFN-γ. I then assessed the expression of HLA class II in COs under a range of more physiologically relevant pro-inflammatory conditions, both *in vivo* through transplantation in xenogenic immunocompetent mice and differing humanised mouse models and *in vitro* through co-culture with activated human lymphocytes.

4.2 Results

4.2.1 COs upregulate HLA class I and II in response to interferon-γ stimulation

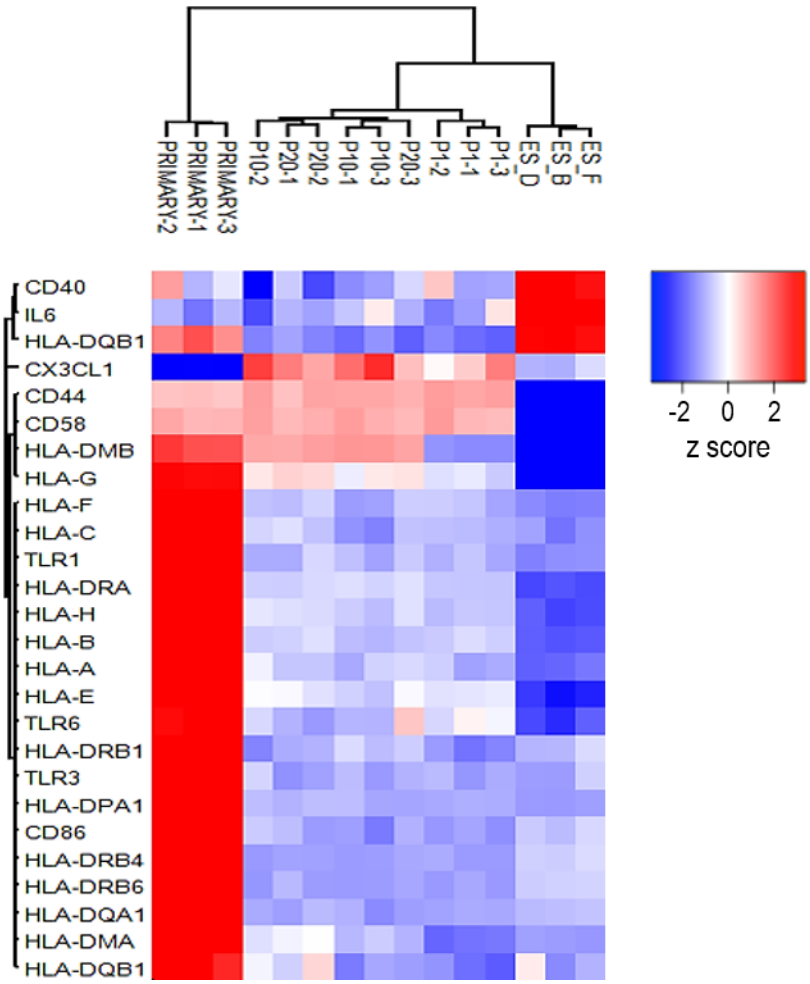

Figure 4.1: Downregulation of HLA molecules and other immune markers in COs compared to primary cholangiocytes
Bulk RNA-Seq analysis of primary cholangiocytes compared to COs at passage 1, passage 10 and passage 20 and embryonic stem cell controls (n=3 biological replicates).

RNA-Seq data provided by Fotios Sampaziotis.

Our previous characterisation of mRNA expression in COs compared to primary cholangiocytes had highlighted that expression of multiple immune markers was significantly downregulated in COs at early (P1), mid (P10) and late (P20) passages compared to primary cholangiocytes (figure 4.1). This included almost all HLA class I and II molecules. Given the importance of HLA molecules in immunogenicity during transplantation, I decided to focus primarily on the expression of HLA and related costimulatory molecules in CO culture and pro-inflammatory conditions. I initially tested HLA expression after stimulation with two pro-inflammatory cytokines, IFN-γ and IL-6 (appendix figure 3),

however, after no noticeable differences in expression of HLA or any other immune genes was seen after IL-6 treatment, I focused on challenging COs with IFN-γ in subsequent experiments.

COs from three different lines (passages 4-6) were treated with recombinant IFN-γ at a concentration of 100ng/ml for 72 hours and then harvested for qPCR (figure 4.2) or fixed for immunofluorescence (figure 4.3) along with untreated control COs from the same CO lines and passage number. RT-qPCR was performed on the IFN-γ treated and untreated CO samples along with primary cholangiocytes from the same donors. Primer functionality was validated using human splenocytes (appendix figure 3). All samples were run in technical duplicates. The expression of the HLA genes HLA-A, HLA-B, HLA-C, HLA-DR, HLA-DQ and HLA-DP and the costimulatory molecules CD80, CD86 and CD40 was quantified relative to the housekeeping gene HMBS. Primary cholangiocytes expressed HLA class I (HLA-A, B and C) and HLA-DR (HLA class II) at high levels, although there was high variability of expression between different donors. HLA-DQ and HLA-DP were expressed at low levels on primary cholangiocytes. Expression of HLA class I was significantly reduced for all three genes following CO culture while expression of HLA-DR was lost completely. HLA-DQ and HLA-DP were downregulated after CO culture but this decrease was not statistically significant, likely due to the comparatively low levels of expression in both the primary and untreated CO groups. Treatment with IFN-γ significantly increased expression of HLA class I and HLA-DR. HLA-A was upregulated to levels equivalent to primary cholangiocytes while HLA-B, C and DR were expressed at higher levels than in primary cholangiocytes. IFN-γ treatment had no effect on HLA-DP expression but was able to significantly upregulate HLA-DQ, although to a much lesser degree than HLA-DR and with a large degree of variability between lines.

I also investigated the expression of the co-stimulatory molecules CD80, CD86 and CD40. Primary cholangiocytes did not express CD80, while CD86 and CD40 were expressed at very low levels. IFN-γ treatment did not upregulate CD80 or CD86 and caused a modest but significant upregulation of CD40. Due to the low or completely lacking expression of costimulatory molecules on COs, I decided to focus further investigation on HLA expression alone.

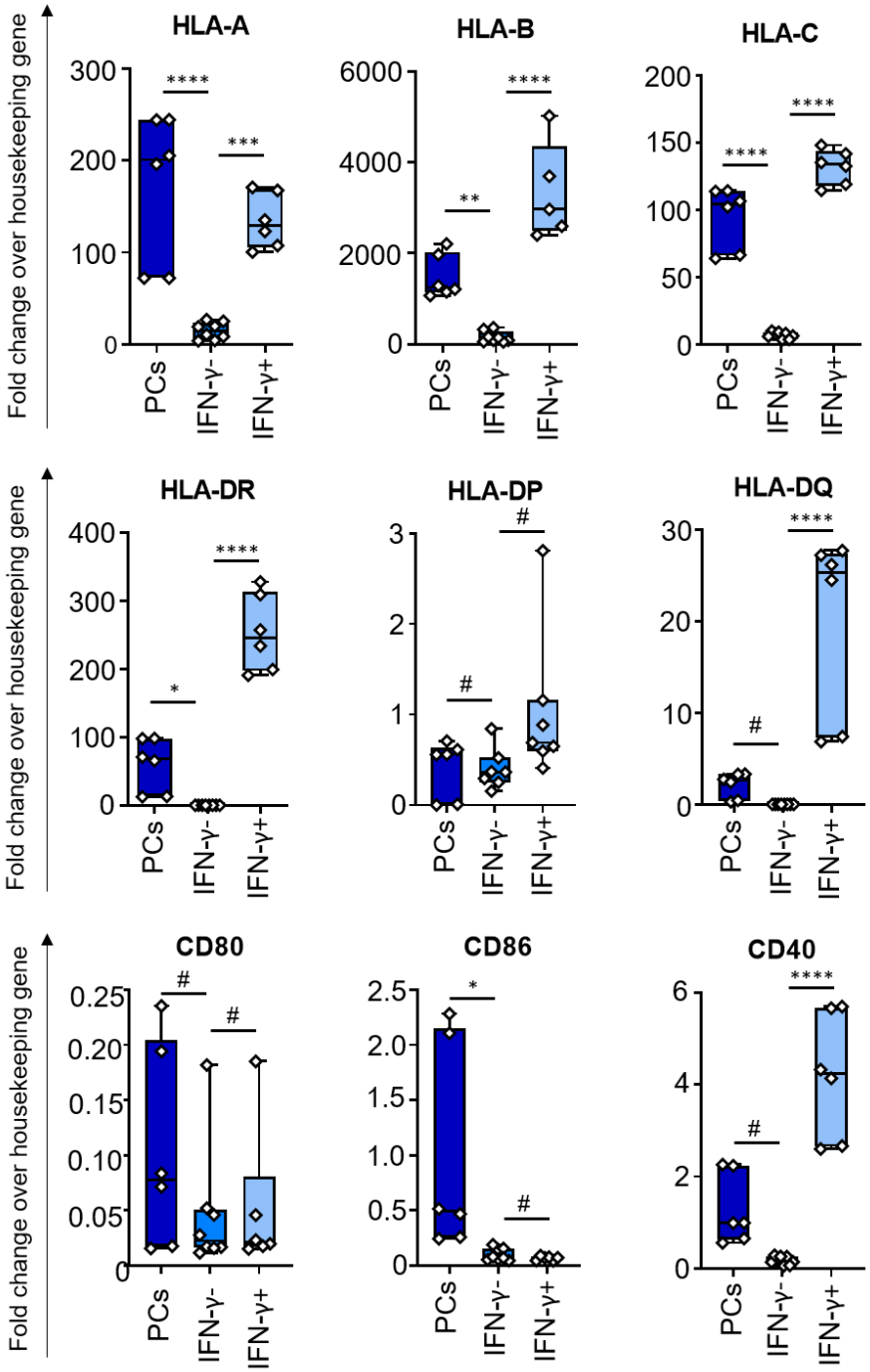

Figure 4.2: RT-qPCR expression of immunogenic markers in COs and primary cholangiocytes
(a) HLA class I (b) HLA class II and (c) co-stimulatory molecules in primary cholangiocytes (PCs) (3 biological replicates, 2 technical replicates) and interferon-γ-treated COs (3 biological replicates, 2 technical replicates*) compared against untreated COs (4 biological replicates, 2 technical replicates). *One technical replicate excluded from HLA B IFN-γ+ group due to a technical error). Centre line, median; box, interquartile range (IQR); whiskers, range (minimum to maximum). Values relative to the housekeeping gene HMBS. # P> 0.05; * P< 0.05; ** P< 0.01; *** P< 0.001; ****P<0.0001 (one-way ANOVA with Dunnett's multiple comparisons).

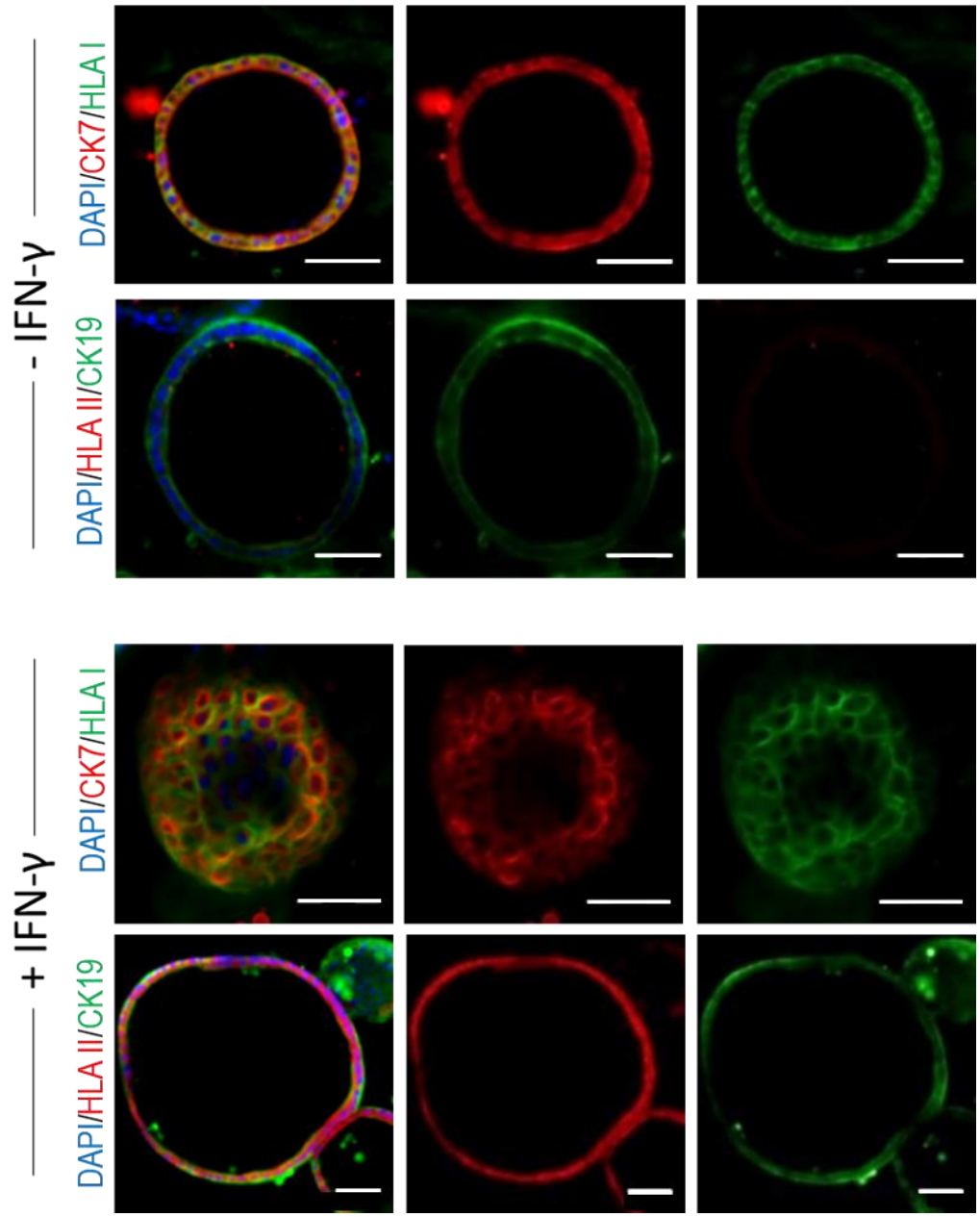

Figure 4.3: HLA expression in COs after IFN-γ treatment
Immunofluorescent images of HLA class I and class II expression in a representative CO line after treatment with 100ng/ml interferon-γ for 72 hours compared to untreated CO controls. Scale bar = 50μm. Untreated COs express HLA class I but not HLA class II while IFN-γ-treated COs express both HLA class I and II.

IFN-γ treated and untreated COs from the same experiment, as described in figure 4.2, were fixed for immunofluorescence and stained with pan HLA class I and II antibodies (figure 4.3). The untreated COs expressed HLA class I but not HLA class II while the IFN-γ treated COs expressed both HLA class I and class II, confirming the results shown by our RT-qPCR analyses.

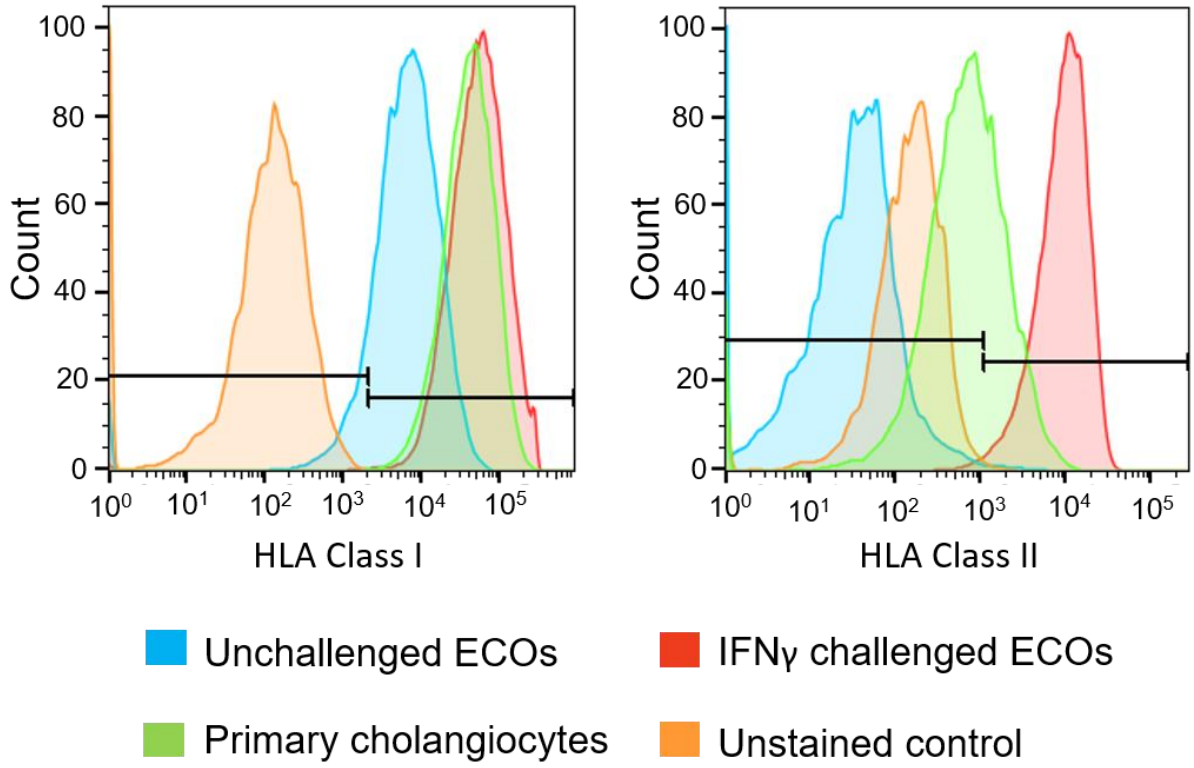

Figure 4.4: Flow cytometry histograms of HLA class I and class II expression in COs and primary cholangiocytes
(**a**) HLA class I expression and (**b**) HLA class II expression in primary cholangiocytes (green) compared to control COs (blue) and IFN-γ-treated COs (red) and an unstained control (yellow). Flow cytometry gating: $>10^3$ = positive expression $< 10^3$ = no expression. All populations shown are EpCAM+ (see appendix figure 4 for gating strategy). HLA class I expression is high in primary cholangiocytes and reduced in unchallenged COs. IFN-γ treatment restores HLA class I expression to levels equivalent to primary cholangiocytes. HLA class II is moderately expressed in primary cholangiocytes but not expressed in COs. IFN-γ treatment upregulated HLA class II expression to levels above primary cholangiocytes.

To confirm the RT-qPCR and IF results, primary cholangiocytes were fixed using 4% PFA as described in section (2.3.3.1) and stored at 4°C while an established CO line was challenged with IFN-γ as described for figures 2.2 and 2.3. The IFN-γ treated COs and matching untreated CO controls were fixed with 4% PFA and all samples were stained with EpCAM and pan-HLA class I and II antibodies and run concurrently on the flow cytometer. EpCAM staining was included in order to ensure the purity of the primary cholangiocyte population, as EpCAM is expressed on cholangiocytes but not leukocytes or other potentially contaminating cell types in the primary cholangiocyte population. In agreement with my RT-qPCR and IF data, HLA class I was expressed at high levels on primary cholangiocytes while untreated COs all expressed HLA class I but at lower levels than primary cholangiocytes. Treatment with IFN-γ restored HLA class I levels to equivalent to primary cholangiocytes. HLA class II was partially expressed on primary cholangiocytes and expression was lost on untreated COs. IFN-γ treatment upregulated HLA class II to levels above primary cholangiocytes.

These results were confirmed by using a total of four different CO lines and primary cholangiocyte samples (figure 4.5), all of which show consistent patterns of HLA class I and II protein expression in primary cholangiocytes and IFN-γ treated and untreated COs. Primary cholangiocytes consistently express HLA class I at levels near 100% of cells examined, while HLA class II expression was more variable across donors, being expressed by an average of 30% of all CO cells (figure 4.5a). Untreated COs express HLA class I at variable levels (figure 4.5b), with a mean expression of 82% of cells, while IFN-γ treatment upregulates expression to a mean expression of 98% of cells (not statistically significant). HLA class II was not expressed on untreated COs and IFN-γ treatment significantly upregulated HLA class II expression to a mean of 92.3% of cells.

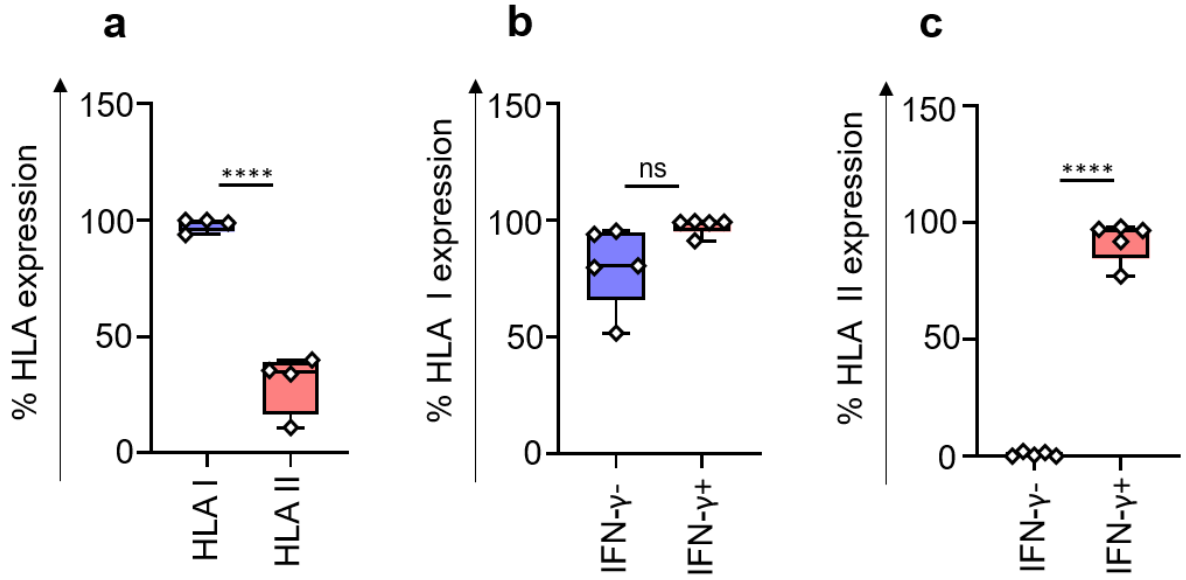

Figure 4.5: Graphs demonstrating HLA class I and II expression in multiple CO lines
(a) A graph showing the percentage of primary cholangiocytes expressing HLA class I and II as measured by flow cytometry (n= 4 biological replicates). Primary cholangiocytes consistently express high levels of HLA class I, while HLA class II expression is consistently lower and shows greater variability between donors. (b) A graph showing the percentage of IFN-γ-treated (100ng/ml, 72 hours) and untreated COs (multiple passages, all >P1) expressing HLA class I as measured by flow cytometry (n=5 biological replicates). Both IFN-γ-treated and untreated COs express high levels of HLA class I although untreated COs show greater variability between lines. (c) A graph showing the percentage of IFN-γ-treated and untreated COs (multiple passages, all >P1) expressing HLA class II as measured by flow cytometry (n=5 biological replicates). Untreated COs do not express HLA class II while IFN-γ-treated COs express HLA class II at high levels. # P> 0.05; **** P<0.0001 (two-tailed Student's t-test).

4.2.2 COs upregulate HLA class II under inflammatory conditions *in vivo*

After characterising the expression of HLA class I and II in COs after exposure to high levels of IFN-γ, I assessed HLA class II expression under more physiological pro-inflammatory conditions. This is important not only to confirm the relevance of the *in vitro* IFN-γ challenge experiments but also to

assess the level of HLA class II expression likely to be expected when transplanting CO cellular therapies or bioengineered biliary tissue using COs. To address, this, I transplanted 1.0 x 10^6 COs from established human CO lines under the kidney capsule of 5 different models: fully immunocompetent C57BL/6 mice (figures 2.6. and 2.7), allogeneic SpMC-reconstituted humanised mice (figure 4.8), allogeneic HSC-reconstituted humanised mice (figure 4.9), autologous SpMC-reconstituted humanised mice (figure 4.9) and autologous HSC-reconstituted mice (figure 4.10). All CO lines used within this experiment had previously been demonstrated to survive for a minimum of two weeks and a maximum of at least twelve weeks in naïve NSG mice. Work is currently ongoing to assess HLA class II levels on CO grafts in non-humanised NSG mice.

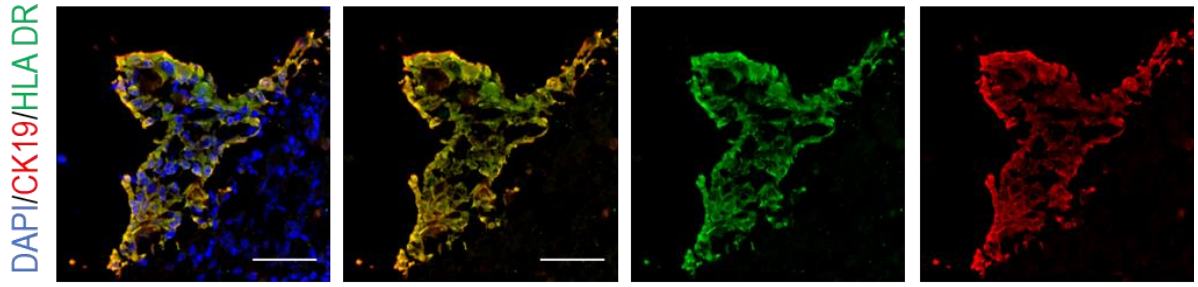

Figure 4.6: HLA class II expression in COs after xenogenic transplantation
Immunofluorescent images of COs transplanted under the kidney capsule of an immunocompetent C57BL/6 mouse stained with cytokeratin 19 (red) and HLA-DR (green). Image taken three days after transplantation. Scale bar = 50μm. COs upregulate HLA-DR in immunocompetent B6 mice.

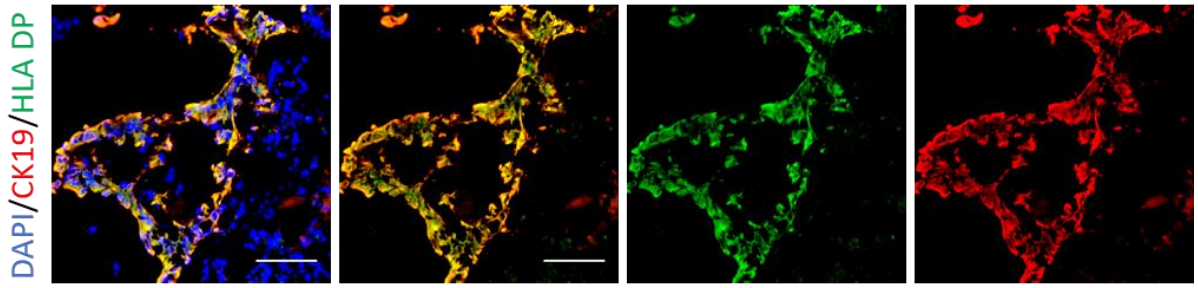

Figure 4.7: COs express HLA-DP after xenogenic transplantation
Immunofluorescent images of COs transplanted under the kidney capsule of an immunocompetent Cb57BL/6 mouse stained with cytokeratin 19 (red) and HLA-DP (green). Image taken three days after transplantation. Scale bar = 50μm. COs upregulate HLA-DP in immunocompetent B6 mice.

HLA-DR was clearly upregulated in fully immunocompetent C57BL/6 mice (figure 4.6), as was HLA-DP (figure 4.7). The level of HLA-DR expression in different humanised mouse models, however, is less clear. COs transplanted into allogeneic SpMC-reconstituted NSG mice show levels of HLA-DR staining above that of background (figure 4.8), however the staining is patchy and does not perfectly

match the graft, unlike the HLA-DR and HLA-DP staining seen in Black6 mice. HLA-DR staining on autologous SpMC-reconstituted (figure 4.10) and allogeneic HSC-reconstituted (figure 4.9) was even less pronounced, and likely represent background staining, while autologous HSC-reconstituted grafts showed no HLA-DR expression (figure 4.11). In confirmation of our earlier *in vitro* data showing consistent expression of HLA class I even without inflammatory stimulation, COs transplanted into non-humanised NSG mice clearly expressed HLA class I (figure 4.12).

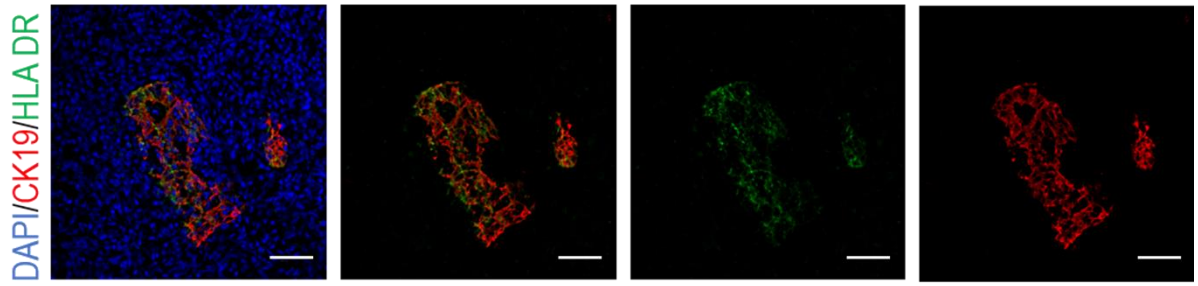

Figure 4.8: HLA-DR expression in allogeneic SpMC-reconstituted NSG mice
Immunofluorescent images of COs transplanted under the kidney capsule of an allogeneic SpMC-reconstituted NSG mouse, stained with cytokeratin 19 (red) and HLA-DR (green). Image taken 12 weeks after CO transplantation. Scale bar = 50μm.

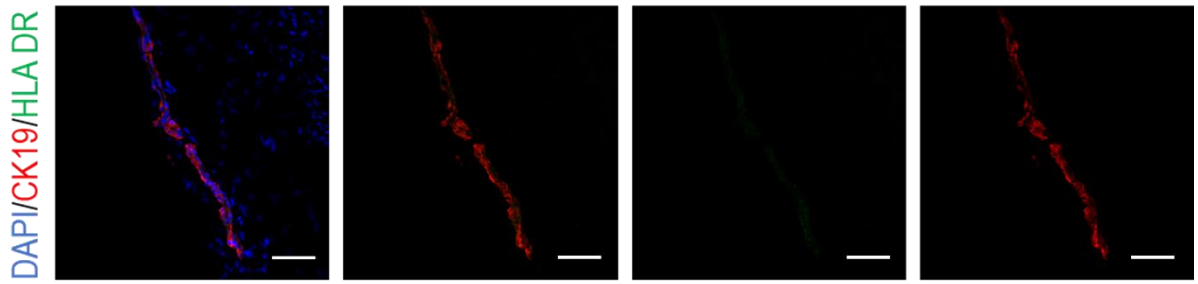

Figure 4.9: HLA-DR expression in allogeneic HSC-reconstituted NSG mice
Immunofluorescent images of COs transplanted under the kidney capsule of an allogeneic HSC-reconstituted stained with cytokeratin 19 (red) and HLA-DR (green). Image taken four weeks after CO transplantation. Scale bar = 50μm.

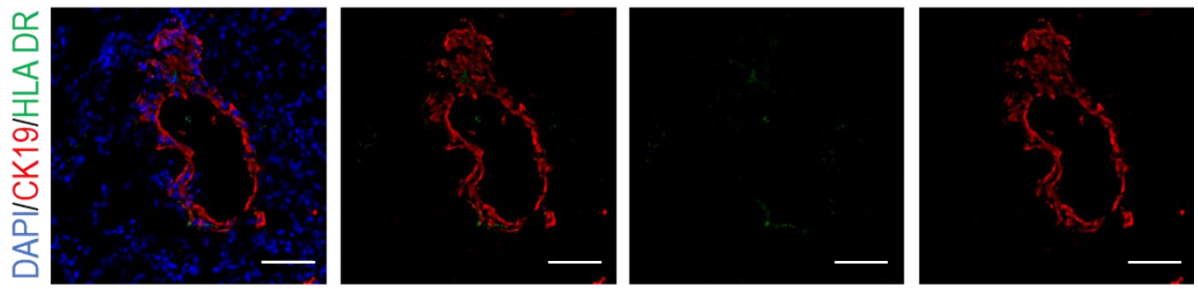

Figure 4.10: HLA-DR expression in autologous SpMC-reconstituted NSG mice
Immunofluorescent images of COs transplanted under the kidney capsule of an autologous SpMC-reconstituted NSG mouse, stained with cytokeratin 19 (red) and HLA-DR (green). Image taken two weeks after CO transplantation. Scale bar = 50μm.

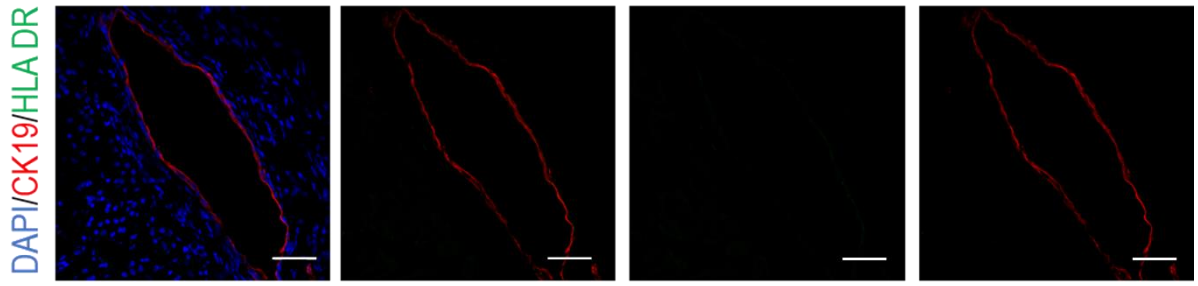

Figure 4.11: HLA-DR expression in autologous HSC-reconstituted NSG mice
Immunofluorescent images of COs transplanted under the kidney capsule of an autologous HSC-reconstituted NSG mouse, stained with cytokeratin 19 (red) and HLA-DR (green). Image taken four weeks after CO transplantation. Scale bar = 50μm.

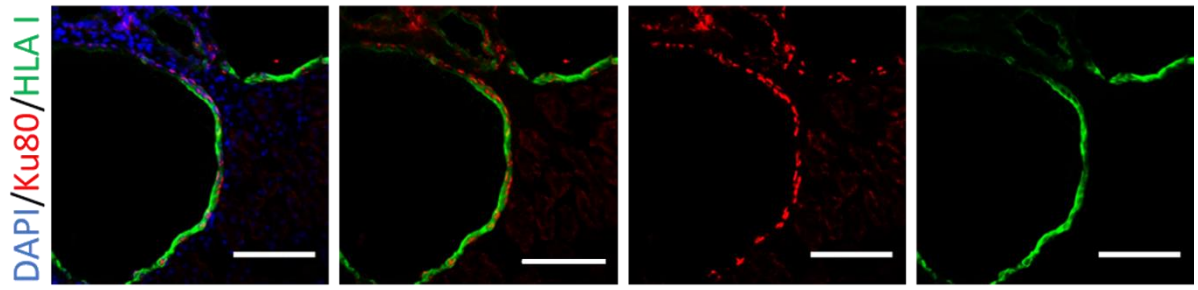

Figure 4.12: HLA class I expression in immunodeficient NSG mice
Immunofluorescent images of COs transplanted under the kidney capsule of a non-reconstituted NSG mouse, stained with the human-specific nuclear marker Ku80 (red) and pan-HLA class I (green). Image taken 10 weeks after CO transplantation. Scale bar = 100μm.

4.2.3 Activated PBMCs upregulate HLA class II expression on COs

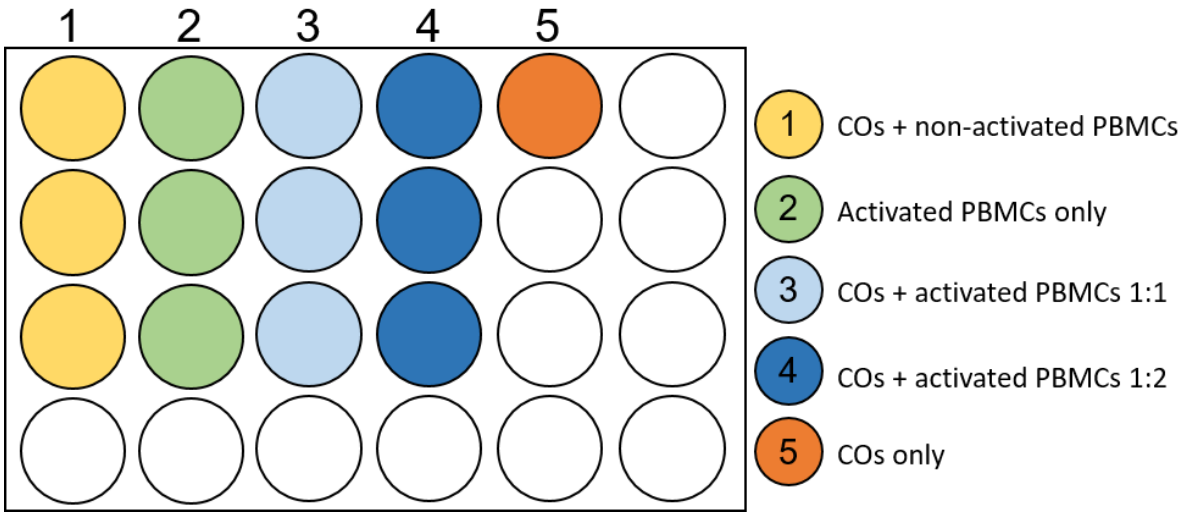

Figure 4.13: Schematic representation of the experimental design for the CO/PBMC co-culture experiment
Experimental design for the co-culture of COs and PBMCs showing the different co-culture groups in a 24 well plate. 1: 1.0 x 10^5 COs/1.0 x 10^5 PBMCs without activation; 2: 1.0 x 10^5 PBMCs with activation only; 3: 1.0 x 10^5 COs/1.0 x 10^5 PBMCs with activation; 4: 1.0 x 10^5 COs/2.0 x 10^5 PBMCs with activation; 5: 1.0 x 10^5 COs only.

I aimed to establish an *in vitro* system to model the interaction between activated lymphocytes and COs in order to determine whether the pro-inflammatory environment resulting from lymphocyte activation (in particular, the production of IFN-γ) was sufficient to cause HLA class II upregulation on COs. This system was established both in order to determine the extent of HLA upregulation on COs under more physiologically relevant concentrations of IFN-γ (in contrast to the super-physiological concentrations used in the IFN-γ challenge experiments described in figures 4.3 – 4.5), and in order to model the effect of a pro-inflammatory, cell-mediated alloimmune response on a CO allograft.

SpMCs were thawed from a liquid nitrogen cryobank as described in section 2.1.3.4 and plated in complete RPMI media a 24 well plate as shown in figure 4.13. SpMCs in groups 2, 3 and 4 were activated using CD3/CD28 dynabeads as described in section 2.1.3.5 and the plate was incubated at 37°C for 24 hours, at which point 100 µl of the supernatant was taken for ELISA and frozen at -20°C and COs were added to wells 1, 3, 4 and 5. The co-culture was incubated for 72 hours. A further 100 µl of supernatant was taken for ELISA and the cells were processed for flow cytometry and stained with 7AAD, CD45 (expressed on SpMCs but not on COs), EpCAM (expressed on COs, but not on SpMCs), pan-HLA class I and pan-HLA class II. All CO groups were from the same line (378 BD, passage 6) and all SpMC groups were from one donor (donor 312) which was allogeneic and fully HLA-mismatched with the CO line (as the CO lines and SpMCs are all from deceased organ donors, records of the HLA types were available for all donors).

HLA class I was expressed on 97% of COs in groups 1 (COs + non-activated SpMCs) and 5 (COs only) and this remained high at 99% on groups 3 (1:1 COs + activated PBMCs) and 4 (1:2 COs + activated SpMCs), however, this increase was not statistically significant (figure 4.14).

Expression of HLA class II, however, was impacted by SpMC co-culture. HLA class II expression on COs in group 5 (COs only) was close to 0 while COs in group 1 (COs + non-activated SpMCs) were at approximately 1% and group 3 (1:1 COs + activated SpMCs) approximately 3.5% (figure 4.14). The mean HLA class II expression in group 4 COs (1:2 COs + activated PBMCs) was 8%. Only this group showed a statistically significant increase in HLA class II expression ($p < 0.01$), however the overall trend showed a small but consistent increase in class II expression appearing to correlate with the presence of PBMCs, particularly activated PBMCs.

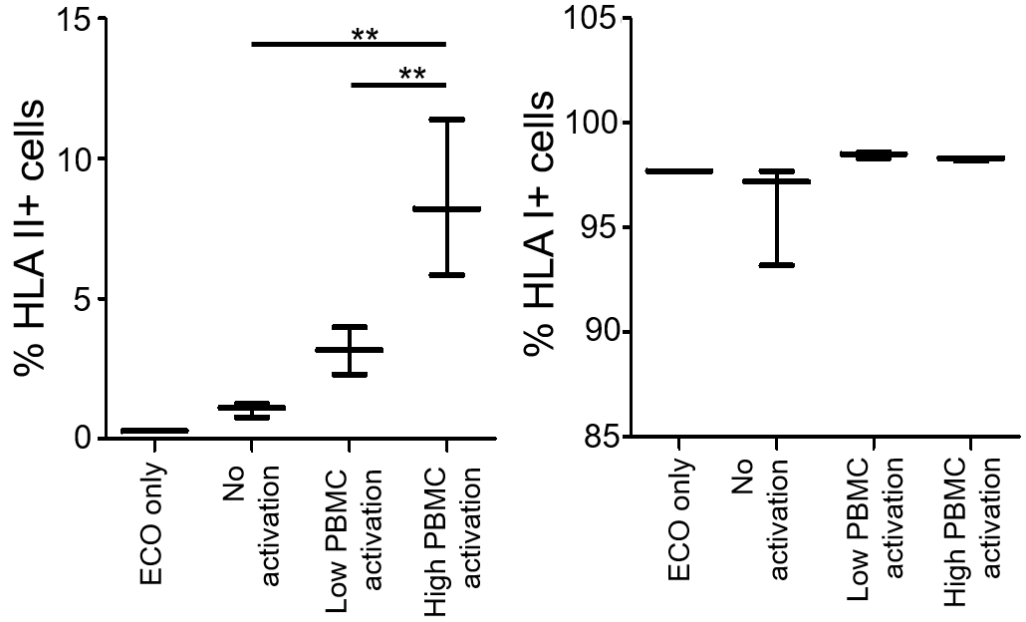

Figure 4.14: COs upregulate HLA class II after exposure to activated PBMCs
Percentage of HLA class II (left) and HLA class I (right) expressing CO cells, as measured by flow cytometry after 72 hours of co-culture with activated PBMCs. EpCAM+ cells shown only. ECO only- COs in suspension culture without any PBMCs; No activation- COs in a 1:1 co-culture with non-activated PBMCs; Low PBMC activation- COs in a 1:1 co-culture with activated PBMCs; High PBMC activation—COs in a 1:2 co-culture with activated PBMCs. (n = 3 biological replicates). **P < 0.01, one-way ANOVA with Tukey's multiple comparisons.

I assessed the levels of IFN-γ in the supernatant of each condition (with the exception of condition 5, COs only), at both 24 hours after activation and at 72 hours of co-culture (a total of 96 hours after activation) using ELISA (figure 4.15). Due to a technical error in the standard curve of the ELISA, it was not possible to calculate the absolute concentrations of IFN-γ in each group and the values given are in relative units. A non-substrate negative control and a positive control (recombinant IFN-γ at a

known dilution) was used to validate the values found in the non-standard samples. As expected, condition 1 (COs + non-activated PBMCs) did not express high levels of IFN-γ, either at 24 or 96 hours after the start of the experiment. All conditions with activated PBMCs resulted in low levels of IFN-γ at 24 hours, increasing significantly ($P < 0.0001$ for all groups) after a further 72 hours incubation. There was no significant difference between any of the conditions at 24 hours, except between C1 and C4 ($P < 0.05$). Out of all the conditions containing activated PBMCs, IFN-γ levels were highest in C4, which was significantly higher than both C2 and C3 ($P < 0.0001$) and lowest in C3, which was significantly lower than C2 and C4 ($P < 0.0001$).

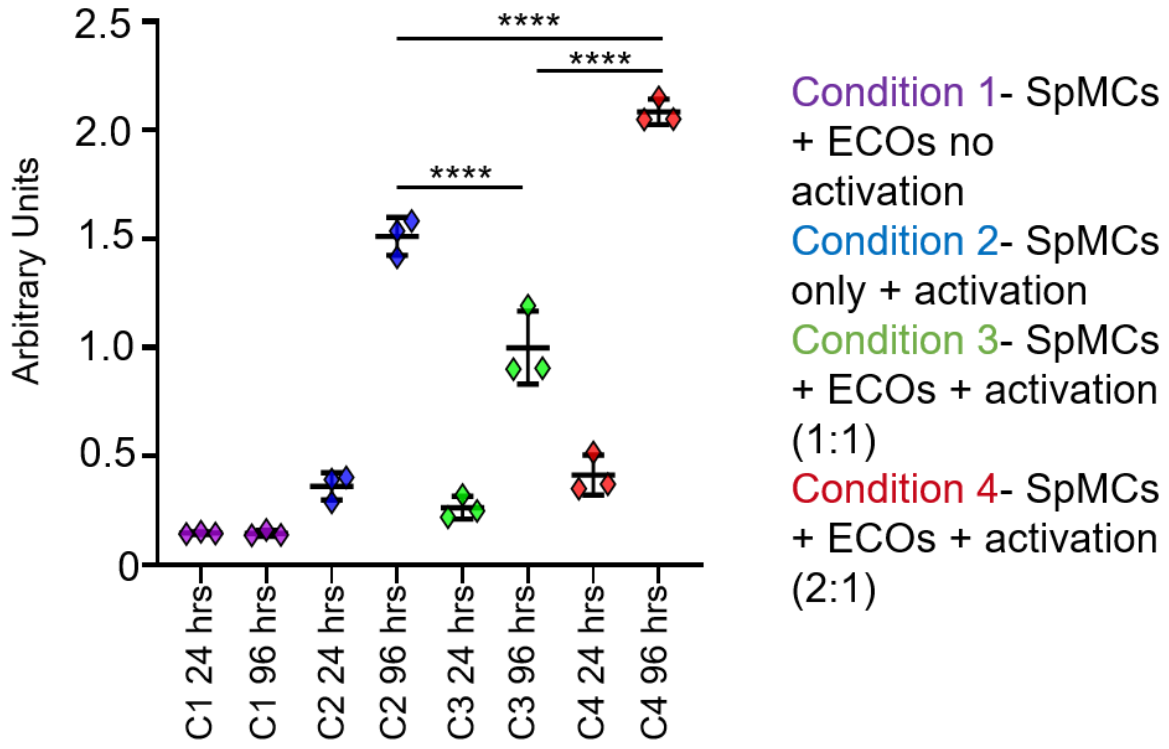

Figure 4.15: IFN-γ levels in CO/PBMC co-culture conditions, before and after co-culture
Levels of IFN-γ (relative units) as measured by ELISA in all co-culture conditions containing PBMCs. Samples taken for ELISA at 24 hours after activation and 96 hours after activation. (n = 3 biological replicates). **** $P < 0.0001$ one-way ANOVA with Tukey's multiple comparisons. C2, C3 and C4 24 vs 96 hrs all $P < 0.0001$ (significance bars omitted from graph for clarity).

4.3 Discussion

HLA expression *in vitro* after IFN-γ challenge

HLA class I and HLA class II was expressed on primary cholangiocytes and was shown to be downregulated following *in vitro* culture compared to primary cholangiocytes. This downregulation may be due to the lack of normal immune signalling from pro-inflammatory cytokines and other immune mediators that would be present *in vivo*, as well as the lack of exposure to bile and other antigens. Challenge with IFN-γ induced expression of HLA class I and II (HLA-DR and DQ but not HLA-DP) in COs to levels higher than primary cholangiocytes, which agrees with established reports that IFN-γ upregulates HLA class I and causes expression of HLA class II on many cell types, including intrahepatic cholangiocytes[26,266-268]. My RT-qPCR analyses showed that the HLA class II HLA-DR was most significantly upregulated both in primary tissue and in COs after IFN-γ challenge. This is in keeping with the established research on HLA class II expression in non-APC cell types, which also shows a dominance of HLA-DR expression over HLA-DP or DQ[266,268,269].

This is the first time, to my knowledge, that the immune profile of extrahepatic cholangiocytes, either cultured or primary, and their response to inflammatory cytokines has been studied. My cytokine challenge experiments also have the advantage of being performed on a novel cholangiocyte culture system that encourages the formation of ductal organoids. This represents a more physiologically relevant culture system than the monolayer systems used in previous studies. This cytokine challenge method is limited as it only exposes the cells to one pro-inflammatory cytokine at a time, in a concentration that is not reflective of physiological conditions. It is nonetheless an informative approach, as it allows preliminary comparison of the immune profile of COs with their primary cell type. My *in vitro* IFN-γ challenge experiments provide an initial starting point for investigation of the alloimmune response to cellular therapies as they provide an indication of how a pro-inflammatory environment can change the cells' phenotype and inform design of more complex *in vitro* or *in vivo* studies.

A limitation of my characterisation of HLA expression on primary cholangiocytes is that the primary tissue is isolated from deceased organ donors, both DBD and DCD, and it is highly likely that these donors will be undergoing a systemic inflammatory process, potentially resulting in upregulation of HLA class I and II to levels not typically seen within healthy individuals. Expression of HLA class II has been reported on primary cholangiocytes, however this finding is not consistent and reports differ on whether healthy primary cholangiocytes typically express HLA class II[24,26,275]. It is therefore possible that the present finding that HLA class II is upregulated on primary cholangiocytes is influenced by the systemic inflammation in the tissue donors. Due to the requirement to match the primary cholangiocyte donors with their corresponding CO lines (all of which were derived from deceased donors) whenever possible, it was not possible to avoid this limitation in this current study. However, I plan to gain access

to primary biliary tissue from living donors (e.g. patients undergoing a cholestectomy) and to compare the expression of HLA class I and II in these samples to the primary cholangiocyte samples from deceased donors to confirm the validity of my initial finding.

An additional limitation of my primary cholangiocyte data is that there was no reasonable way to purify the primary cholangiocyte samples when collecting RNA for RT-qPCR analysis, as MACS or FACS sorting would have detrimentally impacted the viability and yield of the cholangiocyte population. While flow cytometric analysis of the extrahepatic primary cholangiocyte populations demonstrates that my isolation method yields a >90% pure cholangiocyte population, the remaining <10% are comprised mostly of PBMCs (data not shown), which typically express high levels of HLA class I and II and other immune markers, and so may impact on the RT-qPCR results seen for the primary cholangiocytes. My flow cytometric analyses on EpCAM+ gated primary cholangiocytes demonstrated that primary cholangiocytes do express HLA class II, validating the RT-qPCR data. However, it cannot confirm whether the relative quantification of HLA class II expression shown by RT-qPCR is accurate, or if the values are artificially elevated by lymphocyte contamination in the primary RNA samples.

A limitation of my IFN-γ challenge experiments is that the concentration of IFN-γ used is super-physiological and the degree of upregulation of HLA class I and II seen in these *in vitro* experiments may not reflect the phhysiological levels of HLA expression seen *in vivo* in a pro-inflammatory environment. To address this limitation, I tested HLA expression *in vivo* under a variety of pro-inflammatory conditions. I focussed in particular on HLA class II expression as this was not detected in COs under normal culture conditions, whereas COs consistently expressed HLA class I, both *in vitro* and *in vivo* when transplanted into non-humanised NSG mice.

HLA class II expression *in vivo*

I demonstrated that COs transplanted into immunocompetent mice were able to significantly upregulate HLA class II, likely due to the highly pro-inflammatory response that occurs during xenogenic graft rejection. Interestingly, in addition to upregulation of HLA-DR (consistent with *in vitro* IFN-γ challenge data), I detected upregulation of HLA-DP *in vivo*; This was not detected in the *in vitro* IFN-γ challenge assays, suggesting that other factor(s) may influence the expression of HLA-DP. My earliest cytokine challenge experiments with the cytokines IFN-γ, TNF-α, IL-6 and TGF-β (data not shown) did not detected cytokines other than IFN-γ as able to induce HLA class II expression on COs. However, it may be that a combination of cytokines present during an *in vivo* immune response is required to upregulate HLA-DP expression, rather than any single factor, as previously shown in other cell types for HLA class II expression overall[278]. Additionally, HLA-DP is known to have allelic variation leading to either high or low HLA-DP expression, which is correlated with greater or lesser susceptibility to conditions such as GVHD and Hepatitis B. It is possible that the CO line in these *in vivo* experiments

in immunocompetent mice carried the allelic variant of HLA-DP responsible for higher expression and as such was able to express HLA-DP upon exposure to IFN-γ while other CO lines carried the allele for low expression and so did not express HLA-DP even after exposure to high levels of IFN-γ. In order to test this possibility, further *in vivo* experiments should be complemented by RT-qPCR analyses of HLA expression in the specific CO lines used *in vivo after in vitro* IFN-γ challenge.

HLA class II expression on CO grafts in humanised mice was less definitive. While allogeneic humanised mice appear to show some HLA class II staining above the level of background, the staining is patchy and variable, while autologous humanised mice do not appear to express HLA class II. Work is ongoing to confirm if this potential expression in allogeneic humanised mice is consistent. Alternative methods may be needed to assess HLA class II expression, such as flow cytometry, which is able to give a quantitative assessment of varying expression levels. Quantitative assessment of marker expression would also allow for a more complete assessment of HLA class I expression, which is present on COs transplanted into naïve immunocompromised NSG mice (figure 4.12) but may be upregulated in humanised and immunocompetent mice, which is not readily established through qualitative assessment methods such as immunofluorescence.

A lack of HLA class II expression on grafts in humanised mice is not surprising, as it is well established that the humanised mouse model, either HSC or PBMC/SpMC-reconstituted, does not fully recapitulate all features of the immunocompetent human immune system[135] (see chapter 5) and so the pro-inflammatory response may not be as strong or as complete as that seen in a xenogenic model or an immunocompetent human. In addition to assessing the expression of HLA class II on the CO allograft, determining the extent of the systemic pro-inflammatory response post-transplantation through serum ELISAs for pro-inflammatory cytokines such as IFN-γ and IL-6 would also be informative. Comparison of the serum levels of pro-inflammatory cytokines of each mouse model (immunocompetent, SpMC-humanised, HSC-humanised and immunodeficient) with CO transplantation, Matrigel-only transplantation and no transplantation would determine the extent to which CO allografts are able to induce a pro-inflammatory response above the baseline level of inflammation induced by transplantation alone.

HLA class II expression after co-culture with activated lymphocytes

My initial co-culture experiment with COs and PBMCs demonstrated no statistically significant increase in HLA class I expression between any of the conditions. This is in keeping with my earlier flow cytometric data, which showed that several CO lines express HLA class I on close to 100% of cells. While IFN-γ stimulation can increase the overall intensity of HLA class I expression (figure 4.3), it will not greatly increase the proportion of cells expressing HLA class I, as that is already very close to the maximum.

Expression of HLA class II, however, did increase in a manner that appeared to be dose-dependent upon the number and activation status of the PBMCs in co-culture. While only the difference in the percentage of HLA class II-expressing cells was statistically significant between conditions 3 (1:1 COs + activated PBMCs) and 4 (1:2 CO + activated PBMCs), the overall trend appeared to be that the presence of activated PBMCs caused an increase in HLA class II expression compared to non-activated PBMCs, which in turn caused an increase in HLA class II expression compared to no PBMCs.

I also measured the levels of IFN-γ in the supernatant of the different conditions, both at the start of co-culture (24 hours after activation) and after 72 hours of co-culture (96 hours of co-culture). COs were added 24 hours after activation to ensure that all PBMCs were activated at the beginning of co-culture and co-culture was maintained for 72 hours to match the 72 hour time course of my earlier IFN-γ challenge experiments (figures 2.2-2.5) and to ensure that the COs had sufficient time to fully upregulate HLA class I and II. IFN-γ levels were measured both to confirm that the PBMCs had been successfully activated and to investigate whether or not any observed upregulation of HLA class II on COs correlated to an increased quantity of IFN-γ produced by the PBMCs.

My IFN-γ ELISA showed that all conditions containing activated PBMCs had significantly ($P < 0.0001$) increased levels of IFN-γ at 96 hours post-activation compared to 24 hours, confirming that activation had been successful. Levels of IFN-γ at 96 hours were highest in condition 4, which was also the condition that showed the greatest upregulation of HLA class II on COs. This finding complements a previous report[269] showing that epithelial cells exposed to the supernatant of activated PBMCs were able to upregulate HLA class II due to the IFN-γ released by the activated PBMCs. The correlation between HLA class II expression and IFN-γ levels at 96 hours was not exact, however, as C2 (activated PBMCs only) had significantly ($P < 0.0001$) higher levels of IFN-γ than C3 (1:1 COs + activated PBMCs). Further work is needed to validate and investigate this finding, however one potential explanation could be that the levels of IFN-γ in the supernatant of C3 wells is lower as some proportion of the IFN-γ has bound to IFN-γ receptors on the COs.

This was only a preliminary experiment, however, and requires repeating to confirm the results shown here. This work is currently ongoing. Further experimental groups of higher PBMC numbers (e.g. 1:4 COs:PBMCs and 1:8 COs:PBMCs) will be added to confirm the apparent dose-dependent relationship between activated PBMC ratio and CO HLA class II expression. Additionally, a CO-only group treated with recombinant IFN-γ will be added to the experiment as a positive control and to compare the percentage of HLA class II expression seen after PBMC co-culture with the levels shown by our earlier IFN-γ challenge assays. The activation status of the PBMCs will be confirmed through flow cytometric analysis of activation markers such as CD25 as well as IFN-γ production. Additionally, a limitation of this initial experimental set up was that the PBMCs were added without determining the proportion of T cells to other PBMC cell types. Only T cells are able to be stimulated by CD3/CD28 activation beads

and to resultantly produce IFN-γ, so if some groups contained greater proportions of other PBMC types (e.g. B cells), this could have affected the results. For that reason, future co-culture experiments will assess the proportion of T cells to other PBMCs in each condition, and, if judged necessary, remove other cell types through MACS sorting.

These results demonstrate the COs are capable of upregulating HLA class II (specifically, HLA-DR and possibly HLA-DP), not only after super-physiological stimulation with IFN-γ but also after exposure to physiologically relevant pro-inflammatory environments. This suggests that COs or CO-derived therapies would upregulate HLA class II after transplantation into an immunocompetent patient. This would be likely to exacerbate the immune response against a CO allograft as the recipient's immune system would respond to both the HLA class I and class II molecules presented on the CO graft. The high levels of both HLA class I and II on COs exposed to a pro-inflammatory setting suggests that immunosuppression is likely to be required after transplantation, and that HLA matching at HLA-DR and DP (as well as on HLA class I loci) may be beneficial to graft survival.

CHAPTER 5: ASSESSMENT OF THE IMMUNOGENICITY OF CHOLANGIOCYTE ORGANOIDS

5.1 introduction

Thorough assessment of the immunogenicity of potential cellular therapies is essential before these therapies can be utilised in a clinical setting. Due to the logistical and financial challenges of generating autologous cellular therapies for each patient, it is highly likely that future cellular therapies will originate from allogeneic donors. Therefore it is important to assess the extent to which an allogeneic human immune system would respond to a transplanted cellular therapy, and whether interventions to ameliorate immunogenicity, such as immunosuppression, HLA matching or gene editing to remove HLA, would be effective.

Humanised mouse models are an important tool for studying the immunogenicity of cellular therapies in the context of a human immune system. Humanised mice are defined as severely immunodeficient mice that have been reconstituted with human immune cells, either haematopoietic stem cells or adult leukocytes, to recapitulate key features of the human immune system[135]. There are currently three types of humanised mouse model: the Hu-BLT model, which reconstitutes mice with foetal bone marrow, liver and thymus; the Hu-SRC model, which reconstitutes mice with HSCs from adult or neonatal donors and the Hu-PBL model, which reconstitutes mice with human peripheral blood leukocytes from adult donors[135]. SpMCs can also be used in place of peripheral blood leukocytes in this model.

Within the Saeb-Parsy group, we utilise Hu-SRC and Hu-PBL mice (described from this point on as HSC-reconstituted and SpMC-reconstituted) to assess the immunogenicity of cellular therapies as these two models allow for concurrent derivation of organoid lines from autologous donor tissue to serve as autologous controls. These models are complementary to each other, with both having strengths and limitations. The SpMC-reconstituted model elicits a strong CD3+ T cell response that can effectively reject allogeneic grafts, however successful engraftment inevitably leads to a strong GVHD response that can confound interpretation of the immune response[135]. Additionally, the engraftment of immune cells other than T cells is not well supported in this model, with B cells surviving only in the spleen and other cell types such as macrophages and NK cells not surviving at all[205,279].

Conversely, the HSC-reconstituted model can support the engraftment of a wider variety of human immune cells, including B cells, NK cells and macrophages and rarely develops GVHD within the time frame of a typical experiment[279], as the human T cells are educated on murine thymic epithelial cells. However, many of the cell types produced in this model are immature or not fully functional[135]. This reduced functionality is due to a variety of factors, mainly stemming from the inability of the murine environment to support the differentiation of human leukocytes and the lack of adequate lymphoid

structures within immunodeficient mice. Many cytokines required for the survival and differentiation of human HSCs, such as GM-CSF (required for myeloid cell differentiation) and IL-15 (required for NK cell differentiation), are not compatible between human and murine cells, reducing the ability of such cell types to adequately differentiate and mature within an HSC-reconstituted humanised mouse system. Dendritic cells (DCs) are among the leukocyte subtypes that fail to adequately mature within humanised mice and this impacts on the functionality of the adaptive immune system, as DCs are required for effective antigen presentation to CD4+ T cells and costimulatory activation of B cells through CD40L. The lack of human HLA molecules on thymic epithelial cells can also reduce the effectiveness of the T cell response as human T cells are incapable of recognising and mounting a response to HLA-restricted human antigens. Furthermore, immunodeficient mouse strains such as NSG and NOG mice lack adequately developed secondary lymphoid structures such as lymph nodes and splenic germinal centres, which are important for T cell maturation, B cell class switching and the development of antigen-specific antibodies.

Additionally, the ability of this model to reject allogeneic grafts is variable and highly dependent on the strain of immunocompetent mouse used, the age of the mice at reconstitution and the source of the reconstituting human HSCs[135,280,281]. Only the most immunodeficient strains available, such as NSG or NOG mice are capable of adequate reconstitution with human HSCs, with younger mice (particularly neonates) and females tending to engraft more effectively. Additionally, human HSCs from cord blood or foetal tissue are typically more effective than adult HSCs from sources such as bone marrow.

It is likely that allogeneic cellular therapies will elicit an immune response in patients, necessitating interventions to prevent graft rejection. Immunosuppression is highly effective in preventing graft rejection in solid organ transplantation, however long-term immunosuppression can have significant negative side-effects[158-160] and so alternative strategies are also being explored for cellular therapies. One promising option is the generation of gene-edited "universal" cellular therapies that do not express HLA class I, and this option is being widely explored[172,175,282,283]. Gene editing, however, is likely to be costly, time-consuming and carries the potential risk of off-target effects and other safety implications[284,285].

Another strategy is the generation of banks of cellular therapies to allow for HLA matching of donor and recipient. HLA matching is known to be effective at improving graft survival of the majority of solid organs after allogeneic transplantation, and several studies have suggested that HLA matching may reduce the immunogenicity of allogeneic cellular therapies[167,168,170], although this is still uncertain[286]. Therefore HLA-matching is a potential strategy for reducing the immunogenicity of allogeneic CO grafts. The role of HLA matching in liver transplantation is controversial- HLA matching is generally considered to not affect liver transplantation outcomes[154,155], however multiple reports suggest that HLA matching may increase the likelihood of developing operational tolerance[287-289].

Additionally, others have found an association between HLA class I mismatch and the development of vanishing bile duct syndrome[290], or shown HLA-A matching to be positively associated with ten-year graft survival[291].

In this chapter, I present the results of my assessment of the immunogenicity of CO grafts in SpMC-reconstituted and HSC-reconstituted humanised mice. I assess the capacity of the SpMC-reconstituted and HSC-reconstituted humanised mouse models to reject allogeneic grafts and compare the response to autologous and allogeneic CO grafts in both models. I describe the refinements I have made to the humanised mouse models through the use of bioluminescent imaging (BLI) and present preliminary data on the impact of HLA-matching on the immune response to allogeneic CO grafts in an HSC-reconstituted humanised mouse model.

5.2 Results

5.2.1 Development of the SpMC-reconstituted humanised mouse model

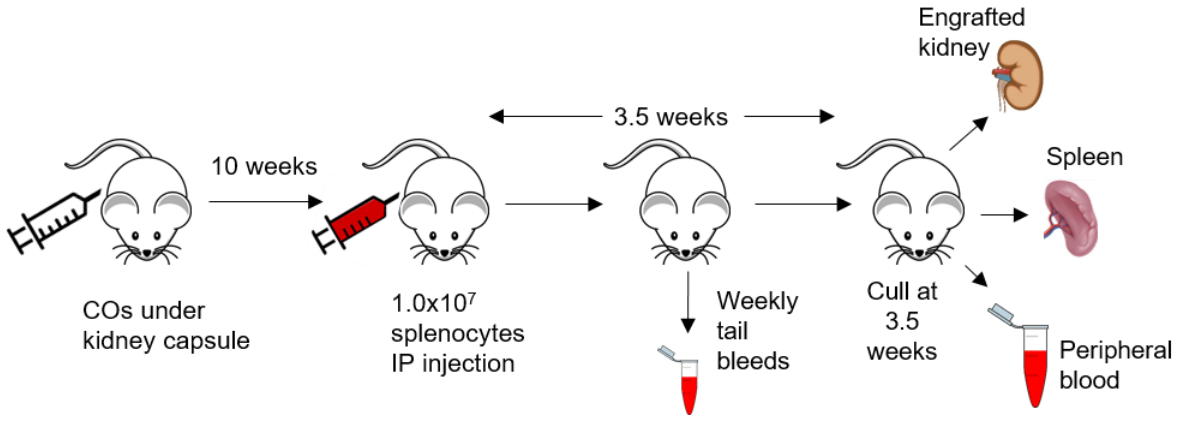

Figure 5.1: Schematic representation of the initial SpMC-reconstituted humanised mouse model Schematic demonstrating the timetable and key steps of the initial SpMC-reconstituted humanised mouse model. Steps in order (left to right): transplantation of organoids under the kidney capsule of naïve NSG mice; reconstitution with adult SpMCs (splenocytes) via intraperitoneal (IP) injection; weekly monitoring of engraftment; final cull and harvesting of the graft and immune tissues.

Three NSG mice were transplanted with 1.0 x 10^6 COs from donor 200 under the capsule of the left kidney and reconstituted 10 weeks later with 1.0 x 10^7 allogeneic splenocytes (SpMCs) from donor 150 via intraperitoneal (IP) injection (figure 5.1). Three non-humanised NSG mice were simultaneously transplanted with 1.0 x 10^6 COs from donor 200 and culled at ten weeks after transplantation. Tail bleeds were performed every week on the SpMC-reconstituted mice and the PBMCs analysed by flow cytometry to monitor engraftment with human leukocytes (figure 5.2). The SpMC-reconstituted mice showed rapid engraftment with human leukocytes after the first week, with only minor variation in engraftment between individual animals. The human CD45+ cell engraftment was almost entirely composed of CD3+ T cells, with almost no CD19+ B cell presence in the peripheral blood (figure 5.3). The majority of T cells in the peripheral blood were CD4+, although proportions of CD4+ and CD8+ T cells varied slightly at each time point. The mice were culled at 3.5 weeks when the proportion of human CD45+ cells in the peripheral blood reached 60%. Peripheral blood and spleen were taken for flow cytometric analysis and the kidneys, both the CO-transplanted left kidney and the control right kidney, were taken for cryosectioning and immunofluorescence imaging, along with the kidneys from the non-humanised control NSG mice.

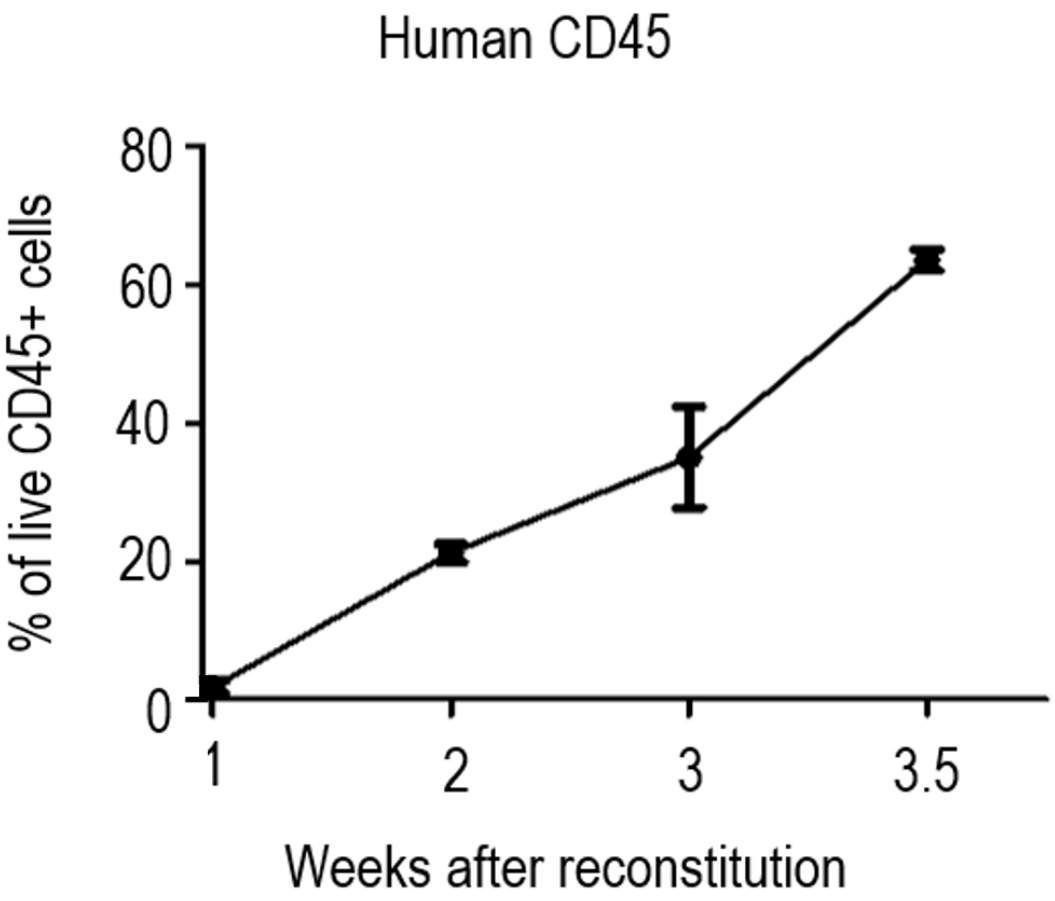

Figure 5.2: Human CD45+ cell engraftment in SpMC-reconstituted mice
Timecourse of the engraftment of human CD45+ cells in the peripheral blood of NSG mice as a proportion of all live CD45+ cells, as measured by flow cytometry. N = 3 biological replicates. Flow cytometric gating strategy shown in appendix figure 5.

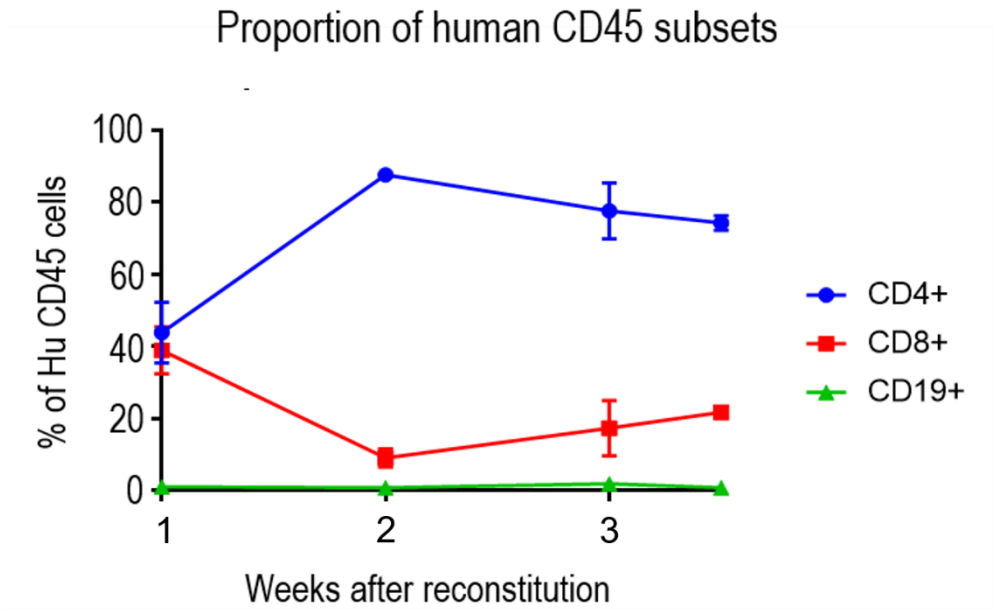

Figure 5.3: Human CD45+ subtype engraftment in SpMC-reconstituted mice
Timecourse of the engraftment of human CD4+ and CD8+ T cells and CD19+ B cells in the peripheral blood of NSG mice. T cells and B cells measured as a proportion of all live human CD45+ cells, as measured by flow cytometry. N = 3 biological replicates. Flow cytometric gating strategy shown in appendix figure 5.

The spleens of the SpMC-reconstituted humanised mouse showed a mean proportion of 30% live human CD45+ leukocytes (figure 5.4), although there was variability between animals. The spleens also showed engraftment with human CD19+ B cells (40% of all splenic human CD45+ cells) and CD4+ and CD8+ T cells (figure 5.4). As in the peripheral blood, the proportion of CD4+ T cells was greater than CD8+ T cells, although the difference between the two subtypes was less in the spleen than the peripheral blood.

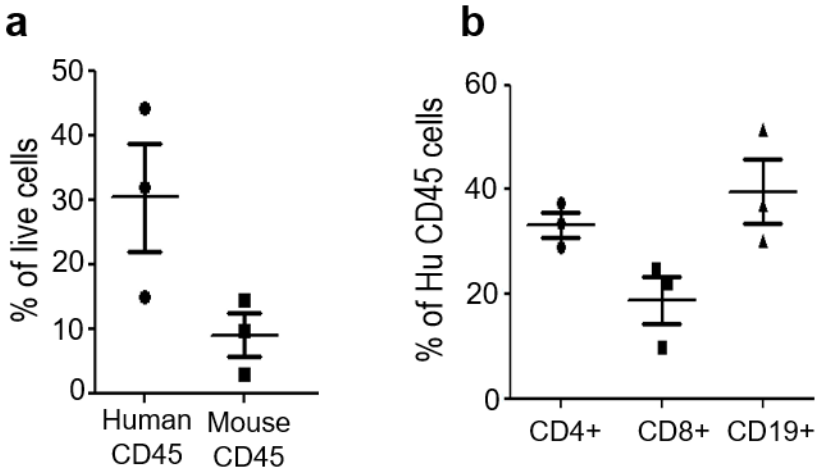

Figure 5.4: Engraftment of human leukocytes in the spleen of SpMC-reconstituted mice
(a) Proportion of human CD45+ cells compared to murine CD45+ cells in the spleen of SpMC-reconstituted mice, as measured by flow cytometry. (b) Proportion of human CD4+ and CD8+ T cells and CD19+ B cells as a percentage of all live human CD45+ cells in the spleen, as measured by flow cytometry. Splenic engraftment measured at the experimental endpoint (3.5 weeks after reconstitution). N=3 biological replicates. Flow cytometric gating strategy shown in appendix figure 5.

The kidneys were cryosectioned at 7µm thickness until the graft area was located. The cryosections were initially stained for the human-specific markers Ku80 and HLA class I (figure 5.5). COs in the non-humanised control were shown to have formed large, duct-like structures under the kidney capsule, with CO cells arranged in a single-cell cystic structure around a lumen. In contrast, COs in the SpMC-humanised mice showed a collapsed, irregular graft structure, with thickened cells and a high density of infiltrating cells expressing the human-specific marker Ku80 but not the cholangiocyte marker CK7 (figure 5.5). Further immunofluorescent imaging confirmed these infiltrating human cells to be human CD45+ leukocytes (figure 5.6). These images also confirmed that the disordered graft structure seen in figure 5.5 continued throughout the extent of the CO graft.

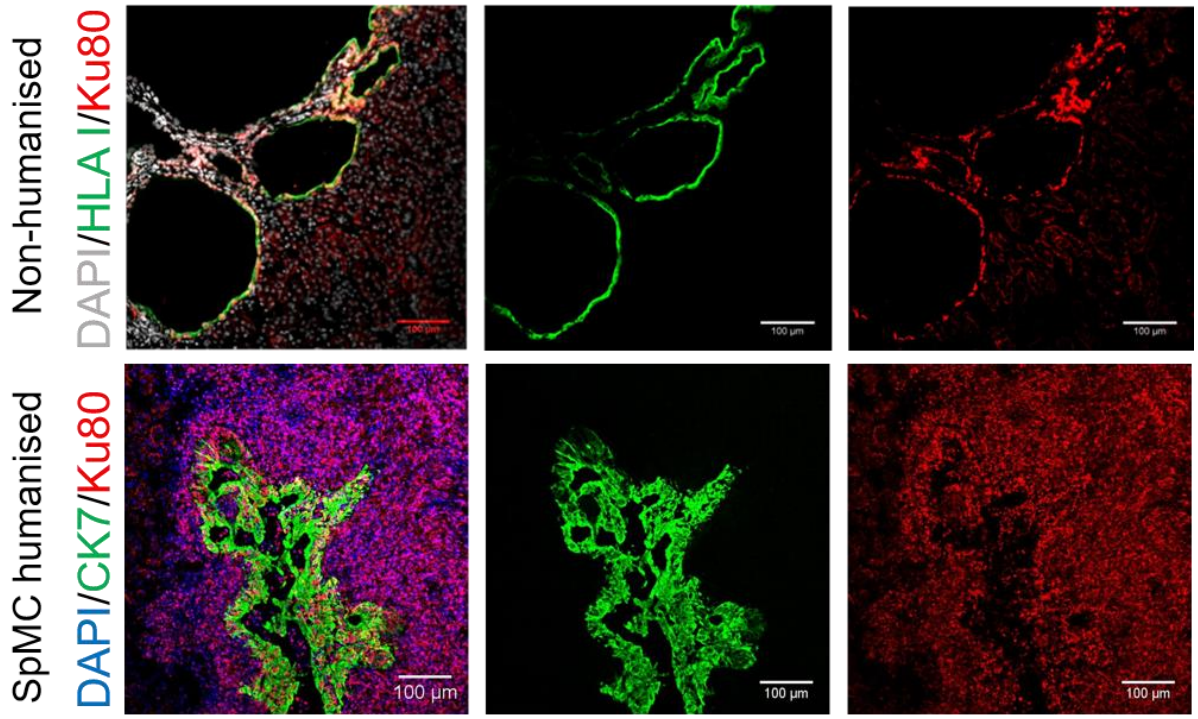

Figure 5.5: Graft infiltration in SpMC-reconstituted mice
Immunofluorescence images demonstrating CO grafts from line 200 under the kidney capsule of non-humanised (top) and SpMC-humanised (bottom) NSG mice. The CO graft in the non-humanised mouse is stained for two human-specific markers, HLA class I (green) and Ku80 (red) and the CO graft forms cystic duct-like structures. The CO graft in the SpMC-reconstituted mouse is stained for the cholangiocyte marker CK7 (green) and Ku80 (red) and is surrounded by CK7-/Ku80+ cells. The CO graft has lost the cystic, duct-like morphology seen in the non-humanised graft. Scale bar = 100µm.

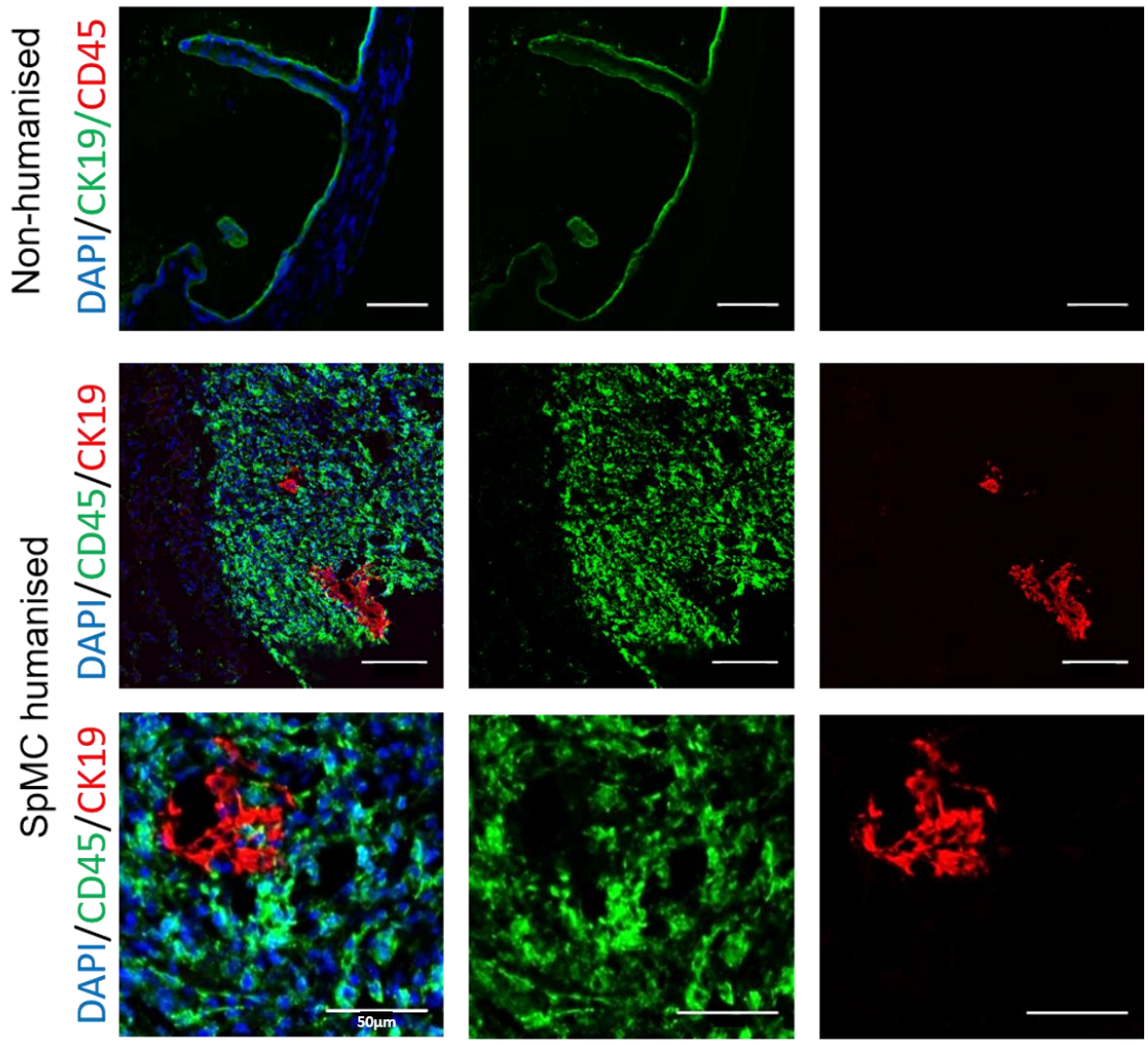

Figure 5.6: Leukocyte infiltration into CO grafts in SpMC-reconstituted mice
Immunofluorescence images of a non-humanised CO graft (top) showing CK19 expression (green) but no CD45+ leukocytes (red) compared to an SpMC-reconstituted CO graft (middle and bottom) showing CK19+ CO cells (red) surrounded by CD45+ leukocytes (green). Scale bar (top and bottom rows) = 50µm. Scale bar (middle row) = 100µm.

After this preliminary experiment, I continued to investigate the immunogenicity of COs using the SpMC model, following the experimental parameters outlined in figure 5.1. However, SpMCs from donor 150 were no longer available and alternative SpMC donors failed to engraft to any extent, even after a significantly longer engraftment time course (data not shown). As a result, and in order to reduce the time required for each reconstitution experiment, I modified the design of the SpMC-reconstituted humanised mouse experiments. The animals were reconstituted with 1.0 x 10^7 SpMCs and the SpMC engraftment monitored through weekly tail bleeds until a threshold of approximately 5% live human CD45+ cells in the peripheral blood was reached, at which point the mice were transplanted under the

left kidney capsule with 1.0 x 10^6 COs. The mice were culled two weeks after transplantation with COs (figure 5.7).

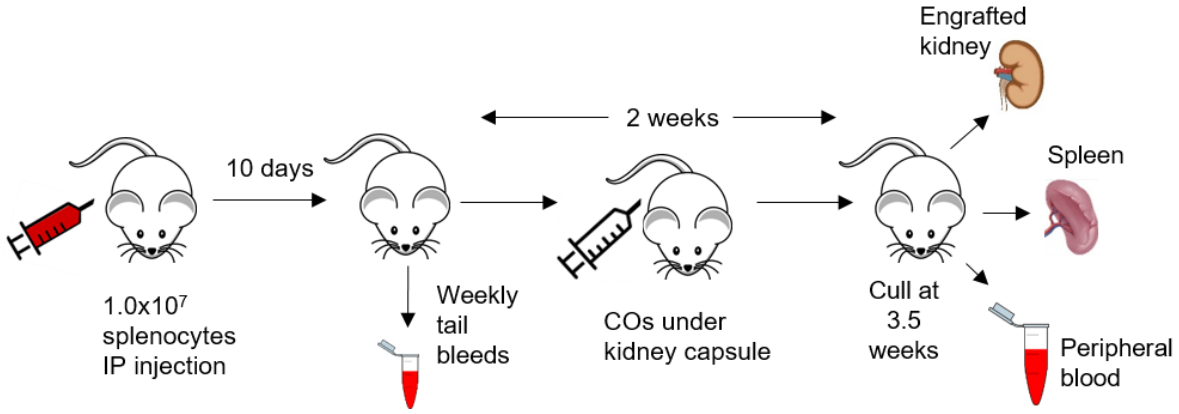

Figure 5.7: Schematic representation of the modified SpMC-reconstituted humanised mouse model
Schematic demonstrating the timetable and key steps of the modified SpMC-reconstituted humanised mouse model. Steps in order (left to right): reconstitution with adult SpMCs (splenocytes) via intraperitoneal (IP) injection; weekly monitoring of engraftment; transplantation of organoids under the kidney capsule of naïve NSG mice; final cull and harvesting of the graft and immune tissues.

I aimed to investigate the immunogenicity of allogeneic COs compared to autologous COs through the use of the SpMC-reconstituted humanised mouse model and bilateral transplantation of two different CO lines under the left and right kidney of SpMC-reconstituted mice (figure 5.8).

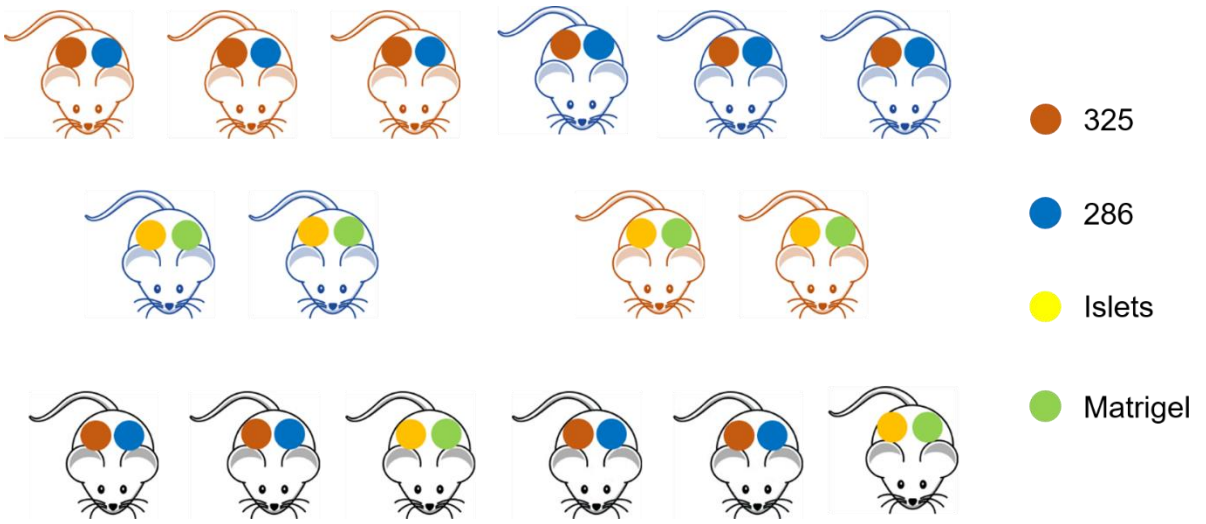

Figure 5.8: Schematic representation of the experimental design for the bilateral SpMC-reconstituted humanised mouse experiment
Five mice were reconstituted with SpMCs from donor 325 (brown) and five with SpMCs from donor 286 (blue). Three mice of each group were transplanted under the left kidney with 325 COs (brown dot) and under the right kidney with 286 COs (blue dot). Two mice of each group were transplanted under the left kidney with primary islets (yellow dot) and Matrigel only (green dot). Four non-humanised NSG mice were transplanted under the left kidney with 325 COs (brown dot) and under the right kidney with 286 COs (blue dot) and two non-humanised NSG mice were transplanted under the left kidney with primary islets (yellow dot) and Matrigel only (green dot).

I selected donors 325 and 286 as these were donors for which both CO lines and a high number of SpMCs were available. Additionally, both donors had previously been shown to survive *in vivo* (table 3.1) and had been used in an HSC-reconstituted humanised mouse experiment conducted earlier (discussed later in this chapter). SpMC engraftment of donor 325 was rapid, while donor 286 entirely failed to engraft (figure 5.9). The reason for this failure is unclear, however one possible explanation is that immune cells from donor 286 were cryopreserved for longer and were derived from an older donor, both of which may have impacted on the quality of the SpMCs.

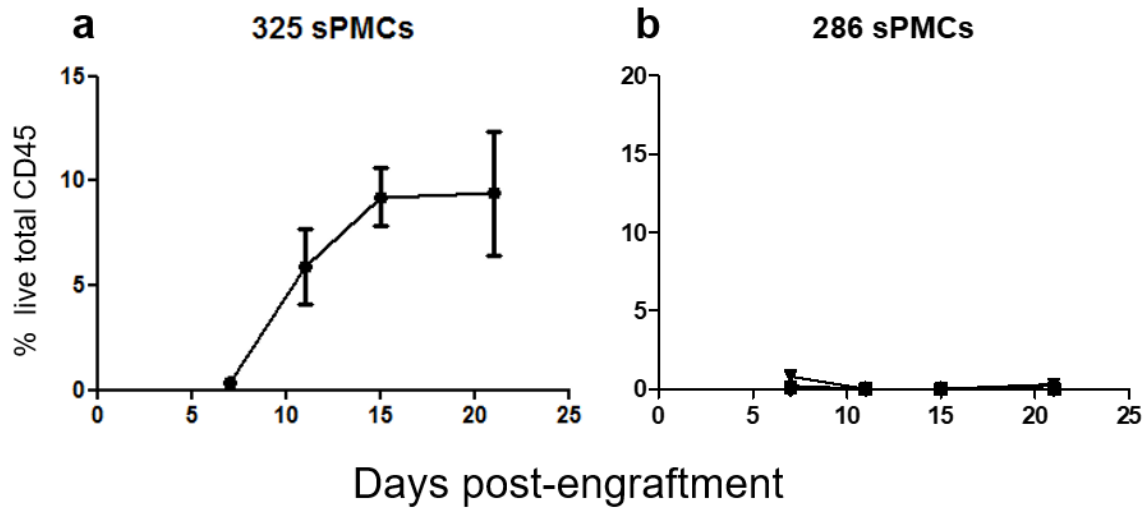

Figure 5.9: Human CD45+ cell engraftment in SpMC-reconstituted mice
Timecourse of the engraftment of human CD45+ cells in the peripheral blood of SpMC-reconstituted NSG mice as a proportion of all live CD45+ cells, as measured by flow cytometry. (a) Engraftment timecourse of SpMCs from donor 325. (b) Engraftment timecourse of SpMCs from donor 286. N = 5 biological replicates per donor. Flow cytometric gating strategy shown in appendix figure 5.

The mice were transplanted one week after SpMC reconstitution with the CO lines 325 BD and 286 GB as shown in figure 5.8, along with the positive (primary islets) and negative (Matrigel only) control SpMC-reconstituted mice and non-humanised controls. All mice were culled two weeks after transplantation and the kidneys were harvested for cryosectioning and immunofluorescence imaging. Processing and analysis of the samples from this experiment is still ongoing and the majority of control SpMC-reconstituted kidney samples and non-humanised kidney samples have not yet been analysed. Initial analysis of the SpMC-reconstituted/CO engrafted kidney samples reconstituted with SpMC donor 325 shows infiltration of CD45+ leukocytes into the graft area of both allogeneic and autologous (figure 5.10) grafts. Autologous 325 BD grafts can be seen under the kidney capsule, forming cystic duct-like structures containing CD45+ cells while no surviving 286 GB cells can be found in the graft area of the allogeneic right kidney graft. Importantly, however, no surviving 286 GB cells could also be found under the kidney capsule of a non-humanised NSG mouse (data not shown), although analysis of all samples is still ongoing. One possible explanation for the lack of survival of 286 GB cells is that the 286 CO line was cryopreserved for longer than the 325 CO line and underwent a greater number of freeze-thaw events, which could have damaged the quality of the CO line. Infiltration of CD45+ leukocytes was also seen in the positive control primary islet grafts (figure 5.11).

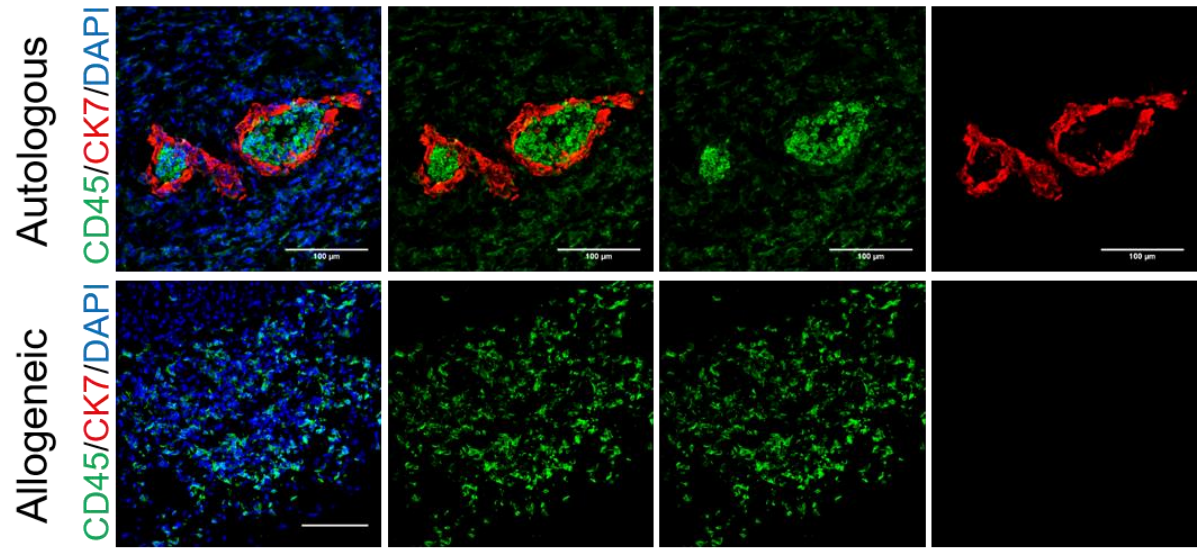

Figure 5.10: Leukocyte infiltration in autologous and allogeneic CO grafts
Immunofluorescence images of CO grafts in autologous (top) and allogeneic (bottom) SpMC-reconstituted humanised mice three weeks after SpMC-reconstitution and two weeks after CO transplantation, showing CD45+ leukocyte infiltration into the CO graft area. CO grafts stained for CK7 (red). No remaining evidence of CO graft survival in allogeneic SpMC-reconstituted mice. Autologous CO grafts from line 325, allogeneic grafts from line 286. Both allogeneic and autologous humanised mice reconstituted with SpMCs from donor 325. Scale bar = 100µm.

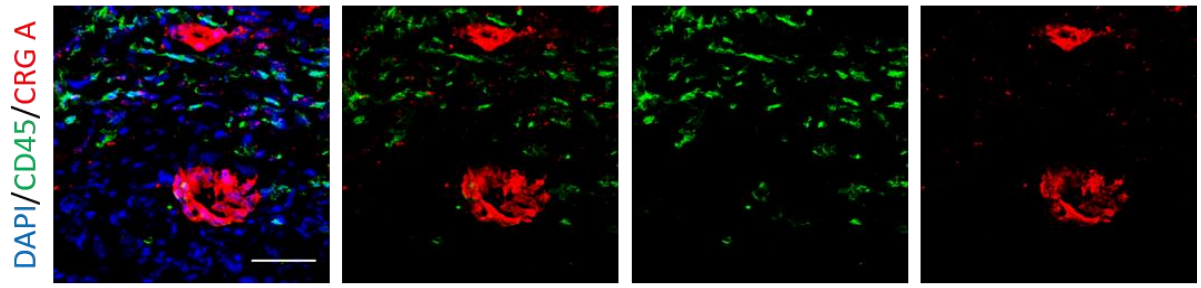

Figure 5.11: Leukocyte infiltration into a positive control primary islet graft
Immunofluorescent images of SpMC-reconstituted humanised mice engrafted with SpMCs from donor 325 and allogeneic primary human islets showing CD45+ leukocyte infiltration (green) into chromogranin A+ (red) primary islet grafts under the kidney capsule. Scale bar = 50µm.

5.2.2: Differential graft infiltration of allogeneic vs autologous grafts in HSC-reconstituted humanised mice

The aim of our first HSC-reconstituted humanised mouse experiment was to investigate the immunogenicity of allogeneic and autologous CO grafts and to determine the extent to which allogeneic CO grafts would be rejected in an HSC-reconstituted humanised mouse model. Twelve female mice were irradiated with 2.4Gy of gamma irradiation and reconstituted six hours later with 1.0 x 10^7 CD3-depleted bone marrow cells - six mice were reconstituted with donor 256 and four with donor 261 (I was unable to reconstitute more than four mice with donor 261 due to a lack of adequate bone marrow cells). The mice were from two separate cages, one 5.5 weeks old and one 6.5 weeks old. The engraftment of human CD45+ cells was monitored by bi-weekly tail bleeds, starting 8 weeks after reconstitution and ending at 17 weeks, when the animals were transplanted with COs. One 261-reconstituted humanised mouse had to be culled soon after HSC reconstitution for health reasons. Engraftment of human CD45+ cells in the peripheral blood was variable across mice (figure 5.12).

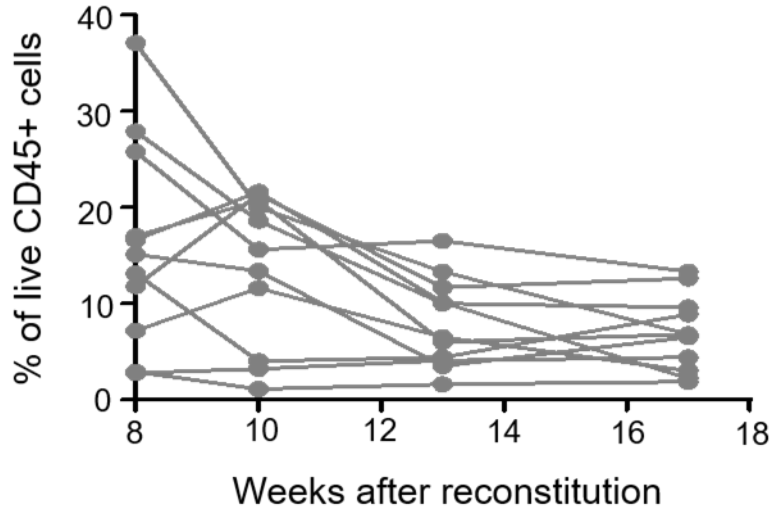

Figure 5.12: Leukocyte engraftment timecourse in HSC-reconstituted humanised mice
Timecourse of the engraftment of human CD45+ cells in the peripheral blood of HSC-reconstituted NSG mice as a proportion of all live CD45+ cells, as measured by flow cytometry. Each line represents engraftment in an individual animal. Engraftment monitored from 8 weeks after reconstitution to 17 weeks, at which point the animals were transplanted with CO grafts.

In order to ensure that both CO lines were tested in both an allogeneic and autologous humanised immune system, four 256-reconstituted humanised mice were transplanted with COs from line 256 (256 autologous) and four with COs from line 261 (261 allogeneic). Two 261-reconstituted humanised mice were transplanted with COs from line 261 (261 autologous) and one 261-reconstituted humanised mouse was transplanted with COs from line 256 (256 allogeneic). The mice were culled four weeks after transplantation, a total of 21 weeks after HSC reconstitution. At the time of the final cull, the 261-

reconstituted humanised mice were noticeably less well engrafted than the 256-reconstituted humanised mice, with two out of the three 261 animals showing less than 5% human CD45+ cells in the spleen, compared to a mean engraftment of 40% human CD45+ cells in the spleens of 256-reconstituted humanised mice (figure 5.13).

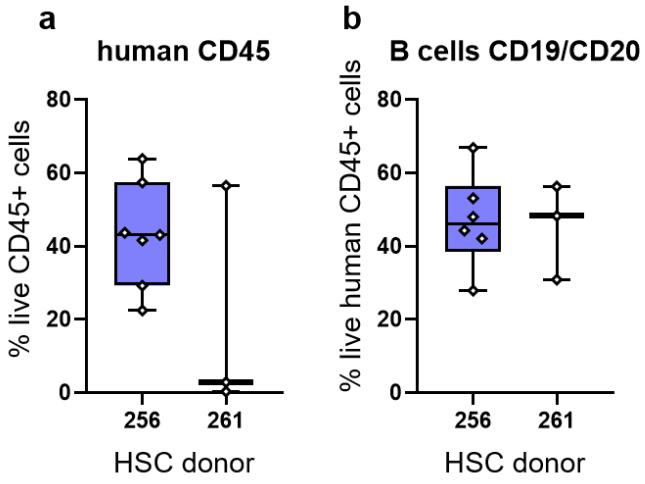

Figure 5.13: Leukocyte engraftment in the spleen of HSC-reconstituted humanised mice
Engraftment of human leukocytes in the spleen of HSC-reconstituted humanised mice at the end of the experimental time course, 21 weeks after initial HSC reconstitution, as measured by flow cytometry. (a) Engraftment of live human CD45+ leukocytes as a percentage of all live CD45+ cells in the spleen of HSC-reconstituted humanised mice reconstituted with HSCs from either donor 256 or donor 261.

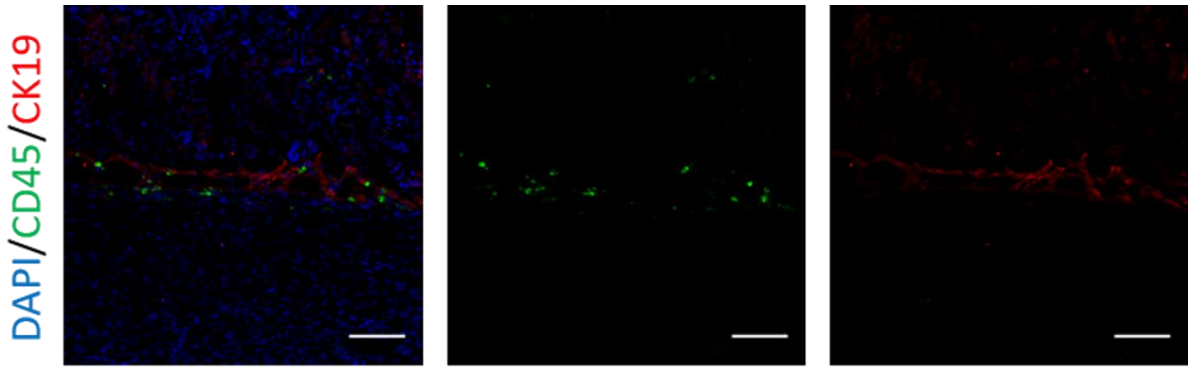

Figure 5.14: Lack of survival of 261 CO grafts
Immunofluorescent image demonstrating the lack of survival of 261 CO grafts. No specific CK19 (red) staining was seen. Some infiltrating CD45+ (green) cells were seen in proximity to the graft area. Scale = 100 µm.

No survival was seen of any 261 CO grafts, in either the allogeneic, autologous or non-humanised mice, although evidence of graft death could be seen, along with infiltrating leukocytes in the allogeneic graft areas (figure 5.14). 256 CO grafts showed good survival within all conditions (figure 5.15) and there was no noticeable difference in graft structure or size in the allogeneic, autologous or non-humanised grafts. CD45+ staining was seen in both allogeneic and autologous grafts (figure 5.15), but a greater

degree of lymphocyte infiltration was seen in allogeneic grafts. This difference was significant ($P < 0.05$) although there was a high level of variation was seen between different areas of the CO grafts (figure 5.16). When the number of infiltrating leukocytes was normalised to the percentage of human leukocytes in the peripheral blood at the point of transplantation (infiltrating leukocytes/percentage peripheral blood leukocytes), the difference in leukocyte infiltration between allogeneic and autologous grafts became more pronounced ($P < 0.01$) (Figure 5.16).

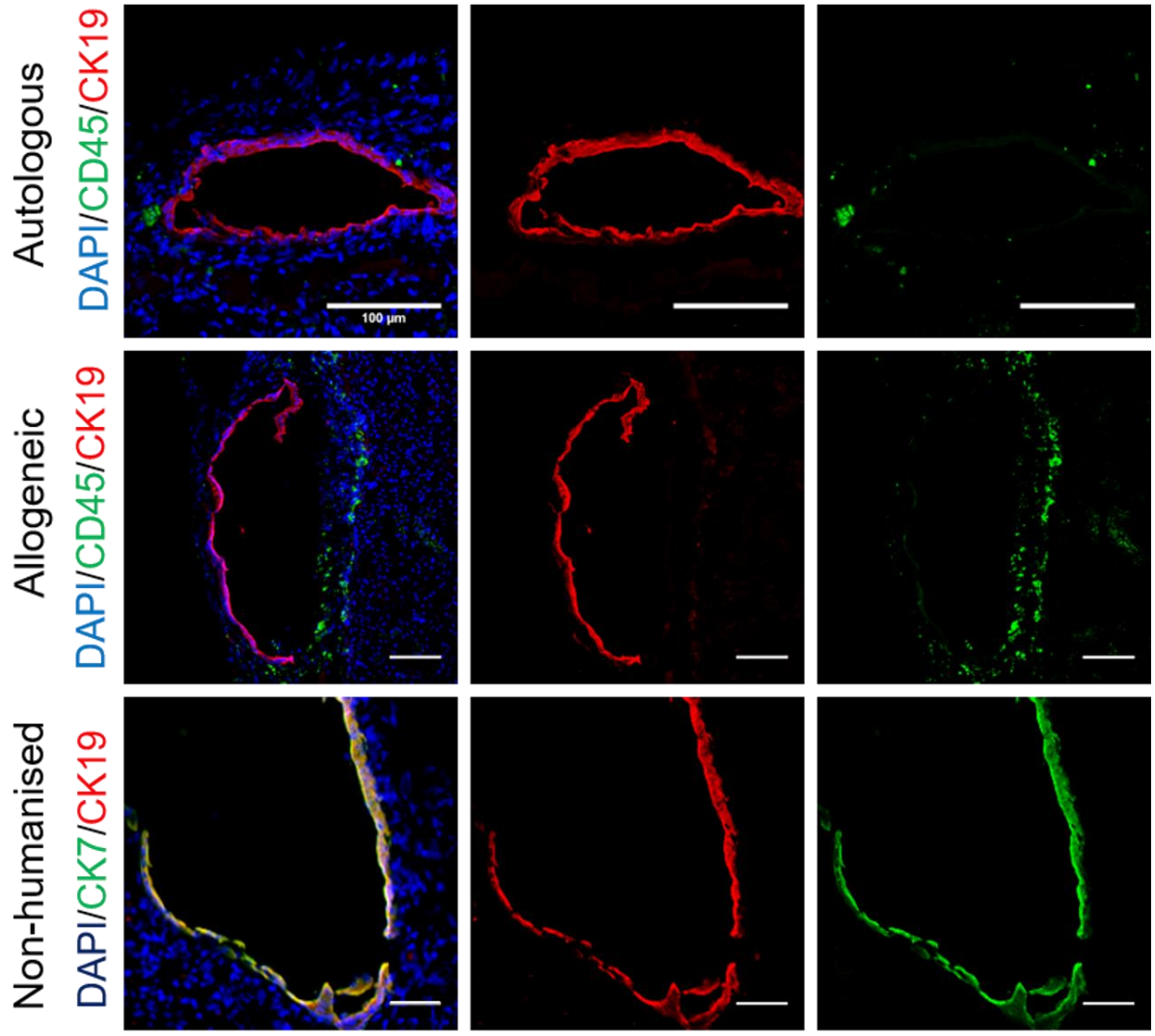

Figure 5.15: Graft infiltration into CO grafts in HSC-reconstituted humanised mice
Immunofluorescent images showing CD45+ leukocyte (green) infiltration into CK19+ CO grafts (red) in autologous (top) and allogeneic (middle) HSC-reconstituted mice. Allogeneic and autologous grafts compared to CO grafts in non-humanised NSG mice (bottom). All CO grafts are from line 256. Autologous HSCs are from donor 256 and allogeneic HSCs from donor 261. All grafts shown four weeks after transplantation. Scale bar = 100µm (top and middle rows). Scale bar = 50µm (bottom row).

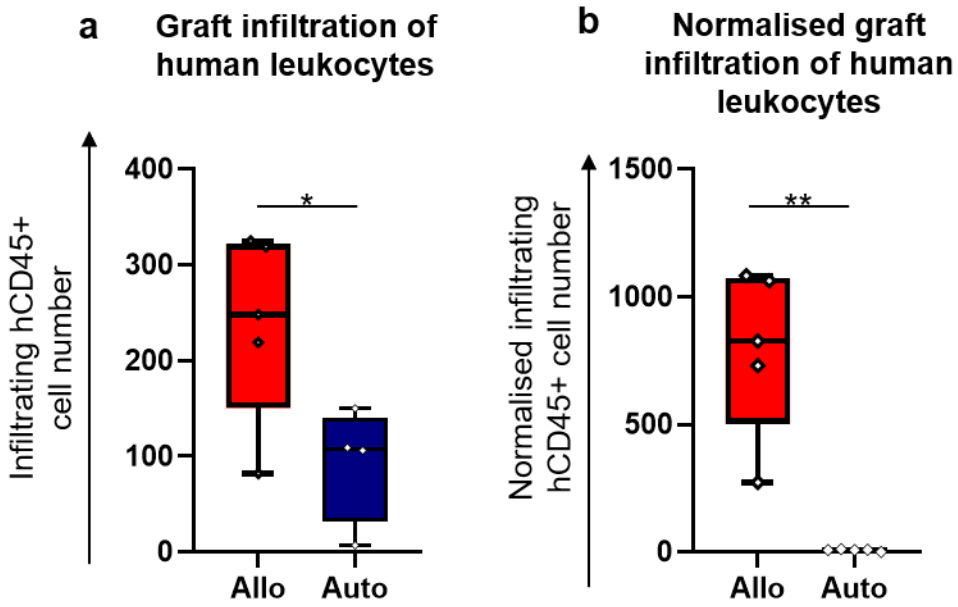

Figure 5.16: Allogeneic grafts show higher numbers of infiltrating leukocytes than autologous grafts in HSC-reconstituted humanised mice
(a) Numbers of infiltrating leukocytes in CD45/CK19 stained cryosections of CO grafts taken from autologous (n=2 biological replicates) and allogeneic (n= 1 biological replicate) HSC-reconstituted humanised mice. Representative cryosections of the graft area containing live CK19+ CO cells were randomly sampled from throughout the extent of the graft and imaged at 10x magnification, with the CO graft in the centre of the image. Surrounding/infiltrating CD45+ leukocytes were counted using Image J. $P < 0.05$ (Student's T-test). (b) Numbers of infiltrating leukocytes from the same CD45/CK19 cryosections after normalisation to the total percentage of human CD45+ cells in the peripheral blood at 17 weeks post-engraftment (immediately before CO transplantation). $P < 0.01$ (Welch's T-test).

5.2.3: CO line quality is the greatest indicator of survival in HSC-humanised mice

Fourteen NSG mice were irradiated at 2.4Gy and reconstituted with 1.0 x 10^7 CD3-depleted bone marrow cells from donor 286. The time course of engraftment in the peripheral blood was monitored from week 12 to week 18, at which point the mice were transplanted with COs under the kidney capsule (figure 5.17). Two mice were culled before transplantation for health reasons (weight loss <20% of initial weight). Four mice were transplanted with 1.0 x 10^6 COs from line 286 GB, four mice were transplanted with 1.0 x 10^6 COs from line 325 BD and four mice were transplanted with 600 IEQ primary islets from an allogeneic donor. Animals were sorted into groups for transplantation in a manner that ensured that each group had an approximately even distribution of well-engrafted, moderately engrafted and poorly engrafted animals. One animal from the 286 autologous group was culled after transplantation due to health reasons. Two non-humanised mice were transplanted with 325 BD COs, two non-humanised mice were transplanted with 286 GB COs and two non-humanised mice were transplanted with primary allogeneic islets.

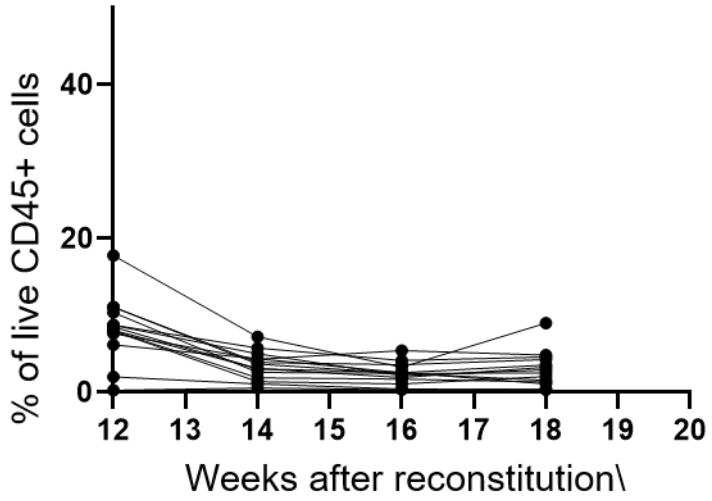

Figure 5.17: Leukocyte engraftment timecourse in HSC-reconstituted humanised mice (donor 286)

Timecourse of the engraftment of human CD45+ cells in the peripheral blood of HSC-reconstituted humanised NSG mice as a proportion of all live CD45+ cells, as measured by flow cytometry. Each line represents engraftment in an individual animal. All animals engrafted with CD3-depleted BM cells from donor 286. Engraftment monitored from 12 weeks after reconstitution to 18 weeks, at which point the animals were transplanted with CO grafts.

The animals were culled at 2 weeks after transplantation and tissue taken for analysis. Engraftment levels of human CD45+ cells and CD19+/CD20+ B cells in the spleen and peripheral blood was highly variable between individual animals, with no difference in engraftment levels between autologous, allogeneic or islet positive control groups (figure 5.18).

Survival was seen in both 325 allogeneic and 286 autologous grafts (figure 5.19), however the degree of graft survival and the formation of typical duct-like structures was much greater in the 325 BD grafts. 325 BD grafts showed a greater degree of survival and proliferation than any other CO line transplanted *in vivo*, while the 286 CO line showed much poorer engraftment than typical. A greater degree of CD45+ cell infiltration was seen into the allogeneic 325 CO grafts, however. Analysis of these samples is ongoing, including of the islet positive control samples, and lymphocyte counting has not yet been conducted to determine whether the higher numbers of leukocytes observed in the 325 allogeneic grafts (figure 5.19) is statistically significant.

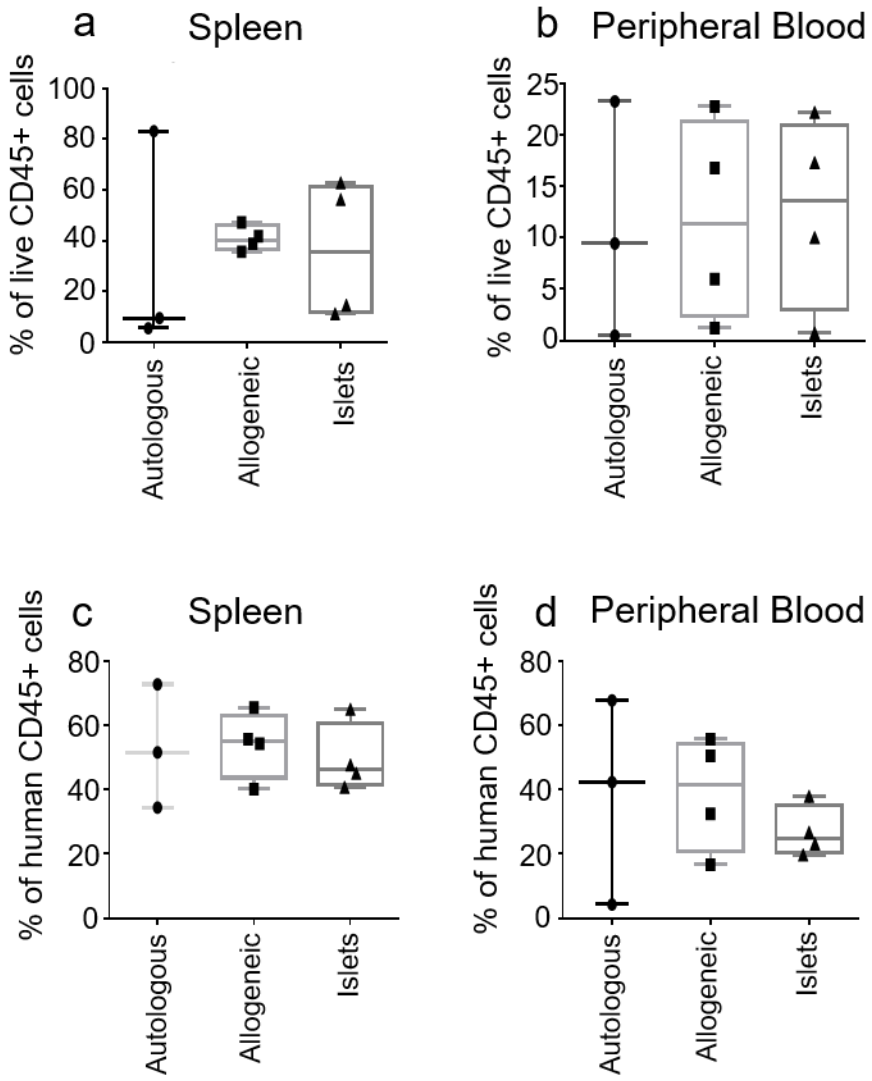

Figure 5.18: Leukocyte engraftment in the spleen and peripheral blood of HSC-reconstituted humanised mice

(**a**) Engraftment of live human CD45+ leukocytes as a percentage of all live CD45+ cells in the spleen of HSC-reconstituted humanised mice transplanted with either allogeneic COs, autologous COs or positive control allogeneic primary islets. (**b**) Engraftment of live human CD45+ leukocytes as a percentage of all live CD45+ cells in the peripheral blood of HSC-reconstituted humanised mice transplanted with either allogeneic COs, autologous COs or positive control allogeneic primary islets. (**c**) Engraftment of live human CD19+/CD20+ B cells as a percentage of all live human CD45+ leukocytes in the spleen of HSC-reconstituted humanised mice transplanted with either allogeneic COs, autologous COs or positive control allogeneic primary islets. (**d**) Engraftment of live human CD19+/CD20+ B cells as a percentage of all live human CD45+ leukocytes in the peripheral blood of HSC-reconstituted humanised mice transplanted with either allogeneic COs, autologous COs or positive control allogeneic primary islets. Engraftment percentages measured by flow cytometry. Flow cytometric gating strategy shown in appendix figure 5. Each data point represents an individual mouse. Data collected at final cull, two weeks after transplantation with CO or islet grafts, 20 weeks after HSC reconstitution.

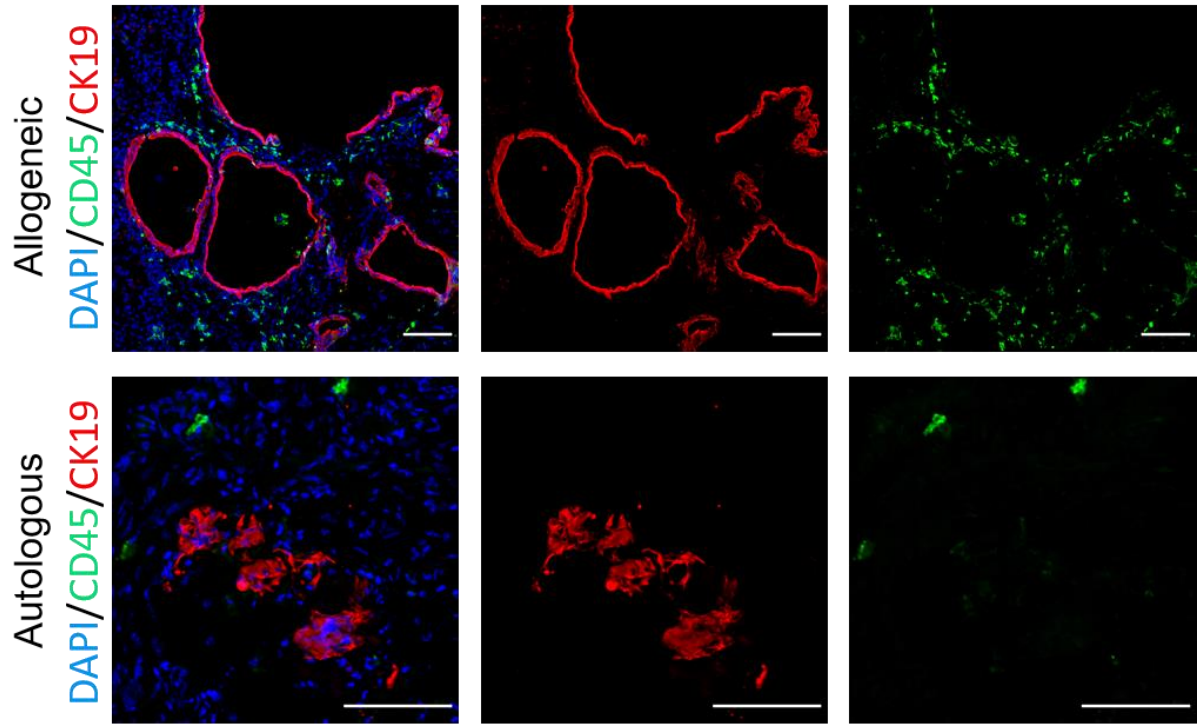

Figure 5.19: Leukocyte infiltration and graft survival in HSC-reconstituted humanised mice
Immunofluorescent images of allogeneic (top) and autologous (bottom) CK19+ CO grafts (red) under the kidney capsule of HSC-reconstituted mice engrafted with HSCs from donor 286, showing infiltration of CD45+ leukocytes (green). Autologous COs are from line 286 and allogeneic COs are from line 325. Grafts shown at 2 weeks after transplantation (20 weeks after HSC-reconstitution). Scale bar = 100µm.

5.2.3: Humanised mice as a method for comparing the immunogenicity of HLA-matched and HLA-mismatched cellular therapies

Following these pilot experiments, I aimed to investigate the immunogenicity of HLA-matched CO lines compared to HLA-mismatched CO lines using the HSC-reconstituted humanised mouse model. As the CO lines, bone marrow and splenocyte samples are all from deceased organ donors, records of the HLA types were available for all donors. I used standard kidney transplantation matching criteria to determine the criteria for a "complete" HLA match- defined as matching on both alleles for HLA A, B and DR. I defined a "partial" HLA match as matching only on HLA A and B, ignoring HLA-DR and any other HLA class II molecules.

I identified one CO line, 299 BD, as being a complete HLA match for one bone marrow/SpMC donor, donor 263 (table 5.1). This donor had 5.0 x 10^8 bone marrow cells and 1.0 x 10^9 SpMCs available at the time of identification - enough for one group of HSC-reconstituted humanised mice and several groups

of SpMC-reconstituted humanised mice. Additionally, I identified one donor, 354, as being a partial match (HLA A and B) for the 299 BD line. No bone marrow was available from this donor, but 8.0 x 10^8 SpMCs were available for use, making it suitable for SpMC-reconstituted humanised mouse experiments. There were multiple available candidates for a complete HLA mismatch donor for the 299 BD line but I initially chose donor 235 due to the high numbers of both bone marrow cells (9.0 x 10^8) and SpMCs (1.2 x 10^9).

Donor	HLA A	HLA B	HLA DR	Role	SpMCs	BM
235	A11 A19:29	B5:51 B12:45	DR7 DR10 DR53	Full mismatch 299 and 337	1.2 x 10^9	9 x 10^8
263	A1 A2	B8 B40:B60 Bw6	DR3:17 DR6:13 DR52	Full match 299	1.0 x 10^9	5 x 10^8
299	A*01 A*02	B*08 B40:61 Bw6	DR3:17 DR6:13 DR52	CO line	3.5x10^8	None
354	A*01 A*02	B*08 B*40:01	DRB1*03:01 DRB1*04	Partial match 299	7.0 x 10^8	None

Table 5.1: Donors identified as HLA matches/mismatches for CO line 299
A table showing the details of donors identified to be a complete (HLA A, B and DR) HLA match, partial (HLA A and B) HLA match or complete HLA mismatch for the BD CO donor 299. The table includes: donor ID, HLA A, B and DR type and numbers of available SpMCs and bone marrow (BM) cells at the time of donor identification.

Once I had identified suitable HLA matched and mismatched lines, I set up an HSC-reconstitution humanised mouse experiment to investigate the immune response to a fully HLA matched and fully HLA mismatched CO graft. I was not able to include an autologous group or a partially mismatched group in this experiment due to lack of bone marrow cells for donors 299 and 354. I irradiated ten female NSG mice with 2.4Gy of gamma irradiation and reconstituted eight mice each with 1.0 x 10^7 CD3-depleted bone marrow cells from donor 325 (complete mismatch) and two with 1.0 x 10^7 CD3-depleted bone marrow cells from donor 263 (complete HLA match). I had initially aimed to reconstitute up to eight animals in each donor group, however due to a technical error in the CD3-depletion process, the majority of the 263 bone marrow cells were lost and I was left with only enough cells to reconstitute two animals.

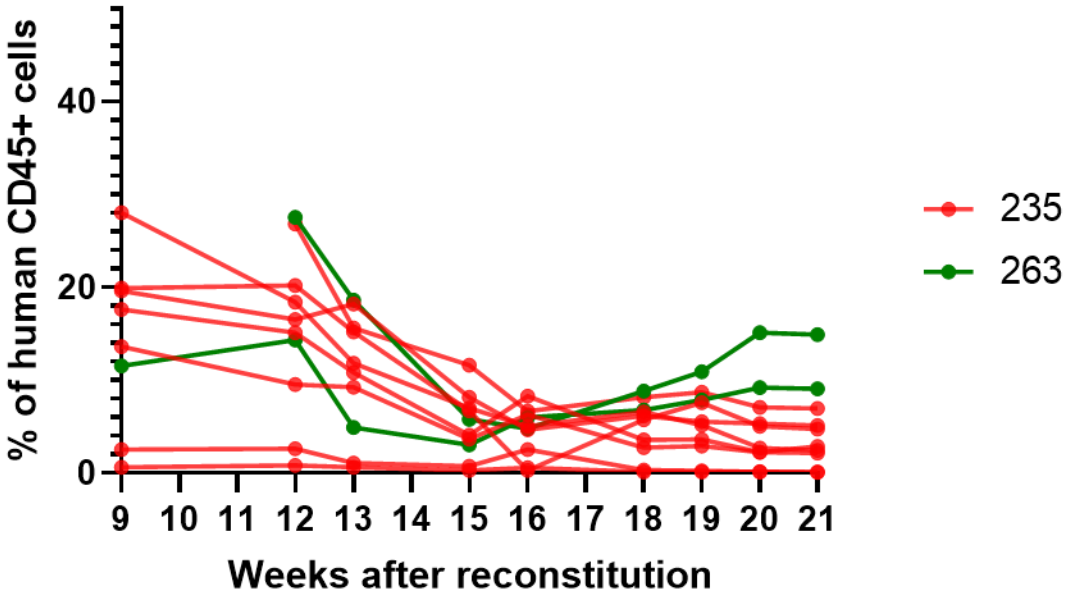

Figure 5.20: Leukocyte engraftment timecourse in HSC-reconstituted humanised mice
Timecourse of the engraftment of human CD45+ cells in the peripheral blood of HSC-reconstituted NSG mice as a proportion of all live CD45+ cells, as measured by flow cytometry. Mice were engrafted with HSCs from donor 263 (green) or 235 (red). Each line represents engraftment in an individual animal. Engraftment monitored from 9 weeks after reconstitution to 21 weeks, one week after transplantation with CO or positive control grafts.

I monitored the time course of leukocyte engraftment from week nine to week 21, one week after transplantation. Engraftment remained mostly stable after week 18 for 325-reconstituted mice, with engraftment in 263-reconstituted mice increasing slightly from week 18 onwards (figure 5.20). The two animals reconstituted with donor 263 showed slightly higher peripheral blood engraftment overall than the animals reconstituted with donor 235, possibly due to the noticeably higher proportion of CD3+ cells in the 263-reconstituted animals (figure 5.21). All animals except two (both donor 235) showed peripheral blood engraftment of >2% human CD45+ cells (figure 5.20).

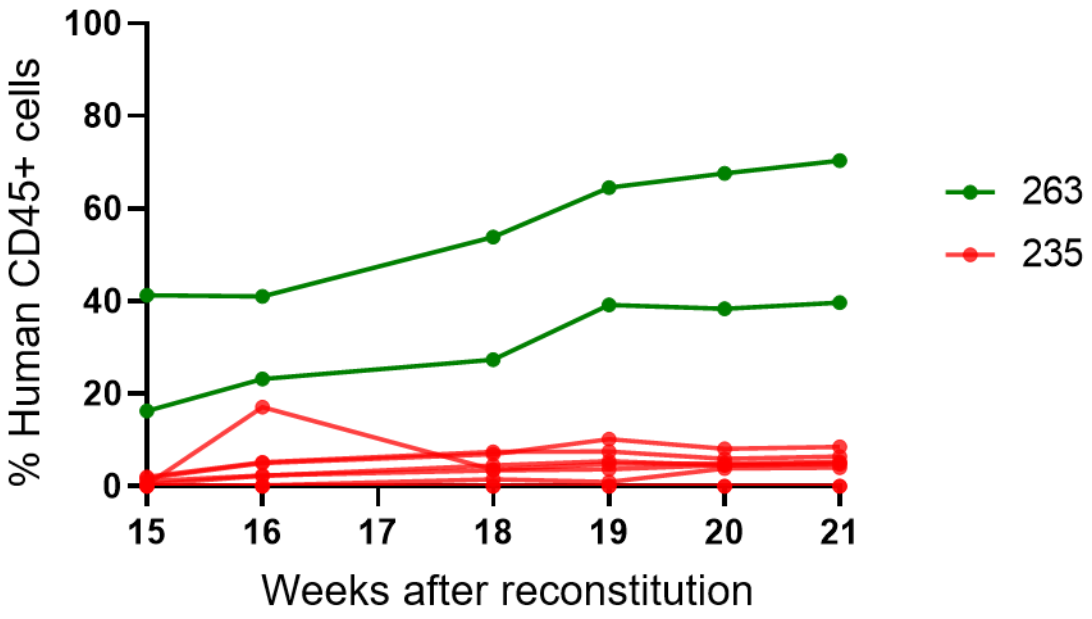

Figure 5.21: T cell engraftment timecourse in HSC-reconstituted humanised mice
Engraftment of CD3+ T-cells as a proportion of all human CD45+ leukocytes in the peripheral blood of NSG mice engrafted with HSCs from donors 263 (green) or 235 (red) from 15 weeks post-reconstitution to 21 weeks post-reconstitution. CD3+ T cell proportion measured by flow cytometry. Flow cytometric gating strategy shown in appendix figure 5.

As discussed in chapter 3, I decided to use bioluminescent imaging in this humanised mouse experiment (and all future humanised mouse experiments, wherever possible) to aid with tracking and quantification of the transplanted CO or positive control grafts. During the engraftment time course, I transduced the 299 BD line with a suitable luciferase construct, a process outlined in chapter 3. Once I was confident that I had created a suitable construct and had successfully generated the 299-RFP-Luc CO line, the next step was to identify a suitable positive control and transduce it with the Ef1α-RFP-Luciferase construct. I had previously used primary human islets as a positive control, however due to their very poor rate of survival after transplantation, even in non-humanised NSG mice, I elected to use a different cell type for this experiment. The three criteria for selection were: good survival *in vivo* for at least 3-4 weeks; high immunogenicity; ability to be transduced with the luciferase construct. I selected three potential options that met at least one of these criterion: primary endothelial cells, which can express high levels of HLA class I and II after IFN-γ treatment; HEK 293T (Human Embryonic Kidney) 293T, an immortalised cell line), which are easily transduced and likely to have good *in vivo* survival due to being an immortalised cell line; and LX2 cells, an immortalised human hepatic stellate cell line, which have moderate levels of HLA expression, are an immortalised cell line and are able to be transduced easily.

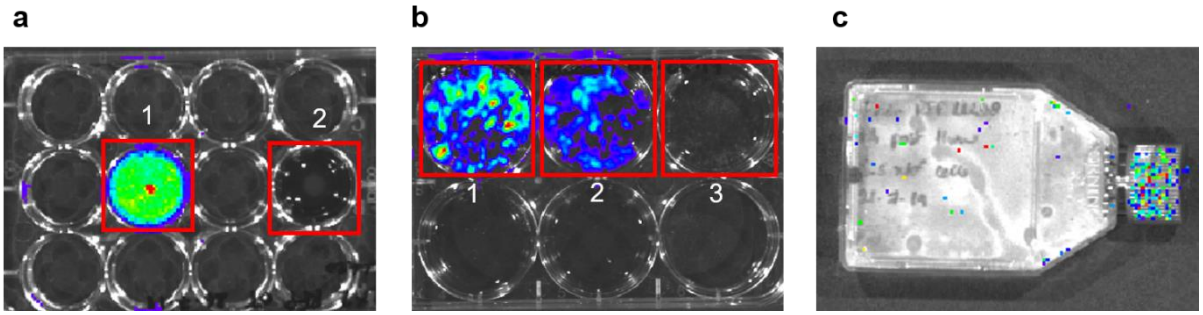

Figure 5.22: Testing of luciferase expression in three potential positive control cell types
(a) Luciferase expression (luminescence) in LX2-RFP-Luc cells (1) compared to a wild-type control (2). Both wells received 7.5µl/ml (150µg) luciferin substrate. (b) Luciferase expression (luminescence) in HEK-293T-RFP-Luc cells receiving 15µl/ml (300µg) of luciferin (1), HEK-293T-RFP-Luc cells receiving 7.5µl/ml (150µg) of luciferin (2) and wild-type HEK-293T cells receiving 7.5µl/ml (150µg) of luciferin (3). (c) Luciferase expression (luminescence) in primary endothelial cells transduced with the Ef1α-luciferase-RFP construct receiving 7.5µl/ml luciferin. All images taken with automatic exposure.

I was unable to transduce the primary endothelial cells with my luciferase construct, ruling it out of consideration (figure 5.22), while transduction was successful in both HEK 293T cells and LX2 cells. I then tested the ability of both cell types to upregulate HLA class I and II, in order to make the positive control graft as immunogenic as possible. I treated both cell types with increasing concentrations of IFN-γ (all super-physiological levels) for 72 hours and then performed flow cytometry to test the levels of HLA class I and II with and without IFN-γ treatment.

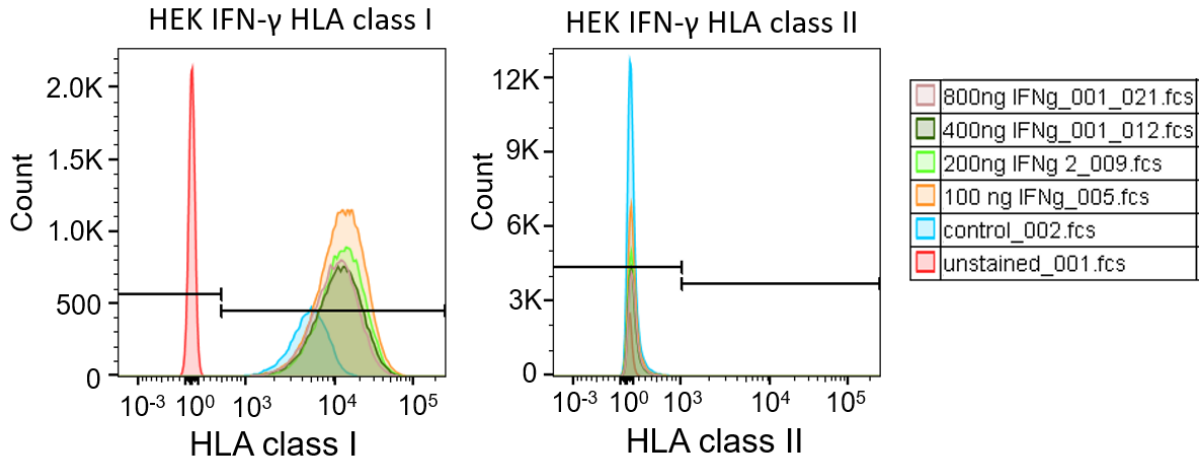

Figure 5.23: Testing HLA upregulation in HEK 293T cells
Flow cytometric analyses of HLA class I (left) and HLA class II (right) expression in HEK 293T cells. HLA expression in untreated HEK 293T cells (blue) compared to expression after 72 hours treatment with 100ng/ml (orange), 200ng/ml (light green), 400ng/ml (dark green) and 800ng/ml (purple) recombinant IFN-γ and to an unstained control (red).

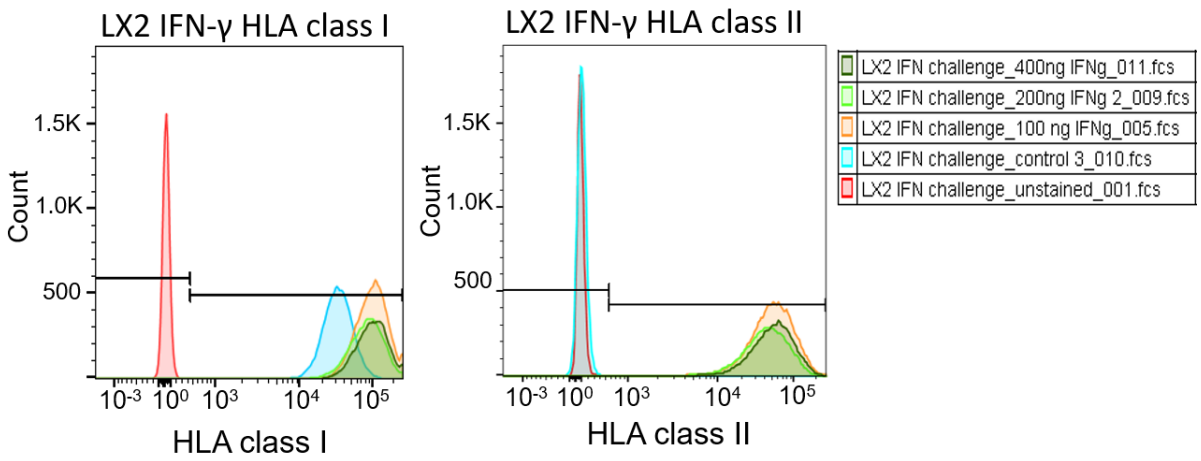

Figure 5.24: Testing HLA upregulation in LX2 cells
Flow cytometric analyses of HLA class I (left) and HLA class II (right) expression in LX2 cells. HLA expression in untreated LX2 cells (blue) compared to expression after 72 hours treatment with 100ng/ml (orange), 200ng/ml (light green), 400ng/ml (dark green) and 800ng/ml (purple) recombinant IFN-γ and to an unstained control (red).

HEK 293T cells were unable to upregulate HLA class II at any concentration of IFN-γ and IFN-γ treatment was only able to upregulate HLA class I to a very minor extent (figure 5.23). Conversely, LX2 cells upregulated HLA class II to a high level after IFN-γ treatment and showed a noticeable increase in HLA class I expression after IFN-γ treatment, from an already high baseline expression (figure 5.24). Based on this, I opted to use LX2-RFP-Luc cells as positive controls.

Four 235-reconstituted mice and two 263-reconstituted mice were transplanted at week 20 with 299-RFP-Luc COs, as were five non-humanised NSG mice. Two 235-reconstituted mice were transplanted at week 21 with LX2-RFP-Luc cells, and a further two mice were transplanted with 299-RFP-Luc COs. Four non-humanised NSG mice were transplanted with LX2-RFP-Luc cells. The two groups were transplanted a week apart due to the positive control cells not being ready for transplantation until week 21. Four mice had initially been intended to receive LX2-RFP-Luc cells, however, due to technical reasons, two of the four initial 235-reconstituted mice transplanted with 299-RFP-Luc COs did not receive adequate CO cell numbers, so we decided to transplant a further two mice with COs instead of LX2 cells.

I imaged each group of mice 24 hours after transplantation, and again at 7 and 14 days after transplantation, and at the final cull, 21 days after transplantation (figure 5.25). Similar technical issues led to three of the five non-humanised NSG mice receiving low cell numbers, limiting the ability to adequately detect the grafts in those mice using BLI (figure 5.25).

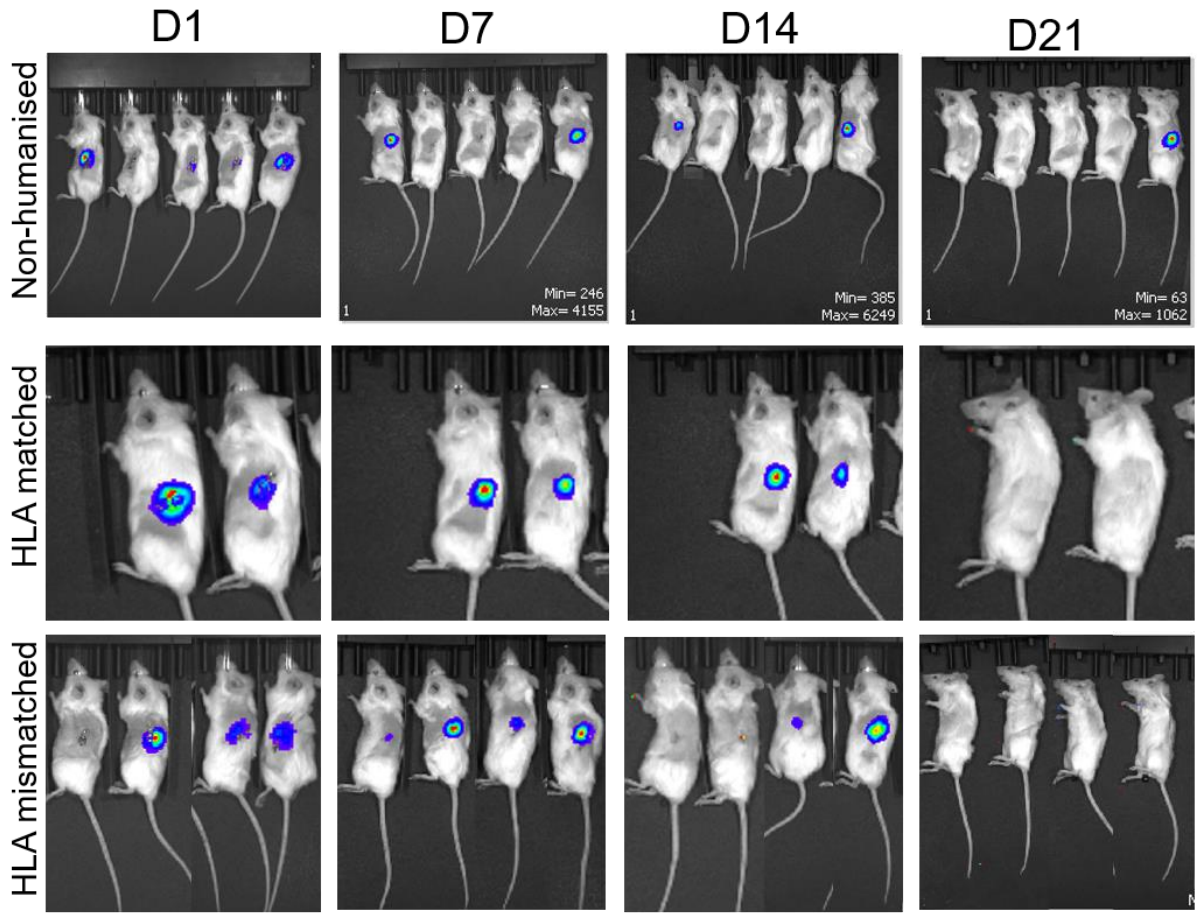

Figure 5.25: Bioluminescent images of CO grafts after transplantation in HLA-matched and mismatched humanised mice
Bioluminescent images of 299-RFP-Luc CO grafts transplanted into non-humanised NSG mice; HLA-matched (donor 263) HSC-reconstituted humanised mice; or HLA-mismatched (donor 235) HSC-reconstituted humanised mice at day 1, day 7, day 14 and day 21 post-transplantation. Day 21 images were taken post-mortem. All images taken with automatic exposure.

All groups showed a large decrease in luminescence over time, both visibly (figure 5.25) and through quantification of luminescence (figure 5.26), with luminescence in all groups decreasing to between 10^5 and 10^4 photons, a level similar to background. Normalising luminescence to the values shown at day 1 (24 hours after transplantation) to remove the variability between initial cell numbers showed a similar trend (figure 5.27). One animal in the 299 non-humanised group, however, did show a visible CO graft at D21, while no animals in any other group showed any sign of graft survival through BLI (figure 5.25). Due to the low number of animals in each group, particularly the HLA matched group and the positive control group, statistical analysis is not possible for this experiment.

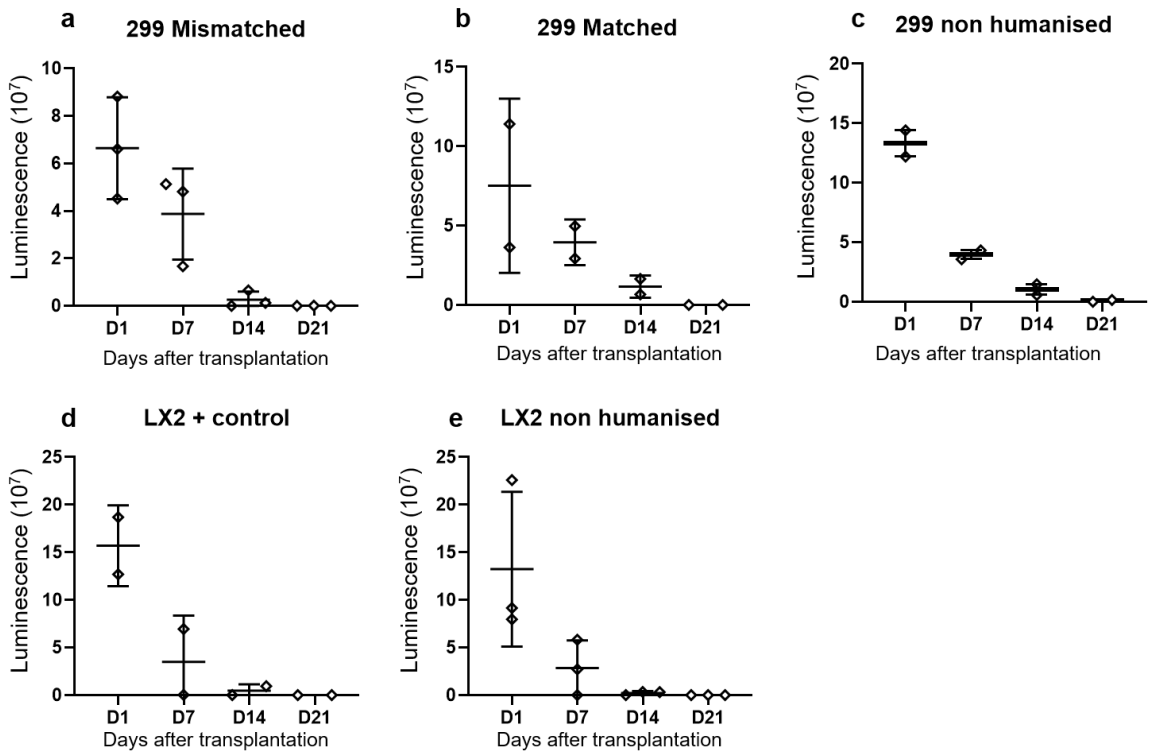

Figure 5.26: Time course of luminescence of CO and LX2 grafts after transplantation in HSC-reconstituted humanised mice

Luminescence measurements (10^7 photons) of 299-RFP-Luc and LX2-RFP-Luc grafts transplanted under the kidney capsule of HSC-reconstituted humanised mice or non-humanised controls. (a) 299-RFP-Luc COs transplanted into fully HLA-mismatched humanised mice (donor 235) (n=3). (b) 299-RFP-Luc COs transplanted into fully HLA-matched humanised mice (donor 263) (n=2). (c) 299-RFP-Luc COs transplanted into non-humanised NSG mice (n=2). (d) LX2-RFP-Luc positive control cells transplanted into fully HLA-mismatched humanised mice (donor 235) (n=2). (e) LX2-RFP-Luc positive control cells transplanted into non-humanised NSG mice (n=3). BLI performed at 24 hours, 7 days, 14 days and 21 days after transplantation. Imaging on D21 was performed post-mortem. Exposure time for all images= 7 seconds. Each data point represents an individual animal. Animals with BLI measurements below the threshold of visible detection on D1 were excluded from analysis. No statistical analysis performed due to inadequate numbers in each group.

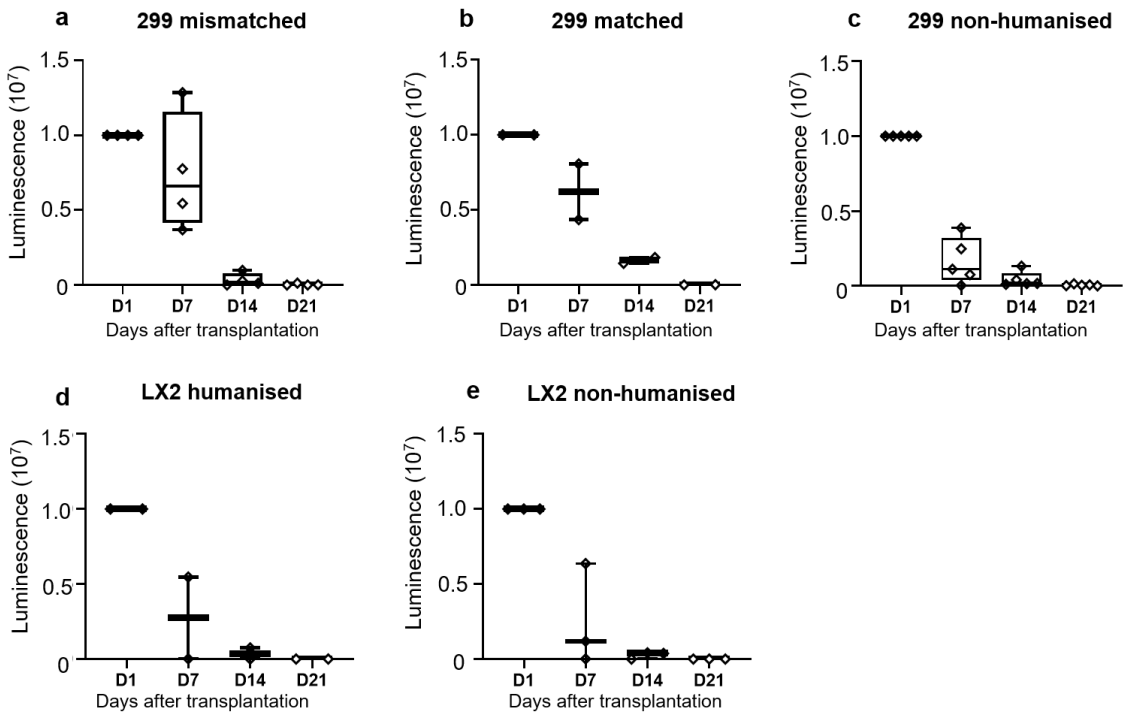

Figure 5.27: Time course of luminescence of CO and LX2 grafts after transplantation in HSC-reconstituted humanised mice normalised to D1

Luminescence measurements (10^7 photons) of 299-RFP-Luc and LX2-RFP-Luc grafts transplanted under the kidney capsule of HSC-reconstituted humanised mice or non-humanised controls normalised to luminescence at D1. (a) 299-RFP-Luc COs transplanted into fully HLA-mismatched humanised mice (donor 235) (n=3). (b) 299-RFP-Luc COs transplanted into fully HLA-matched humanised mice (donor 263) (n=2). (c) 299-RFP-Luc COs transplanted into non-humanised NSG mice (n=2). (d) LX2-RFP-Luc positive control cells transplanted into fully HLA-mismatched humanised mice (donor 235) (n=2). (e) LX2-RFP-Luc positive control cells transplanted into non-humanised NSG mice (n=3). BLI performed at 24 hours, 7 days, 14 days and 21 days after transplantation. Imaging on D21 was performed post-mortem. Exposure time for all images= 7 seconds. Each data point represents an individual animal.

Hisological analysis of the kidney samples from this experiment is ongoing, however preliminary immunofluorescence results show a greater degree of human leukocyte (CD45+) infiltration into the HLA matched CO graft area compared to the HLA mismatched CO graft (figure 5.28). As only one HLA matched and one HLA mismatched graft have currently been analysed, quantification of the leukocyte infiltration and comparison between the two groups is not yet possible. Leukocyte infiltration is seen in both the matched and micmatched grafts, however, with many CD45+ cells in direct contact with or very close to the CO graft, with no CD45+ leukocytes observed in the surrounding kidney parenchyma. Additionally, preliminary immunofluorescence assessment of the leukocyte subtypes within the HLA matched graft demonstrates a high proportion of CD4+ lymphocytes among the infiltrating leukocytes (figure 5.29). Further histological analysis is ongoing to identify other leukocyte

subtypes and to quantify and compare the proportion of different leukocyte subtypes within HLA matched and mismatched grafts.

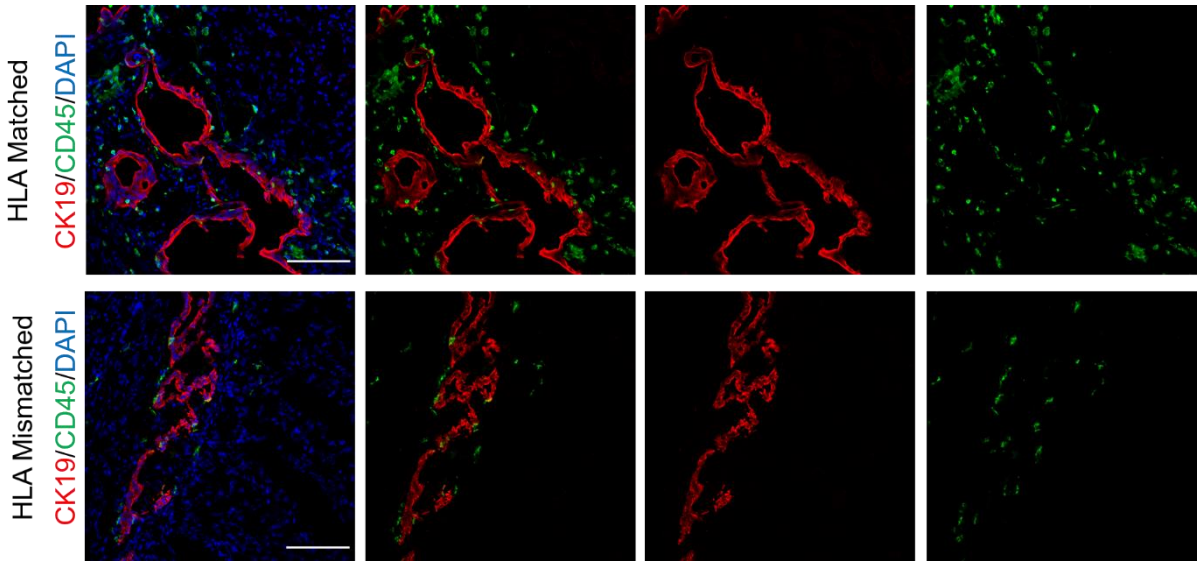

Figure 5.28: Leukocyte infiltration and graft survival in HLA matched compared to HLA mismatched HSC-reconstituted humanised mice
Immunofluorescent images of allogeneic CK19+ CO grafts (red) under the kidney capsule of HSC-reconstituted mice engrafted with HSCs from donor 263 (top, HLA matched) and donor 235 (bottom, HLA mismatched) showing infiltration of CD45+ leukocytes (green). All CO grafts were from CO line 299 RFP (passage 9). Grafts shown at 3 weeks after transplantation (20 weeks after HSC-reconstitution). Scale bar = 100µm.

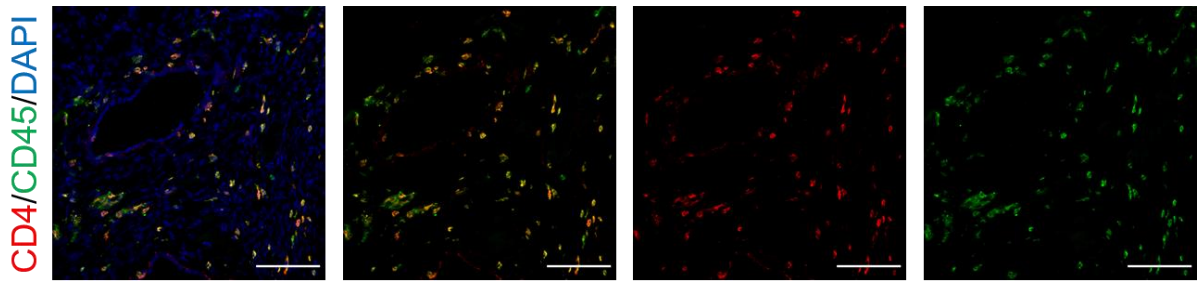

Figure 5.29: Infilatration of CD45+ and CD45+/CD4+ leukocytes into an HLA matched HSC-reconstituted graft
Immunofluorescent images of allogeneic CK19+ CO grafts (unstained cystic structures) under the kidney capsule of an HLA matched HSC-reconstituted mice engrafted with HSCs from donor 263 showing infiltration of CD45+ leukocytes (green) and CD4+ T cells (red). Graft shown at 3 weeks after transplantation (20 weeks after HSC-reconstitution). Scale bar = 100µm.

5.2.4: Investigation of the immunogenicity of HLA matched and mismatched CO grafts using the SpMC-reconstituted humanised mouse model

Investigation of the immunogenicity of CO grafts with and without HLA matching is ongoing, and the next step is to use the SpMC-reconstituted humanised model to address this question. As shown in table 5.1, high numbers of SpMCs are available for not only complete HLA-matched and complete HLA-mismatched donors but also for the autologous 299 donor and a partial HLA-match donor, allowing a more extensive future investigation into the role of HLA matching on CO immunogenicity (figure 5.30).

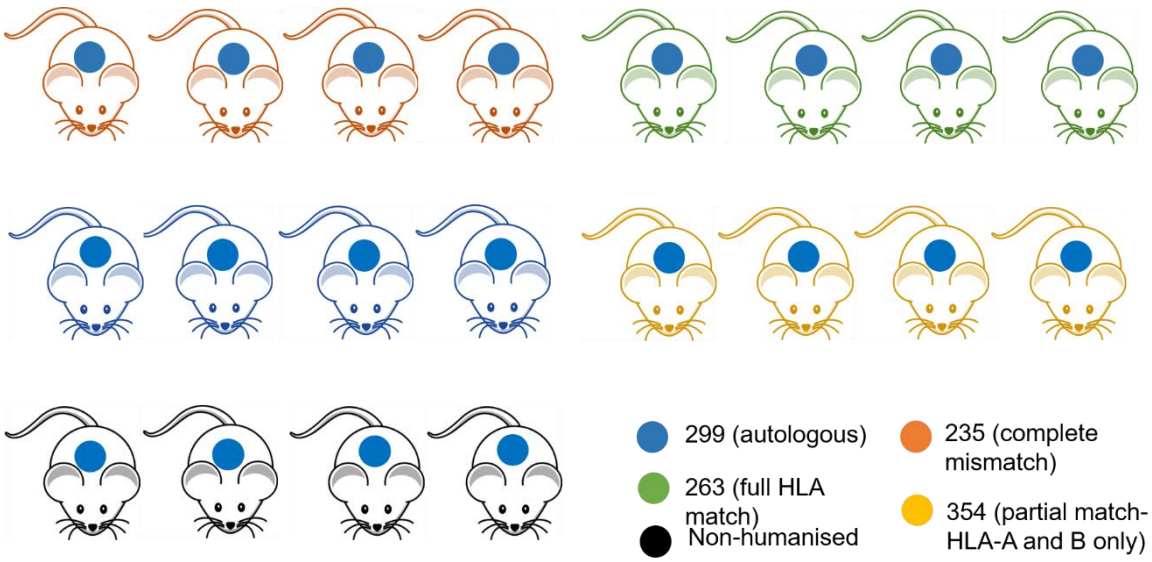

Figure 5.30: Schematic representation of the planned SpMC-reconstituted humanised mouse experiment to investigate the role of HLA matching in CO immunogenicity

2.4Gy-irradiated NSG mice will be reconstituted with 1.0 x 10^7 SpMCs from one of the four key donors (autologous, fully HLA-matched, fully HLA-mismatched and partially HLA-matched). Each group will contain a minimum of four animals to allow for statistical analysis. All mice will be transplanted under the left kidney capsule with 1.0 x 10^6 299-RFP-Luc COs. In addition, at least four non-humanised NSG mice will be transplanted under the left kidney capsule with 1.0 x 10^6 299-RFP-Luc COs. LXs-RFP-Luc will be transplanted under the right kidney capsule as a positive control to test humanisation efficacy.

As shown in previous SpMC-reconstituted humanised mouse experiments, engraftment of SpMCs can be highly variable across donors, so in order to ensure I could generate adequately humanised mice from all key SpMC donors, I first tested the engraftment of the four donors identified in table 5.1 (299, 263, 235 and 354). In order to improve the reliability of engraftment, I first irradiated the NSG mice and then reconstituted two mice with SpMCs from each donor (eight mice in total). The purpose of this experiment was only to test the engraftment of each SpMC donor, and so no CO grafts (or grafts of any other cell type) were transplanted into these animals at any point throughout the experiment. The engraftment of each donor was monitored weekly through tail bleeds and flow cytometry (figure 5.31).

Donor 354 and 263 engrafted rapidly, and one animal from each group had to be culled before the planned experimental endpoint of nine weeks, due to very high (>60%) peripheral blood engraftment. The second animal reconstituted with donor 263 showed a decrease in engraftment after five weeks, however this is unlikely to affect any humanised mouse experiments as the experimental time course after CO transplantation is unlikely to last longer than four weeks. Donor 299 showed only modest engraftment in one animal, with a much slower rate of engraftment than donors 354 or 263, however peripheral blood engraftment at the end of the experiment was >5%, a sufficient level of humanisation.

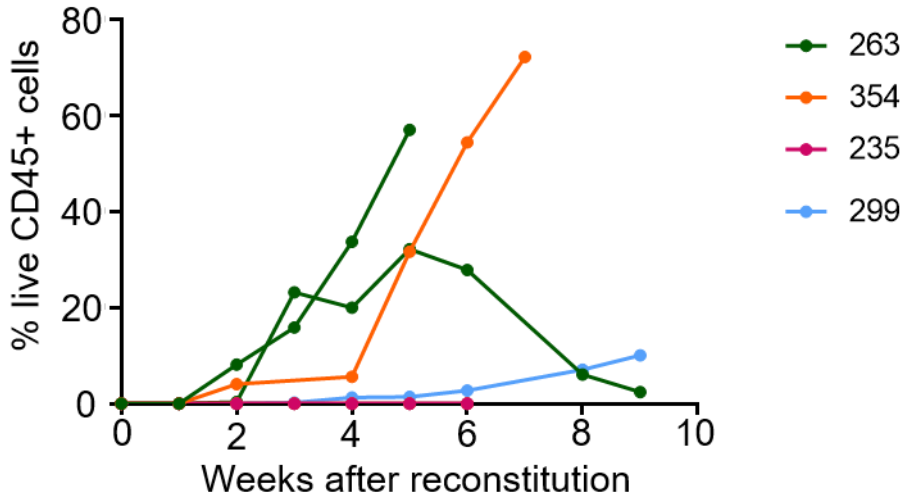

Figure 5.31: Testing reconstitution capacity of SpMCs from key donors
Timecourse of the engraftment of live human CD45+ cells in the peripheral blood of SpMC-reconstituted NSG mice as a proportion of all live CD45+ cells, as measured by flow cytometry. Each line represents an individual animal, reconstituted with 1.0 x 10^7 SpMCs from one of four key SpMC donors. Donor 263 (green) - complete HLA match for the 299 BD CO line. Donor 354 (orange) – partial HLA-mismatch (HLA A and B) for the 299 BD CO line. Donor 235 (pink) – complete HLA-mismatch for the 299 BD CO line. 299 (blue) – autologous SpMCs for the 299 BD CO line. N = 2 biological replicate for each donor.

Donor 235, the complete HLA-mismatch for 299 BD, showed no engraftment in either animal. As discussed above, however, there were multiple options for complete HLA-mismatch donors available, many of which had high numbers of SpMCs. I selected three of these donors with the highest numbers of SpMCs and tested their engraftment capacity in NSG mice, using the same method as outlined above. All donors showed rapid engraftment, in particular donor 283 (figure 5.32). Donor 318 showed the steadiest rate of engraftment, however this was not consistent between both animals in the group, unlike the animals engrafted with donors 283 and 322. As with donor 263, engraftment levels of donors 283 and 322 dropped rapidly after 16 days. Due to logistical reasons, these animals were all culled at 3.5 weeks post-reconstitution, so further investigation is required to determine whether the loss of

engraftment seen in these donors would continue or remain stable at approximately 5-10%, as seen in figure 5.32. However, these two SpMC-reconstitution time courses demonstrate that donors 263, 254 and 299 are suitable for SpMC-reconstituted humanised mouse experiments and that multiple promising options are available for a fully HLA-mismatched SpMC donor.

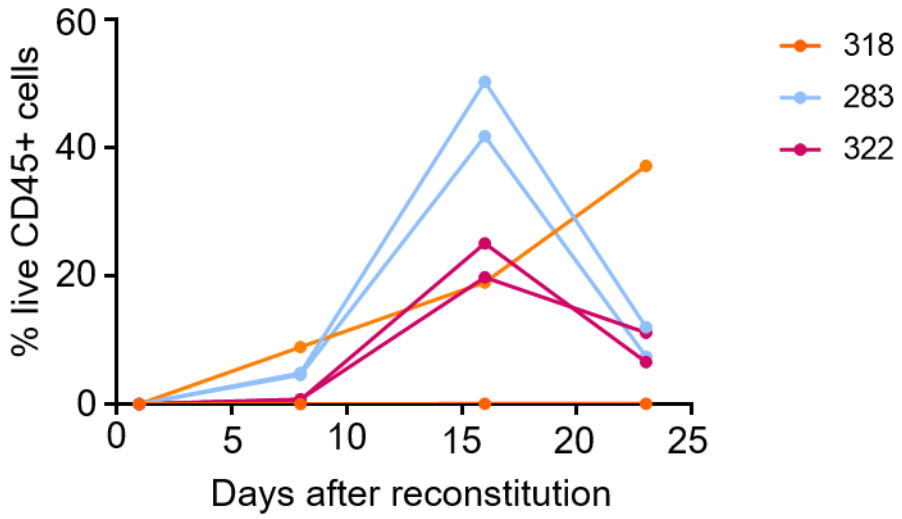

Figure 5.32: Testing reconstitution capacity of SpMCs from HLA-mismatched donors
Timecourse of the engraftment of live human CD45+ cells in the peripheral blood of SpMC-reconstituted NSG mice as a proportion of all live CD45+ cells, as measured by flow cytometry. Each line represents an individual animal, reconstituted with 1.0 x 10^7 SpMCs from one of three SpMC donors identified as being complete HLA-mismatches for the 299 BD CO line. N = 2 biological replicate for each donor.

5.3 Discussion

Assessment of the SpMC-reconstituted humanised mouse model

The early SpMC-reconstituted humanised mouse experiments suggested that I could effectively reconstitute NSG mice with SpMCs and produce a humanised mouse model capable of a strong immune response against allogeneic CO grafts, as evidenced by the high level of leukocyte infiltration around the CO graft compared to very minimal infiltration in the surrounding murine tissue. I adapted the SpMC-reconstitution method from a similar model of PBMC-reconstitution used by others[218] – our group had previously tried to generate SpMC and PBMC-reconstituted humanised mice through IV injection of 1.0×10^6 cells but had been unsuccessful. I demonstrated that reconstitution through IP injection of a higher cell number (1.0×10^7) produced a high level of engraftment. As this IP injection method was demonstrated to be successful, further attempts to engraft via IV injection were discontinued. The engraftment in the peripheral blood was largely of CD4+ and CD8+ T cells, which is consistent with established reports of the Hu-PBL model[279] . However, I did also observe some engraftment of human CD19+ B cells in the mouse spleen.

I observed both a high level of human CD45+ cell infiltration into the CO graft area and a noticeable change in the graft structure compared to non-humanised controls. The CO grafts lost the typical duct-like structures and became highly disordered, including a thickening of individual cells and loss of the cuboidal, monolayer structure. This was also seen in the CO grafts transplanted into immunocompetent C57BL/6 mice (figures 4.6 and 4.7), suggesting that this is a common consequence of a strong xenogenic or alloimmune response, and could be a result of the pro-inflammatory environment seen during a strong immune response[130]. The very dense infiltration of human leukocytes into the graft area, combined with the high levels of human T cells in the peripheral blood and the enlarged spleens (appendix figure 6) suggests that the response to the CO graft may have been at least partially due to GVHD[292]. The development of GVHD is a well-known limitation of the Hu-PBL model[279,293] and can complicate interpretation of data relating to rejection of the CO graft observed in this experiment. However, no human CD45+ lymphocyte infiltration was observed in the right kidney, which was not transplanted, suggesting that the infiltration and rejection of the CO graft was at least partially antigen-specific and not just a systemic GVHD response.

Another possibility is that the inflammation and injury caused by the CO transplantation procedure could have led the human leukocytes to home to the CO graft, making the infiltration a response to inflammation and damage generally, rather than a specific alloimmune response. However, this is unlikely as the transplantation was performed ten weeks previous to the SpMC reconstitution, at which point the impact of the transplantation injury would have disappeared. The design of later SpMC-reconstituted humanised mouse experiments was altered such that the SpMC reconstitution occurred before CO transplantation, in order to ensure that the CO grafts were transplanted into a model already

capable of mounting an immune response, and so this initial inflammation (which would also occur in the case of CO transplantation into a human patient) was taken into account. This was done in order to ensure that the immune response seen in these experiments was as physiologically accurate as possible, however it did reintroduce the possibility that the immune response seen could be simply a result of transplant-related inflammation and not a true alloimmune response. In order to account for this, Matrigel-only negative controls were included in SpMC-reconstituted humanised mouse experiments wherever possible. Assessment of these Matrigel-only control grafts is ongoing and will provide further clarity on this aspect of the immune response, as they will provide a site of similar tissue damage and inflammation without the possibility of an antigen-specific allograft response.

My initial SpMC-reconstituted experiment was a preliminary test to assess the ability to use the SpMC-reconstituted humanised mouse model and as such suffers from several major limitations. The main limitation is the lack of adequate controls; while non-humanised controls were used, there was no positive or negative controls to determine the extent of the model to reject allogeneic grafts, nor was there an autologous control to confirm that the infiltration seen was a result of a genuine and specific alloimmune response. Additionally, the low numbers of animals used in each group makes quantitative comparison of the humanised and non-humanised groups challenging. A further limitation was the inability to consistently compare the graft size at the point of transplantation to the graft at the end of the experiment. While cell death and/or cell proliferation can be assessed in grafts using TUNEL and Ki67 staining respectively (this work is in progress), it was not possible to quantify the level of graft loss, either within individual grafts or between grafts. Therefore, while the lymphocyte infiltration and graft deformity point strongly to immune rejection, I was unable to adequately assess the proportion of graft loss due to the immune response. This limitation is currently being addressed through the use of luciferase-expressing CO lines and BLI in humanised mice (discussed further below).

My later SpMC-reconstituted humanised mouse experiments aimed to address several of the limitations outlined above, through the use of a "crossover" experimental design, where two SpMC donors and their corresponding CO lines were used, with both CO lines receiving autologous and allogeneic reconstitution. The aim of this experimental design was to ensure that differences in both donor SpMC engraftment capacity and CO line proliferation were controlled for in the assessment of immunogenicity. I selected two CO lines that had previously been shown to survive *in vivo*. However, there was no assessment of the capacity for SpMC engraftment of either donor before the start of the experiment, and the SpMCs from donor 286 did not show any engraftment over the 20-day time course of the experiment. This, coupled with the unexpected lack of survival of the 286 CO line *in vivo* in either humanised or non-humanised animals, limit interpretation of the data as as it rendered the entire allogeneic arm of the experiment ineffective. The 325 CO graft was able to survive *in vivo* but there was no 286 SpMC engraftment to produce an immune response, while there was effective 325 SpMC

engraftment in 325-reconstituted mice but no survival of the 286 CO graft, for reasons unrelated to any alloimmune response.

Human CD45+ infiltration was observed in the 325 autologous CO grafts, primarily clustering within the lumen of the duct-like structures (figure 5.10). This suggests that the immune response in SpMC-reconstituted humanised mice, while not simply a result of systemic GVHD, is also not a specific alloimmune response, as leukocytes are infiltrating autologous grafts. This could be due to the inflammatory environment as a result of the CO transplantation procedure, which involves damage to the kidney parenchyma through the use of Hamilton needles. Additionally, this SpMC-reconstituted humanised mouse experiment was performed by first reconstituting the mice with SpMCs and then transplanting COs once the immune engraftment was underway, meaning that human leukocytes would be present at the time of transplantation injury. However, another possibility is that these infiltrating leukocytes are Tregs, which are known to home to areas of inflammation and to help to maintain graft tolerance[294]. The lack of an adequate allogeneic group in this experiment prevented the comparison of the graft infiltration in autologous compared to allogeneic grafts. Further assessment of the graft area is required, including TUNEL staining to detect CO cell apoptosis and immunofluorescence staining to determine the subtype of the infiltrating leukocytes. In addition, BLI in future SpMC-reconstituted humanised mice experiments will help to clarify the role of infiltrating leukocytes in autologous grafts as it will be able to determine if autologous graft loss is occurring and, if so, how the rate of graft loss compares to both non-humanised and allogeneic grafts. A further adjustment to the current SpMC-reconstituted humanised model that is planned for future experiments is the use of NSG-$(K^bD^b)^{null}(IA)^{null}$ mice, which do not express MHC class I or II on any cells, preventing the development of GVHD.

Assessment of the HSC-reconstituted humanised mouse model

My first HSC-reconstituted experiment demonstrated reasonable engraftment of HSCs from donors 256 and 261, however, as with the SpMC-reconstituted experiment described above, the 261 CO line did not survive in any conditions, including non-humanised NSG mice, preventing adequate analysis of any 261 CO grafts. Combined with the initial low number of 261 HSC-reconstituted mice at the start of the experiment and the loss of one of the 261 HSC-reconstituted mice engrafted with allogeneic 256 COs due to health concerns, the ability of this experiment to quantitatively assess the allogeneic immune response was significantly limited. Additionally, while levels of human CD45+ engraftment were roughly equivalent in the peripheral blood between 256-reconstituted and 261-reconstituted animals, the splenic engraftment of 261-reconstituted mice was much lower than that of 256-reconstituted mice, in all but one animal (figure 5.13).

There was no noticeable difference in the size of the allogeneic 256 CO grafts compared to either the autologous or non-humanised grafts (figure 5.15), nor was there any structural deformity observed in the allogeneic graft, as was seen in both SpMC-reconstituted and xenogenic CO grafts. There was a significantly greater number of infiltrating leukocytes observed in the allogeneic 256 graft compared to the autologous grafts (figure 5.16), and this difference persisted after normalisation to the overall systemic humanisation of each experimental animal (as measured by the percentage of human CD45+ cells in the peripheral blood). Indeed, the difference between allogeneic and autologous grafts became more pronounced after normalisation, as the allogeneic graft originated from a 261-reconstituted animal which had very low levels of peripheral blood humanisation and yet high levels of graft infiltration, while the autologous grafts originated from 256-reconstituted animals, which had much higher levels of peripheral blood humanisation but low levels of graft infiltration despite this fact. The limitations of the experimental groups outlined above, however, means that this conclusion required validation from further experiments.

The ambiguity of the immune response against allogeneic and autologous grafts was replicated in the second HSC-reconstituted humanised mouse experiment. In this experiment, I reconstituted NSG mice with only one HSC donor in order to simplify the experiment and to allow for greater numbers of animals in each group. I also aimed to include a positive control group using primary islets, which were chosen due to their successful use as positive controls by other groups in humanised mouse experiments[218]. While there was a noticeably greater level of human CD45+ cell infiltration into the allogeneic 325 CO grafts, there was no evidence of graft loss or damage in the allogeneic grafts. The 325 allogeneic graft showed evidence of being highly proliferative and healthy, forming large, regular, duct-like structures. The 325 allogeneic grafts were larger than any CO graft observed previously or since, from any CO line, including the initial line 200 CO non-humanised grafts that had remained *in vivo* for ten weeks (figure 5.5) - eight weeks longer than the 325 CO grafts. In contrast, while the autologous 286 CO grafts showed lower levels of infiltrating leukocytes compared to the allogeneic grafts, the grafts themselves were noticeably less robust. While the 286 CO grafts did survive *in vivo*, they were much smaller in size than the 325 grafts and showed a much less ordered structure. Due to the low numbers of infiltrating leukocytes, this was unlikely to be due to an autoimmune response but instead due to the inherently poor *in vivo* survival capability of the 286 CO line. This assessment is supported by the fact that the 286 line was entirely unable to survive in the later 235/286 SpMC-reconstituted humanised mouse experiment (figure 5.10), even in non-humanised controls where there was no possibility of immune rejection.

In general, the immune response was notably less in all HSC-reconstituted humanised mice than in SpMC-reconstituted humanised mice, both in terms of the levels of peripheral blood engraftment, the extent of human lymphocyte infiltration into the graft area and any effect on graft morphology and survival. This is likely partially due to the lack of a GVHD response in the HSC-reconstituted model,

however, there are also multiple limitations of the HSC-reconstituted humanised model itself that likely contributed to the sub-optimal immune response observed in this experiment. These limitations include the lack of mature T cells due to improper thymic education, the inability of B cells to undergo class switching and the subsequent lack of IgG, and the lack of fully developed lymph nodes and splenic germinal centres in immunodeficient mouse strains[135]

The humanised mouse models I used utilised young adult (5-6 weeks) NSG mice rather than neonates as the use of neonates was found to result in a high rate of accidental death within our group and so was abandoned. This has led to a much greater rate of survival for the animals in the experiments, however the engraftment of older mice may not be as effective as with neonates[280,295]. Equally, while HSCs from cord blood donors can provide better engraftment[296], due to the experimental requirement for autologous controls wherever possible, I used HSCs from adult donors. This enabled me to better experimental design, however it does mean the immune engraftment may be less effective. Our group previously attempted to improve efficacy of our HSC-reconstituted model using HLA II DR4 transgenic mice but this was shown to be ineffective and showed no improvement in humanisation, either overall or of any specific cell type (personal communication).

The impact of HLA matching on the immunogenicity of CO allografts

I aimed to investigate whether HLA matching could reduce the immunogenicity of CO grafts, using humanised mouse models. Reports have indicated that iPSC-derived cellular therapies show reduced immunogenicity and graft rejection when transplanted into non-human primates[168,170], although this finding remains controversial[286], however this is the first time, to our knowledge that the question of HLA matching has been addressed with primary-derived cellular therapies in a humanised mouse model. While the importance of HLA matching in liver transplantation remains unclear, with the majority of reports suggesting that it has no impact on patient or graft survival outcomes[154,155], the question of whether or not cholangiocyte cellular therapies are improved by HLA matching is worth investigating as it is likely that a purified CO graft or bioengineered biliary tissue would elicit a different immune response than a solid organ liver graft. In solid organ transplantation, the liver is the organ most likely to achieve operational tolerance[288] – the absence of graft rejection after an allogeneic transplant without the requirement for immunosuppressive treatment[297]. While the exact causes of this tolerising effect is unclear, it is unlikely to be seen in a purified cholangiocyte cellular therapy allograft or bioengineered extrahepatic bile duct as liver tolerance is likely the result of factors specific to the anatomy and physiology of the liver as a whole, such as the presence of tolerising APCs such as Kupffer cells, sinusoidal endothelial cells and dendritic cells[130] and the ability of hepatocytes to express tolerance-inducing ligands such as Programmed Death 1 ligand (PD-L1) and Fas ligand (FasL), which induce apoptosis in autoreactive and alloreactive T cells[298]. These factors would not be present in a CO-

derived cellular therapy, increasing the likelihood that other methods to reduce immunogenicity, such as HLA-matching, may be required.

In accordance with the current practice for kidney transplantation[299,300], I defined a complete HLA match as matching on both alleles for HLA A, B and DR. While it is typically thought that HLA matching for cellular therapies would likely involve the use of homozygous HLA donors[163], due to generating our CO lines from deceased organ donors, I did not have ready access to such homozygous donors. Equally, using gene editing techniques to generate homozygous HLA CO lines, as has been reported for other cellular therapies[171], was beyond the scope of this project. I instead relied on identifying a complete HLA match within our banks of CO lines and SpMC/HSC donors, which I was able to do by virtue of having generated over sixty CO lines and banked immune cells from over 300 donors (immune cells were banked primarily by the Cambridge Biorepository for Translational Medicine, with assistance from myself and other members of the Saeb-Parsy group).

Assessment of the role of HLA matching in CO immunogenicity is still ongoing and will require further *in vitro* and *in vivo* experiments. I conducted a first set of experiments by an HSC-reconstituted humanised mouse model. As I had only identified one fully HLA matched CO line and HSC donor pair (299 and 263 respectively), I was unable to perform a crossover experiment of the kind described in figures 5.12 - 5.16 and so the experimental set up was vulnerable to potential quality issues with the 263 HSCs and 299 CO lines in terms of humanisation and *in vivo* graft survival. Additionally, while HSC engraftment can vary between donors, it is not possible to test the quality of an HSC donor before the start of an experiment due to the long timecourse of humanisation and the typically low numbers of available HSCs for each donor. I elected to use HSCs from donor 235 as a fully mismatched donor due to the relatively high number of available HSCs (table 5.1).

While both donors engrafted well in the majority of animals (figure 5.20) the 263 HSC-reconstituted mice showed higher levels of peripheral blood engraftment than the 235 HSC-reconstituted mice, likely in part due to the higher, and steadily increasing, proportion of CD3+ T cells in the peripheral blood of the 263 HSC-reconstituted mice (figure 5.21), which could be an indicator of the beginning of a GVHD response. This discrepancy between the engraftment of the HLA-matched and HLA-mismatched donors is problematic, as it represents a potential confounding factor in the comparison of the immunogenicity of both groups. However, the analysis of the engraftment in the peripheral blood, spleen and bone marrow at the experimental endpoint is still ongoing and it remains to be seen if this difference between donors will be consistent across all immune compartments. While this experiment cannot be repeated due both to logistical considerations and the lack of any further 263 HSCs, one potential way in which the difference between 263 and 235 engraftment could be controlled for would be to repeat the fully mismatched arm of the experiment with a variety of HSC donors with different capacities for humanisation.

A major difference to the design of this experiment compared to previous HSC-reconstituted and SpMC-reconstituted humanised mouse experiments was the use of BLI to assess the degree of graft survival across different groups. I had previously assessed immunogenicity through lymphocyte infiltration into the CO graft area alone. While graft infiltration is an important aspect of an immune response and an indicator of rejection, it is not able to provide information on the extent of graft loss or growth *in vivo*, which is essential for a complete understanding of the immunogenicity of a cellular therapy. Additionally, the method of assessing lymphocytic infiltration into the graft required the cryosectioning of the entire graft area, the immunostaining of multiple randomly-selected sections from different areas of the graft and the manual counting of all leukocytes in the graft area of the chosen sections using the Image J programme. This method is susceptible to bias in the selection and counting process, and, importantly, is highly time consuming, making the completion of graft infiltration assessment for a humanised mouse experiment very challenging within the timeframe of this project. To address these limitations, I incorporated BLI of CO grafts *in vivo* to compare the survival of grafts between groups in both a qualitative and quantitative manner, while supporting these data with a qualitative assessment of lymphocyte infiltration into the CO grafts.

Despite the advantages of BLI outlined above, there are several limitations to the technique, particularly as I was only able to establish a BLI system and reliable luciferase CO lines immediately before the point at which those lines had to be transplanted into HSC-reconstituted humanised mice. The limitations of the 299-RFP-Luc CO line specifically, including uncertainty as to the stability of the Ef1α-RFP-Luciferase construct and the efficacy of our line purification, are detailed in the discussion of chapter 3. In addition, while I have begun assessment of the sensitivity of BLI in terms of detecting low cell numbers under the kidney capsule (figure 3.15), this work is still ongoing and the ability of the system to detect small changes in graft size and to detect grafts of small overall size is uncertain. Furthermore, throughout this HSC-reconstituted humanised mouse experiment, I was limited in the number of occasions animals could be imaged (up to three times in live mice), which prevented me from extending the time course of the experiment or from performing BLI more than once a week. I am currently in the process of amending this aspect of our project licence to ensure that this limitation will not affect any future humanised mouse experiments.

During the time course of our experiment I observed a large decrease in the CO graft size both qualitatively (figure 5.25) and quantitatively (figures 5.26 and 5.27) in all animals across all groups, regardless of humanisation status or HLA matching. I have observed histological evidence of a similar loss of initial graft mass in previous lines transplanted *in vivo*, including in lines that survived well overall. This suggests that this early loss of cells after transplantation is an unavoidable aspect of transplantation for all CO grafts, regardless of immune response, likely due to the stress caused to the cells during the preparation for transplantation and the transplantation process itself. In experiments in which graft survival is assessed immediately after transplantation and for a short duration (3 weeks),

this initial loss of cells across all groups significantly limits the ability to assess the impact of the immune response on graft size. This limitation is likely to be most significant in the HSC-reconstituted humanised mouse model, however, which shows a less substantial immune response than the SpMC-reconstituted humanised mouse model, and so any effects of immune rejection are likely to be more subtle. Due to the nature of the HSC-reconstituted humanised mouse model, which provides a window of between 8-4 weeks of optimal engraftment (16-24 weeks after reconstitution) for transplantation experiments, it is not possible to first transplant the CO grafts and wait until after the initial graft loss has passed and the graft begins to proliferate again to the point of BLI detection before humanising the mice. However this strategy could potentially be used in SpMC-reconstituted humanised mice, as demonstrated in the initial SpMC-reconstituted humanised mouse experiments.

At the final imaging time point, I observed that CO grafts were not detectable in any animals of any of the groups with the exception of one non-humanised NSG mouse transplanted with 299-RFP-Luc COs (figure 5.25). There was no difference in the extent or rate of graft loss in the HLA-matched and HLA-mismatched groups. While it is promising that one animal in the non-humanised group retained a visible CO graft, it cannot be decisively concluded that this was due to the lack of humanisation, or that the loss of the grafts in other groups was due to immune rejection. This is due to the fact that only one animal in the non-humanised group retained a visible graft and that animal had initially received a higher number of cells than most other animals (as determined by quantification of luminescence at the D1 time point). Additionally, it is not certain that grafts have been truly lost in all other animals without histological assessment, which is still in progress.

The preliminary data shown by BLI suggest that there is no difference between the immune response to HLA-matched and HLA-mismatched CO grafts. This is in agreement with a recent report[286] showing that both HLA-matched and HLA-mismatched iPSC-derived neurons are rejected in non-human primates. However, histological analysis is needed to confirm these findings. Additionally, the HLA-matched (donor 263) humanised mice showed a noticeably higher proportion of CD3+ T cells in the peripheral blood compared to the HLA-mismatched (donor 235) humanised mice (figure 5.21) and a higher level of CD45+ cell engraftment overall (figure 5.20) and it is possible that the apparent equivalence of the immune response to HLA matched and mismatched grafts is largely due to the more robust humanisation in the HLA-matched humanised mice.

Preliminary histological assessment of one HLA matched and one HLA mismatched graft (figure 5.28) demonstrate graft survival in both instances, despite the lack of visible luciferase signal in these animals at and after 14 days post-transplantation. This suggests either that the luciferase construct was silenced *in vivo* or that the luciferase signal fell below the level of detection due to CO cell death between D1 and D14 post-transplantation. Silencing of the luciferase construct is unlikely as The 299 RFP CO line has been demonstrated to retain luciferase expression at passage 20 *in vitro*, 18 passages after viral

transduction with the Efl α-luciferase-RFP construct (figure 3.23). It is possible, however, that the *in vivo* environment results in construct silencing despite persistent *in vitro* expression. Immunofluorescence staining for luciferase protein will be required to determine whether the construct has been silenced *in vivo*.

The CO graft in the HLA matched kidney sections was noticeably larger than the graft in the HLA mismatched sections (figure 5.28), which could indicate that HLA matching promotes overall graft survival. However, due to a technical error, a greater number of CO cells was transplanted into the HLA matched animals compared to the HLA mismatched animals, and so the larger size of HLA matched grafts at the point of the final cull could be due either partially or entirely to the higher number of cells delivered at transplantation. Due to the loss of luciferase signal in both the HLA matched and mismatched groups at D14 post-transplantation, it is not possible to accurately determine whether or not the extent of graft survival at the final cull relative to the initial graft size is greater in HLA matched grafts compared to HLA mismatched grafts.

Human leukocyte infiltration in and around the CO graft appears to be greater in HLA matched sections compared to HLA mismatched sections (figure 5.28), however this is likely at least partially due to the overall greater degree of humanisation, particularly the greater degree of CD3+ leukocyte engraftment, within the HLA matched animals (figure 5.21). Once histological analysis of all kidney grafts is completed, quantification of leukocyte infiltration normalised to overall human leukocyte engraftment at the point of the final cull will be required to accurately determine the comparable degree of leukocyte infiltration into HLA matched and mismatched grafts.

Preliminary immunofluorescence staining of an HLA matched graft demonstrated a high proportion of CD4+ lymphocytes in the graft area (figure 5.29). Immunofluorescence staining for other lymphocyte subtypes is still being optimised so it is not currently possible to determine whether these CD4+ lymphocytes are T effector cells or T helper cells, and so not currently possible to determine whether this CD4+ infiltration represents an immunogenic or immunomodulatory response. Further immunofluorescence staining for markers such as CD8, granzyme B, FoxP3 and CD25, combined with TUNEL staining on CO cells for evidence of apoptosis, will be required to assess the nature of this immune response. Additionally, histological analysis of the HLA mismatched grafts is also required, to determine whether the proportions of leukocyte subtypes and apoptotic cells differ between HLA matched and mismatched grafts, and so to determine whether the nature of the immune response is the same or different between these two groups.

I have begun preparation for further humanised mouse experiments to assess HLA matching in CO grafts, this time using the SpMC-reconstituted humanised mouse model. I have confirmed that SpMCs from all key donors are able to adequately engraft in NSG mice (figures 5.31 and 5.32), although, due to variation in the rate of engraftment, adjustments may need to be made to the timing of SpMC

reconstitution or CO transplantation to ensure that all groups are equally engrafted at the time of the experiment. Further preliminary experiments will be needed to address the limitations discussed above before this SpMC-reconstitution experiment can be conducted, including a thorough assessment of the capacity of the BLI system to assess graft survival under different conditions and a determination of the stability of our luciferase construct over time. Once these concerns have been addressed, however, it is hoped that the planned SpMC-reconstitution experiment, combined with the ongoing analysis of my recent HSC-reconstitution experiment, will provide definitive insight into the role of HLA matching on the immunogenicity of CO cellular therapies.

CHAPTER 6: FUTURE WORK AND CONCLUSIONS

6.1 Future work

6.1.1 Refinement of the method for generating bioengineered biliary tissue

I have demonstrated that COs can be used to generate bioengineered biliary tissue in the form of artificial bile ducts capable of rescuing a model of extrahepatic biliary injury. I further demonstrated that this procedure can be further refined to produce more physiologically relevant constructs with COs seeded in the lumen of the collagen construct. The next step for this project is to refine the seeding process to improve the survival rate of seeded cells and to characterise the length of time needed in culture before full confluence is reached. Additionally, work is ongoing by Fotios Sampaziotis and Teresa Brevini to develop human-sized bioengineered bile ducts. These larger constructs are being generated using COs seeded on either densified collagen scaffolds[125] or decellularised[301,302] porcine bile ducts and are currently being tested *in vivo* in large animal models to determine the efficacy of the construct to rescue a model of biliary injury and the survival of the graft itself. Additionally, work is ongoing to investigate the impact of incorporating elastin[303] and other extracellular matrix components into our densified collagen scaffolds.

Additionally, a future application of the murine-sized seeded bile duct constructs is to assess the immunogenicity of COs in a more physiologically relevant niche - while the current model involves the transplantation of COs as a cell suspension under the kidney capsule, many future CO-based therapies would involve the transplantation of a bioengineered extrahepatic bile duct and so it is important to investigate the immunogenicity of COs in an extrahepatic biliary niche.

6.1.2 Refinement of the method for *in vivo* bioluminescent imaging

In response to the challenges encountered with monitoring and assessing the survival of the CO grafts *in vivo* in both humanised and non-humanised mice, I have developed CO lines expressing luciferase to enable bioluminescent live imaging *in vivo* and the quantification of CO graft size by the measurement of luminescence. BLI is increasingly becoming an essential tool in humanised mouse studies of graft rejection[173,175,221] and so fully establishing the BLI system for use in future experiments is an important priority. While I have successfully generated luciferase lines capable of BLI monitoring *in vivo*, and utilised these lines in a humanised mouse experiment, some unanswered questions still remain before this system can be fully effective. I generated the luciferase CO lines using a construct with an Ef1α promoter, known to produce stable expression of integrated constructs. However, I have not yet tested the long-term stability of the luciferase constructs in COs either *in vitro* or *in vivo*. Moreover, I have not yet assessed whether or not the random integration method used to deliver the

construct has any negative effects on the transduced COs. This will be done by a combination of *in vitro* analysis of cholangiocyte marker expression and function and *in vivo* comparison of the survival of luciferase CO lines and WT lines. It is also important to assess the sensitivity of BLI detection *in vivo,* as it is possible that any differences in CO graft survival detected in future humanised mouse experiments (for example, between fully and partially HLA-matched lines) may be subtle and it is critical to better understand the extent to which the BLI system is capable of detecting such differences.

6.1.3 Continued assessment of HLA class II expression in COs under inflammatory conditions

I have assessed the expression of HLA class I and II on COs under a range of different pro-inflammatory conditions, including exposure to super-physiological levels of IFN-γ *in vitro*, *in vitro* co-culture with activated leukocytes and transplantation *in vivo* in immunocompetent and humanised mice. While the effect of *in vitro* cytokine challenge with recombinant IFN-γ has been well-established throughout this dissertation, the assessment of the impact of lymphocyte co-culture and an *in vivo* inflammatory environment is preliminary and requires further investigation. I aim to confirm the findings of these preliminary experiments and to expand upon them, for example through assessing HLA class II expression in non-humanised NSG mice, quantifying HLA class II expression on CO grafts through flow cytometry and extending *in vitro* co-culture experiments with activated lymphocytes through the addition of further experimental conditions and controls. Additionally, while I have extensively assessed the impact of IFN-γ on COs, it is important to investigate the expression of HLA and other immunogenic markers on COs after exposure to other pro-inflammatory cytokines such as TNF-α, IL-1 and IL-6. It would also be useful to investigate combinations of two or more pro-inflammatory cytokines on CO antigenicity, particularly as I have already demonstrated that COs are not capable of expressing HLA-DP after stimulation with purified IFN-γ but that HLA-DP can be upregulated on COs during a strong xenogenic immune response *in vivo*.

6.1.4 Refinement of the SpMC humanised mouse model

One of the major limitations of the SpMC-reconstituted humanised mouse model is the inevitable development of GVHD[279] following successful engraftment. While this does not prevent the assessment of allograft rejection using this model[304], it can limit the timeframe available for experiments and can potentially complicate the interpretation of experimental data without the use of adequate autologous and negative controls. To address this problem, several strains of NSG mice lacking murine MHC class I and II have been generated and have been shown to limit the development of GVHD in an SpMC/PBMC-reconstituted humanised mouse model, while still allowing for alloimmune rejection of human grafts[209]. Our group has recently acquired the NSG-$(K^bD^b)^{null}(IA)^{null}$ strain and the engraftment

capacity of these mice is currently being tested by several group members. I plan to assess the capacity of these mice to reject allogeneic CO grafts after SpMC reconstitution and, if the results are favourable, continue to use this strain in all future SpMC-reconstituted humanised mouse experiments, including the assessment of HLA-matched and mismatched CO grafts.

6.1.5 Further assessment of the role of HLA matching in CO immunogenicity

I have presented the preliminary results of HSC-reconstituted humanised mouse experiments to investigate the immunogenicity of HLA-matched compared to HLA-mismatched CO grafts. The analysis of this experiment is still ongoing, so the first step is the completion of this work. I will assess the humanisation at the point of the final cull in the peripheral blood, spleen and bone marrow and compare the engraftment between the two groups of HSC reconstituted mice (HLA-matched and mismatched). I will also analyse the CO grafts through histological analysis, including assessment of graft morphology, lymphocyte infiltration and CO cell apoptosis or proliferation.

I will also assess the survival of fully HLA-matched, partially HLA-matched and fully HLA-mismatched CO grafts using the SpMC-reconstituted humanised mouse model. Solid organ transplants are, when applicable, typically matched on both HLA class I (A and B) and HLA class II (DR). However, a purified population of one non-haematopoietic cell type (such as cholangiocytes) may not express HLA class II under normal circumstances: Matching for HLA class II may, therefore, not be as important as in solid organ transplantation, where there donor passenger HLA class II-expressing antigen presenting eclls are expected to be transferred to the recipient in the transplanted organ. My investigation into the antigenicity of COs suggests that they may express HLA class II after transplantation into immunocompetent recipients, however the impact of this has not yet been fully assessed in a humanised mouse experiment.

An important method of investigating immunogenicity is the use of lymphocyte co-culture assays, where the cells of interest are exposed to allogeneic lymphocytes and the degree of lymphocyte activation and cytotoxic cell killing are monitored. I plan to use this method to complement the *in vivo* humanised mouse studies, to investigate the ability of COs to activate allogeneic T cells. I will investigate the ability of COs to activate T cells through the direct alloimmune pathway by co-culture of T cells and COs alone, and through the indirect pathway by co-culture of COs with T cells and professional antigen presenting cells. I will compare the activation of T cells by HLA-matched, partially matched and mismatched CO lines. Additionally, I will investigate the ability of cytotoxic CD8+ T cells to kill COs of different degrees of HLA matching.

6.1.6 Amelioration of CO immunogenicity through gene editing

In this dissertation, I have focused on assessing the immunogenicity of WT COs, or on the use of HLA matching to ameliorate immunogenicity. However, this is only one possible mechanism for producing cellular therapies with reduced immunogenicity. Another promising option is the development of "universal" cellular therapies through genetic engineering by removing or silencing HLA expression, particularly HLA class I expression, on allogeneic cells[283,305]. While the complete knock-out of HLA class I can lead to graft detection and cytotoxic killing by NK cells, human ESCs have recently been edited using CRISPR technology to lack all expression of HLA-A, B and C while overexpressing HLA-E[175]. This strategy enabled the cells to evade immune detection by cytotoxic T cells, anti-HLA antibodies and NK cells. I aim to generate similar "universal" COs in collaboration with the Ghevaert group, using a CRISPR/Cas nickase system[306]. The Ghevaert group have already generated HLA class I KO iPSCs from six iPSC lines using this method. These iPSC lines can be successfully differentiated into multiple cell types and the differentiated cells can survive *in vivo.* Furthermore, these cells retain HLA class I KO status at all times, including after stimulation with IFN-γ. I will initially generate HLA class I KO COs without HLA-E overexpression, and assess their antigenicity and immunogenicity both *in vitro* through lymphocyte co-culture and cytokine challenge and *in vivo* through the use of HSC-reconstituted and SpMC-reconstituted humanised mice. I will additionally assess the impact of NK cell cytotoxicity on HLA I KO COs using *in vitro* co-culture assays and humanised mice. If these HLA I KO COs are found to be vulnerable to NK cell cytotoxic killing then I will additionally generate HLA I/HLA E overexpression COs and assess their ability to evade detection by both cytotoxic T cells and NK cells and for HLA I/HLA E overexpression CO grafts to survive *in vivo.*

6.2 Conclusions

The key outputs of my experimental work are summarised below:

- Refining the existing method for deriving and culturing COs by aiding in the development of a protocol for deriving COs from intrahepatic bile ducts
- Refining the existing method for the generation of bioengineered biliary tissue by aiding in the development of a protocol for seeding COs on the luminal surface of densified collagen tubular scaffolds
- Demonstrating and quantifying the ability of COs to upregulate HLA class II molecules upon exposure to a range of *in vivo* and *in vitro* pro-inflammatory environments
- Comparing the expression of HLA molecules on primary cholangiocytes and COs across multiple donors
- Generating a bank of over 60 CO lines from over 40 unique, HLA-matched donors and identifying HLA-matched immune cell donors
- Generating luciferase-expressing COs and demonstrating their utility in monitoring CO grafts *in vivo*, including in humanised mouse models. The use of BLI in live mice also allows for a reduction in the total number of animals required for timecourse experiments, in keeping with the principles of the 3Rs (Replacement, Reduction and Refinement) of humane animal research.
- Demonstrating that COs can induce an immune response in an allogeneic SpMC-reconstituted humanised mouse model
- Comparing the immune response to allogeneic and autologous COs in two complementary humanised mouse models
- Generating preliminary results of the comparison of the immunogenicity of HLA-matched and HLA-mismatched CO grafts

In conclusion, the results and methods presented here have provided new tools for the development of cholangiocyte cellular therapies and the assessment of their immunogenicity, as well as advancing our knowledge in the fields of both the transplant of cellular therapies and humanised mouse models. These results have laid the groundwork for exciting future experiments, both currently ongoing and in the years to come.

CHAPTER 7. APPENDIX

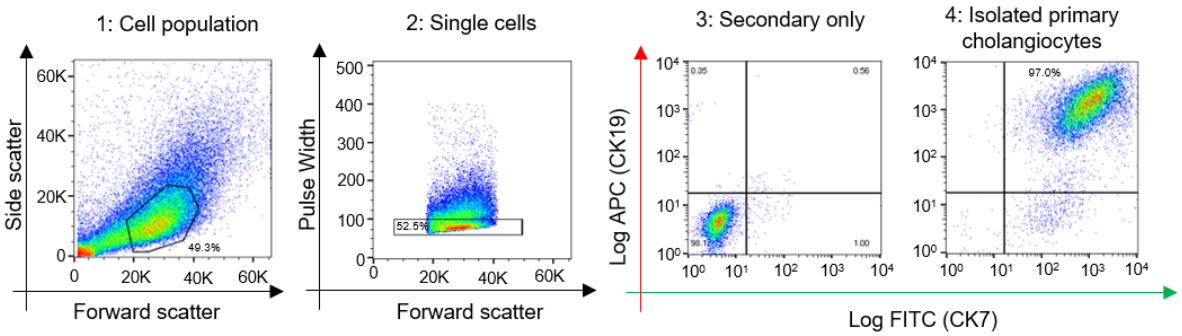

Appendix Figure 1: Gating strategy for flow cytometric analyses of cholangiocytes

Representative flow cytometry plots showing gating strategy for CK7+/CK19+ flow cytometric analyses, gating on: 1: exclusion of debris; 2: exclusion of doublets; 3: secondary-only control to exclude negative population; 4: representative C19+/CK7+ population.

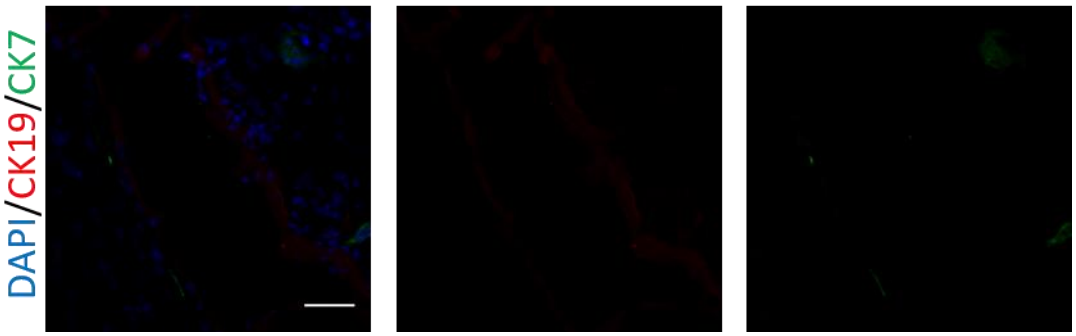

Appendix Figure 2: Lack of survival of CO line 261 BD
Immunofluorescence image showing a lack of survival of the 261 BD line 4 weeks after transplantation. CK19 (red) and CK7 (green) show background staining but no specific staining of surviving cells. Scale bar- 100 µm.

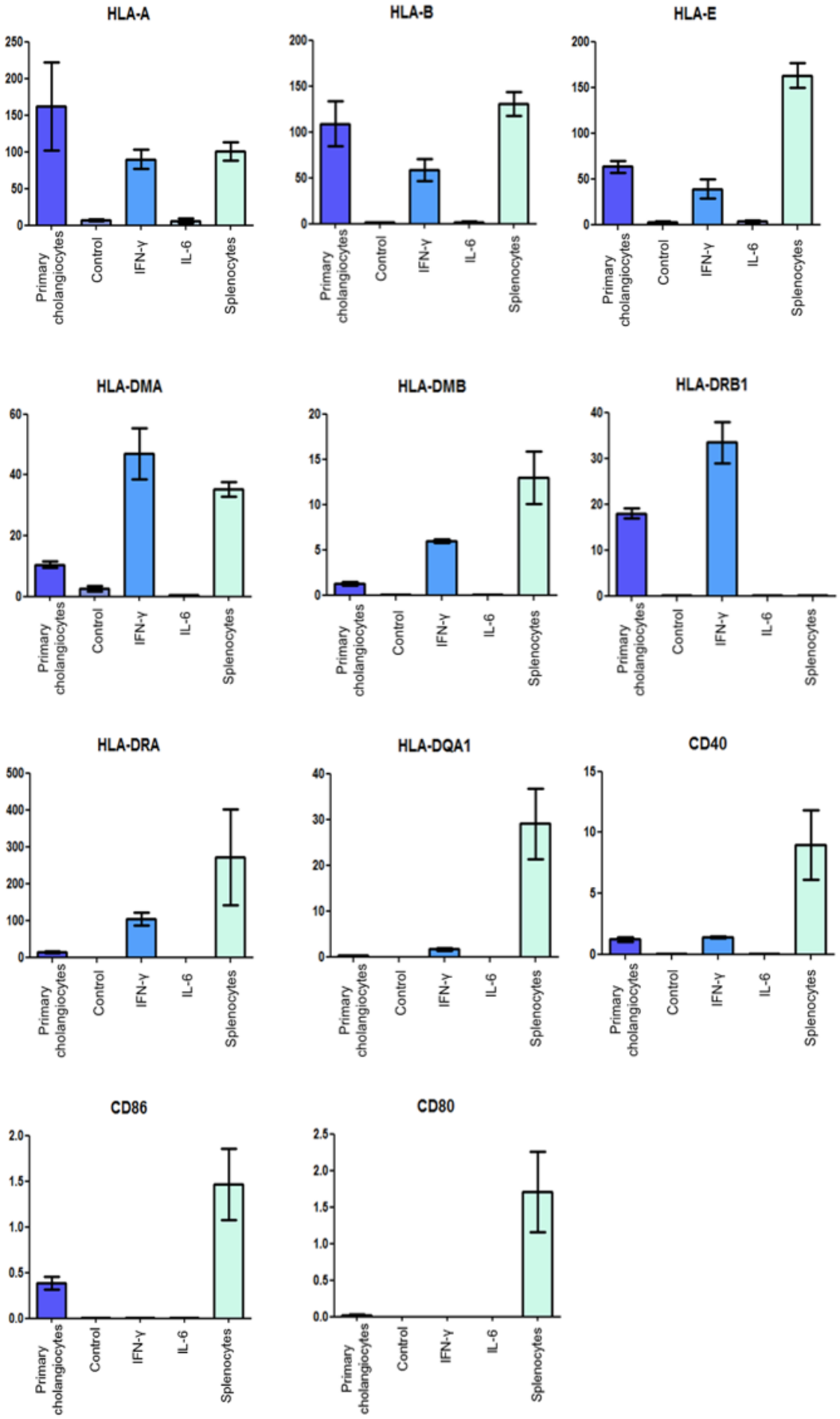
HLA-A
HLA-B
HLA-E
HLA-DMA
HLA-DMB
HLA-DRB1
HLA-DRA
HLA-DQA1
CD40
CD86
CD80
Primary cholangiocytes
Control
IFN-γ
IL-6
Splenocytes

Appendix Figure 3: Expression of immunogenic markers in primary cholangiocytes and COs after cytokine challenge
RT-qPCR analyses showing expression of immunogenic markers in primary cholangiocytes, control (untreated) COs, IFN-γ treated COs, IL-6 treated COs and splenocytes as a positive control. Values relative to the housekeeping gene HMBS. IFN-γ and IL-6 treatment for 72 hours at 100 ng/ml.

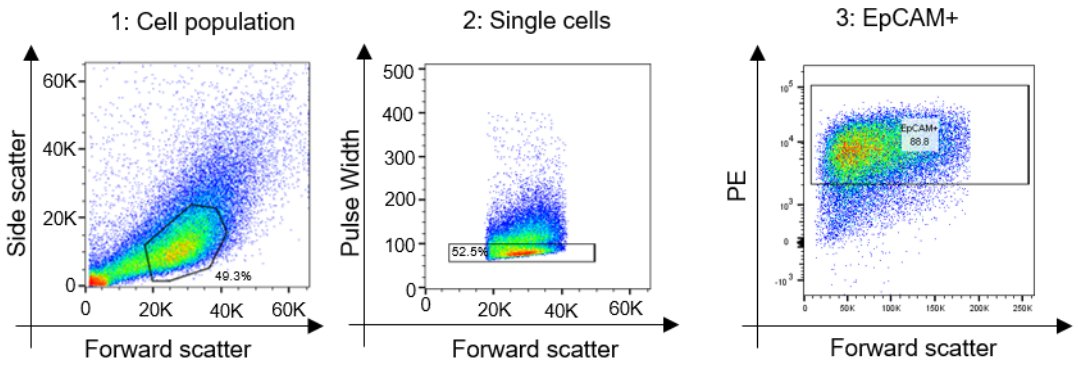

Appendix Figure 4: Gating strategy for CO and primary cholangiocytes HLA expression
Representative flow cytometry plots showing gating strategy for flow cytometric analyses of HLA expression, gating on: 1: exclusion of debris; 2: exclusion of doublets; 3: EpCAM+ cells.

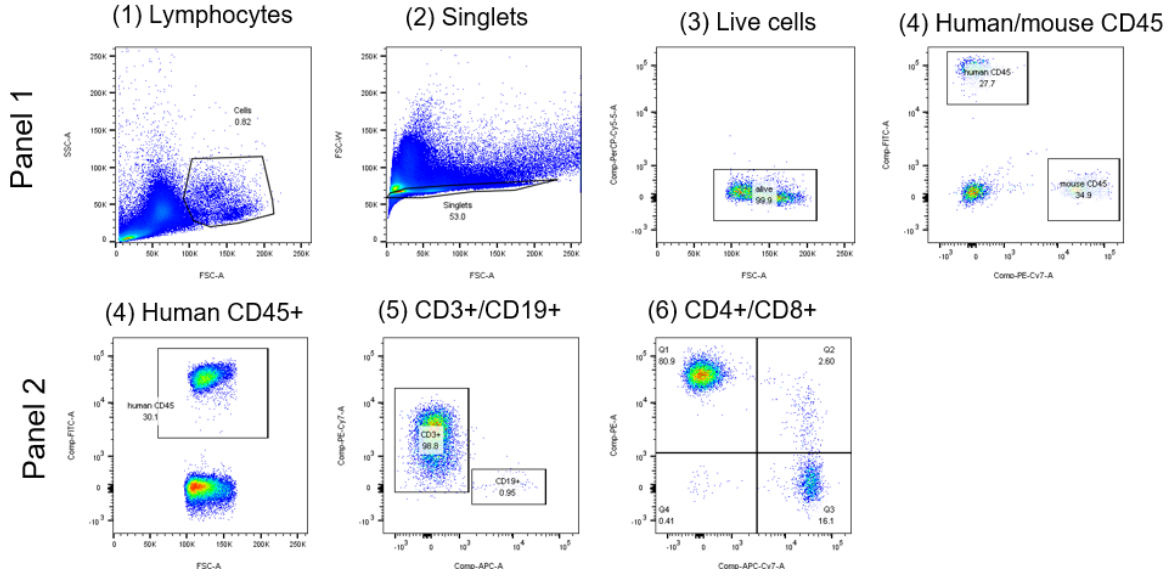

Appendix Figure 5: Gating strategy for flow cytometric analyses of lymphocyte populations in humanised mice from peripheral blood, bone marrow and spleen
Representative flow cytometry plots showing gating strategy for flow cytometric analyses of leukocytes from humanised mice, gating on: (1) exclusion of debris; (2) exclusion of doublets; (3) live cells. Panel 1: (4) Human CD45+/mouse CD54.1+ Panel 2: (4) Human CD45+; (5) CD3+/CD19+; (6) CD4+/CD8+.

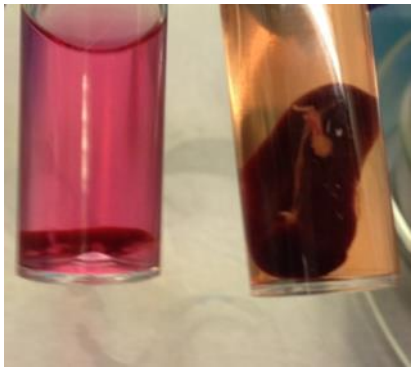

Appendix Figure 6: Enlarged spleen of a SpMC-reconstituted humanised mouse
Image of the spleen of a non-humanised NSG mouse (left) compared to an SpMC-reconstituted humanised mouse (right) after 3.5 weeks of engraftment with human SpMCs (peripheral blood engraftment: 60% human CD45+).

Media	Ingredients	Company	Amount/Dilution
LX2 media	High glucose DMEM, GlutaMAX™ Supplement	Life Technologies (10566-016)	490 ml
	Fetal Bovine Serum (FBS)	GE Life Sciences (SH30070.03)	50 ml
	Pen/Strep	Life Technologies (15140122)	5 ml
MEF media	Advanced DMEM F12	Thermo Fisher Scientific (12634010)	450 ml
	Fetal Bovine Serum (FBS)	GE Life Sciences (SH30070.03)	50 ml
	Pen/Strep	Life Technologies (15140122)	5 ml
	B-mercaptoethanol	Sigma Aldrich (M6250-10ML)	3.5 µl
Complete RPMI	RPMI 1640 Medium, GlutaMAX™ Supplement	Life Technologies (61870-010)	500 ml
	Fetal Bovine Serum (FCS)	GE Life Sciences (SH30070.03)	50 ml
	Pen/Strep	Life Technologies (15140122)	5 ml
William's E	William's E	Gibco, Life Technologies	443 ml
	Nicotinamide	Sigma Aldrich	10mM (12.5 ml)
	Sodium Bicarbonate	Sigma Aldrich	17mM (8.5 ml)
	Sodium Pyruvate	Invitrogen	6.3mM (3.15 ml)
	Glucose	Sigma Aldrich	14mM (7 ml)
	HEPES	Invitrogen	20mM (10 ml)
	ITS+	BD Biosciences	5 ml
	Pen/Strep	Life Technologies (15140122)	5 ml
	Dexamethasone	R&D Systems	0.1µM (5µl)
	Glutamine	Life Technologies (25030)	2mM (5.3 ml)

Appendix Table 1: List of all media used in cell cuture

Gene	Forward primer sequence	Reverse primer sequence
HMBS	GGAGCCATGTCTGGTAACGG	CCACGCGAATCACTCTCATCT
CK7	GATTGCTGGCCTTCGGGGT	TCATCACAGAGATATTCACGGCTC
CK19	ACGACCATCCAGGACCTGCGG	TCCCACTTGGCCCCTCAGCGTA
Sox9	CTCTGGAGACTTCTGAACGAGAG	CCTTGAAGATGGCGTTGGGG
GGT	GTGAGAGCAGTTGGCTGTGC	GTTGAACTCTGCTGTGGGGC
HLA-A	TCACAGACTGACCGAGTGGA	ATGGTGTGAGAACCGGCCT
HLA-B	CGAGGCCGGGTCTCACA	TAGGCTCTCCGCTGCTCC
HLA-E	ACTCTAAGGCTGAGTGGAGC	AAGACACATAGGGGAGGCGT
HLA-DMA	TCCAGAGGGTTTCCTATCGC	ACAGGGACGGAATGATGCTG
HLA-DMB	AGCTGGCCACTCTAGTTACAC	AGGAATGAGGTCCCCCAAGT
HLA-DRA	AGCACTGGGAGTTTGATGCT	GCTTTTGCGCAATCCCTTGA
HLA-DRB1	GGCAGCCTAAGAGGGAGTGT	CTTAGGTTGGACTCGCCGCT
HLA-DQA1	GTGGCAAAACACAACTTGAACA	TGACCTCAGGAACCTCATTGG
CD40	CACCCTTGGACAAGCTGTGA	GATAAAGACCAGCACCAAGAGG
CD80	GGGGAAATGTCGCCTCTCTG	GTGGATTTAGTTTCACAGCTTGC
CD86	ATATTAGGTCACAGCAGAAGCAGCC	TCAGAGGAGCAGCACCAGAGA

Appendix Table 2: List of all primers used for RT-qPCR analyses

	Donor ID	GB/BD	Age	M/F	DBD/DCD	Blood group	Successful line
1	241	BD	76	M	DCD	AB+	Y
2	241	GB	76	M	DCD	AB+	Y
3	241	IHD (tissue)	76	M	DCD	AB+	Y
4	241	IHD (EpCAM)	76	M	DCD	AB+	N
5	242	BD	50	M	DCD	O+	Y
6	242	IHD	50	M	DCD	O+	Y
7	243	BD	37	M	DCD	O-	Y
8	243	GB	37	M	DCD	O-	Y
9	247	BD	27	F	DBD	O-	N
10	256	BD	56	M	DBD	B+	Y
11	261	BD	77	M	DCD	A+	Y
12	261	GB	77	M	DCD	A+	Y
13	261	IHD	77	M	DCD	A+	Y
14	263	GB	51	F	DCD	A+	Y
15	274	GB	68	M	DCD	A	Y
16	274	IHD	68	M	DCD	A	Y
17	275	GB	63	M	DCD	O+	Y
18	275	BD	63	M	DCD	O+	Y
19	275	IHD (EpCAM)	63	M	DCD	O+	Y
20	283	GB	73	M	DCD	AB+	Y
21	283	BD	73	M	DCD	AB+	Y
22	283	IHD	73	M	DCD	AB+	Y
23	286	BD	54	M	DCD	AB+	Y
24	286	GB	54	M	DCD	AB+	Y
25	292	BD	57	M	DBD	A+	Y
26	292	GB	57	M	DBD	A+	Y
27	292	IHD (EpCAM)	57	M	DBD	A+	Y
28	295	GB	79	F	DBD	O+	Y
29	299	BD	46	M	DBD	O+	Y
30	302	IHD (tissue)	44	M	DCD	B+	Y
31	302	BD	44	M	DCD	B+	Y
32	310	BD	51	M	DBD	O+	Y
33	312	BD	77	F	DCD	O+	Y
34	313	BD	35	F	DCD	O-	Y
35	325	BD	44	F	DCD	O+	Y
36	325	GB	44	F	DCD	O+	Y
37	328	GB	52	F	DCD	B+	Y
38	337	GB	25	F	DCD	A+	Y
39	339	GB	73	F	DCD	A+	Y
40	343	GB	70	F	DBD	A+	Y
41	351	BD	43	F	DBD	A+	Y
42	356	GB	41	F	DCD	O+	Y
43	356	BD (not flushed)	41	F	DCD	O+	N
44	362	GB	60	M	DCD	A+	Y
45	367	GB	70	M	DCD	O+	Y
46	368	GB	58	M	DCD	AB+	Y
47	368	BD (not flushed)	58	M	DCD	AB+	N

48	376	GB	55	M	DCD	A+	Y
49	378	BD	49	M	DCD	O+	Y
50	382	BD (not flushed)	60	F	DBD	O+	Y
51	385	BD	31	M	DBD	O+	Y
52	386	BD (not flushed)	75	F	DCD	O+	N
53	386	GB	75	F	DCD	O+	Y
54	386	IHD (tissue)	75	F	DCD	O+	Y
55	390	BD (not flushed)	68	F	DCD	O+	Y
56	390	GB	68	F	DCD	O+	Y
57	390	IHD	68	F	DCD	O+	Y
58	PBC-1a	IHD (biopsy)	23	F	N/A	AB+	Y
59	PBC-1b	IHD (biopsy)	23	F	N/A	AB+	Y
60	PSC-1C	BD (ERCP)	44	M	N/A	O+	Y
61	PSC-2a	IHD (biopsy)	38	M	N/A	O+	Y
62	PSC-2b	IHD (biopsy)	42	M	N/A	O+	Y
63	PSC-2c	BD (ERCP)	42	M	N/A	O+	Y
64	400	BD	57	M	DBD	B+	Y
65	402	BD	63	F	DBD	O+	Y
66	405	BD	58	F	DBD	O+	Y
67	410	IHD	-	-	N/A	-	Y
68	414	GB	52	M	DCD	O-	Y
69	415	IHD	-	-	N/A	-	Y
70	422	BD	50	M	DBD	O+	Y
71	440	BD	48	M	DCD	A+	Y

Appendix Table 3: List of all CO donors isolated between September 2016 and August 2019
Table showing key details of all CO lines derived between September 2016 and August 2019: anonymised donor ID number; tissue type (bile duct (BD), gallbladder (GB) or intrahepatic ducts (IHD)); age; sex; donor type (if applicable) (donation after brain death (DBD) or donation after cardiac death (DCD); blood group; and the success of the line derivation.

Antibody	Company	Product Number	Dilution
Albumin	Bethyl Laboratories	A80-129A	1:100
CK19	Abcam	ab7754	1:100
CK7	Abcam	ab68459	1:100
MHC Class I	Abcam	Ab23755	1:1000
MHC Class II	Abcam	ab157210	1:200
Human CD45	Abcam	ab10558	1:100
Human CD45	BD Biosciences	555480	1:100
Ku80	Takara	Y40400	1:50
PerCP-7AAD	eBiosciences	00-6993-50	1:50
FITC-hCD45	MACS Miltenyi	51401276779	1:40
PE-Cy7-mCD45.1	Biolegend	110730	1:40
APC-CD19	eBiosciences	17-0199-41	1:50
PE-Cy7-CD3	Biolegend	300316	1:50
PE-CD4	Biolegend	317410	1:40
APC-Cy7-CD8	BD Pharminogen	557834	1:40
PE-EpCAM	Biolegend	324205	1:40
PE/Cy7-HLA I	Biolegend	311430	1:100
APC-HLA II	MACS Miltenyi	130-104-824	1:300
PerCP-mCD45.1	BD Biosciences	561047	1:100
PE-CD19	BD Biosciences	555413	1:50
PE Dazzle-CD20	Biolegend	302348	1:200
Zombie Aqua	Biolegend	423102	1:200

Appendix table 4: List of all antibodies used in immunofluorescence and flow cytometry analyses

I have included the published version of my first-author publication as an appendix to this thesis. Material from:

O. C. Tysoe, A. W. Justin, T. Brevini, S. E. Chen, K. T. Mahbubani, A. K. Frank, H. Zedira, E. Melum, K. Saeb-Parsy, A. E. Markaki, L. Vallier, F. Sampaziotis. Isolation and propagation of primary human cholangiocyte organoids for the generation of bioengineered biliary tissue. Nat Protocols

Published 2019

Publisher: Springer Nature Limited

CHAPTER 8. REFERENCES

1 Lazaridis, K. N. & LaRusso, N. F. The Cholangiopathies. *Mayo Clinic proceedings* **90**, 791-800, doi:10.1016/j.mayocp.2015.03.017 (2015).

2 Strazzabosco, M. & Fabris, L. Functional anatomy of normal bile ducts. *The Anatomical Record: Advances in Integrative Anatomy and Evolutionary Biology: Advances in Integrative Anatomy and Evolutionary Biology* **291**, 653-660 (2008).

3 Zhang, L., Theise, N., Chua, M. & Reid, L. M. The stem cell niche of human livers: Symmetry between development and regeneration. *Hepatology* **48**, 1598-1607, doi:10.1002/hep.22516 (2008).

4 Maroni, L. *et al.* Functional and Structural Features of Cholangiocytes in Health and Disease. *Cellular and Molecular Gastroenterology and Hepatology* **1**, 368-380, doi:https://doi.org/10.1016/j.jcmgh.2015.05.005 (2015).

5 Alpini, G. *et al.* Large but not small intrahepatic bile ducts are involved in secretin-regulated ductal bile secretion. *American Journal of Physiology-Gastrointestinal and Liver Physiology* **272**, G1064-G1074, doi:10.1152/ajpgi.1997.272.5.G1064 (1997).

6 Mancinelli, R. *et al.* After Damage of Large Bile Ducts by Gamma-Aminobutyric Acid, Small Ducts Replenish the Biliary Tree by Amplification of Calcium-Dependent Signaling and de Novo Acquisition of Large Cholangiocyte Phenotypes. *The American Journal of Pathology* **176**, 1790-1800, doi:https://doi.org/10.2353/ajpath.2010.090677 (2010).

7 Kanno, N., LeSage, G., Glaser, S., Alvaro, D. & Alpini, G. Functional heterogeneity of the intrahepatic biliary epithelium. *Hepatology* **31**, 555-561 (2000).

8 Tabibian, J. H., Masyuk, A. I., Masyuk, T. V., O'Hara, S. P. & LaRusso, N. F. Physiology of cholangiocytes. *Comprehensive Physiology* **3**, 541-565 (2013).

9 Masyuk, A. I. & LaRusso, N. F. Aquaporins in the hepatobiliary system. *Hepatology* **43**, S75-S81 (2006).

10 Si-Tayeb, K. *et al.* Highly efficient generation of human hepatocyte-like cells from induced pluripotent stem cells. *Hepatology (Baltimore, Md.)* **51**, 297-305, doi:10.1002/hep.23354 (2010).

11 Douarin, N. An experimental analysis of liver development. *Medical biology* **53**, 427-455 (1975).

12 Zaret, K. S. Regulatory phases of early liver development: paradigms of organogenesis. *Nature Reviews Genetics* **3**, 499 (2002).

13 Zorn, A. Liver development. StemBook. *The Stem Cell Research Community* (2008).

14 Zong, Y. & Stanger, B. Z. Molecular mechanisms of bile duct development. *The international journal of biochemistry & cell biology* **43**, 257-264, doi:10.1016/j.biocel.2010.06.020 (2011).

15 Zong, Y. *et al.* Notch signaling controls liver development by regulating biliary differentiation. *Development* **136**, 1727-1739 (2009).

16 Antoniou, A. *et al.* Intrahepatic bile ducts develop according to a new mode of tubulogenesis regulated by the transcription factor SOX9. *Gastroenterology* **136**, 2325-2333 (2009).

17 Strazzabosco, M. & Fabris, L. Development of the bile ducts: Essentials for the clinical hepatologist. *Journal of Hepatology* **56**, 1159-1170, doi:https://doi.org/10.1016/j.jhep.2011.09.022 (2012).
18 Fischer, E. *et al.* Defective planar cell polarity in polycystic kidney disease. *Nature genetics* **38**, 21 (2006).
19 Spence, J. R. *et al.* Sox17 regulates organ lineage segregation of ventral foregut progenitor cells. *Developmental cell* **17**, 62-74 (2009).
20 Banales, J. M. *et al.* Cholangiocyte pathobiology. *Nature Reviews Gastroenterology & Hepatology* **16**, 269-281, doi:10.1038/s41575-019-0125-y (2019).
21 O'Hara, S. P., Tabibian, J. H., Splinter, P. L. & LaRusso, N. F. The dynamic biliary epithelia: Molecules, pathways, and disease. *Journal of Hepatology* **58**, 575-582, doi:https://doi.org/10.1016/j.jhep.2012.10.011 (2013).
22 Pinto, C., Giordano, D. M., Maroni, L. & Marzioni, M. Role of inflammation and proinflammatory cytokines in cholangiocyte pathophysiology. *Biochimica et Biophysica Acta (BBA) - Molecular Basis of Disease* **1864**, 1270-1278, doi:https://doi.org/10.1016/j.bbadis.2017.07.024 (2018).
23 Gobin, S. J. & van den Elsen, P. J. in *Seminars in cancer biology.* 55-59 (Elsevier).
24 Tsuneyama, K. *et al.* Abnormal expression of the E2 component of the pyruvate dehydrogenase complex on the luminal surface of biliary epithelium occurs before major histocompatibility complex class II and BB1/B7 expression. *Hepatology* **21**, 1031-1037, doi:10.1002/hep.1840210422 (1995).
25 Roberts, S. K., Ludwig, J. & Larusso, N. F. The pathobiology of biliary epithelia. *Gastroenterology* **112**, 269-279, doi:http://dx.doi.org/10.1016/S0016-5085(97)70244-0 (1997).
26 Cruickshank, S. M., Southgate, J., Selby, P. J. & Trejdosiewicz, L. K. Expression and cytokine regulation of immune recognition elements by normal human biliary epithelial and established liver cell lines in vitro. *Journal of Hepatology* **29**, 550-558, doi:http://dx.doi.org/10.1016/S0168-8278(98)80149-9 (1998).
27 Park, S. M. The Crucial Role of Cholangiocytes in Cholangiopathies. *Gut and Liver* **6**, 295-304, doi:10.5009/gnl.2012.6.3.295 (2012).
28 Toy, E., Balasubramanian, S., Selmi, C., Li, C.-S. & Bowlus, C. L. The prevalence, incidence and natural history of primary sclerosing cholangitis in an ethnically diverse population. *BMC Gastroenterology* **11**, 83, doi:10.1186/1471-230x-11-83 (2011).
29 Eaton, J. E., Talwalkar, J. A., Lazaridis, K. N., Gores, G. J. & Lindor, K. D. Pathogenesis of primary sclerosing cholangitis and advances in diagnosis and management. *Gastroenterology* **145**, 521-536, doi:10.1053/j.gastro.2013.06.052 (2013).
30 Aoki, C. A., Bowlus, C. L. & Gershwin, M. E. The immunobiology of primary sclerosing cholangitis. *Autoimmunity Reviews* **4**, 137-143, doi:https://doi.org/10.1016/j.autrev.2004.09.003 (2005).
31 Pollheimer, M. J., Trauner, M. & Fickert, P. Will we ever model PSC?–"it's hard to be a PSC model!". *Clinics and research in hepatology and gastroenterology* **35**, 792-804 (2011).
32 Martin, E. F. & Levy, C. Timing, Management, and Outcomes of Liver Transplantation in Primary Sclerosing Cholangitis. *Semin Liver Dis* **37**, 305-313, doi:10.1055/s-0037-1608655 (2017).
33 Jones, D. E. Pathogenesis of primary biliary cirrhosis. *Gut* **56**, 1615-1624 (2007).
34 Kaplan, M. M. Primary biliary cirrhosis. *New England Journal of Medicine* **335**, 1570-1580 (1996).
35 Lindor, K. D. *et al.* Primary biliary cirrhosis. *Hepatology* **50**, 291-308 (2009).
36 Poupon, R. E., Poupon, R., Balkau, B. & group, U.-P. s. Ursodiol for the long-term treatment of primary biliary cirrhosis. *New England Journal of Medicine* **330**, 1342-1347 (1994).
37 Poupon, R. E., Balkau, B., Eschwège, E., Poupon, R. & Group*, U. P. S. A multicenter, controlled trial of ursodiol for the treatment of primary biliary cirrhosis. *New England Journal of Medicine* **324**, 1548-1554 (1991).

38 Mendes, F. D., Kim, W. R., Pedersen, R., Therneau, T. & Lindor, K. D. Mortality attributable to cholestatic liver disease in the United States. *Hepatology* **47**, 1241-1247, doi:10.1002/hep.22178 (2008).
39 Murray, K. F. & Carithers, R. L. AASLD practice guidelines: Evaluation of the patient for liver transplantation. *Hepatology* **41**, 1407-1432, doi:10.1002/hep.20704 (2005).
40 Markus, B. H. *et al.* Efficacy of liver transplantation in patients with primary biliary cirrhosis. *New England Journal of Medicine* **320**, 1709-1713 (1989).
41 Engelmann, G. *et al.* Indications for pediatric liver transplantation. Data from the Heidelberg pediatric liver transplantation program. *Nephrology Dialysis Transplantation* **22**, viii23-viii28 (2007).
42 Murray, K. F. & Carithers Jr., R. L. AASLD practice guidelines: Evaluation of the patient for liver transplantation. *Hepatology* **41**, 1407-1432, doi:10.1002/hep.20704 (2005).
43 Gallo, A. & Esquivel, C. O. Current options for management of biliary atresia. *Pediatric transplantation* **17**, 95-98 (2013).
44 Bates, M. D., Bucuvalas, J. C., Alonso, M. H. & Ryckman, F. C. in *Seminars in liver disease.* 281-293 (© 1998 by Thieme Medical Publishers, Inc.).
45 Asai, A., Miethke, A. & Bezerra, J. A. Pathogenesis of biliary atresia: defining biology to understand clinical phenotypes. *Nature reviews Gastroenterology & hepatology* **12**, 342 (2015).
46 Ramachandran, P. *et al.* The extended Kasai portoenterostomy for biliary atresia: A preliminary report. *J Indian Assoc Pediatr Surg* **21**, 66-71, doi:10.4103/0971-9261.176941 (2016).
47 Hadžic, N. *et al.* Long-term survival following Kasai portoenterostomy: is chronic liver disease inevitable? *Journal of pediatric gastroenterology and nutrition* **37**, 430-433 (2003).
48 Li, L. *et al.* Alagille syndrome is caused by mutations in human Jagged1, which encodes a ligand for Notch1. *Nature Genetics* **16**, 243-251, doi:10.1038/ng0797-243 (1997).
49 McDaniell, R. *et al.* NOTCH2 Mutations Cause Alagille Syndrome, a Heterogeneous Disorder of the Notch Signaling Pathway. *The American Journal of Human Genetics* **79**, 169-173, doi:https://doi.org/10.1086/505332 (2006).
50 Turnpenny, P. D. & Ellard, S. Alagille syndrome: pathogenesis, diagnosis and management. *Eur J Hum Genet* **20**, 251-257, doi:10.1038/ejhg.2011.181 (2012).
51 Danks, D. M., Campbell, P. E., Jack, I., Rogers, J. & Smith, A. L. Studies of the aetiology of neonatal hepatitis and biliary atresia. *Arch Dis Child* **52**, 360-367, doi:10.1136/adc.52.5.360 (1977).
52 Alagille, D., Odièvre, M., Gautier, M. & Dommergues, J. P. Hepatic ductular hypoplasia associated with characteristic facies, vertebral malformations, retarded physical, mental, and sexual development, and cardiac murmur. *The Journal of Pediatrics* **86**, 63-71, doi:https://doi.org/10.1016/S0022-3476(75)80706-2 (1975).
53 Geisler, F. & Strazzabosco, M. Emerging roles of Notch signaling in liver disease. *Hepatology (Baltimore, Md.)* **61**, 382-392, doi:10.1002/hep.27268 (2015).
54 Saleh, M., Kamath, B. M. & Chitayat, D. Alagille syndrome: clinical perspectives. *Appl Clin Genet* **9**, 75-82, doi:10.2147/TACG.S86420 (2016).
55 Transplant, N. B. a. NHS Blood and Transplant annual report and accounts: 2018 to 2019. (NHS Blood and Transplant, 2018).
56 Johnson, R. J., Bradbury, L. L., Martin, K., Neuberger, J. & Registry, O. b. o. t. U. T. Organ Donation and Transplantation in the UK—The Last Decade: A Report From the UK National Transplant Registry. *Transplantation* **97**, S1-S27, doi:10.1097/01.tp.0000438215.16737.68 (2014).
57 Citerio, G. *et al.* Organ donation in adults: a critical care perspective. *Intensive Care Medicine* **42**, 305-315, doi:10.1007/s00134-015-4191-5 (2016).
58 Cunningham, E. C., Sharland, A. F. & Bishop, G. A. Liver Transplant Tolerance and Its Application to the Clinic: Can We Exploit the High Dose Effect? *Clinical and Developmental Immunology* **2013**, 419692, doi:10.1155/2013/419692 (2013).
59 de la Garza, R. G. *et al.* Trial of complete weaning from immunosuppression for liver transplant recipients: Factors predictive of tolerance. *Liver Transplantation* **19**, 937-944, doi:10.1002/lt.23686 (2013).

60 Sherston, S. N., Carroll, R. P., Harden, P. N. & Wood, K. J. Predictors of Cancer Risk in the Long-Term Solid-Organ Transplant Recipient. *Transplantation* **97**, 605-611, doi:10.1097/01.TP.0000436907.56425.5c (2014).
61 Jardine, A. G., Gaston, R. S., Fellstrom, B. C. & Holdaas, H. Prevention of cardiovascular disease in adult recipients of kidney transplants. *The Lancet* **378**, 1419-1427, doi:http://dx.doi.org/10.1016/S0140-6736(11)61334-2.
62 Peleg, A. Y. *et al.* Opportunistic Infections in 547 Organ Transplant Recipients Receiving Alemtuzumab, a Humanized Monoclonal CD-52 Antibody. *Clinical Infectious Diseases* **44**, 204-212, doi:10.1086/510388 (2007).
63 Amit, M. *et al.* Clonally Derived Human Embryonic Stem Cell Lines Maintain Pluripotency and Proliferative Potential for Prolonged Periods of Culture. *Developmental Biology* **227**, 271-278, doi:http://dx.doi.org/10.1006/dbio.2000.9912 (2000).
64 Martin, G. R. Isolation of a pluripotent cell line from early mouse embryos cultured in medium conditioned by teratocarcinoma stem cells. *Proceedings of the National Academy of Sciences* **78**, 7634-7638 (1981).
65 Thomson, J. A. *et al.* Embryonic Stem Cell Lines Derived from Human Blastocysts. *Science* **282**, 1145-1147, doi:10.1126/science.282.5391.1145 (1998).
66 Schwartz, S. D. *et al.* Embryonic stem cell trials for macular degeneration: a preliminary report. *The Lancet* **379**, 713-720, doi:http://dx.doi.org/10.1016/S0140-6736(12)60028-2.
67 Menasché, P. *et al.* Human embryonic stem cell-derived cardiac progenitors for severe heart failure treatment: first clinical case report. *European Heart Journal* **36**, 2011-2017, doi:10.1093/eurheartj/ehv189 (2015).
68 Chong, J. J. H. *et al.* Human embryonic-stem-cell-derived cardiomyocytes regenerate non-human primate hearts. *Nature* **510**, 273-277, doi:10.1038/nature13233

http://www.nature.com/nature/journal/v510/n7504/abs/nature13233.html#supplementary-information (2014).
69 Bretzner, F., Gilbert, F., Baylis, F. & Brownstone, R. M. Target Populations for First-In-Human Embryonic Stem Cell Research in Spinal Cord Injury. *Cell Stem Cell* **8**, 468-475, doi:http://dx.doi.org/10.1016/j.stem.2011.04.012 (2011).
70 Ambasudhan, R. *et al.* Potential for cell therapy in Parkinson's disease using genetically programmed human embryonic stem cell–derived neural progenitor cells. *Journal of Comparative Neurology* **522**, 2845-2856, doi:10.1002/cne.23617 (2014).
71 Drukker, M. *et al.* Human Embryonic Stem Cells and Their Differentiated Derivatives Are Less Susceptible to Immune Rejection Than Adult Cells. *STEM CELLS* **24**, 221-229, doi:10.1634/stemcells.2005-0188 (2006).
72 Wood, K. J., Issa, F. & Hester, J. Understanding Stem Cell Immunogenicity in Therapeutic Applications. *Trends in Immunology* **37**, 5-16, doi:http://dx.doi.org/10.1016/j.it.2015.11.005 (2016).
73 Takahashi, K. & Yamanaka, S. Induction of Pluripotent Stem Cells from Mouse Embryonic and Adult Fibroblast Cultures by Defined Factors. *Cell* **126**, 663-676, doi:http://dx.doi.org/10.1016/j.cell.2006.07.024 (2006).
74 Takahashi, K. *et al.* Induction of Pluripotent Stem Cells from Adult Human Fibroblasts by Defined Factors. *Cell* **131**, 861-872, doi:http://dx.doi.org/10.1016/j.cell.2007.11.019 (2007).
75 Okita, K., Ichisaka, T. & Yamanaka, S. Generation of germline-competent induced pluripotent stem cells. *Nature* **448**, 313-317, doi:http://www.nature.com/nature/journal/v448/n7151/suppinfo/nature05934_S1.html (2007).
76 Wernig, M., Meissner, A., Cassady, J. P. & Jaenisch, R. c-Myc Is Dispensable for Direct Reprogramming of Mouse Fibroblasts. *Cell Stem Cell* **2**, 10-12, doi:http://dx.doi.org/10.1016/j.stem.2007.12.001 (2008).
77 Fang, I. M., Yang, C.-M., Yang, C.-H., Chiou, S.-H. & Chen, M.-S. Transplantation of induced pluripotent stem cells without C-Myc attenuates retinal ischemia and reperfusion injury in rats. *Experimental Eye Research* **113**, 49-59, doi:http://dx.doi.org/10.1016/j.exer.2013.05.007 (2013).

78 Wang, C.-Y. *et al.* Induced Pluripotent Stem Cells Without c-Myc Reduce Airway Responsiveness and Allergic Reaction in Sensitized Mice. *Transplantation* **96**, 958-965, doi:10.1097/TP.0b013e3182a53ef7 (2013).
79 Soldner, F. *et al.* Parkinson's Disease Patient-Derived Induced Pluripotent Stem Cells Free of Viral Reprogramming Factors. *Cell* **136**, 964-977, doi:http://dx.doi.org/10.1016/j.cell.2009.02.013 (2009).
80 Fusaki, N., Ban, H., Nishiyama, A., Saeki, K. & Hasegawa, M. Efficient induction of transgene-free human pluripotent stem cells using a vector based on Sendai virus, an RNA virus that does not integrate into the host genome. *Proceedings of the Japan Academy, Series B* **85**, 348-362, doi:10.2183/pjab.85.348 (2009).
81 Warren, L. *et al.* Highly Efficient Reprogramming to Pluripotency and Directed Differentiation of Human Cells with Synthetic Modified mRNA. *Cell Stem Cell* **7**, 618-630, doi:http://dx.doi.org/10.1016/j.stem.2010.08.012 (2010).
82 Zhou, H. *et al.* Generation of Induced Pluripotent Stem Cells Using Recombinant Proteins. *Cell Stem Cell* **4**, 381-384, doi:10.1016/j.stem.2009.04.005 (2009).
83 Zhao, T., Zhang, Z.-N., Rong, Z. & Xu, Y. Immunogenicity of induced pluripotent stem cells. *Nature* **474**, 212-215, doi:http://www.nature.com/nature/journal/v474/n7350/abs/10.1038-nature10135-unlocked.html#supplementary-information (2011).
84 Lister, R. *et al.* Hotspots of aberrant epigenomic reprogramming in human induced pluripotent stem cells. *Nature* **471**, 68-73, doi:http://www.nature.com/nature/journal/v471/n7336/abs/10.1038-nature09798-unlocked.html#supplementary-information (2011).
85 Herberts, C. A., Kwa, M. S. G. & Hermsen, H. P. H. Risk factors in the development of stem cell therapy. *Journal of Translational Medicine* **9**, 29, doi:10.1186/1479-5876-9-29 (2011).
86 Scharp, D. W. *et al.* Insulin Independence After Islet Transplantation Into Type I Diabetic Patient. *Diabetes* **39**, 515-518, doi:10.2337/diab.39.4.515 (1990).
87 Shapiro , A. M. J. *et al.* Islet Transplantation in Seven Patients with Type 1 Diabetes Mellitus Using a Glucocorticoid-Free Immunosuppressive Regimen. *New England Journal of Medicine* **343**, 230-238, doi:doi:10.1056/NEJM200007273430401 (2000).
88 Kubota, C. *et al.* Six cloned calves produced from adult fibroblast cells after long-term culture. *Proceedings of the National Academy of Sciences* **97**, 990-995, doi:10.1073/pnas.97.3.990 (2000).
89 Dunn, J. C., Yarmush, M. L., Koebe, H. G. & Tompkins, R. G. Hepatocyte function and extracellular matrix geometry: long-term culture in a sandwich configuration. *The FASEB Journal* **3**, 174-177 (1989).
90 Sreejit, P., Kumar, S. & Verma, R. S. An improved protocol for primary culture of cardiomyocyte from neonatal mice. *In Vitro Cellular & Developmental Biology - Animal* **44**, 45-50, doi:10.1007/s11626-007-9079-4 (2008).
91 Schnabel, M. *et al.* Dedifferentiation-associated changes in morphology and gene expression in primary human articular chondrocytes in cell culture. *Osteoarthritis and Cartilage* **10**, 62-70, doi:http://dx.doi.org/10.1053/joca.2001.0482 (2002).
92 Chamley, J. H., Campbell, G. R., McConnell, J. D. & Gröschel-Stewart, U. Comparison of vascular smooth muscle cells from adult human, monkey and rabbit in primary culture and in subculture. *Cell and Tissue Research* **177**, 503-522, doi:10.1007/bf00220611 (1977).
93 Greetje, E. *et al.* Molecular Mechanisms Underlying the Dedifferentiation Process of Isolated Hepatocytes and Their Cultures. *Current Drug Metabolism* **7**, 629-660, doi:http://dx.doi.org/10.2174/138920006778017759 (2006).
94 Tuschl, G., Hrach, J., Walter, Y., Hewitt, P. G. & Mueller, S. O. Serum-free collagen sandwich cultures of adult rat hepatocytes maintain liver-like properties long term: A valuable model for in vitro toxicity and drug–drug interaction studies. *Chemico-Biological Interactions* **181**, 124-137, doi:http://dx.doi.org/10.1016/j.cbi.2009.05.015 (2009).
95 Godoy, P. *et al.* Extracellular matrix modulates sensitivity of hepatocytes to fibroblastoid dedifferentiation and transforming growth factor β–induced apoptosis. *Hepatology* **49**, 2031-2043, doi:10.1002/hep.22880 (2009).

96 Rossi, G., Manfrin, A. & Lutolf, M. P. Progress and potential in organoid research. *Nature Reviews Genetics* **19**, 671-687, doi:10.1038/s41576-018-0051-9 (2018).
97 Drost, J. & Clevers, H. Translational applications of adult stem cell-derived organoids. *Development* **144**, 968-975, doi:10.1242/dev.140566 (2017).
98 Yin, X. *et al.* Engineering Stem Cell Organoids. *Cell Stem Cell* **18**, 25-38, doi:https://doi.org/10.1016/j.stem.2015.12.005 (2016).
99 Sato, T. *et al.* Single Lgr5 stem cells build crypt–villus structures in vitro without a mesenchymal niche. *Nature* **459**, 262 (2009).
100 MacDonald, B. T., Tamai, K. & He, X. Wnt/β-Catenin Signaling: Components, Mechanisms, and Diseases. *Developmental Cell* **17**, 9-26, doi:https://doi.org/10.1016/j.devcel.2009.06.016 (2009).
101 Logan, C. Y. & Nusse, R. The Wnt signaling pathway in development and disease. *Annu. Rev. Cell Dev. Biol.* **20**, 781-810 (2004).
102 Korinek, V. *et al.* Depletion of epithelial stem-cell compartments in the small intestine of mice lacking Tcf-4. *Nature genetics* **19**, 379 (1998).
103 Barker, N. *et al.* Identification of stem cells in small intestine and colon by marker gene Lgr5. *Nature* **449**, 1003 (2007).
104 Kim, K.-A. *et al.* Mitogenic influence of human R-spondin1 on the intestinal epithelium. *Science* **309**, 1256-1259 (2005).
105 Kleinman, H. K. & Martin, G. R. Matrigel: Basement membrane matrix with biological activity. *Seminars in Cancer Biology* **15**, 378-386, doi:https://doi.org/10.1016/j.semcancer.2005.05.004 (2005).
106 Dignass, A. U. & Sturm, A. Peptide growth factors in the intestine. *European journal of gastroenterology & hepatology* **13**, 763-770 (2001).
107 Haramis, A.-P. G. *et al.* De novo crypt formation and juvenile polyposis on BMP inhibition in mouse intestine. *Science* **303**, 1684-1686 (2004).
108 Barkauskas, C. E. *et al.* Type 2 alveolar cells are stem cells in adult lung. *The Journal of Clinical Investigation* **123**, 3025-3036, doi:10.1172/JCI68782 (2013).
109 Broutier, L. *et al.* Culture and establishment of self-renewing human and mouse adult liver and pancreas 3D organoids and their genetic manipulation. *Nature Protocols* **11**, 1724, doi:10.1038/nprot.2016.097

https://www.nature.com/articles/nprot.2016.097#supplementary-information (2016).
110 Huch, M. *et al.* In vitro expansion of single Lgr5+ liver stem cells induced by Wnt-driven regeneration. *Nature* **494**, 247, doi:10.1038/nature11826

https://www.nature.com/articles/nature11826#supplementary-information (2013).
111 Lei, M. *et al.* Self-organization process in newborn skin organoid formation inspires strategy to restore hair regeneration of adult cells. *Proceedings of the National Academy of Sciences* **114**, E7101-E7110, doi:10.1073/pnas.1700475114 (2017).
112 Lo, A. T., Mori, H., Mott, J. & Bissell, M. J. Constructing Three-Dimensional Models to Study Mammary Gland Branching Morphogenesis and Functional Differentiation. *Journal of Mammary Gland Biology and Neoplasia* **17**, 103-110, doi:10.1007/s10911-012-9251-7 (2012).
113 Barker, N. *et al.* Lgr5+ve Stem Cells Drive Self-Renewal in the Stomach and Build Long-Lived Gastric Units In Vitro. *Cell Stem Cell* **6**, 25-36, doi:https://doi.org/10.1016/j.stem.2009.11.013 (2010).
114 Gotoh, S. *et al.* Generation of Alveolar Epithelial Spheroids via Isolated Progenitor Cells from Human Pluripotent Stem Cells. *Stem Cell Reports* **3**, 394-403, doi:https://doi.org/10.1016/j.stemcr.2014.07.005 (2014).
115 Lancaster, M. A. *et al.* Cerebral organoids model human brain development and microcephaly. *Nature* **501**, 373 (2013).
116 Pham, M. T. *et al.* Generation of human vascularized brain organoids. *Neuroreport* **29**, 588-593, doi:10.1097/WNR.0000000000001014 (2018).
117 Voges, H. K. *et al.* Development of a human cardiac organoid injury model reveals innate regenerative potential. *Development* **144**, 1118-1127, doi:10.1242/dev.143966 (2017).

118 McCracken, K. W. *et al.* Modelling human development and disease in pluripotent stem-cell-derived gastric organoids. *Nature* **516**, 400, doi:10.1038/nature13863 (2014).
119 Spence, J. R. *et al.* Directed differentiation of human pluripotent stem cells into intestinal tissue in vitro. *Nature* **470**, 105, doi:10.1038/nature09691

https://www.nature.com/articles/nature09691#supplementary-information (2010).
120 Nadkarni, R. R., Abed, S. & Draper, J. S. Organoids as a model system for studying human lung development and disease. *Biochemical and Biophysical Research Communications* **473**, 675-682, doi:https://doi.org/10.1016/j.bbrc.2015.12.091 (2016).
121 Koledova, Z. & Lu, P. in *Mammary Gland Development: Methods and Protocols* (eds Finian Martin, Torsten Stein, & Jillian Howlin) 217-231 (Springer New York, 2017).
122 Bertaux-Skeirik, N. *et al.* in *Gastrointestinal Physiology and Diseases: Methods and Protocols* (ed Andrei I. Ivanov) 23-31 (Springer New York, 2016).
123 Nozaki, K. *et al.* Co-culture with intestinal epithelial organoids allows efficient expansion and motility analysis of intraepithelial lymphocytes. *Journal of Gastroenterology* **51**, 206-213, doi:10.1007/s00535-016-1170-8 (2016).
124 Sampaziotis, F. *et al.* Reconstruction of the mouse extrahepatic biliary tree using primary human extrahepatic cholangiocyte organoids. *Nature Medicine* **23**, 954, doi:10.1038/nm.4360

https://www.nature.com/articles/nm.4360#supplementary-information (2017).
125 Tysoe, O. C. *et al.* Isolation and propagation of primary human cholangiocyte organoids for the generation of bioengineered biliary tissue. *Nature Protocols* **14**, 1884-1925, doi:10.1038/s41596-019-0168-0 (2019).
126 Ali, J. M., Bolton, E. M., Bradley, J. A. & Pettigrew, G. J. Allorecognition Pathways in Transplant Rejection and Tolerance. *Transplantation* **96**, 681-688, doi:10.1097/TP.0b013e31829853ce (2013).
127 Klein, U. & Dalla-Favera, R. Germinal centres: role in B-cell physiology and malignancy. *Nature Reviews Immunology* **8**, 22, doi:10.1038/nri2217 (2008).
128 Ali, J. M., Bolton, E. M., Bradley, J. A. & Pettigrew, G. J. Allorecognition pathways in transplant rejection and tolerance. *Transplantation* **96**, 681-688, doi:10.1097/TP.0b013e31829853ce (2013).
129 Herrera, O. B. *et al.* A Novel Pathway of Alloantigen Presentation by Dendritic Cells. *The Journal of Immunology* **173**, 4828-4837, doi:10.4049/jimmunol.173.8.4828 (2004).
130 Sánchez–Fueyo, A. & Strom, T. B. Immunologic Basis of Graft Rejection and Tolerance Following Transplantation of Liver or Other Solid Organs. *Gastroenterology* **140**, 51-64.e52, doi:http://dx.doi.org/10.1053/j.gastro.2010.10.059 (2011).
131 Boussiotis, V. *et al.* Prevention of T cell anergy by signaling through the gamma c chain of the IL-2 receptor. *Science* **266**, 1039-1042, doi:10.1126/science.7973657 (1994).
132 Zanders, E. D., Lamb, J. R., Feldmann, M., Green, N. & Beverley, P. C. L. Tolerance of T-cell clones is associated with membrane antigen changes. *Nature* **303**, 625-627 (1983).
133 Harding, F. A., McArthur, J. G., Gross, J. A., Raulet, D. H. & Allison, J. P. CD28-mediated signalling co-stimulates murine T cells and prevents induction of anergy in T-cell clones. *Nature* **356**, 607-609 (1992).
134 Land, W. G., Agostinis, P., Gasser, S., Garg, A. D. & Linkermann, A. Transplantation and Damage-Associated Molecular Patterns (DAMPs). *American Journal of Transplantation*, n/a-n/a, doi:10.1111/ajt.13963 (2016).
135 Shultz, L. D., Brehm, M. A., Garcia-Martinez, J. V. & Greiner, D. L. Humanized mice for immune system investigation: progress, promise and challenges. *Nat Rev Immunol* **12**, 786-798 (2012).
136 Wecker, H., Winn, H. J. & Auchincloss, H. CD4+ T cells, without CD8+ or B lymphocytes, can reject xenogeneic skin grafts. *Xenotransplantation* **1**, 8-16, doi:10.1111/j.1399-3089.1994.tb00045.x (1994).
137 Pietra, B. A., Wiseman, A., Bolwerk, A., Rizeq, M. & Gill, R. G. CD4 T cell–mediated cardiac allograft rejection requires donor but not host MHC class II. *The Journal of Clinical Investigation* **106**, 1003-1010, doi:10.1172/JCI10467.

138 Michaels, P. J. *et al.* Humoral rejection in cardiac transplantation: risk factors, hemodynamic consequences and relationship to transplant coronary artery disease. *The Journal of Heart and Lung Transplantation* **22**, 58-69, doi:http://dx.doi.org/10.1016/S1053-2498(02)00472-2 (2003).
139 Pelletier, R. P. *et al.* Clinical Significance of MHC-Reactive Alloantibodies that Develop after Kidney or Kidney–pancreas Transplantation. *American Journal of Transplantation* **2**, 134-141, doi:10.1034/j.1600-6143.2002.020204.x (2002).
140 Yang, J. *et al.* Allograft rejection mediated by memory T cells is resistant to regulation. *Proceedings of the National Academy of Sciences* **104**, 19954-19959, doi:10.1073/pnas.0704397104 (2007).
141 Curci, C. *et al.* Potential role of effector memory T cells in chronic T cell-mediated kidney graft rejection. *Nephrology Dialysis Transplantation*, doi:10.1093/ndt/gfw245 (2016).
142 Dengler, T. J. & Pober, J. S. Human Vascular Endothelial Cells Stimulate Memory But Not Naive CD8+ T Cells to Differentiate into CTL Retaining an Early Activation Phenotype. *The Journal of Immunology* **164**, 5146-5155, doi:10.4049/jimmunol.164.10.5146 (2000).
143 Li, X. C., Strom, T. B., Turka, L. A. & Wells, A. D. T Cell Death and Transplantation Tolerance. *Immunity* **14**, 407-416, doi:http://dx.doi.org/10.1016/S1074-7613(01)00121-2 (2001).
144 Li, Y. *et al.* Blocking both signal 1 and signal 2 of T-cell activation prevents apoptosis of alloreactive t cells and induction of peripheral allograft tolerance. *Nature Medicine* **5**, 1298-1302, doi:10.1038/15256 (1999).
145 Cederbom, L., Hall, H. & Ivars, F. CD4+CD25+ regulatory T cells down-regulate co-stimulatory molecules on antigen-presenting cells. *European Journal of Immunology* **30**, 1538-1543, doi:10.1002/1521-4141(200006)30:6<1538::AID-IMMU1538>3.0.CO;2-X (2000).
146 Wood, K. J. & Sakaguchi, S. Regulatory T cells in transplantation tolerance. *Nat Rev Immunol* **3**, 199-210 (2003).
147 Grazia Roncarolo, M. *et al.* Interleukin-10-secreting type 1 regulatory T cells in rodents and humans. *Immunological Reviews* **212**, 28-50, doi:10.1111/j.0105-2896.2006.00420.x (2006).
148 Qin, S. *et al.* "Infectious" transplantation tolerance. *Science* **259**, 974-977, doi:10.1126/science.8094901 (1993).
149 Choo, S. Y. The HLA system: genetics, immunology, clinical testing, and clinical implications. *Yonsei medical journal* **48**, 11-23 (2007).
150 Ayala García, M. A., González Yebra, B., López Flores, A. L. & Guaní Guerra, E. The major histocompatibility complex in transplantation. *Journal of transplantation* **2012**, 842141-842141, doi:10.1155/2012/842141 (2012).
151 Takemoto, S., Port, F. K., Claas, F. H. & Duquesnoy, R. J. HLA matching for kidney transplantation. *Human immunology* **65**, 1489-1505 (2004).
152 Ansari, D., Bućin, D. & Nilsson, J. Human leukocyte antigen matching in heart transplantation: systematic review and meta-analysis. *Transplant International* **27**, 793-804, doi:10.1111/tri.12335 (2014).
153 Petersdorf, E. W. Optimal HLA matching in hematopoietic cell transplantation. *Current Opinion in Immunology* **20**, 588-593, doi:https://doi.org/10.1016/j.coi.2008.06.014 (2008).
154 Nikaein, A. *et al.* HLA compatibility and liver transplant outcome. Improved patient survival by HLA and cross-matching. *Transplantation* **58**, 786-792 (1994).
155 Navarro, V., Herrine, S., Katopes, C., Colombe, B. & Spain, C. V. The effect of HLA class I (A and B) and class II (DR) compatibility on liver transplantation outcomes: An analysis of the OPTN database. *Liver Transplantation* **12**, 652-658, doi:10.1002/lt.20680 (2006).
156 Kirk, A. D. Induction immunosuppression. *Transplantation* **82**, 593-602 (2006).
157 Moini, M., Schilsky, M. L. & Tichy, E. M. Review on immunosuppression in liver transplantation. *World J Hepatol* **7**, 1355-1368, doi:10.4254/wjh.v7.i10.1355 (2015).
158 Bamoulid, J. *et al.* The need for minimization strategies: current problems of immunosuppression. *Transplant International* **28**, 891-900, doi:10.1111/tri.12553 (2015).
159 Vajdic, C. M. & van Leeuwen, M. T. Cancer incidence and risk factors after solid organ transplantation. *International Journal of Cancer* **125**, 1747-1754, doi:10.1002/ijc.24439 (2009).

160 Duncan, M. D. & Wilkes, D. S. Transplant-related immunosuppression: a review of immunosuppression and pulmonary infections. *Proceedings of the American Thoracic Society* **2**, 449-455 (2005).
161 Hallett, P. J. *et al.* Successful function of autologous iPSC-derived dopamine neurons following transplantation in a non-human primate model of Parkinson's disease. *Cell Stem Cell* **16**, 269-274, doi:10.1016/j.stem.2015.01.018 (2015).
162 Gourraud, P.-A., Gilson, L., Girard, M. & Peschanski, M. The Role of Human Leukocyte Antigen Matching in the Development of Multiethnic "Haplobank" of Induced Pluripotent Stem Cell Lines. *STEM CELLS* **30**, 180-186, doi:10.1002/stem.772 (2012).
163 Taylor, Craig J., Peacock, S., Chaudhry, Afzal N., Bradley, J. A. & Bolton, Eleanor M. Generating an iPSC Bank for HLA-Matched Tissue Transplantation Based on Known Donor and Recipient HLA Types. *Cell Stem Cell* **11**, 147-152, doi:http://dx.doi.org/10.1016/j.stem.2012.07.014 (2012).
164 Okita, K. *et al.* A more efficient method to generate integration-free human iPS cells. *Nature Methods* **8**, 409, doi:10.1038/nmeth.1591

https://www.nature.com/articles/nmeth.1591#supplementary-information (2011).
165 Pappas, D. J. *et al.* Proceedings: human leukocyte antigen haplo-homozygous induced pluripotent stem cell haplobank modeled after the california population: evaluating matching in a multiethnic and admixed population. *Stem cells translational medicine* **4**, 413-418, doi:10.5966/sctm.2015-0052 (2015).
166 Solomon, S., Pitossi, F. & Rao, M. S. Banking on iPSC- Is it Doable and is it Worthwhile. *Stem Cell Reviews* **11**, 1-10, doi:10.1007/s12015-014-9574-4 (2015).
167 Shiba, Y. *et al.* Allogeneic transplantation of iPS cell-derived cardiomyocytes regenerates primate hearts. *Nature* **538**, 388, doi:10.1038/nature19815

https://www.nature.com/articles/nature19815#supplementary-information (2016).
168 Kawamura, T. *et al.* Cardiomyocytes Derived from MHC-Homozygous Induced Pluripotent Stem Cells Exhibit Reduced Allogeneic Immunogenicity in MHC-Matched Non-human Primates. *Stem Cell Reports* **6**, 312-320, doi:10.1016/j.stemcr.2016.01.012 (2016).
169 Deleidi, M., Hargus, G., Hallett, P., Osborn, T. & Isacson, O. Development of histocompatible primate-induced pluripotent stem cells for neural transplantation. *Stem cells* **29**, 1052-1063 (2011).
170 Morizane, A. *et al.* MHC matching improves engraftment of iPSC-derived neurons in non-human primates. *Nature Communications* **8**, 385, doi:10.1038/s41467-017-00926-5 (2017).
171 Jang, Y. *et al.* Development of immunocompatible pluripotent stem cells via CRISPR-based human leukocyte antigen engineering. *Experimental & Molecular Medicine* **51**, 3, doi:10.1038/s12276-018-0190-2 (2019).
172 Wang, D., Quan, Y., Yan, Q., Morales, J. E. & Wetsel, R. A. Targeted Disruption of the β2-Microglobulin Gene Minimizes the Immunogenicity of Human Embryonic Stem Cells. *Stem cells translational medicine* **4**, 1234-1245, doi:10.5966/sctm.2015-0049 (2015).
173 Deuse, T. *et al.* Immunobiology of naïve and genetically modified HLA-class-I-knockdown human embryonic stem cells. *Journal of Cell Science* **124**, 3029-3037, doi:10.1242/jcs.087718 (2011).
174 Karre, K. Express yourself or die: peptides, MHC molecules, and NK cells. *Science* **267**, 978-980 (1995).
175 Gornalusse, G. G. *et al.* HLA-E-expressing pluripotent stem cells escape allogeneic responses and lysis by NK cells. *Nature Biotechnology* **35**, 765, doi:10.1038/nbt.3860

https://www.nature.com/articles/nbt.3860#supplementary-information (2017).
176 Bosma, G. C., Custer, R. P. & Bosma, M. J. A severe combined immunodeficiency mutation in the mouse. *Nature* **301**, 527-530 (1983).
177 Fulop, G. M. & Phillips, R. A. The scid mutation in mice causes a general defect in DNA repair. *Nature* **347**, 479-482 (1990).
178 Mombaerts, P. *et al.* RAG-1-deficient mice have no mature B and T lymphocytes. *Cell* **68**, 869-877, doi:http://dx.doi.org/10.1016/0092-8674(92)90030-G (1992).

179 Shinkai, Y. *et al.* RAG-2-deficient mice lack mature lymphocytes owing to inability to initiate V(D)J rearrangement. *Cell* **68**, 855-867, doi:http://dx.doi.org/10.1016/0092-8674(92)90029-C (1992).
180 Shultz, L. D. *et al.* Multiple defects in innate and adaptive immunologic function in NOD/LtSz-scid mice. *The Journal of Immunology* **154**, 180-191 (1995).
181 Ito, M. *et al.* NOD/SCID/gamma(null)(c) mouse: an excellent recipient mouse model for engraftment of human cells. *Blood* **100**, 3175-3182, doi:10.1182/blood-2001-12-0207 (2002).
182 Leonard, W. J. Cytokines and immunodeficiency diseases. *Nature Reviews Immunology* **1**, 200, doi:10.1038/35105066

https://www.nature.com/articles/nri35105066#supplementary-information (2001).
183 Kennedy, M. K. *et al.* Reversible defects in natural killer and memory CD8 T cell lineages in interleukin 15–deficient mice. *Journal of Experimental Medicine* **191**, 771-780 (2000).
184 Suzuki, H. *et al.* Deregulated T cell activation and autoimmunity in mice lacking interleukin-2 receptor beta. *Science* **268**, 1472-1476 (1995).
185 Shultz, L. D. *et al.* Human Lymphoid and Myeloid Cell Development in NOD/LtSz-scid IL2Rγnull Mice Engrafted with Mobilized Human Hemopoietic Stem Cells. *The Journal of Immunology* **174**, 6477-6489, doi:10.4049/jimmunol.174.10.6477 (2005).
186 Shultz, L. D., Brehm, M. A., Garcia-Martinez, J. V. & Greiner, D. L. Humanized mice for immune system investigation: progress, promise and challenges. *Nature Reviews Immunology* **12**, 786 (2012).
187 Lapidot, T. *et al.* Cytokine stimulation of multilineage hematopoiesis from immature human cells engrafted in SCID mice. *Science* **255**, 1137-1141, doi:10.1126/science.1372131 (1992).
188 Ishikawa, F. *et al.* Development of functional human blood and immune systems in NOD/SCID/IL2 receptor γ chain^{null} mice . *Blood* **106**, 1565-1573, doi:10.1182/blood-2005-02-0516 (2005).
189 Legrand, N., Weijer, K. & Spits, H. Experimental Models to Study Development and Function of the Human Immune System In Vivo. *The Journal of Immunology* **176**, 2053-2058, doi:10.4049/jimmunol.176.4.2053 (2006).
190 Ito, M. *et al.* NOD/SCID/γ mouse: an excellent recipient mouse model for engraftment of human cells. *Blood* **100**, 3175-3182, doi:10.1182/blood-2001-12-0207 (2002).
191 Brehm, M. A. *et al.* Parameters for establishing humanized mouse models to study human immunity: Analysis of human hematopoietic stem cell engraftment in three immunodeficient strains of mice bearing the IL2rγnull mutation. *Clinical Immunology* **135**, 84-98, doi:http://dx.doi.org/10.1016/j.clim.2009.12.008 (2010).
192 Watanabe, Y. *et al.* The analysis of the functions of human B and T cells in humanized NOD/shi-scid/γcnull (NOG) mice (hu-HSC NOG mice). *International Immunology* **21**, 843-858, doi:10.1093/intimm/dxp050 (2009).
193 Matsumura, T. *et al.* Functional CD5+ B cells develop predominantly in the spleen of NOD/SCID/γcnull (NOG) mice transplanted either with human umbilical cord blood, bone marrow, or mobilized peripheral blood CD34+ cells. *Experimental Hematology* **31**, 789-797, doi:http://dx.doi.org/10.1016/S0301-472X(03)00193-0 (2003).
194 Brehm, M., Bortell, R., Verma, M., Shultz, L. & Greiner, D. Humanized mice in translational immunology. *Translational Immunology: Mechanisms and Pharmacological Approaches*, 285-326 (2016).
195 Manz, M. G. Human-Hemato-Lymphoid-System Mice: Opportunities and Challenges. *Immunity* **26**, 537-541, doi:https://doi.org/10.1016/j.immuni.2007.05.001 (2007).
196 Yahata, T. *et al.* Functional Human T Lymphocyte Development from Cord Blood CD34+ Cells in Nonobese Diabetic/Shi-scid, IL-2 Receptor γ Null Mice. *The Journal of Immunology* **169**, 204-209, doi:10.4049/jimmunol.169.1.204 (2002).
197 King, M. A. *et al.* Human peripheral blood leucocyte non-obese diabetic-severe combined immunodeficiency interleukin-2 receptor gamma chain gene mouse model of xenogeneic graft-versus-host-like disease and the role of host major histocompatibility complex. *Clinical & Experimental Immunology* **157**, 104-118, doi:10.1111/j.1365-2249.2009.03933.x (2009).

198 Harui, A., Kiertscher, S. M. & Roth, M. D. Reconstitution of huPBL-NSG Mice with Donor-Matched Dendritic Cells Enables Antigen-Specific T-cell Activation. *Journal of Neuroimmune Pharmacology* **6**, 148-157, doi:10.1007/s11481-010-9223-x (2011).
199 King, M. *et al.* A new Hu-PBL model for the study of human islet alloreactivity based on NOD-scid mice bearing a targeted mutation in the IL-2 receptor gamma chain gene. *Clinical Immunology* **126**, 303-314, doi:http://dx.doi.org/10.1016/j.clim.2007.11.001 (2008).
200 Pober, J. S. *et al.* Immunopathology of human T cellresponses to skin, artery and endothelial cell grafts in thehuman peripheral blood lymphocyte/severe combinedimmunodeficient mouse. *Springer Seminars inImmunopathology* **25**, 167-180, doi:10.1007/s00281-003-0135-1 (2003).
201 Issa, F. *et al.* Ex vivo-expanded human regulatory T cells prevent the rejection of skin allografts in a humanised mouse model(). *Transplantation* **90**, 1321-1327, doi:10.1097/TP.0b013e3181ff8772 (2010).
202 Chin, M. H. *et al.* Induced Pluripotent Stem Cells and Embryonic Stem Cells Are Distinguished by Gene Expression Signatures. *Cell Stem Cell* **5**, 111-123, doi:http://dx.doi.org/10.1016/j.stem.2009.06.008 (2009).
203 Nadig, S. N. *et al.* In vivo prevention of transplant arteriosclerosis by ex vivo-expanded human regulatory T cells. *Nat Med* **16**, 809-813, doi:http://www.nature.com/nm/journal/v16/n7/abs/nm.2154.html#supplementary-information (2010).
204 Antin, J. & Ferrara, J. Cytokine dysregulation and acute graft-versus-host disease. *Blood* **80**, 2964-2968 (1992).
205 Covassin, L. *et al.* Human peripheral blood CD4 T cell-engrafted non-obese diabetic-scid IL2rγnull H2-Ab1 tm1Gru Tg (human leucocyte antigen D-related 4) mice: a mouse model of human allogeneic graft-versus-host disease. *Clinical & Experimental Immunology* **166**, 269-280, doi:10.1111/j.1365-2249.2011.04462.x (2011).
206 Racki, W. J. *et al.* NOD-scid IL2rγ(null) (NSG) Mouse Model of Human Skin Transplantation and Allograft Rejection. *Transplantation* **89**, 527-536, doi:10.1097/TP.0b013e3181c90242 (2010).
207 Andrade, D. *et al.* Engraftment of peripheral blood mononuclear cells from systemic lupus erythematosus and antiphospholipid syndrome patient donors into BALB-RAG-2−/−IL-2Rγ−/− mice: A promising model for studying human disease. *Arthritis & Rheumatism* **63**, 2764-2773, doi:10.1002/art.30424 (2011).
208 Yaguchi, T. *et al.* Human PBMC-transferred murine MHC class I/II-deficient NOG mice enable long-term evaluation of human immune responses. *Cellular & molecular immunology* (2017).
209 Brehm, M. A. *et al.* Lack of acute xenogeneic graft-versus-host disease, but retention of T-cell function following engraftment of human peripheral blood mononuclear cells in NSG mice deficient in MHC class I and II expression. *The FASEB Journal* **33**, 3137-3151 (2018).
210 van Bilsen, K. *et al.* The neonatal Fc receptor is expressed by human retinal pigment epithelial cells and is downregulated by tumour necrosis factor-alpha. *British Journal of Ophthalmology* **95**, 864-868, doi:10.1136/bjo.2010.187930 (2011).
211 Ito, R. *et al.* Establishment of a Human Allergy Model Using Human IL-3/GM-CSF–Transgenic NOG Mice. *The Journal of Immunology* **191**, 2890-2899 (2013).
212 Billerbeck, E. *et al.* Development of human CD4+ FoxP3+ regulatory T cells in human stem cell factor–, granulocyte-macrophage colony-stimulating factor–, and interleukin-3–expressing NOD-SCID IL2Rγnull humanized mice. *Blood* **117**, 3076-3086 (2011).
213 Katano, I. *et al.* Long-term maintenance of peripheral blood derived human NK cells in a novel human IL-15-transgenic NOG mouse. *Scientific reports* **7**, 17230 (2017).
214 Herndler-Brandstetter, D. *et al.* Humanized mouse model supports development, function, and tissue residency of human natural killer cells. *Proceedings of the National Academy of Sciences* **114**, E9626-E9634 (2017).
215 Brehm, M. A. *et al.* Human Immune System Development and Rejection of Human Islet Allografts in Spontaneously Diabetic NOD-Rag1^{null} IL2rγ^{null} Ins2^{Akita} Mice. *Diabetes* **59**, 2265-2270, doi:10.2337/db10-0323 (2010).

216 Rayner, D., Nelson, R. & Murray, A. G. Noncytolytic human lymphocytes injure dermal microvessels in the huPBL-SCID skin graft model. *Human Immunology* **62**, 598-606, doi:https://doi.org/10.1016/S0198-8859(01)00252-X (2001).
217 Noyan, F. *et al.* Prevention of Allograft Rejection by Use of Regulatory T Cells With an MHC-Specific Chimeric Antigen Receptor. *American Journal of Transplantation* **17**, 917-930, doi:10.1111/ajt.14175 (2017).
218 Wu, D. C. *et al.* Ex Vivo Expanded Human Regulatory T Cells Can Prolong Survival of a Human Islet Allograft in a Humanized Mouse Model. *Transplantation* **96**, 707-716, doi:10.1097/TP.0b013e31829fa271 (2013).
219 Aoyama, N. *et al.* Transgenic mice that accept Luciferase- or GFP-expressing syngeneic tumor cells at high efficiencies. *Genes to Cells* **23**, 580-589, doi:10.1111/gtc.12592 (2018).
220 Deuse, T. *et al.* Hypoimmunogenic derivatives of induced pluripotent stem cells evade immune rejection in fully immunocompetent allogeneic recipients. *Nature Biotechnology* **37**, 252-258, doi:10.1038/s41587-019-0016-3 (2019).
221 Kooreman, N. G. *et al.* Alloimmune Responses of Humanized Mice to Human Pluripotent Stem Cell Therapeutics. *Cell Reports* **20**, 1978-1990, doi:https://doi.org/10.1016/j.celrep.2017.08.003 (2017).
222 Sakuma, T., Barry, M. A. & Ikeda, Y. Lentiviral vectors: basic to translational. *Biochemical Journal* **443**, 603-618 (2012).
223 Sampaziotis, F. *et al.* Cholangiocytes derived from human induced pluripotent stem cells for disease modeling and drug validation. *Nature Biotechnology* **33**, 845, doi:10.1038/nbt.3275

https://www.nature.com/articles/nbt.3275#supplementary-information (2015).
224 Sato, T. *et al.* Long-term Expansion of Epithelial Organoids From Human Colon, Adenoma, Adenocarcinoma, and Barrett's Epithelium. *Gastroenterology* **141**, 1762-1772, doi:https://doi.org/10.1053/j.gastro.2011.07.050 (2011).
225 Kessler, M. *et al.* The Notch and Wnt pathways regulate stemness and differentiation in human fallopian tube organoids. *Nature Communications* **6**, 8989, doi:10.1038/ncomms9989

https://www.nature.com/articles/ncomms9989#supplementary-information (2015).
226 Huch, M. *et al.* Long-Term Culture of Genome-Stable Bipotent Stem Cells from Adult Human Liver. *Cell* **160**, 299-312, doi:10.1016/j.cell.2014.11.050 (2015).
227 Karthaus, Wouter R. *et al.* Identification of Multipotent Luminal Progenitor Cells in Human Prostate Organoid Cultures. *Cell* **159**, 163-175, doi:https://doi.org/10.1016/j.cell.2014.08.017 (2014).
228 Koo, B.-K. & Clevers, H. Stem Cells Marked by the R-Spondin Receptor LGR5. *Gastroenterology* **147**, 289-302, doi:https://doi.org/10.1053/j.gastro.2014.05.007 (2014).
229 Glinka, A. *et al.* Dickkopf-1 is a member of a new family of secreted proteins and functions in head induction. *Nature* **391**, 357, doi:10.1038/34848 (1998).
230 Fedi, P. *et al.* Isolation and Biochemical Characterization of the Human Dkk-1 Homologue, a Novel Inhibitor of Mammalian Wnt Signaling. *Journal of Biological Chemistry* **274**, 19465-19472, doi:10.1074/jbc.274.27.19465 (1999).
231 Bafico, A., Liu, G., Yaniv, A., Gazit, A. & Aaronson, S. A. Novel mechanism of Wnt signalling inhibition mediated by Dickkopf-1 interaction with LRP6/Arrow. *Nature Cell Biology* **3**, 683, doi:10.1038/35083081 (2001).
232 Cui, S., Capecci, L. M. & Matthews, R. P. Disruption of planar cell polarity activity leads to developmental biliary defects. *Developmental Biology* **351**, 229-241, doi:https://doi.org/10.1016/j.ydbio.2010.12.041 (2011).
233 Yoshimura, Y. *et al.* Mouse embryonic stem cells with a multi-integrase mouse artificial chromosome for transchromosomic mouse generation. *Transgenic Research* **24**, 717-727, doi:10.1007/s11248-015-9884-6 (2015).
234 Thibaudeau, L. *et al.* Mimicking breast cancer-induced bone metastasis in vivo: current transplantation models and advanced humanized strategies. *Cancer and Metastasis Reviews* **33**, 721-735, doi:10.1007/s10555-014-9499-z (2014).

235 de Jong, M., Essers, J. & van Weerden, W. M. Imaging preclinical tumour models: improving translational power. *Nature Reviews Cancer* **14**, 481, doi:10.1038/nrc3751 (2014).
236 Harari, D. *et al.* Bridging the species divide: transgenic mice humanized for type-I interferon response. *PloS one* **9**, e84259 (2014).
237 Li, Z. *et al.* Optimization of Mesenchymal Stem Cells (MSCs) Delivery Dose and Route in Mice with Acute Liver Injury by Bioluminescence Imaging. *Molecular Imaging and Biology* **17**, 185-194, doi:10.1007/s11307-014-0792-6 (2015).
238 Chen, A. A. *et al.* Humanized mice with ectopic artificial liver tissues. *Proceedings of the National Academy of Sciences* **108**, 11842-11847, doi:10.1073/pnas.1101791108 (2011).
239 Billerbeck, E. *et al.* Humanized mice efficiently engrafted with fetal hepatoblasts and syngeneic immune cells develop human monocytes and NK cells. *Journal of Hepatology* **65**, 334-343, doi:https://doi.org/10.1016/j.jhep.2016.04.022 (2016).
240 Hofmann, C. *et al.* Cell-Cell Contacts Prevent Anoikis in Primary Human Colonic Epithelial Cells. *Gastroenterology* **132**, 587-600, doi:https://doi.org/10.1053/j.gastro.2006.11.017 (2007).
241 Olson, M. F. Applications for ROCK kinase inhibition. *Current Opinion in Cell Biology* **20**, 242-248, doi:https://doi.org/10.1016/j.ceb.2008.01.002 (2008).
242 Gilmore, A. P. Anoikis. *Cell Death & Differentiation* **12**, 1473-1477, doi:10.1038/sj.cdd.4401723 (2005).
243 Chen, C. *et al.* Bioengineered bile ducts recapitulate key cholangiocyte functions. *Biofabrication* **10**, 034103, doi:10.1088/1758-5090/aac8fd (2018).
244 Hassanein, W. *et al.* Recellularization via the bile duct supports functional allogenic and xenogenic cell growth on a decellularized rat liver scaffold. *Organogenesis* **13**, 16-27 (2017).
245 Pauwels, K. *et al.* State-of-the-Art Lentiviral Vectors for Research Use: Risk Assessment and Biosafety Recommendations. *Current Gene Therapy* **9**, 459-474, doi:10.2174/156652309790031120 (2009).
246 Fujii, M., Matano, M., Nanki, K. & Sato, T. Efficient genetic engineering of human intestinal organoids using electroporation. *Nature Protocols* **10**, 1474, doi:10.1038/nprot.2015.088

https://www.nature.com/articles/nprot.2015.088#supplementary-information (2015).
247 Laperrousaz, B. *et al.* Direct transfection of clonal organoids in Matrigel microbeads: a promising approach toward organoid-based genetic screens. *Nucleic Acids Research* **46**, e70-e70, doi:10.1093/nar/gky030 (2018).
248 Schwank, G. *et al.* Functional Repair of CFTR by CRISPR/Cas9 in Intestinal Stem Cell Organoids of Cystic Fibrosis Patients. *Cell Stem Cell* **13**, 653-658, doi:https://doi.org/10.1016/j.stem.2013.11.002 (2013).
249 Matano, M. *et al.* Modeling colorectal cancer using CRISPR-Cas9–mediated engineering of human intestinal organoids. *Nature medicine* **21**, 256 (2015).
250 Oceguera-Yanez, F. *et al.* Engineering the AAVS1 locus for consistent and scalable transgene expression in human iPSCs and their differentiated derivatives. *Methods* **101**, 43-55, doi:https://doi.org/10.1016/j.ymeth.2015.12.012 (2016).
251 Tiyaboonchai, A. *et al.* Utilization of the AAVS1 safe harbor locus for hematopoietic specific transgene expression and gene knockdown in human ES cells. *Stem Cell Research* **12**, 630-637, doi:https://doi.org/10.1016/j.scr.2014.02.004 (2014).
252 Rivière, I., Dunbar, C. E. & Sadelain, M. Hematopoietic stem cell engineering at a crossroads. *Blood* **119**, 1107-1116 (2012).
253 Nusse, R., van Ooyen, A., Cox, D., Fung, Y. K. T. & Varmus, H. Mode of proviral activation of a putative mammary oncogene (int-1) on mouse chromosome 15. *Nature* **307**, 131 (1984).
254 Rivella, S. & Sadelain, M. in *Seminars in hematology.* 112-125.
255 Ellis, J. Silencing and variegation of gammaretrovirus and lentivirus vectors. *Human gene therapy* **16**, 1241-1246 (2005).
256 Sadelain, M., Papapetrou, E. P. & Bushman, F. D. Safe harbours for the integration of new DNA in the human genome. *Nature reviews Cancer* **12**, 51 (2012).
257 Qin, J. Y. *et al.* Systematic comparison of constitutive promoters and the doxycycline-inducible promoter. *PloS one* **5**, e10611 (2010).

258 Moore, J. C. *et al.* Efficient, high-throughput transfection of human embryonic stem cells. *Stem Cell Research & Therapy* **1**, 23, doi:10.1186/scrt23 (2010).
259 Woods, N.-B., Ooka, A. & Karlsson, S. Development of gene therapy for hematopoietic stem cells using lentiviral vectors. *Leukemia* **16**, 563 (2002).
260 Salmon, P. *et al.* High-level transgene expression in human hematopoietic progenitors and differentiated blood lineages after transduction with improved lentiviral vectors. *Blood* **96**, 3392-3398 (2000).
261 Berlinghoff, S. *et al.* Susceptibility of mesothelioma cell lines to adeno-associated virus 2 vector-based suicide gene therapy. *Lung Cancer* **46**, 179-186 (2004).
262 Neefjes, J., Jongsma, M. L. M., Paul, P. & Bakke, O. Towards a systems understanding of MHC class I and MHC class II antigen presentation. *Nature Reviews Immunology* **11**, 823-836, doi:10.1038/nri3084 (2011).
263 Mulder, D. J. *et al.* Antigen Presentation and MHC Class II Expression by Human Esophageal Epithelial Cells: Role in Eosinophilic Esophagitis. *The American Journal of Pathology* **178**, 744-753, doi:http://dx.doi.org/10.1016/j.ajpath.2010.10.027 (2011).
264 Bland, P. MHC class II expression by the gut epithelium. *Immunology today* **9**, 174-178 (1988).
265 Onoé, K., Yanagawa, Y., Minami, K., Iijima, N. & Iwabuchi, K. Th1 or Th2 balance regulated by interaction between dendritic cells and NKT cells. *Immunologic Research* **38**, 319-332, doi:10.1007/s12026-007-0011-5 (2007).
266 Basham, T. Y. & Merigan, T. C. Recombinant interferon-gamma increases HLA-DR synthesis and expression. *The Journal of Immunology* **130**, 1492-1494 (1983).
267 Berrih, S. *et al.* Interferon-gamma modulates HLA class II antigen expression on cultured human thymic epithelial cells. *The Journal of Immunology* **135**, 1165-1171 (1985).
268 Hohlfeld, R. & Engel, A. G. Induction of HLA-DR expression on human myoblasts with interferon-gamma. *The American journal of pathology* **136**, 503-508 (1990).
269 Geppert, T. D. & Lipsky, P. E. Antigen presentation by interferon-gamma-treated endothelial cells and fibroblasts: differential ability to function as antigen-presenting cells despite comparable Ia expression. *The Journal of Immunology* **135**, 3750-3762 (1985).
270 Darnell, J., Kerr, I. & Stark, G. Jak-STAT pathways and transcriptional activation in response to IFNs and other extracellular signaling proteins. *Science* **264**, 1415-1421, doi:10.1126/science.8197455 (1994).
271 Muhlethaler-Mottet, A., Di Berardino, W., Otten, L. A. & Mach, B. Activation of the MHC Class II Transactivator CIITA by Interferon-γ Requires Cooperative Interaction between Stat1 and USF-1. *Immunity* **8**, 157-166, doi:https://doi.org/10.1016/S1074-7613(00)80468-9 (1998).
272 Steimle, V., Siegrist, C., Mottet, A., Lisowska-Grospierre, B. & Mach, B. Regulation of MHC class II expression by interferon-gamma mediated by the transactivator gene CIITA. *Science* **265**, 106-109, doi:10.1126/science.8016643 (1994).
273 Hu, G. *et al.* miR-221 suppresses ICAM-1 translation and regulates interferon-γ-induced ICAM-1 expression in human cholangiocytes. *American Journal of Physiology - Gastrointestinal and Liver Physiology* **298**, G542-G550, doi:10.1152/ajpgi.00490.2009 (2010).
274 Ayres, R. C., Neuberger, J. M., Shaw, J., Joplin, R. & Adams, D. H. Intercellular adhesion molecule-1 and MHC antigens on human intrahepatic bile duct cells: effect of pro-inflammatory cytokines. *Gut* **34**, 1245-1249 (1993).
275 Snover, D. C. MHC antigen expression in human liver grafts: Its role in rejection. *Hepatology* **11**, 704-706, doi:10.1002/hep.1840110428 (1990).
276 Leon, M. P. *et al.* Immunogenicity of biliary epithelium: Investigation of antigen presentation to CD4+ T cells. *Hepatology* **24**, 561-567, doi:10.1002/hep.510240317 (1996).
277 Shimoda, S. *et al.* Biliary epithelial cells and primary biliary cirrhosis: The role of liver-infiltrating mononuclear cells. *Hepatology* **47**, 958-965, doi:10.1002/hep.22102 (2008).
278 Pujol–Borrell, R. *et al.* HLA class II induction in human islet cells by interferon-γ plus tumour necrosis factor or lymphotoxin. *Nature* **326**, 304-306, doi:10.1038/326304a0 (1987).
279 Brehm, M. A. & Shultz, L. D. Human allograft rejection in humanized mice: a historical perspective. *Cellular & Molecular Immunology* **9**, 225-231, doi:10.1038/cmi.2011.64 (2012).
280 Brehm, M. A. *et al.* Human Immune System Development and Rejection of Human Islet Allografts in Spontaneously Diabetic NOD-

Rag1^{null} IL2rγ^{null} Ins2^{Akita} Mice . *Diabetes* **59**, 2265-2270, doi:10.2337/db10-0323 (2010).

281 Jacobson, S. *et al.* Alloreactivity but failure to reject human islet transplants by humanized Balb/c/Rag2−/− gc−/− mice. *Scandinavian journal of immunology* **71**, 83-90 (2010).

282 Torikai, H. *et al.* Toward eliminating HLA class I expression to generate universal cells from allogeneic donors. *Blood* **122**, 1341-1349, doi:10.1182/blood-2013-03-478255 (2013).

283 Börger, A.-K. *et al.* Generation of HLA-Universal iPSC-Derived Megakaryocytes and Platelets for Survival Under Refractoriness Conditions. *Molecular Medicine* **22**, 274-285, doi:10.2119/molmed.2015.00235 (2016).

284 Howard, H. C. *et al.* One small edit for humans, one giant edit for humankind? Points and questions to consider for a responsible way forward for gene editing in humans. *European Journal of Human Genetics* **26**, 1-11, doi:10.1038/s41431-017-0024-z (2018).

285 Yin, H., Kauffman, K. J. & Anderson, D. G. Delivery technologies for genome editing. *Nature Reviews Drug Discovery* **16**, 387, doi:10.1038/nrd.2016.280 (2017).

286 Aron Badin, R. *et al.* MHC matching fails to prevent long-term rejection of iPSC-derived neurons in non-human primates. *Nature Communications* **10**, 4357, doi:10.1038/s41467-019-12324-0 (2019).

287 Devlin, J. *et al.* Defining the outcome of immunosuppression withdrawal after liver transplantation. *Hepatology* **27**, 926-933, doi:10.1002/hep.510270406 (1998).

288 Orlando, G., Soker, S. & Wood, K. Operational tolerance after liver transplantation. *Journal of Hepatology* **50**, 1247-1257, doi:https://doi.org/10.1016/j.jhep.2009.03.006 (2009).

289 Ohe, H. *et al.* Factors affecting operational tolerance after pediatric living-donor liver transplantation: impact of early post-transplant events and HLA match*. *Transplant International* **25**, 97-106, doi:10.1111/j.1432-2277.2011.01389.x (2012).

290 Donaldson, P. T. *et al.* EVIDENCE FOR AN IMMUNE RESPONSE TO HLA CLASS I ANTIGENS IN THE VANISHING-BILEDUCT SYNDROME AFTER LIVER TRANSPLANTATION. *The Lancet* **329**, 945-948, doi:https://doi.org/10.1016/S0140-6736(87)90293-5 (1987).

291 Balan, V. *et al.* Long-term outcome of human leukocyte antigen mismatching in liver transplantation: results of the National Institute of Diabetes and Digestive and Kidney Diseases Liver Transplantation Database. *Hepatology* **48**, 878-888 (2008).

292 Dilly, S. A. & Sloane, J. P. Enlargement of the human spleen in graft-versus-host disease. *Transplantation* **45**, 741-743 (1988).

293 Kenney, L. L., Shultz, L. D., Greiner, D. L. & Brehm, M. A. Humanized Mouse Models for Transplant Immunology. *American Journal of Transplantation* **16**, 389-397, doi:10.1111/ajt.13520 (2016).

294 Walsh, P. T., Taylor, D. K. & Turka, L. A. Tregs and transplantation tolerance. *The Journal of Clinical Investigation* **114**, 1398-1403, doi:10.1172/JCI23238 (2004).

295 Okada, S., Harada, H., Ito, T., Saito, T. & Suzu, S. Early development of human hematopoietic and acquired immune systems in new born NOD/Scid/Jak3null mice intrahepatic engrafted with cord blood-derived CD34+ cells. *International Journal of Hematology* **88**, 476-482, doi:10.1007/s12185-008-0215-z (2008).

296 Lepus, C. M. *et al.* Comparison of human fetal liver, umbilical cord blood, and adult blood hematopoietic stem cell engraftment in NOD-scid/γc−/−, Balb/c-Rag1−/−γc−/−, and C.B-17-scid/bg immunodeficient mice. *Human Immunology* **70**, 790-802, doi:https://doi.org/10.1016/j.humimm.2009.06.005 (2009).

297 Ezekian, B. *et al.* Contemporary Strategies and Barriers to Transplantation Tolerance. *Transplantation* **102**, 1213-1222, doi:10.1097/TP.0000000000002242 (2018).

298 Newton, J. M. & Levitsky, J. Mechanisms and Strategies for Tolerance in Liver Transplantation. *Current Transplantation Reports* **3**, 325-333, doi:10.1007/s40472-016-0119-4 (2016).

299 Milner, J. *et al.* HLA Matching Trumps Donor Age: Donor-Recipient Pairing Characteristics That Impact Long-Term Success in Living Donor Kidney Transplantation in the Era of Paired

Kidney Exchange. *Transplant Direct* **2**, e85-e85, doi:10.1097/TXD.0000000000000597 (2016).
300 Breda, A. *et al.* in *Edn. presented at the EAU Annual Congress London.*
301 Yu, Y., Alkhawaji, A., Ding, Y. & Mei, J. Decellularized scaffolds in regenerative medicine. *Oncotarget* **7**, 58671-58683, doi:10.18632/oncotarget.10945 (2016).
302 Keane, T. J., Swinehart, I. T. & Badylak, S. F. Methods of tissue decellularization used for preparation of biologic scaffolds and in vivo relevance. *Methods* **84**, 25-34, doi:https://doi.org/10.1016/j.ymeth.2015.03.005 (2015).
303 Ryan, A. J. & O'Brien, F. J. Insoluble elastin reduces collagen scaffold stiffness, improves viscoelastic properties, and induces a contractile phenotype in smooth muscle cells. *Biomaterials* **73**, 296-307 (2015).
304 King, M., Pearson, T., Rossini, A. A., Shultz, L. D. & Greiner, D. L. Humanized mice for the study of type 1 diabetes and beta cell function. *Annals of the New York Academy of Sciences* **1150**, 46-53, doi:10.1196/annals.1447.009 (2008).
305 Lipsitz, Y. Y., Bedford, P., Davies, A. H., Timmins, N. E. & Zandstra, P. W. Achieving Efficient Manufacturing and Quality Assurance through Synthetic Cell Therapy Design. *Cell Stem Cell* **20**, 13-17, doi:https://doi.org/10.1016/j.stem.2016.12.003 (2017).
306 Ran, F. A. *et al.* Double Nicking by RNA-Guided CRISPR Cas9 for Enhanced Genome Editing Specificity. *Cell* **154**, 1380-1389, doi:https://doi.org/10.1016/j.cell.2013.08.021 (2013).

nature protocols

PROTOCOL

https://doi.org/10.1038/s41596-019-0168-0

Isolation and propagation of primary human cholangiocyte organoids for the generation of bioengineered biliary tissue

Olivia C. Tysoe[1,2,12], Alexander W. Justin[3,12], Teresa Brevini[1,4,12], Si Emma Chen[1], Krishnaa T. Mahbubani[2], Anna K. Frank[5,6,7], Hajer Zedira[1], Espen Melum[5,6,8,9], Kourosh Saeb-Parsy[2,13], Athina E. Markaki[3,13], Ludovic Vallier[1,2,13*] and Fotios Sampaziotis[1,2,10,11,13*]

Pediatric liver transplantation is often required as a consequence of biliary disorders because of the lack of alternative treatments for repairing or replacing damaged bile ducts. To address the lack of availability of pediatric livers suitable for transplantation, we developed a protocol for generating bioengineered biliary tissue suitable for biliary reconstruction. Our platform allows the derivation of cholangiocyte organoids (COs) expressing key biliary markers and retaining functions of primary extra- or intrahepatic duct cholangiocytes within 2 weeks of isolation. COs are subsequently seeded on polyglycolic acid (PGA) scaffolds or densified collagen constructs for 4 weeks to generate bioengineered tissue retaining biliary characteristics. Expertise in organoid culture and tissue engineering is desirable for optimal results. COs correspond to mature functional cholangiocytes, differentiating our method from alternative organoid systems currently available that propagate adult stem cells. Consequently, COs provide a unique platform for studies in biliary physiology and pathophysiology, and the resulting bioengineered tissue has broad applications for regenerative medicine and cholangiopathies.

Introduction

Cholangiopathies comprise a diverse group of disorders characterized by damage to the biliary tree and loss of bile ducts resulting in cholestasis, hepatic injury and ultimately liver failure[1,2]. However, treatment options are limited to liver transplantation. Indeed, biliary disease remains the leading indication for this intervention in children, with >70% of pediatric liver grafts being used to treat biliary atresia[3]. The generation of healthy biliary tissue suitable for replacing or reconstructing damaged bile ducts could address the clinical need for alternative therapeutic approaches and reduce pressure on the transplant waiting list. However, progress in this area has been hampered by challenges in the long-term culture and large-scale expansion of primary cholangiocytes. Here, we describe a protocol for the fabrication of functional bioengineered biliary tissue, using biocompatible and biodegradable scaffolds and a method for the isolation and propagation of primary cholangiocytes in organoid format.

Development of the protocol

To generate bioengineered biliary tissue suitable for surgical manipulation and biliary reconstruction, we decided to combine primary biliary epithelium with appropriate matrices.

[1]Wellcome Trust-Medical Research Council Stem Cell Institute, Cambridge Stem Cell Institute, Anne McLaren Laboratory, Department of Surgery, University of Cambridge, Cambridge, UK. [2]Department of Surgery, University of Cambridge, Cambridge, UK. [3]Department of Engineering, University of Cambridge, Cambridge, UK. [4]Department of Medical Biotechnology and Translational Medicine (BIOMETRA), Università degli Studi di Milano, Milan, Italy. [5]Norwegian PSC Research Center, Department of Transplantation Medicine, Division of Surgery, Inflammatory Diseases and Transplantation, Oslo University Hospital, Rikshospitalet, Oslo, Norway. [6]Research Institute of Internal Medicine, Division of Surgery, Inflammatory Diseases and Transplantation, Oslo University Hospital, Rikshospitalet, Oslo, Norway. [7]Department of Medicine III, University Hospital Aachen, Aachen, Germany. [8]Section for Gastroenterology, Department of Transplantation Medicine, Division of Surgery, Inflammatory Diseases and Transplantation, Oslo University Hospital Rikshospitalet, Oslo, Norway. [9]Institute of Clinical Medicine, Faculty of Medicine, University of Oslo, Oslo, Norway. [10]Department of Hepatology, Cambridge University Hospitals NHS Foundation Trust, Cambridge, UK. [11]Department of Medicine, University of Cambridge, Cambridge, UK. [12]These authors contributed equally: Olivia C. Tysoe, Alexander W. Justin, Teresa Brevini. [13]These authors jointly supervised this work: Kourosh Saeb-Parsy, Athina E. Markaki, Ludovic Vallier and Fotios Sampaziotis. *e-mail: lv225@cam.ac.uk; fs347@cam.ac.uk

Development of the protocol for CO culture

First, we developed a culture protocol for the propagation and large-scale expansion of primary adult, functional cholangiocytes[4]. Because biliary reconstruction is predominantly performed on the common bile duct (CBD), we initially focused on the isolation of CBD cholangiocytes, using excised bile ducts from deceased organ donors. To achieve expansion of the isolated cholangiocytes, the cells are embedded in Matrigel and treated with a combination of epidermal growth factor (EGF), R-spondin-1 and DKK-1. We have previously demonstrated that the combination of EGF and 3D culture can promote limited growth of partially mature, fetal cholangiocyte-like cell (CLC) organoids derived from induced pluripotent stem (iPS) cells[5,6]. In addition, primary adult stem cell organoids have been isolated from murine biliary tissue[7]. To support the long-term expansion of adult cholangiocytes, we use R-spondin-1, a WNT agonist reported to stimulate organoid derivation from multiple adult epithelia[8–13]. However, R-spondin promotes the propagation of adult stem cells rather than mature epithelial populations by enhancing canonical Wnt signaling[14]. To avoid the amplification of adult stem cells, we introduce DKK-1[15], a canonical WNT/β-catenin pathway antagonist[16,17]. When used in combination with R-spondin, DKK-1 inhibits canonical and enhances non-canonical WNT signaling through the planar cell polarity pathway[4], which has been reported to play a role in cholangiocyte maturation[18,19]. The combination of EGF, R-spondin-1 and DKK-1 allows for long-term, large-scale expansion of functional, genetically stable, primary adult COs.

Our system was developed and optimized for the culture of CBD COs isolated from fresh excised bile ducts. However, this isolation method requires a complex operation, thereby posing substantial limitations related to access to biliary tissue. To overcome this issue, we subsequently validated the capacity of our culture system for the derivation of COs from multiple sources, such as excised gallbladders, endoscopic retrograde cholangiopancreatography (ERCP) brushings and liver biopsy samples. With this platform, COs can be isolated and expanded using samples from any area of the biliary tree and acquired by any of these isolation methods.

Choice of scaffolds

Our next goal was to identify appropriate scaffolds that could be combined with the cells to generate tissue-like constructs. Important considerations for the choice of scaffolds were their potential to support growth of the cells, their capacity to be integrated into the host tissue following transplantation with minimal inflammatory response and the use of biodegradable materials allowing for tissue remodeling, which is critical to neo-vascularization. Furthermore, to support future clinical translation, the materials used should be compatible with human transplantation.

Importantly, both synthetic and biological polymer scaffolds with these specifications are available. As there are advantages and disadvantages associated with each approach, we decided to explore both. Synthetic polymer scaffolds are widely used, as they can be easily processed using a wide range of techniques and adapted for multiple tissue engineering applications[20]. They have tunable and reproducible physicochemical properties, mechanical strength and degradation rates, making them highly customizable as a scaffold material[20,21]. Biological polymer scaffolds are more challenging to tailor to a particular application, owing to purity, immunogenicity, and scaffold homogeneity and reproducibility issues[22]. However biological polymer scaffolds have superior bioactive properties (e.g., cell attachment, migration, cell scaffold remodeling) and thus better cell and tissue interactions[22,23].

Generation of bioengineered tissue using synthetic scaffolds

First, we focused on synthetic scaffolds commercially available 'off the shelf' to optimize cell seeding, attachment and culture of the resulting tissue. We decided to use a PGA matrix because of its biodegradability, flexibility and lack of inflammatory response in vivo[24]. In addition, synthetic PGA scaffolds can be easily processed into tailored architectures[22,23]. For these reasons, PGA is one of the most commonly used synthetic polymers in tissue engineering[21] and has been approved by the FDA for use in human studies[25].

We subsequently identified the optimal method for seeding COs on the scaffolds. Our results demonstrated that the use of cell clumps concentrated in small volumes is the optimal seeding method. Small volumes of cell suspension are absorbed by the scaffold, maximizing cell-to-scaffold contact. An alternative method, the dissociation of organoids into single cells, requires aggressive enzymatic digestion, which reduces cell viability and attachment because of the cleavage of multiple cell-to-matrix adhesion molecules[26]. Seeding cell clumps resulted in the generation of confluent PGA scaffolds seeded with COs, which were used to successfully repair biliary tree wall defects in immunocompromised mice following transplantation.

Generation of bioengineered tissue using biological scaffolds

We subsequently used the same seeding methodology to populate biological scaffolds. Here, we chose densified collagen hydrogel because of its biocompatibility, low immunogenicity, ability to favor cell attachment and growth, biodegradability and ability to be naturally remodeled by cells[27]. Importantly, as compared with standard collagen gel, densified collagen gel demonstrates superior mechanical properties for surgical applications[27,28]. Densification expels the majority of the water content of the collagen gel, vastly reducing its volume, resulting in a polymer scaffold of higher concentration and fibrillar alignment[28]. Through the use of appropriate molds, the densification process can be customized to generate constructs of more complex geometries, which can be successfully seeded with COs.

Generation of bioengineered mouse bile ducts

One of the most relevant clinical applications of bioengineered biliary tissue is the generation of tubular constructs suitable for biliary reconstruction. However, bile duct transplantation can be associated with a substantial inflammatory response, epithelial damage and the formation of anastomotic strictures in humans[29,30]. Consequently, in vivo validation of the function, biocompatibility and patency of bioengineered ducts following reconstruction is required. To achieve this goal, we decided to generate bioengineered constructs populated with human COs, transplant them into immunocompromised mice and characterize them.

The fabrication of tubular structures with dimensions comparable to those of the mouse CBD (250-μm inner diameter and 30-μm wall thickness) was a key challenge. Indeed, commercially available fibrous PGA scaffolds[31] were incompatible with these requirements because their minimum thickness (300 μm) is substantially larger than the required wall thickness. Appropriate-thickness predensified collagen gel sheets could be fashioned into a tube using sutures; however, interruption of the collagen fibrils along the seam led to partial collapse of the lumen under the weight of the wall. To overcome these challenges, we developed a method in which collagen was cast around a central rod and densified afterward, to yield a seamless tube with a thin and robust wall. Furthermore, a conical funnel mold was used, which allowed a proportionately large volume of collagen to densify into a short length of tube and enabled efficient water removal via multiple routes (through on-axis absorption and radial evaporation). These techniques yielded bioengineered tubes with a patent lumen and dimensions similar to those of the mouse CBD[32].

We subsequently used the approach that we developed for seeding COs on flat collagen scaffolds to seed the luminal surface of the construct with cells and generate mouse-sized bioengineered bile ducts populated with human cells. Importantly, the potential of these constructs for biliary reconstruction in vivo was illustrated through their successful transplantation into immunocompromised mice[4].

Applications and target audience

The propagation of COs and the generation of bioengineered biliary tissue are likely to be of interest to a broad scientific audience, including clinician scientists focusing on translation of new therapies to the clinic, bioengineers working on whole-organ reconstruction, groups focusing on biliary physiology and disease and the pharmaceutical industry. Currently the only therapeutic option for biliary disorders is liver transplantation. The generation of bioengineered biliary tissue could provide one of the first alternative treatments and pioneer the use of regenerative medicine for cholangiopathies[33,34].

Furthermore, a limitation of complex liver co-culture systems is the lack of a biliary system. The capacity of COs to grow in a variety of matrices and scaffolds makes them an ideal addition to complex tissue engineering applications that focus on recapitulating the microanatomy of the liver and the development of artificial whole-organ systems[35].

Cholangiocytes constitute a rare liver cell type, and access to primary tissue has limited large-scale analyses in the past. COs closely resemble primary biliary epithelium in terms of transcriptional profile and function[4]. Consequently, extrahepatic COs (ECOs) and intrahepatic COs (ICOs) could serve as surrogates for primary cholangiocytes from any region of the biliary tree, enabling in-depth, large-scale studies of biliary physiology and pathophysiology. Similarly, COs recapitulate the effects of compounds such as verapamil and somatostatin, rendering them suitable for drug-screening applications.

Comparison to other methods

A unique feature of our culture system is that it enables the long-term culture of mature cholangiocytes through inhibition of canonical WNT signaling by DKK-1, maintaining adult

characteristics and functionality with no need for additional differentiation. Therefore, our system is distinct from alternative primary organoid platforms based on canonical WNT signaling, which propagate adult stem cells[8,11,13,36] rather than bona fide biliary epithelium. Consequently, COs may be better suited to studies on biliary physiology and disease requiring high-fidelity cholangiocytes, whereas adult stem cells are optimal for studies on liver repair and regeneration.

Although methods for short-term culture of murine[37] and human primary cholangiocytes have been reported[38,39], these systems are technically challenging and allow for only limited expansion, restricting large-scale analyses, and the function of the resulting cells has not been extensively characterized. COs combine high proliferative capacity, increased functionality and the potential for large-scale expansion, which is critical to regenerative medicine or for high-throughput applications.

Importantly, cholangiocytes can be derived from iPS cells[5,6,40,41]. However, these cells have the characteristics of fetal intrahepatic cholangiocytes, whereas our method can generate cells similar to both intrahepatic and extrahepatic adult cholangiocytes. In addition, COs can be rapidly isolated and expanded, unlike iPS cell systems, which require a lengthy differentiation process and cannot be further propagated once terminally differentiated. Consequently, stem cell–derived cholangiocytes are optimal for studies of intrahepatic bile duct development and its disorders, whereas COs are better suited to studies of adult intra- and extrahepatic cholangiocyte physiology or regenerative medicine applications requiring large numbers of highly functional cells in little time.

Our system provides multiple advantages for tissue engineering and regenerative medicine. The generation of bioengineered tissue is versatile, allowing the use of synthetic (PGA) or biological scaffolds (collagen). Furthermore, it is compatible with Good Manufacturing Practice (GMP)-compliant materials, such as collagen, which has an excellent in vivo profile and is used extensively in clinical applications[24]. The method by which the densified collagen tubes are formed allows their generation at customizable length scales compatible with small animal studies. Furthermore, the densification process does not impart substantial stress upon the cells, which can be mixed in the gel if required. The resulting constructs can be maintained for >2 months in culture, enabling the generation of large batches of bioengineered tissue with prolonged 'shelf life'. Importantly, our bioengineered biliary tissue provides the first proof of principle for organ reconstruction using primary epithelial organoids, in which the resulting bioengineered construct was used to fully replace the native organ[4].

Limitations

A limitation of our system is that COs, as adult primary cholangiocytes, are not suitable for studying biliary development, an application for which stem cell–derived systems are more appropriate. In addition, as COs represent a pure epithelial population, this system does not currently allow for the study of epithelial and mesenchymal interactions, although the potential exists within our system to generate bioengineered tissue with additional cell types. A further, technical, limitation is that COs currently rely on the use of Matrigel, a non-GMP-compliant extracellular matrix. However, multiple chemically defined hydrogel matrices, which could replace Matrigel, are currently in development[42].

For research groups without access to a hospital with hepatobiliary services, access to primary tissue may present a challenge, as primary samples must be processed promptly following isolation. We note that samples can be obtained in any hospital that offers a cholecystectomy, ERCP or liver biopsy service, and that organoid derivation is still feasible after small delays associated with tissue transfer over short distances. Nevertheless, to compensate for transport-associated delays when multiple samples from distal centers are processed, a team of trained technicians working in parallel may be required.

Finally, although mouse-sized (submillimeter) constructs serve as proof of principle for the generation of bioengineered ducts populated with human cells, their mechanical properties do not translate to those of the human bile duct (7-mm diameter, 1-mm wall thickness). Therefore, optimization of our technique for the generation of human-sized constructs with appropriate physical attributes will be required before clinical translation.

Experimental design

Our method describes a system for isolating primary extrahepatic and intrahepatic cholangiocytes from primary tissue, culturing these primary cholangiocytes in a 3D organoid system and generating bioengineered biliary tissue using artificial scaffolds (Fig. 1). In this section, we describe infrastructure and experimental setup considerations that one must take into account before using this protocol.

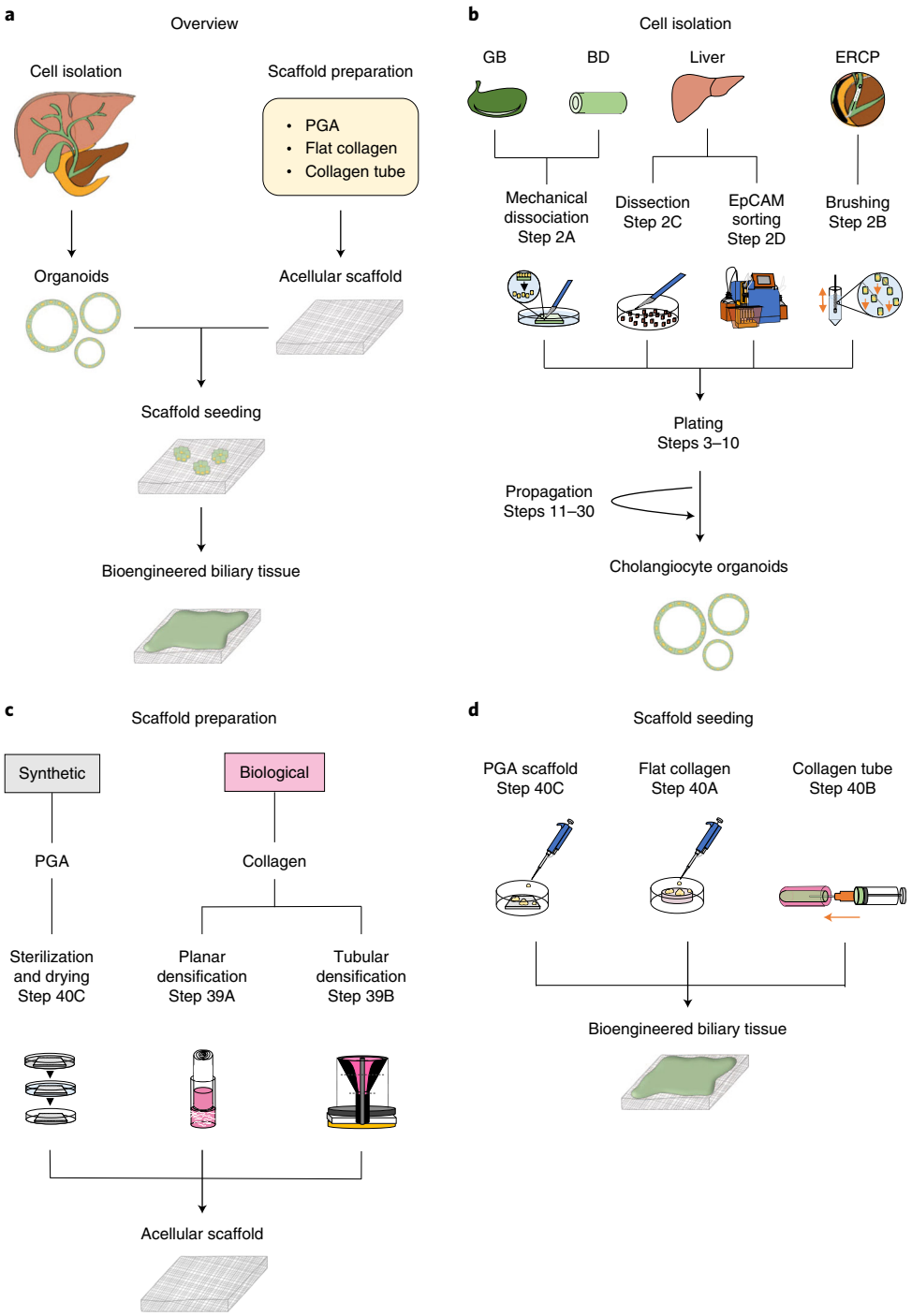

Fig. 1 | Flowchart of key steps in the generation of bioengineered biliary tissue. a, Overview flowchart showing the three major protocol steps: cell isolation, scaffold preparation and generation of bioengineered biliary tissue. **b**, Flowchart summarizing the process of cell isolation from different biliary tissue samples with reference to the relevant protocol sections. **c**, Flowchart illustrating the different types of biological or synthetic scaffolds used, with reference to the relevant protocol sections. **d**, Flowchart summarizing the seeding of acellular scaffolds with CO cells, with reference to the relevant protocol sections. BD, primary bile duct; GB, gallbladder.

Isolation of cholangiocytes from primary tissue

Our protocol requires the isolation of cholangiocytes from primary human tissue, either from living patients or from deceased organ donors. As such, appropriate ethical approval from the relevant regulatory bodies is required, and informed consent is essential before any human tissue samples are acquired.

Obtaining fresh human tissue samples will require access to a hospital with one of the following services: hepatology, advanced endoscopy, hepatobiliary surgery, transplant organ procurement or liver transplantation. Importantly, donor tissue viability decreases in proportion to ex vivo storage and bile exposure. Therefore, bile must be flushed from the tissue, which should then be stored immediately in cold preservation solution (such as University of Wisconsin (UW) solution) or supplemented William's E+ medium at 4 °C until it can be processed[43].

When multiple tissue samples are obtained simultaneously (such as from a deceased organ donor), the tissue should be processed in order of sensitivity to cold storage (Supplementary Fig. 1). Liver biopsies require immediate processing, whereas extrahepatic tissue can be stored at 4 °C for several hours, provided that it is appropriately flushed of bile. Furthermore, all tissue handling should be performed under aseptic conditions to avoid contamination. Consequently, good communication with the clinicians obtaining the sample is critical. Long-distance transport of samples is likely to impact the viability of explanted tissue, so samples must ideally be processed in a facility close to the site of collection. Tissue must be processed in a class II biological safety cabinet under aseptic conditions, and sterile surgical equipment must be used.

CO lines can be generated using multiple approaches, depending on the source of available tissue and the method of sample collection (Fig. 1). Surgically excised tissue samples, such as gallbladders and bile ducts, can be used for the generation of COs following isolation of the luminal layer of cholangiocytes through mechanical scraping (Fig. 2). ERCP brushings provide an alternative source of tissue for patients having endoscopy (Fig. 3). One can isolate COs from liver biopsy tissue by dividing a liver biopsy core into small pieces (~1 mm^3) and plating them directly in CO organoid culture conditions (Fig. 4). Alternatively, CO lines can be derived from a population of $EpCAM^+$ sorted single cells (Supplementary Fig. 2). Tissue can be enzymatically digested to a single-cell suspension and then EpCAM-sorted through either FACS or magnetic-activated cell sorting (MACS).

Provided the tissue has been appropriately and promptly processed, the methods described should produce CO lines with almost 100% efficiency, apart from EpCAM sorting, which yields viable lines with an efficacy of 66% (Supplementary Table 1) owing to the impact of single-cell dissociation on cell viability. This method of derivation will produce a highly purified CO population, in contrast to derivation from whole-liver tissue, which can take up to three passages to establish a pure CO population. Flushing the tissue of bile is critical to achieving these results. Indeed, derivation efficiency is reduced from 95% to 40% if flushing is not performed (Supplementary Table 1). The optimal technique for CO line derivation should be decided on the basis of sample availability and access to tissue.

Establishment and maintenance of COs

Once plated, primary cholangiocytes should form organoids in 3–10 d. Clump size and seeding density can affect the speed and efficiency of derivation. Single cells tend to require longer culture and yield lower numbers of organoids from the same number of starting cells. Large clumps of >50–100 cells and high seeding density may result in cell attachment and limit organoid growth.

CO lines should be passaged approximately every 5 d (Fig. 5), although the cells should be monitored daily to check whether confluency has been reached (Fig. 5b, Supplementary Fig. 3). Delays in passaging of confluent wells can result in organoid collapse and affect the long-term health of the organoid line (Supplementary Fig. 4b). The same considerations as for organoid derivation apply with regard to clump size and seeding density during passaging (Supplementary Fig. 4b). Importantly, our protocol relies on Matrigel as an extracellular matrix, which has a profound impact on the quality of the resulting organoid lines. Therefore, Matrigel must be batch-tested before use. It is also important to ensure that no reagent or medium used in the maintenance of CO lines is used for longer than 3 months, as this can impact organoid quality.

Organoids can be analyzed through a variety of methods, such as qPCR, immunofluorescence (IF) and flow cytometry, as we have previously described[5,6]. COs should show robust expression of key biliary markers such as cytokeratin 19, cytokeratin 7, Sox9 and gamma-glutamyl transferase (GGT), as well as key cholangiocyte functions such as alkaline phosphatase (ALP) and GGT activity (Fig. 6), which can be used to assess the quality of CO derivation and culture.

Scaffold preparation

Bioengineered tissue can be generated using both synthetic (PGA) and biological (densified collagen gel) polymeric scaffolds, each of which may be suited to different applications. PGA scaffolds can be commercially sourced, are cheap and require minimal processing to yield positive results.

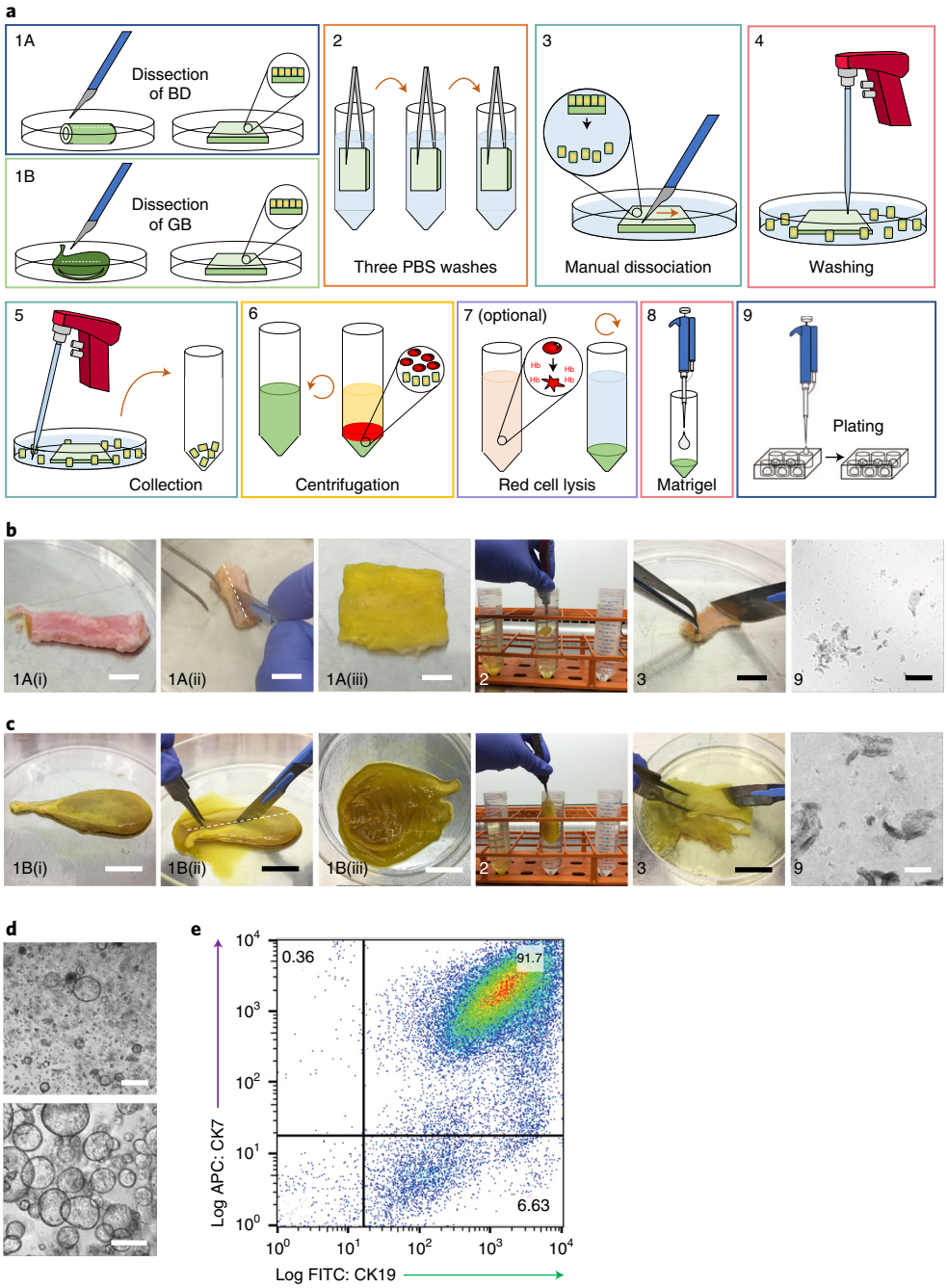

Fig. 2 | Derivation of ECOs from extrahepatic biliary tissue. a, Schematic representation of key stages of the derivation of ECOs from primary bile duct (BD) and gallbladder (GB) tissue (Step 2A). **b**,**c**, Representative images of key stages of the derivation of cholangiocytes from primary BD (**b**) and GB (**c**) tissue. Numbers in **b** and **c** correspond to the schematic stages illustrated in **a**. 1A(i), 1B(i): resected biliary tissue before dissection. 1A(ii), 1B(ii): tissue dissection. 1A(iii), 1B(iii): exposed luminal surface following dissection. 2: PBS wash. 3: Mechanical dissociation of the biliary epithelium. 9: Primary cholangiocytes in suspension following dissociation. Scale bars: **b**, images 1A(i)–3, 1 cm; **c**, images 1B(i)–3, 2 cm; **b**, image 9 and **c**, image 9, 100 μm. **d**, Representative bright-field images demonstrating key time points of ECO derivation. Scale bars, 200 μm. (Top) Primary cholangiocytes 24 h after plating, demonstrating the formation of early organoid structures. (Bottom) ECOs following long-term culture (passage 20). **e**, Flow cytometry analysis of the primary cell suspension, demonstrating >90% cholangiocyte isolation efficiency (Step 2A(i–viii); gating strategy demonstrated in Supplementary Fig. 6). APC, allophycocyanin; FITC, fluorescein isothiocyanate.

The mechanical properties of the scaffold (e.g., Young's modulus, strength) are tunable and can be customized through adjustment of the density and pore size. Furthermore, PGA constructs can be easily fabricated into custom architectures[22,23].

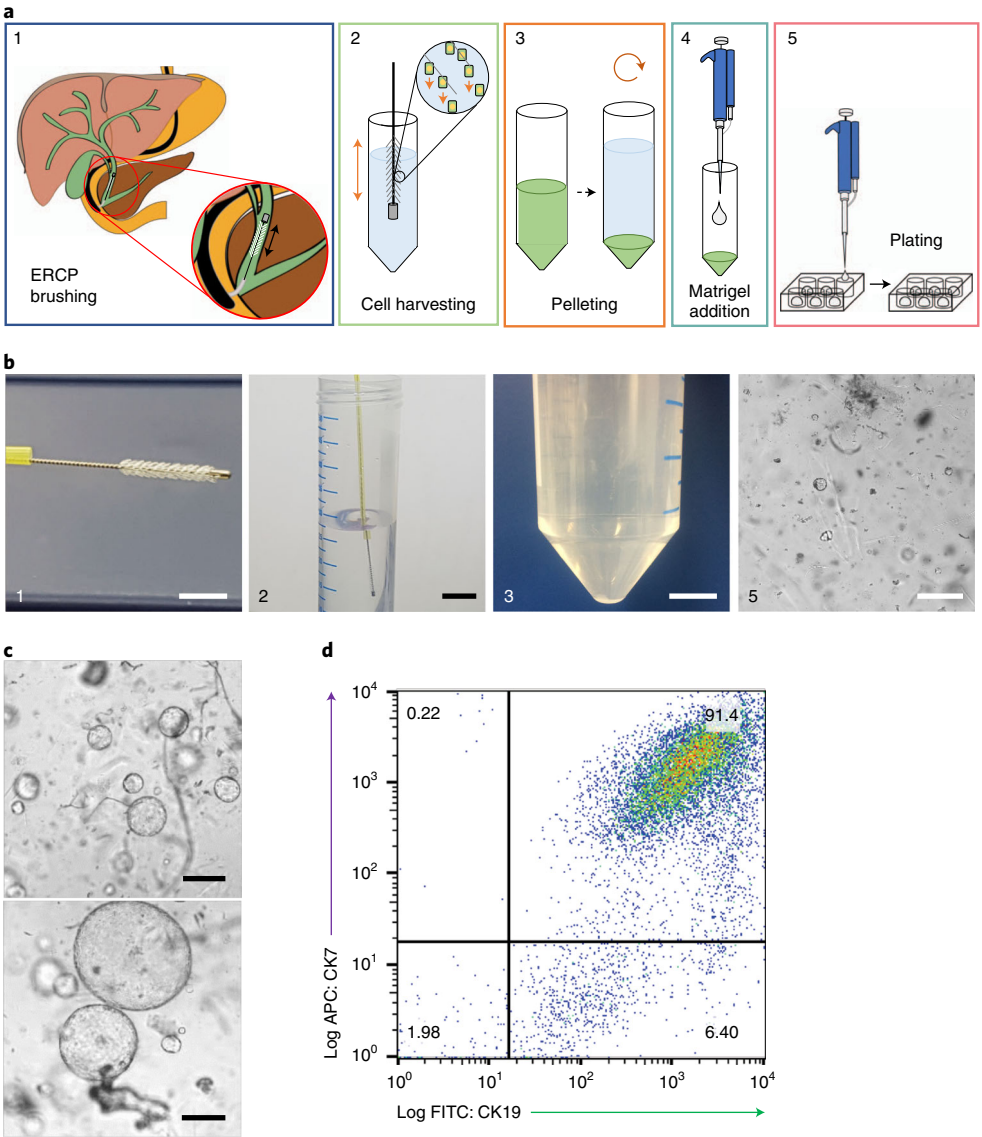

Fig. 3 | Derivation of ECOs through ERCP brushings. a, Schematic representation of stages of ECO derivation from ERCP brushings (Step 2B). **b**, Representative images of key stages of the derivation procedure. Numbers correspond to schematic stages in **a**. 1: ERCP brush. 2: Medium wash to dislodge the collected cholangiocytes from the brush. 3: Representative cell pellet after isolation. 5: Bright-field image of ERCP isolated cholangiocytes following plating. Scale bars, 1 cm (1–3) or 200 μm (5). **c**, Bright-field images demonstrating representative time points in the derivation of organoids from cholangiocytes obtained through ERCP brushings. (Top) Primary cholangiocytes 24 h after plating, demonstrating the formation of early organoid structures. (Bottom) COs 1 week after plating. Scale bars, 200 μm. **d**, Flow cytometry analysis of the cell suspension obtained through ERCP, demonstrating >90% cholangiocyte isolation efficiency (Step 2B(i–v); gating strategy demonstrated in Supplementary Fig. 6). APC, allophycocyanin; FITC, fluorescein isothiocyanate.

Collagen constitutes a physiological component of the extracellular matrix[44] with high bioactivity[45], which can interact with cells and present multiple cues that enhance attachment, survival, proliferation and tissue remodeling[44,46]. Furthermore, unlike PGA, cells can be mixed directly into the collagen gel precursor solution before gelation and densification, generating a uniform network of cells throughout the scaffold, which is useful for applications such as complex co-culture systems. However, it is more expensive than synthetic alternatives, and scaffolds with adequate mechanical strength for surgical manipulation[47,48] are not commercially available and need to be custom-made. Indeed, densified collagen sheets must be fabricated from collagen gels through water absorption (Fig. 7), whereas densified collagen tubes must be formed through molding of collagen gel around a cylindrical template and water removal by evaporation from the gel surface (Fig. 8). Consequently,

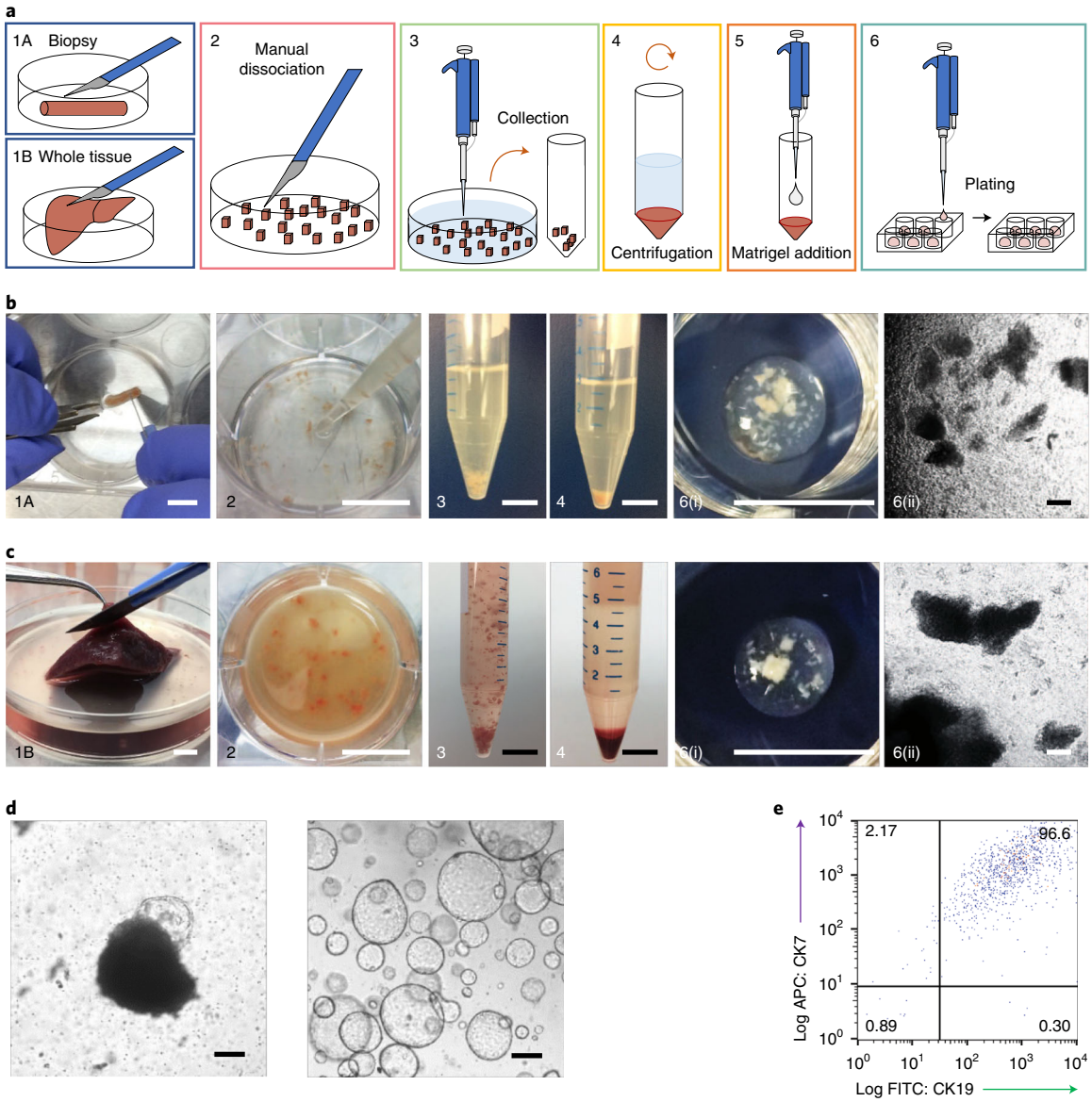

Fig. 4 | Derivation of intrahepatic organoids. a, Schematic representation of stages of ICO derivation (Step 2C). **b**,**c**, Representative images of key stages of ICO derivation for liver biopsies (**b**) and surgically resected liver tissue (**c**). Numbers correspond to schematic stages in **a**. 1: Dissection of liver tissue. 2: Manual dissociation and collection of dissected tissue. 3 and 4: Dissected tissue before (3) and after (4) centrifugation. 6: Plating. 6(i): Representative images of liver tissue after embedding in Matrigel, before medium addition. Scale bars, 1 cm (1–6(i)). 6(ii): Representative bright-field images of liver tissue after plating. Scale bars, 200 μm. **d**, Representative bright-field images demonstrating key time points of ICO derivation. (Left) ICO culture 5 d after plating, demonstrating the emergence of an organoid from a segment of liver tissue. (Right) Established ICO line (passage 20). Scale bars, 200 μm. **e**, Flow cytometry analysis of ICO cells, demonstrating >95% cholangiocyte isolation efficiency (gating strategy in Supplementary Fig. 6). APC, allophycocyanin; FITC, fluorescein isothiocyanate.

densified collagen scaffolds are more physiological but require a higher level of expertise and pose a greater number of potential pitfalls, whereas PGA scaffolds may be appropriate for settings in which the expertise and equipment for the generation of custom-made scaffolds are not available.

Scaffold seeding

PGA and densified collagen scaffolds (both flat and tubular) can be seeded with COs to generate bioengineered biliary tissue within 2–4 weeks. The cells are seeded as clumps in small volumes to maximize their contact with the scaffold and are incubated for 1 h to allow attachment before the addition of medium. For tubular scaffolds, cannulation with a small-gauge (<30-gauge) needle is necessary for seeding. This procedure is technically challenging and may require the assistance of a surgeon to avoid damaging the scaffold.

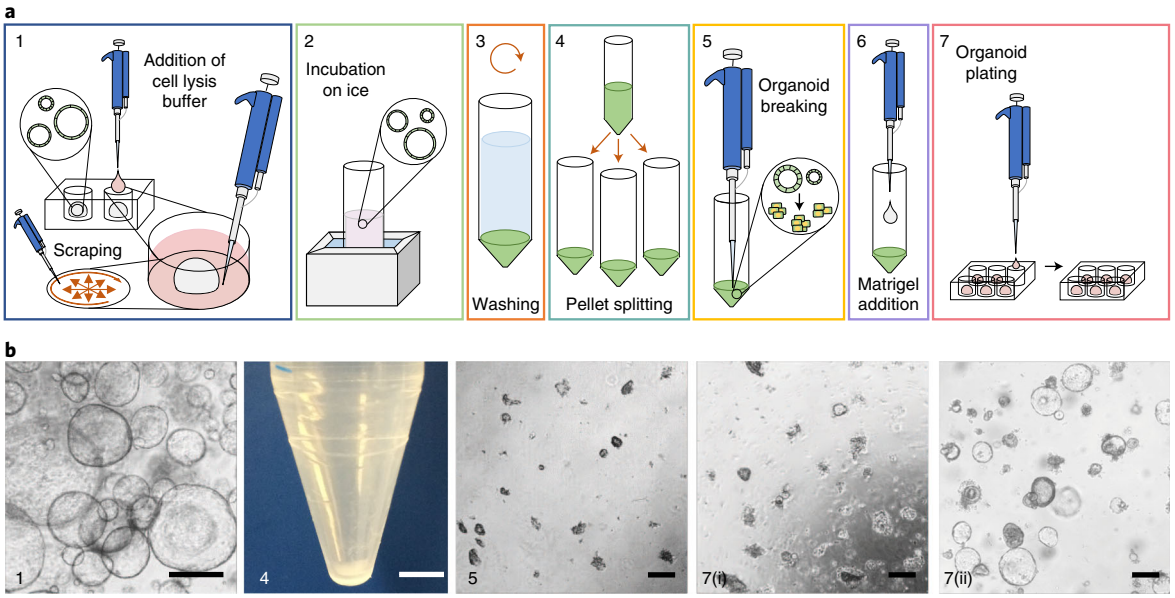

Fig. 5 | Passaging of COs. a, Schematic representation of the stages of the CO passaging procedure (Steps 15–30). **b**, Representative images of key stages of the CO passaging procedure. Numbers correspond to schematic stages in **a**. 1: Confluent COs before passaging. 4: Representative organoid pellet yielding nine organoid wells following plating (~4.0 × 10^5 cells). 5: Suspension of COs after manual dissociation, demonstrating representative clump size for passaging (~30–100 cells per clump) (Step 28). 7(i): COs immediately after plating (Steps 9–13), demonstrating that the majority of cells remain in small clumps and have not yet formed organoids at this stage. 7(ii): COs 24 h after passaging, demonstrating that the majority of CO clumps have remodeled into organoids at this point. Scale bars, 100 µm (1, 5, 7(i) and 7(ii)); 5 mm (4).

The efficiency and quality of cell attachment following seeding (Figs. 9 and 10) depend on clump size, cell number, seeding cell suspension volume and drying time for the scaffold. Single cells and low cell numbers are associated with reduced seeding efficiency, whereas large clumps may attach only partially. Importantly, parts of a clump that have not attached may remodel to form organoid-like structures connected to the scaffold or overlap with neighboring clumps that have attached, generating a pseudostratified epithelium. Consequently, the use of 30–50 cell clumps is critical to achieving optimal seeding results.

Low cell-suspension volumes result in poor scaffold coverage and therefore suboptimal seeding, whereas cell viability may be reduced because of medium evaporation during the incubation period. High volumes may lead to overflow and 'spillage' of the cell suspension from the scaffold to the plate, resulting in a reduced cell-to-surface ratio and poor seeding efficiency. Consequently, the seeding volume must be optimized on the basis of the scaffold surface, as described in the Procedure. This is particularly important when seeding on the luminal surface of a tubular scaffold, where the cell suspension must be optimized for minimal volume and maximal density, to be contained within the tube lumen.

Reduced incubation time does not allow an adequate period for the cells to attach. Consequently, the addition of medium at the end of the incubation phase results in washing of poorly attached cells off the scaffold. Prolonged incubation can result in scaffold drying and reduced cell viability.

Importantly, the scaffold is rarely confluent following seeding. Indeed, in most cases only a proportion of the scaffold is covered with cells. However, these expand to generate a confluent layer within weeks. The time to confluency can be reduced by seeding of higher numbers of cells or by repeated rounds of seeding. Importantly, if an additional round of seeding is performed, the scaffold should not be allowed to dry before the new cells are added, in order to preserve the viability of the cells already attached.

Bioengineered biliary tissue can be analyzed through IF or functional assays as previously described[4] and should show robust expression of key biliary markers such as cytokeratin 19 and cytokeratin 7 (Fig. 11a,c,e), as well as key cholangiocyte functions such as GGT activity (Fig. 11b,d,f). Once confluent, the scaffolds can be transplanted in vivo or maintained in culture for several months.

Scaffold-specific considerations

Pore size is an important consideration for PGA scaffolds. The scaffold pore size will determine the optimal cell clump size for seeding. Scaffolds with large pores would, in principle, allow deeper cell

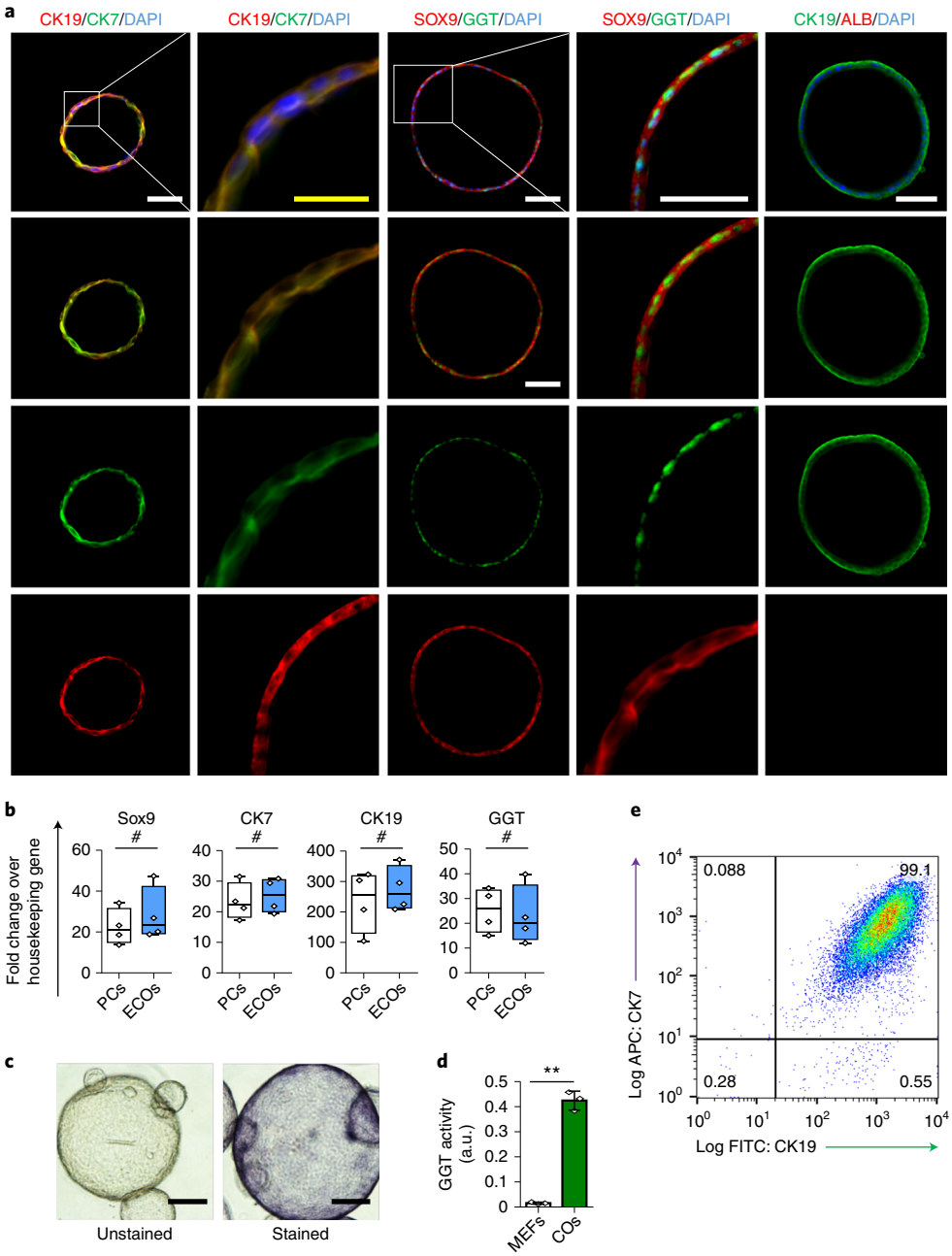

Fig. 6 | Characterization of COs. a, Immunofluorescence images demonstrating expression of key biliary markers in COs (10 passages). Scale bars, 50 μm. (See Supplementary Table 2 for a detailed list of antibodies and concentrations used). **b**, qRT–PCR confirming the expression of key biliary markers in ECOs (20 passages) compared to freshly isolated primary cholangiocytes (PCs); $n = 4$ biological replicates. Center line, median; box, interquartile range (IQR); whiskers, range (minimum to maximum). Values relative to those of the housekeeping gene *HMBS* (for hydroxymethylbilane synthase). $^{\#}P > 0.05$ (two-tailed Student's *t*-test). qRT–PCR analyses were conducted as previously described[49]. **c**, COs (10 passages) demonstrate ALP activity. Scale bars, 100 μm. ALP assays were conducted as previously described[5]. **d**, GGT activity of COs (20 passages) measured in absorbance units (a.u.); $n = 3$; MEFs (mouse embryonic feeders) were used as a negative control. Error bars, s.d.; individual data points are demonstrated; $^{**}P < 0.0001$, two-tailed Student's *t*-test. GGT activity was assessed using a commercially available kit (MaxDiscovery gamma-Glutamyl Transferase (GGT) Enzymatic Assay Kit) according to the manufacturer's instructions and as previously described[5]. **e**, Flow cytometric analyses performed on COs after long-term culture (20 passages), demonstrating >99% $CK7^{+}/CK19^{+}$ expression (gating strategy demonstrated in Supplementary Fig. 6). APC, allophycocyanin; FITC, fluorescein isothiocyanate.

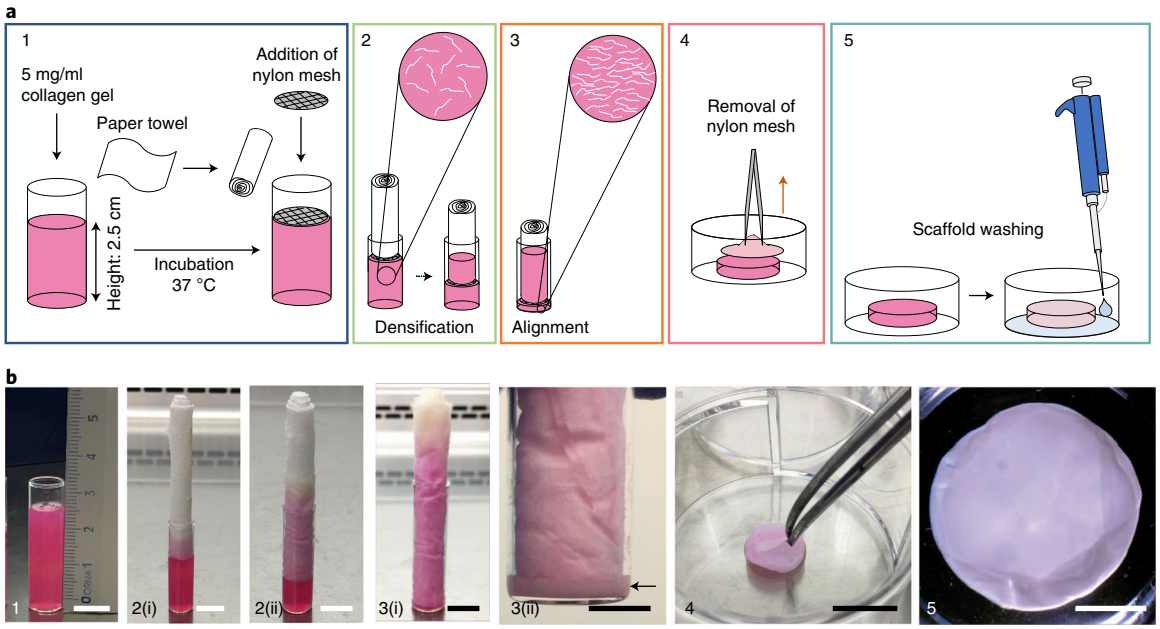

Fig. 7 | Generation of densified collagen sheets. a, Schematic representation of key stages of the procedure for generating densified collagen sheets (Step 39A). **b**, Representative images of key stages of the collagen densification process. Numbers correspond to schematic stages in **a**. 1: Specimen tube containing 5% collagen gel before densification (25-mm height). 2 and 3(i): Representative gel height following water absorption for 0 (2(i)), 30 (2(ii)) and 60 (3(i)) min. 3(ii): Specimen tube containing fully densified collagen scaffold (indicated by the black arrow). 4: Removal of nylon mesh. 5: Representative image of the resulting densified collagen sheet. Scale bars, 1 cm (1–4) or 5 mm (5).

penetration, provided there is good interconnectivity between pores. However, constructs with larger pores are weaker, and seeding with large clumps is required to ensure that the cells do not 'fall through' the spaces between fibers. Furthermore, preparation of the scaffolds for seeding includes treatment with ethanol (EtOH) and concentrated sodium hydroxide (NaOH). It is critical that, at the point of seeding, the scaffold be completely free of EtOH or NaOH remnants, which could result in cell death and poor attachment.

For collagen scaffolds, the quality of collagen plays a key role in the attachment and growth of cells. As collagen solutions are not 100% pure, we recommend testing of each new collagen batch for cell attachment, proliferation, expression of biliary markers and function.

For the generation of tubular densified collagen scaffolds, assistance of an experienced engineer and access to engineering facilities, including a 3D printer, are essential. Furthermore, transplantation of bioengineered ducts into small animal models requires substantial skill because of the construct size, and the procedure must be performed by an experienced surgeon.

Appropriate controls

Freshly isolated primary biliary tissue should be used as a positive control for the expression of biliary markers. For histology or IF analyses, whole tissue can be frozen in optimal cutting temperature compound (OCT) or fixed in 10% (vol/vol) formalin and embedded in paraffin for sectioning. Cells can be isolated as described in Steps 2A and 2D and dissociated to a single-cell suspension for flow cytometry or resuspended in RNA lysis buffer for RNA extraction and qPCR, as described in Step 41C. Alternatively, RNA can be extracted from snap-frozen tissue. Although primary tissue represents the ideal control for CO function and marker expression, it is also possible to compare COs with established cholangiocyte cell lines if access to primary tissue is not possible.

Starting population considerations

We have demonstrated that our protocol for CO derivation is reproducible with >70 CO lines (Supplementary Table 1). In addition, CO lines can be generated from very low numbers (<20,000) of viable primary cells (Supplementary Fig. 5). CO lines can be maintained in culture for >20 passages or 6 months. COs represent primary cells rather than immortalized cell lines; therefore it is possible that a reduction in the growth potential or function of the line will be observed after this time. The 'incubator life' of each line varies, and therefore the expansion potential, expression of

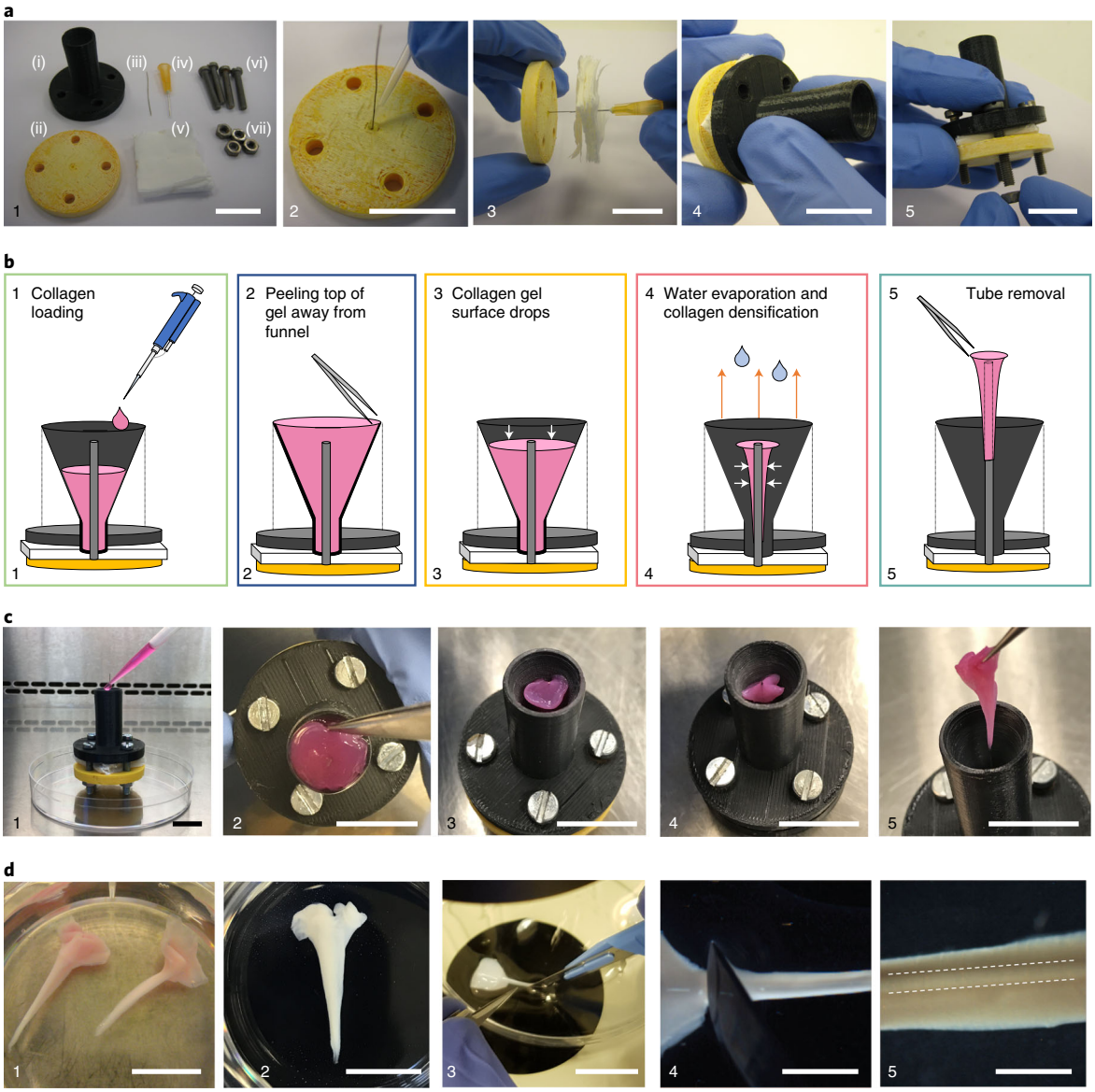

Fig. 8 | Generation of densified collagen tubes. a, Representative images of densification chamber assembly (Equipment setup). 1: Densification chamber components: (i) funnel, (ii) base, (iii) wire, (iv) 23-gauge needle, (v) paper towels, (vi) M4 screws and (vii) nuts. 2: Mounting of the rigid metal wire on the chamber base. 3: Addition of paper towels. 4: Addition of funnel. 5: Chamber assembly. Scale bars: 20 mm. **b**, Schematic representation of stages of collagen tube densification (Step 39B(i–ix)). **c**, Representative images of stages of tube densification. Numbers correspond to schematic stages in **b**. 1: Addition of collagen precursor solution. 2: Peeling of collagen from funnel walls. 3: Gel optimally positioned for evaporation. 4: Completion of densification. 5: Removal of densified tube from wire. Scale bars, 15 mm. **d**, Tube trimming following densification (Step 39B(x–xv)). 1: Collagen tubes immediately after densification. 2: Washed tube. 3, 4: Tube trimming. 5: Trimmed tube with patent lumen (white dashed lines). Scale bars: 2 cm (1–3), 2 mm (4) or 1 mm (5).

biliary markers and function should be regularly tested after passage 20 to periodically validate the quality of the line.

For the generation of bioengineered tissue, some variability in cell attachment and expansion potential following seeding and after transplantation is expected. Therefore, minor optimization may be required for certain CO lines, as described in the following sections.

Materials

Biological materials

- Human bile duct (minimum 1-cm length), gall bladder (minimum 1-cm^2 area) or liver tissue samples (minimum 5-mm^3 whole-liver piece or two core needle biopsies, if following Step 2C, or minimum

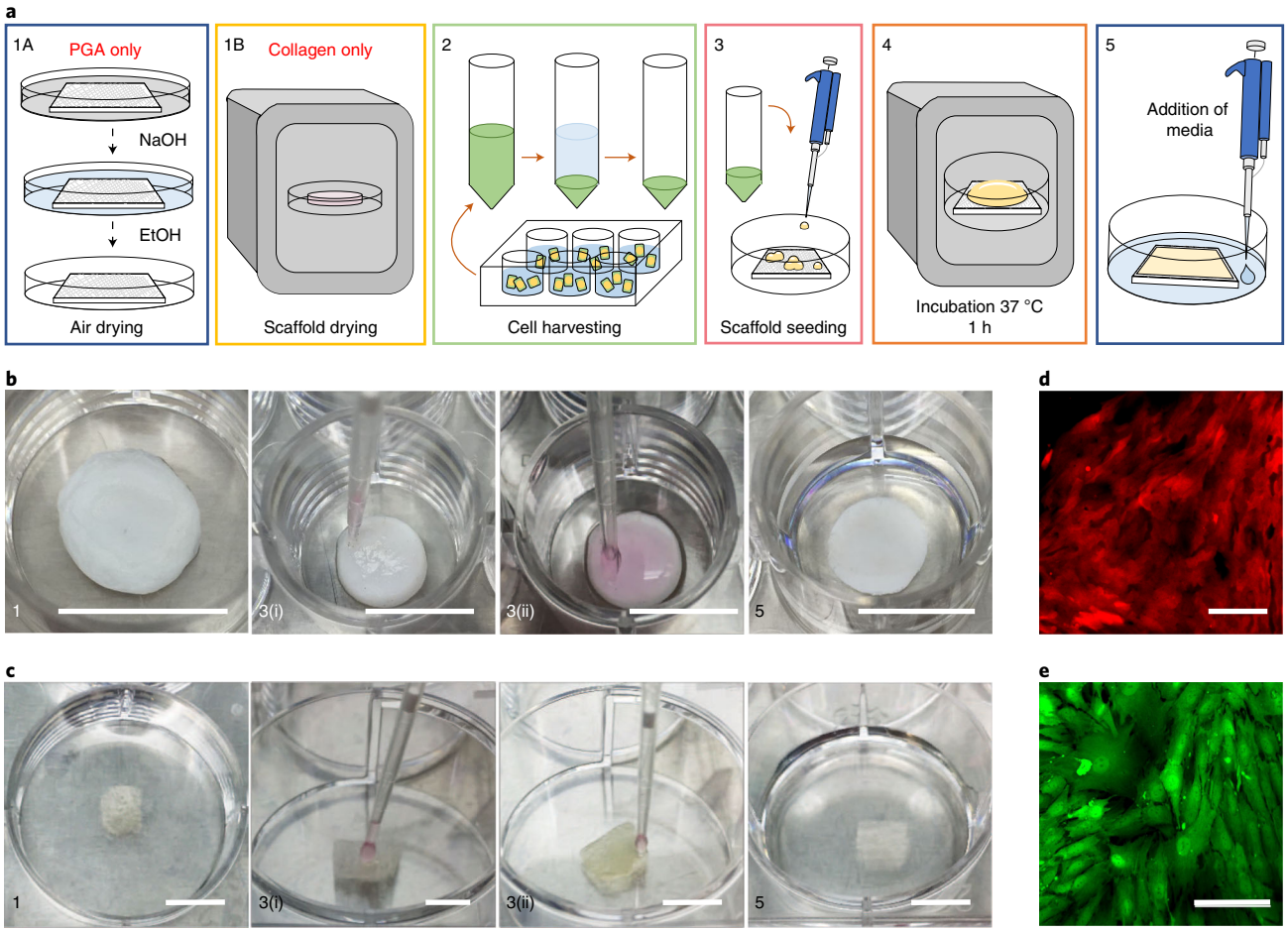

Fig. 9 | Seeding of flat densified collagen or PGA scaffolds. a, Schematic representation of the stages of the procedure for seeding densified collagen sheets and PGA scaffolds (Steps 40A and 40C, respectively). **b**,**c**, Representative images of key stages of the seeding procedure for densified collagen (**b**) and flat PGA (**c**) scaffolds. Numbers correspond to schematic stages in **a**. 1: Dried scaffold before seeding. 3(i): Addition of cell suspension on the scaffold at the start of seeding process. William's E+ medium with phenol red used for illustrative purposes. The use of phenol red in the medium is optional. 3(ii): Scaffold after completion of seeding and before incubation. 5: Seeded scaffold following medium addition. Scale bars, 1 cm. **d**, Representative fluorescent image of a flat densified collagen scaffold confluently seeded with RFP^+ COs (4 weeks after seeding). Scale bar, 100 μm. **e**, Representative fluorescent image of a PGA scaffold confluently seeded with GFP^+ COs (4 weeks after seeding). Scale bar, 50 μm.

$2 \times 1\text{-cm}^2$ whole-liver pieces, if following Step 2D) or cholangiocytes from ERCP brushings. **! CAUTION** All human tissue samples must be collected with the appropriate ethical approval in place and with full informed consent. Donors should be tested to exclude use of HIV-, hepatitis B– or hepatitis C–infected material. Informed consent was obtained for the use of all human tissues used in our experiments. Approval for our experiments was obtained from the NRES Committee East of England, Cambridge South (REC reference 15/EE/0152).

Reagents

- William's E basal medium, no phenol red (Invitrogen, cat. no. A12176-01)
- Nicotinamide (Sigma Life Science, cat. no. N0636-100G)
- Sodium bicarbonate (Sigma Life Science, cat. no. S6014-500G)
- Sodium pyruvate (Invitrogen, cat. no. 11360-070)
- D-Glucose (Gibco, cat. no. 15023-021)
- HEPES (Sigma, cat. no. H0887-20ml)
- ITS+ Universal Cell Culture Premix (20 ml; SLS, cat. no. 354352)
- Dexamethasone (R&D Systems, cat. no. 1126/100)
- L-Glutamine (Life Technologies, cat. no. 25030)
- Penicillin–streptomycin (pen–strep; Life Technologies, cat. no. 15140122)

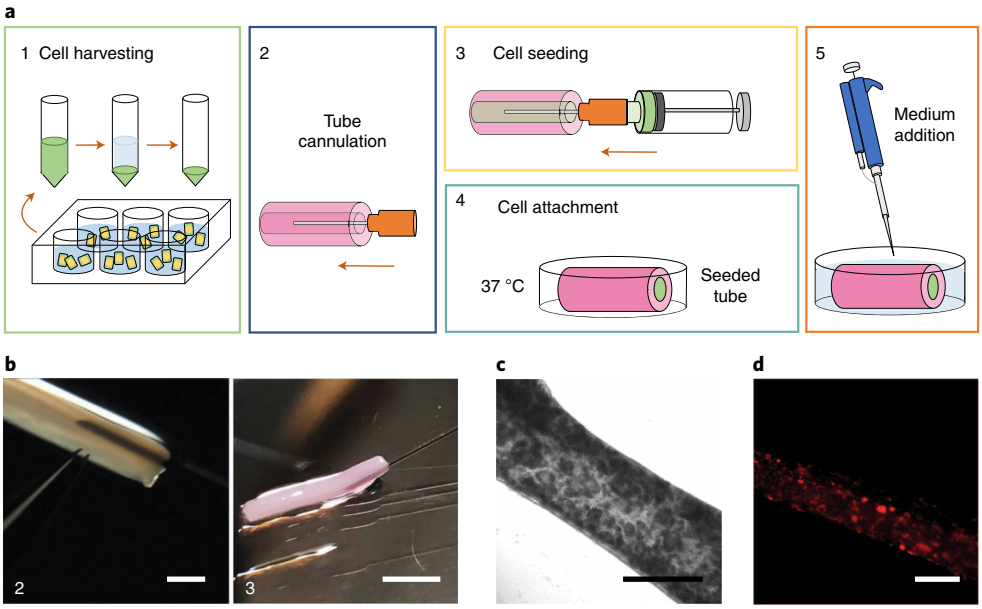

Fig. 10 | Seeding of densified collagen tubular scaffolds. a, Schematic representation of stages of densified collagen tube seeding (Step 40B). **b**, Representative images of the seeding process. Image numbers refer to the corresponding stages illustrated in the schematic in **a**. 2: Cannulation of tube lumen with 34-gauge needle. 3: Seeding of tube lumen with COs. Note the change in the tube color as the lumen fills with phenol red–containing medium. Scale bars: 1 mm (2) or 5 mm (3). **c**, Representative bright-field image of a CO-seeded densified collagen tube (4 weeks after seeding). Scale bar, 200 µm. **d**, Representative fluorescent image of a densified collagen tube (4 weeks after seeding) seeded with RFP^+ COs. Scale bar, 200 µm.

- L-Phospho-ascorbic acid (Sigma Life Sciences, cat. no. 49752-10G)
- Matrigel (BD Biosciences, cat. no. 356237)
- Cell recovery solution (SLS, cat. no. 354253)
- CellBanker 2 (Amsbio, cat. no. 11891)
- Recombinant human epidermal growth factor (EGF; R&D Systems, cat. no. 236-EG)
- Recombinant human DKK-1 protein (R&D Systems, cat. no. 5439-DK-01M/CF)
- Recombinant Human R-spondin-1 (R&D Systems, cat. no. 4645-RS)
- Recombinant Human HGF (PeproTech, cat. no. 100-39)
- Recombinant human forskolin (FSK; Sigma-Aldrich, cat. no. F6886-10MG)
- Y27632 (Stratech Scientific, cat. no. S1049-SEL)
- Liberase DL, research grade (Sigma-Aldrich, cat. no. 5466202001)
- Deoxyribonuclease I (DNase I) from bovine pancreas (Sigma-Aldrich, cat. no. D5025-150KU)
- University of Wisconsin (UW) cold storage solution (Bridge to Life (Europe) Ltd., cat. no. BTLBUW-1000)
- Dulbecco's PBS (PBS; Life Technologies, cat. no. 14190)
- Red blood cell lysis solution (10×; MACS Miltenyi Biotech, cat. no. 130-094-183)
- BSA (Sigma Life Sciences, cat. no. A3059)
- Polyglycolic acid BIOFELT scaffold (1-mm thickness, 50-mg/cm^3 PGA density; Biomedical Structures, custom order)
- CD326 (EpCAM) MicroBeads (human; MACS Miltenyi Biotech, cat. no. 130-061-101)
- FcR blocking reagent (MACS Miltenyi Biotech, cat. no. 130-059-90)
- MACS BSA stock solution (MACS Miltenyi Biotech, cat. no. 130-091-376)
- AutoMACS rinsing solution (MACS Miltenyi Biotech, cat. no. 130-091-222)
- AutoMACS running buffer (MACS Miltenyi Biotech, cat. no. 130-091-221)
- AutoMACS pro washing solution (MACS Miltenyi Biotech, cat. no. 130-092-987)
- Collagen I, high-concentration rat-tail collagen solution (100 mg; Scientific Laboratory Supplies, cat. no. 354249)
- Medium 199 (10×; Sigma-Aldrich, cat. no. M0650)
- Sodium hydroxide (NaOH, 1 M; Sigma-Aldrich, cat. no. 2770) **! CAUTION** NaOH can cause inflammation, irritation or corrosion upon contact with skin or eyes, or when ingested or inhaled. Wear appropriate safety equipment while handling it.

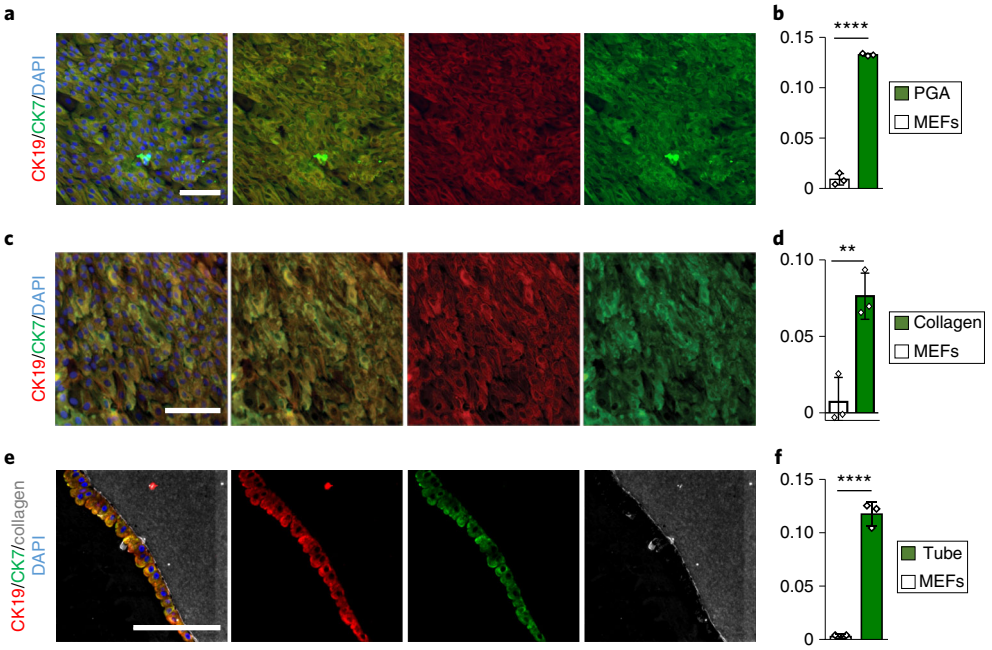

Fig. 11 | Characterization of bioengineered biliary tissue. a, Immunofluorescence images demonstrating expression of key biliary markers in CO-seeded PGA scaffolds (6 weeks after seeding). Scale bar, 100 μm. **b**, CO-seeded PGA scaffolds demonstrate GGT activity (4 weeks after seeding). $n = 3$; MEFs used as a negative control. Error bars, s.d.; individual data points are shown; $^{****}P < 0.0001$, two-tailed Student's *t*-test. **c**, Immunofluorescence images showing expression of key biliary markers in CO-seeded densified collagen sheets (4 weeks after seeding). Scale bar, 100 μm. **d**, CO-seeded collagen scaffolds demonstrate GGT activity (4 weeks after seeding). $n = 3$; MEFs used as a negative control. Error bars, s.d.; individual data points are shown; $^{**}P = 0.0055$, two-tailed Student's *t*-test. **e**, Immunofluorescence images showing expression of key biliary markers in CO-seeded densified collagen tubes (6 weeks after seeding). Scale bar, 100 μm. **f**, CO-seeded collagen tubes demonstrate GGT activity (4 weeks after seeding). $n = 3$; MEFs used as a negative control. Error bars, s.d.; individual data points are shown; $^{****}P = 0.0001$, two-tailed Student's *t*-test. GGT activity was assessed using a commercially available kit (MaxDiscovery gamma-Glutamyl Transferase (GGT) Enzymatic Assay Kit) according to the manufacturer's instructions. a.u., absorbance units; MEFs, mouse embryonic feeders.

- Deionized (DI) water (Evoqua Water Technologies, cat. no. 2111-TR)
- Water for embryo transfer (Sigma, cat. no. W1503)
- Trigene (Distel disinfectant concentrate; Starlab, cat. no. TM309-C)
- Absolute ethanol (EtOH; Fisher Scientific, cat. no. 10041814)
- Trypan blue solution (Thermo Fisher Scientific, cat. no. 15250061) **! CAUTION** Trypan blue is a potential carcinogen and can potentially cause damage to fertility.
- Donkey serum (AbD Serotec, cat. no. c06sb)
- Triton X-100 solution (Sigma, cat. no. X100-500ML)
- Paraformaldehyde (16% (wt/vol) PFA; Alfa Aesar, cat. no. 30525-89-4) **! CAUTION** PFA contains formaldehyde, which is carcinogenic. Paraformaldehyde can cause tissue damage upon inhalation, ingestion, or contact with the skin; it should be handled using appropriate safety measures.
- Cytokeratin 7 antibody (Abcam, cat. no. ab68459; Supplementary Table 1)
- Cytokeratin 19 antibody (Abcam, cat. no. ab7754; Supplementary Table 1)
- Goat anti-human Sox9 (R&D Systems, cat. no. AF3075; Supplementary Table 1)
- Rabbit anti-human albumin (Abcam, cat. no. ab137885; Supplementary Table 1)
- Mouse anti-human GGT-1 (Abcam, cat. no. ab55138; Supplementary Table 1)
- Donkey anti-mouse Alexa Fluor 488 (Life Technologies, cat. no. A2102; Supplementary Table 1)
- Donkey anti-rabbit Alexa Fluor 568 (Life Technologies, cat. no. A10042; Supplementary Table 1)
- Donkey anti-goat Alexa Fluor 488 (Life Technologies, cat. no. A21447; Supplementary Table 1)
- GenElute Mammalian Total RNA Miniprep Kit (Sigma-Aldrich, cat. no. RTN70-1KT)
- MaxDiscovery gamma-Glutamyl Transferase (GGT) Enzymatic Assay Kit (Newmarket Scientific, cat. no. 5601-01)
- Polylactic acid filament (PLA; RS Components, cat. no. 8320214)

- Hoechst 33258 (Sigma-Aldrich, cat. no. B2883)
- Dimethyl sulfoxide (DMSO; Sigma-Aldrich, cat. no. D8418)
- Superglue (Everbuild, cat. no. 78871)
- Red cell lysis buffer (Sigma-Aldrich, cat. no. 11814389001)
- RNA lysis buffer (Sigma-Aldrich, cat. no. L8285)
- Accutase (Thermo Fisher Scientific, cat. no. A1110501)

Equipment

- Plate heater (TAP Biosystems, cat. no. 016-0R10)
- Inverted microscope (Olympus, cat. no. CKX41)
- Tissue culture (TC)-treated culture dish (100 mm; Corning, cat. no. 430167)
- Costar 24-well, clear, TC-treated multiple-well plates (Corning, cat. no. 3526)
- Surgical scalpel blade (no. 22, sterile; Swann Morton, cat. no. 0508)
- Dumont no. 5 fine forceps (FST, cat. no. 11254-20)
- Centrifuge tubes (15 and 50 ml; Corning, cat. nos. 430791 and 430291)
- Vacuum filter/storage bottle system (500 ml; 0.22-μm pore; Corning, cat. no. 431097)
- CO_2 incubator (37 °C, 5% CO_2; Sanyo, cat. no. MCO-18AC)
- Centrifuge (Eppendorf, cat. no. 5804)
- Orbital shaking incubator (New Brunswick Scientific, cat. no. M1299-0082)
- Disposable serological pipettes (5, 10 and 25 ml; Corning, cat. nos. 4487, 4488 and 4489)
- Graduated filter tips (1,000, 200, 20 and 10 μl; Starlab, cat. nos. S1122-1830, S1120-8810, S1120-1810 and S1120-3810)
- Cryotube vials (2 ml; Thermo Scientific, cat. no. 368632)
- AutoMACS Pro Separator (MACS Miltenyi Biotech, cat. no. 130-092-545)
- Cell strainers (40 μm; Corning, cat. no. 352340)
- Countess II automated cell counter (Thermo Fisher Scientific, cat. no. AMQAX1000)
- Countess cell counting chamber slides (Thermo Fisher Scientific, cat. no. C10283)
- Insulin syringes (1 ml; VWR, cat. no. 613-4892)
- Syringes (20 ml; Fisher Scientific, cat. no. 15829152)
- Needles (18 and 23 gauge; Camlab, cat. nos. 305180 and 300700)
- Stainless steel fine tweezers (Onecall, cat. no. 1779183)
- Dissecting scissors (straight; Fisher Scientific, cat. no. 15207266)
- Precision wipes (Kimtech; Fisher Scientific, cat. no. 12660543)
- Self-seal sterilization pouches (Fisher Scientific, cat. no. 15428782)
- Syringe filters (0.2 μm; Fisher Scientific, cat. no. 10268401)
- Six-well plates (Fisher Scientific, cat. no. 10396482)
- Autoclave tape (Greiner Bio-One, cat. no. TAP02)
- Micro-spatula (21-mm length; VWR, cat. no. 231-0446)
- Specimen tubes (flat bottom, 10 mm; Samco, cat. no. G05017)
- Nylon membrane (10-μm pore size, hydrophilic; Millipore, cat. no. NY1002500)
- Syringe (25 μl; model no. 1702; Hamilton, cat. no. 80265)
- Small-hub removable needle (34-gauge; Hamilton, cat. no. 207434) ▲ **CRITICAL** Although the exact make and model of syringe and removable needle can vary according to the researcher's preference, it is essential that small-volume syringes and removable needles with no dead space be used for seeding the tubular scaffolds (Step 40B), because of the very small (25-μl) volumes needed for seeding.
- Funnel (3D-printed in-house)
- Metallic wire (Alfa Aesar, cat. no. 010408.G6)
- Base (3D-printed in-house)
- M4 screws and nuts (4×; RS Components, cat. no. 8199004)
- Screwdriver (RS Components, cat. no. 459-3972)
- Class II biological safety cabinet (Esco Airstream Class II, model no. AC2-6S1)
- Falcon tube (15 ml; Appleton Woods, cat. no. BF031)
- Cryovial (Elkay Laboratory Products, cat. no. 127-T311-200)
- Parafilm (Fisher Scientific, cat. no. 11762644)
- Confocal microscope (Zeiss, model no. LSM 700)
- 3D printer (RS PRO IdeaWerk Pro; RS Components, cat. no. 8625705)
- Hemocytometer or an automated cell counter (Fisher Scientific, cat. no. 13444890)

Software

- FlowJo v.10.4.2 (https://www.flowjo.com/)
- Computer-aided design (CAD) package (Autodesk Inventor; https://www.autodesk.com/products/inventor/overview)
- 3D printer software (Doraware; https://www.dysoncentre.eng.cam.ac.uk/DoraWare)
- ImageJ v1.51h software (Wayne Rasband, NIHR; http://Imagej.nih.gov/ij)

Reagent setup

Human biliary and liver tissue

Primary tissue can be obtained from surgically excised gallbladder or bile duct tissue, ERCP brushings or liver biopsies. Once collected, tissue should be stored immediately at 4 °C in William's E+ medium with 50 ng/ml of EGF and 10 μM Y27632 or in UW cold storage solution. **! CAUTION** Leaving primary tissue in cold storage in either William's E+ or UW for longer than 8 h before processing will negatively affect the viability of the isolated cells.

Nicotinamide 0.4 M stock solution

Dissolve 24.4 g of nicotinamide powder in 500 ml of embryo transfer water. **▲ CRITICAL** Sterilize the nicotinamide stock solution using a vacuum filter/storage bottle system. Mix it well before filtration. Store the solution at 4 °C for up to 3 months.

Sodium bicarbonate 1 M stock solution

Dissolve 42 g of sodium bicarbonate powder in 500 ml of embryo transfer water. **▲ CRITICAL** Sterilize the sodium bicarbonate stock solution using a vacuum filter/storage bottle system. Mix it well before filtration. Store the solution at 4 °C for up to 3 months.

Ascorbic acid trisodium salt 100 mM stock solution

Dissolve 16.1 g of ascorbic acid trisodium salt powder in 500 ml of embryo transfer water. **▲ CRITICAL** Sterilize the ascorbic acid trisodium salt stock solution using a vacuum filter/storage bottle system. Mix the solution well before filtration. Store it at 4 °C for up to 3 months. Protect it from light.

D-Glucose 1 M stock solution

Dissolve 90.1 g of D-glucose powder in 500 ml of embryo transfer water. Warm the mixture to 50 °C to facilitate dissolution. **▲ CRITICAL** Sterilize the D-glucose stock solution using a vacuum filter/storage bottle system. Mix the solution well before filtration. Store it at 4 °C for up to 3 months.

Dexamethasone 10 mM stock solution

Dissolve 100 mg of dexamethasone in 25.4797 ml of DMSO. Prepare 50- to 100-μl aliquots. Store them at −80 °C for up to 12 months.

Supplemented William's E medium (William's E+ medium)

Mix 443 ml of William's E medium with 12.5 ml of nicotinamide stock solution, 8.5 ml of sodium bicarbonate stock solution, 1 ml of ascorbic acid trisodium salt stock solution, 7 ml of glucose stock solution, 3.15 ml of sodium pyruvate, 10 ml of HEPES solution, 5 ml of ITS+ premix, 5 μl of dexamethasone, 5.3 ml of glutamine and 5 ml of pen–strep. **▲ CRITICAL** Sterilize William's E+ medium using a vacuum filter/storage bottle system. Mix the medium well before filtration. Store it at 4 °C for up to 1 month. Warm it to 37 °C before use.

Sodium bicarbonate 7.5% (wt/vol) stock solution

Dissolve 3.75 g of sodium bicarbonate powder in 46.25 ml of DI water. **▲ CRITICAL** Sterilize the sodium bicarbonate stock solution using a 50-ml syringe and a 0.2-μm syringe filter. Mix it well before filtration. Store the solution at 4 °C for up to 3 months.

70% (vol/vol) EtOH

Mix 700 ml of absolute EtOH and 300 ml of DI water. This solution can be stored indefinitely.

Matrigel

10-ml Matrigel vials should be thawed slowly in a refrigerator at 4 °C overnight. Thawed Matrigel should be mixed well and then divided into 1-ml aliquots. Aliquots of Matrigel should always be made in a class II biological safety cabinet to avoid bacterial contamination. Matrigel should be kept constantly on ice to avoid solidification. All equipment coming into contact with Matrigel should be precooled to 4 °C. This includes pipette tips and media for diluting Matrigel. Tubes used for making aliquots should be kept on ice. Store Matrigel aliquots at −20 °C or −80 °C for up to 3 months. ▲ **CRITICAL** Each aliquot should undergo a maximum of two freeze–thaw cycles. This can be achieved by adjusting aliquot volumes accordingly.

3× supplemented William's E+ solution

Supplement William's E+ medium with 1.5 μg/ml R-spondin-1, 300 ng/ml DKK, 150 ng/ml EGF and 3 μM Y27632 (3× is the typical concentration for all supplementary cytokines). The supplemented medium should be prepared immediately before use and should not be stored.

Matrigel–supplemented William's E+ solution droplets

COs are cultured in 3D conditions, suspended in 50-μl droplets composed of a 66.7% (vol/vol) Matrigel and 33.3% (vol/vol) 3× supplemented William's E+ solution, which form a dome after plating (Fig. 4b, image 6(i)). Before plating, prepare a master mix with a volume corresponding to the number of droplets that will be plated (as described in Steps 3–10). Importantly, for generating this master mix, COs or primary cholangiocytes are first resuspended in the 3× supplemented William's E+ solution (Step 3) and Matrigel is subsequently added (Step 5). To calculate the volume of supplemented William's E+ solution needed for resuspension of the CO pellet, the following formula can be used:

$$\text{Volume of supplemented William's E+ medium} = [(\text{Number of CO wells}) \times 50\ \mu\text{l}]/3$$

The master mix must be kept at 4 °C and used immediately after preparation. ▲ **CRITICAL** As the volume of medium needed to resuspend the CO pellet will typically be very small, it is advisable to instead prepare a larger volume of 3× concentrated William's E+ solution. This can then be diluted to 1× and added to the wells after plating as their plating medium. This volume corresponds to 1/3 of the total number of wells to be plated (e.g., if plating 12 wells, prepare 4 ml of 3× William's E+ solution), assuming 1 ml of medium/well is used. A small aliquot of the resulting 3× solution can then be used to resuspend the pellet, and the remaining solution can be diluted to 1× with William's E+ medium devoid of additional cytokines and used as plating medium. For example, if plating 12 wells, resuspend the pellet in 200 μl of 3× supplemented William's E+ solution, taken from the initial 4 ml of 3× supplemented William's E+ solution. After CO plating (Steps 3–10), add 8 ml of non-supplemented William's E+ medium to the 4 ml of supplemented William's E+ solution to make a 1× supplemented William's E+ solution. ▲ **CRITICAL** This solution should be kept on ice for the duration of the Procedure to avoid Matrigel solidification.

Matrigel (66.7% (vol/vol)) solution

To obtain the volume of Matrigel needed when plating, multiply the volume of 3× supplemented William's E+ solution by 2. For example, if plating 12 wells, 200 μl of supplemented William's E+ solution should be added to the pellet, followed by 400 μl of Matrigel. ▲ **CRITICAL** The 3× supplemented William's E+ solution should be precooled to 4 °C. ▲ **CRITICAL** This solution should be kept on ice for the duration of the Procedure to avoid Matrigel solidification.

Liberase

Reconstitute the lyophilized Liberase enzyme with 10 ml of sterile embryo transfer water, per the manufacturer's instructions, to obtain a stock solution. ▲ **CRITICAL** Divide the reconstituted Liberase stock solution into 1-ml aliquots to avoid repeated freeze–thaw cycles and store at −15 °C to −25 °C for up to 6 months. Reconstitution and aliquot preparation should take place in a class II biological safety cabinet to avoid contamination.

DNase I

Reconstitute the lyophilized DNase I to a 4 mg/ml stock solution using sterile PBS. ▲ **CRITICAL** Divide the reconstituted DNase I stock solution into 100-μl aliquots to avoid repeated freeze–thaw cycles and

store at −80 °C for up to 6 months. Reconstitution and aliquot preparation should take place in a class II biological safety cabinet to avoid contamination.

1% (wt/vol) BSA in PBS

Weigh out 5 g of BSA powder and dissolve in 500 ml of PBS to obtain a 1% solution. ▲ CRITICAL Sterilize 1% (wt/vol) BSA in PBS solution using a vacuum filter/storage bottle system. Mix the solution well before filtration. Prepare aliquots in 50-ml centrifuge tubes and store at −20 °C to avoid contamination.

MACS buffer

Prepare a 1-in-20 dilution of MACS BSA stock solution in AutoMACS rinsing solution. ▲ CRITICAL MACS buffer should be freshly prepared at the point of use and should be kept at 4 °C. Buffer preparation should take place in a class II biological safety cabinet to avoid contamination.

0.1% (vol/vol) Triton X-100 solution

Add 50 µl of Triton X-100 to 50 ml of PBS in a 50-ml centrifuge tube. Gently shake the tube by inversion until the Triton X-100 is fully dissolved. This solution can be stored at room temperature (23 °C) for up to 3 months or at 4 °C for up to a year.

Equipment setup

Plate heater setup

Clean the plate heater with Trigene and 70% (vol/vol) EtOH and place it in a class II biological safety cabinet. Set the temperature to 37 °C and place a 24-well plate on the heating surface. ▲ CRITICAL Allow a minimum of 30 min for the plate to warm up before plating Matrigel with cells. If you are using multiple plates, these can be prewarmed in an incubator for a minimum of 30 min, with each plate placed on the plate heater immediately before plating.

AutoMACS Pro Separator setup

Run column exchange before use. Check that the columns are secured and that there are no leaks anywhere in the system. Check that there is sufficient running buffer, washing solution and 70% (vol/vol) EtOH and that the waste bottle is not too full. Run an additional 'Qrinse' before starting cell sorting. To save time, this can be done while the cells are incubating with the MACS beads. To shut down the machine after EpCAM sorting, select the 'Sleep' program. Turn off the machine once the 'Sleep' program has finished.

Fabrication and assembly of densification chamber for densified collagen tubes

The densification chamber, used to form the densified collagen tubes, requires fabrication and assembly ahead of the collagen gel preparation. This involves 3D printing of the base and funnel pieces, mounting a rigid metal wire in the base and fixing paper towels between the base and funnel as follows.

1 Design the chamber geometry using a CAD package (e.g., Autodesk Inventor). See Supplementary Software 1 and 2 for examples of designs we have used successfully.
2 Export the design as a .stl file and prepare the file for 3D printing using 3D printer software (e.g., Doraware).
3 3D-print the chamber model using polylactic acid filament and assemble the components shown in Fig. 8a, image 1.
4 Mount a straight rigid wire in the hole in the base piece of the chamber by gluing it into place with superglue (Fig. 8a, image 2). ▲ CRITICAL STEP Let the superglue cure before continuing (1 h).
5 Fold two sheets of absorbent precision wipes four times and, using scissors, cut to the size of the base plate. Autoclave these paper towels in an autoclave pouch. ▲ CRITICAL STEP Let the towels dry fully before continuing.
6 Sterilize the base plate and funnel piece by immersion in 70% (vol/vol) EtOH.
7 Place the 3D-printed components under a sterile class II biological safety cabinet until dry.
8 Autoclave 4× M4 screws and nuts.
9 Using a sterile 23-gauge needle, punch a hole through the center of the sheets and feed the mounted metallic wire through the needle (Fig. 8a, image 3).

10 Remove the 23-gauge needle and push the paper towels down.

11 Feed the metallic wire through the funnel piece (Fig. 8a, image 4) and fix the funnel piece to the base piece, using 4× M4 screws and nuts (Fig. 8a, image 5).

12 Tighten the screws, using a screwdriver. The chamber is now ready for the densification process. ▲ **CRITICAL STEP** The screws must be tight in order to prevent leakage of water into the towels before a collagen gel forms. ▲ **CRITICAL STEP** The top of the metallic wire must not extrude above the top of the funnel. This is a necessary condition for successful collagen densification for tube formation.

Procedure

Derivation of COs from primary human tissue ● Timing 1.5–10 h

1 Obtain primary tissue from surgically excised gallbladder or bile duct tissue, ERCP brushings or liver biopsies (Fig. 1b). Once collected, tissue should be stored immediately as described in the 'Reagent setup' section.

! CAUTION Dissection of tissue should take place in a class II biological safety cabinet under aseptic conditions.

■ **PAUSE POINT** Tissue can be kept in medium/cold storage solution for up to 8 h, although for optimal viability, tissue should be processed as soon as possible after collection. Guidance on the maximum length of storage before processing for each tissue type is shown in Supplementary Fig. 1.

2 For derivation of COs from excised bile ducts or gall bladders, see option A. For derivation of COs from ERCP brushings, see option B. For derivation of COs from liver tissue, see option C, and for derivation of COs from an $EpCAM^+$ single-cell suspension, see option D.

▲ **CRITICAL STEP** Following of Step 2D is recommended if a highly purified CO population is required in early passages, whereas following of Step 2C is advised in instances in which limited primary tissue is available (e.g., liver biopsies from live donors).

(A) **Derivation of ECOs from deceased organ donors ● Timing 1 h 20 min–1 h 50 min, including plating**

▲ **CRITICAL** All equipment used should be sterile and all work must be done under aseptic conditions in a class II biological safety cabinet.

(i) Transfer the tissue from the storage container to an empty 10-cm plate.

(ii) Using a scalpel and forceps, make a longitudinal incision along the length of the excised bile duct or from the fundus to the neck of the excised gallbladder (Fig. 2b, images 1A(ii) and 2) to expose the lumen. This step should result in a flat sheet of biliary tissue with the biliary epithelium on the luminal surface, usually pigmented yellow by bile, and an 'exterior' surface corresponding to the outer wall of the bile duct or gallbladder.

! CAUTION Ensure the luminal surface is facing upward to avoid the loss of cholangiocytes.

(iii) Wash the tissue by transferring it to a 50-ml centrifuge tube containing PBS to remove excess bile (Fig. 2b,c, image 2). Repeat twice, using a fresh tube each time.

▲ **CRITICAL STEP** PBS washes must be performed cautiously to prevent detachment of the biliary epithelial layer. This is particularly important if the bile duct or gallbladder tissue has been kept on ice for <2–4 h after surgical excision.

? TROUBLESHOOTING

(iv) Transfer the tissue to an empty plate.

(v) Add William's E+ medium to the plate until the tissue is fully submerged in the medium. It is not necessary to supplement the medium with additional cytokines.

! CAUTION The tissue must be submerged in the medium quickly to prevent it from drying.

(vi) Gently scrape the luminal surface of the tissue with a scalpel to release the cholangiocytes into the medium (Fig. 2b,c, image 3).

▲ **CRITICAL STEP** Examine the cell suspension under a microscope after scraping the tissue and before collecting the cells into a centrifuge tube to ensure the mechanical dissociation has been successful. The epithelial cells should be released from the tissue as small clumps and should display columnar morphology (Fig. 2b,c, image 9).

(vii) Collect the medium and cells into a 50-ml centrifuge tube using a 10-ml pipette.

(viii) Wash the tissue again by adding ~10 ml of fresh medium directly to the luminal surface of the tissue in the plate with a 10-ml pipette.

(ix) Repeat the process of scraping and washing until the entire epithelial layer is collected. By the end of this stage, the luminal side of the biliary tissue will appear smooth, losing the characteristic velvet-like appearance of the biliary epithelium (Fig. 2b,c, images 1A(iii) and 1B(iii)).
▲ CRITICAL STEP Scrape cautiously to avoid releasing fibrous tissue and debris into the cell suspension.
? TROUBLESHOOTING

(x) Centrifuge the cells at 444*g* for 4 min at room temperature.
? TROUBLESHOOTING

(xi) Aspirate the supernatant.

(xii) Resuspend the pellet in 10 ml of William's E+ medium (regardless of pellet size) to wash the cells. If there is bile or debris remaining in the suspension, repeat this wash step.
▲ CRITICAL STEP Remove large pieces of debris and fibrous tissue using a p1000 pipette, as these may not be easily removed by washing.
? TROUBLESHOOTING

(xiii) Centrifuge the cells at 444*g* for 4 min at room temperature.

(xiv) If you wish to lyse red cells to avoid erythrocyte contamination, resuspend the cells in 10 ml of ice-cold red cell lysis buffer and incubate the cell suspension on ice for up to 10 min.
▲ CRITICAL STEP If red blood cells can be seen in the pellet after washing, red cell lysis is recommended in order to obtain as pure a population of cholangiocytes as possible upon initial plating, to encourage rapid formation and proliferation of COs. However, this step can be omitted, if the yield of primary cholangiocytes is very low, to avoid cell loss during the incubation and washing steps.

(xv) If you have lysed red cells, wash twice in William's E+ medium as described in Step 2A(xii) before continuing with Step 2A(xvi).

(xvi) Aspirate the supernatant.

(xvii) Wash the pellet in William's E+ medium.

(xviii) Plate the cells as described in Steps 3–10.
▲ CRITICAL STEP Typical morphology for COs plated from gallbladder or bile duct tissue after 1 week and >20 weeks after plating is displayed in Fig. 2d, top and bottom, respectively. COs should begin to form ~3 d after plating, and debris should disappear from the CO culture after the first two passages.
? TROUBLESHOOTING

(B) **Derivation of ECOs from ERCP brushings** ● Timing **30 min**

(i) Prepare a 50-ml centrifuge tube of William's E+ medium with 50 ng/ml of EGF and 10 μM Y27632. Provide this tube to the clinicians before the start of the ERCP procedure.

(ii) Following brushing, wash the ERCP brush in the tube of medium to dislodge the collected cells (Fig. 3a, image 2).

(iii) Transport the centrifuge tube at 4 °C to a class II biological safety cabinet under aseptic conditions.

(iv) Centrifuge the 50-ml tube at 444*g* for 4 min at room temperature.

(v) Plate the resulting pellet of cells as described in the 'Plating of primary cholangiocytes in organoid format' section below (Steps 3–10).
▲ CRITICAL STEP Typical morphology of COs derived from ERCP brushings immediately after plating, 24 h after plating and 1 week after plating are displayed in Fig. 3b (image 5) and 3c (top and bottom), respectively. Organoids should begin to form within 24 h of plating, and debris should disappear from the organoid culture after the first two passages.
? TROUBLESHOOTING

(C) **Derivation of ICOs from liver tissue** ● Timing **30–45 min, including plating**

(i) Place a liver biopsy core into a well of a six-well tissue culture plate. Alternatively, place a small piece of liver tissue (~1 cm^3) on a sterile 10-cm tissue culture dish and cut into small pieces (~3–4 mm^3) before transferring to a well of a six-well plate for further dissection.

(ii) Using a scalpel, carefully dissect the tissue into pieces as small as possible, approximately <1 mm^3 (Fig. 4b, image 1A, and Fig. 4c, image 1B).
▲ CRITICAL STEP Care should be taken to ensure that the tissue is cut as small as possible so it can fit into a p1000 pipette tip (Fig. 4b,c, image 2). Tissue dissection should be done as quickly as possible to prevent the tissue from drying out.

(iii) Add 1 ml of William's E+ medium with 50 ng/ml EGF and 10 μM (1 μl/ml) Y27632 to the dissected liver tissue.
(iv) Transfer the dissected tissue and media to a 15-ml centrifuge tube, using a p1000 pipette (Fig. 4b,c, image 3), and centrifuge at 300*g* for 2 min at room temperature (Fig. 4b,c, image 4).
(v) Carefully aspirate the supernatant.
(vi) Wash the pellet in William's E+ medium.
(vii) Centrifuge at 300*g* for 2 min at room temperature.
(viii) Plate the dissected tissue pieces, following the instructions in the 'Plating of primary cholangiocytes in organoid format' section below (Steps 3–10) (Fig. 4b,c, image 6(i)).
▲ **CRITICAL STEP** Typical morphology for COs plated from diced liver tissue <1 week after plating and >20 weeks after plating is displayed in Fig. 4d, left and right, respectively.
? TROUBLESHOOTING

(D) **Derivation of ICOs through EpCAM MACS sorting** ● **Timing 2–3 h**
▲ **CRITICAL** The Liberase and DNase I solutions should be prewarmed to 37 °C before starting the isolation process.
(i) Place a liver biopsy core into a well of a six-well tissue culture plate. Alternatively, place a small piece of liver tissue (~1 cm^3) on a sterile 10-cm tissue culture dish and cut it into small pieces (~3–4 mm^3) before transferring them to a well of a six-well plate for further dissection.
(ii) Using a sterile scalpel, dissect the tissue into very small pieces (<1 mm^3; Fig. 4b,c, image 2).
(iii) Add 1.5 ml of prewarmed Liberase digestion solution (0.5 U) with 4 mg/ml DNase I (Supplementary Fig. 2b, image 3).
▲ **CRITICAL STEP** DNase I must be added during the dissociation to prevent the cells from forming clumps.
(iv) Place the plate on a heated orbital shaker at 170 r.p.m. and 37 °C for 30 min. Ensure that the plate is secured to the orbital shaker.
(v) Every 10 min, remove the tube from the rocker and gently pipette up and down with a p1000 pipette.
▲ **CRITICAL STEP** Examine the cells under a microscope at these 10-min intervals to check the progress of the dissociation. The dissociation will be finished once all the tissue has been dissociated to a single-cell suspension, with only the collagen scaffold of the tissue remaining (Supplementary Fig. 2b, image 4).
? TROUBLESHOOTING
(vi) After 30 min, or when a single-cell suspension has been obtained, stop the reaction by adding an equivalent volume of cold 1% (wt/vol) BSA in PBS.
(vii) Filter the mixture through a 40-μm filter into a 15-ml centrifuge tube.
▲ **CRITICAL STEP** Filter gently and do not force any material through the filter, as this will reduce viability and result in fibrous material in the final cell suspension.
? TROUBLESHOOTING
(viii) Centrifuge at 444*g* for 4 min at room temperature.
(ix) Aspirate the supernatant, using a p1000 pipette.
(x) Resuspend the pellet in 10 ml of red cell lysis buffer with 4 mg/ml DNase I and 10 μM Y27632.
▲ **CRITICAL STEP** From this stage onward, aspiration of the supernatant should not be done using a vacuum pump aspirator, as this presents a risk of losing the pellet.
(xi) Incubate the cells on ice in red cell lysis buffer for up to 10 min.
(xii) Add an equivalent volume of 1% (wt/vol) BSA in PBS to the red cell lysis buffer and centrifuge at 444*g* for 4 min at room temperature.
(xiii) Aspirate the supernatant, using a p1000 pipette, and resuspend in 1 ml of cold 1% (wt/vol) BSA in PBS with 4 mg/ml DNase I and 10 μM Y27632.
(xiv) Repeat this wash step one more time to ensure the complete removal of the red cell lysis buffer, and resuspend the pellet once more in 1 ml of cold 1% (wt/vol) BSA in PBS with 4 mg/ml DNase I and 10 μM Y27632.
(xv) Take a 10-μl aliquot of the cell suspension and mix it with an equivalent volume of trypan blue. Count the cells using a hemocytometer or an automated cell counter.
? TROUBLESHOOTING

(xvi) Centrifuge the pellet at 444*g* for 4 min at room temperature.

(xvii) Resuspend the pellet in the appropriate volume of MACS buffer, FcR blocking reagent and CD326 (EpCAM) MicroBeads according to the manufacturer's instructions.

▲ **CRITICAL STEP** Use the cell count obtained in Step 2D(xv) to determine the appropriate volume of each reagent to add for the number of cells according to the manufacturer's instructions (300 µl MACS buffer, 100 µl FcR blocking reagent and 100 µl CD326 (EpCAM) MicroBeads for every 5×10^7 total cells).

(xviii) Incubate the cells for 30 min at 4 °C.

(xix) While the cells are incubating, prepare the AutoMACS Pro Separator for cell sorting. See 'AutoMACS Pro Separator setup' in the 'Equipment setup' section for instructions.

(xx) Wash the cells with 5 ml of 1% (wt/vol) BSA in PBS.

(xxi) Centrifuge at 300*g* for 10 min at room temperature.

(xxii) Aspirate the supernatant and resuspend in 5 ml of 1% (wt/vol) BSA in PBS with 4 mg/ml DNase I and 10 µM Y27632.

(xxiii) Filter the sample through a 40-µm filter immediately before sorting (Supplementary Fig. 2b, image 6)

(xxiv) Run the sample through the AutoMACS Pro Separator on a 'POSSELD' program. This will select for the $EpCAM^+$ fraction. Collect the $EpCAM^+$ fraction in a 15-ml centrifuge tube.

▲ **CRITICAL STEP** Ensure this takes place under aseptic conditions; the AutoMACS Pro Separator should be in a class II biological safety cabinet, and all buffers and running solutions should be kept sterile.

▲ **CRITICAL STEP** The MACS centrifuge tube rack should be precooled in the refrigerator for at least an hour before use.

? TROUBLESHOOTING

(xxv) Top up the 15-ml centrifuge tube with 1% (wt/vol) BSA in PBS.

(xxvi) Centrifuge at 444*g* for 4 min at room temperature.

(xxvii) Plate the cell suspension, following the instructions in the 'Plating of primary cholangiocytes in organoid format' section (Steps 3–10) below.

▲ **CRITICAL STEP** Typical morphology for COs plated from $EpCAM^+$ liver tissue <1 week after plating is displayed in Supplementary Fig. 2c. Organoids will grow from single cells over the course of 5–15 d after plating. After the first passage, $EpCAM^+$ organoids will display typical CO morphology, as demonstrated in Supplementary Fig. 4a, image 5.

? TROUBLESHOOTING

Plating of primary cholangiocytes in organoid format ● Timing 10–40 min

▲ **CRITICAL** Preheat an adequate number of 24-well tissue culture plates at 37 °C for at least 1 h before use (preheating overnight is preferable).

▲ **CRITICAL** Thaw Matrigel on ice for 2 h to overnight before starting the isolation procedure. Matrigel will solidify at room temperature and so should always be kept on ice when in use. It is important to work quickly to prevent the Matrigel solidifying during the plating procedure.

▲ **CRITICAL** COs should be plated in 3D Matrigel domes composed of a 2:1 ratio (33.3% to 66.7% (vol/vol) solution) of Matrigel and William's E+ medium. The CO pellet must first be resuspended in 3× supplemented William's E+ solution before the separate addition of Matrigel. See '3× supplemented William's E+ solution' in the 'Reagent setup' section for instructions on how to calculate the volumes of 3× William's E+ and Matrigel required to prepare this solution.

3 Resuspend the CO pellet in a volume of the 3× supplemented William's E+ solution appropriate for the number of wells being plated. For example, if plating nine wells, resuspend in 150 µl of William's E+ medium with 1.5 µg/ml R-spondin, 150 ng/ml EGF, 30 µM (3 µl/ml) Y27632 and 300 ng/ml DKK-1.

▲ **CRITICAL STEP** Y27632 should always be freshly added at this stage and kept in the culture medium for 48 h to ensure maximal survival of the cholangiocyte cells.

4 Mix the Matrigel stock thoroughly with a p1000 pipette.

▲ **CRITICAL STEP** Matrigel should be kept on ice throughout the entire procedure and must be mixed with care to avoid bubbles.

5 Add Matrigel to the cell suspension in a 2:1 ratio (66.7% (vol/vol)) and mix well. See 'Matrigel (66.7% (vol/vol)) solution' in the 'Reagent setup' section for instructions on how to calculate the amount of Matrigel required.

6 Use a p1000 pipette to plate the organoids in 50-µl Matrigel–medium domes, each in a well of a 24-well plate. To plate the dome, hold the tip of the p1000 pipette very close to the surface of the well, in the center, and slowly start pipetting. Move the pipette upward as the droplet forms.
▲ CRITICAL STEP Do not go down to the second stop of the pipette, as this will form bubbles in the Matrigel dome.
▲ CRITICAL STEP Mix thoroughly before plating each dome.
? TROUBLESHOOTING

7 Allow the Matrigel to solidify for 1–2 min in the plate heater. Gently tilt the plate to test that the Matrigel has solidified.

8 Invert the plate and keep it in the 37 °C incubator for 30 min. This step should be omitted when plating dissected liver tissue (Step 2C) or $EpCAM^+$ single cells (Step 2D).
▲ CRITICAL STEP Without the plate inversion step, cell clumps are likely to migrate to the bottom of the well and attach to the plate. If this happens, the cells will not be able to form organoids.
? TROUBLESHOOTING

9 Make up the 3× William's E+ medium solution to a final concentration of 500 ng/ml R-spondin, 50 ng/ml EGF, 10 µM (1 µl/ml) Y27632 and 100 ng/ml DKK-1 (±50 ng/ml HGF) by following the formula below:

$$\text{Final volume of medium} = \text{Initial volume of medium prepared in Step 5} + [\text{Initial volume of medium prepared in Step 5} \times 2]$$

For example, if 1 ml of medium was initially prepared with 1.5 µg/ml R-spondin, 150 ng/ml EGF, 30 µM (3 µl/ml) Y27632 and 300 ng/ml DKK-1 (±50 ng/ml HGF and 6 µM FSK), add a further 2 ml of William's E+ medium without cytokines, for a total of 3 ml of medium with 500 ng/ml R-spondin, 50 ng/ml EGF, 10 µM (1 µl/ml) Y27632 and 100 ng/ml DKK-1 (±50 ng/ml HGF and 2 µM FSK).

10 Add 1 ml of this supplemented medium per organoid well, using a 5- or 10-ml pipette. Place the cell cultures in the cell culture incubator.
▲ CRITICAL STEP Add the medium slowly to the side of each well to avoid disrupting the Matrigel domes.
▲ CRITICAL STEP When plating from primary cells, organoids from the CBD and gallbladder should begin to form within 2 d of plating and should be ready for the first passage within 5–7 d of initial plating (Fig. 2d, bottom, and Fig. 3c, bottom). Organoids from liver biopsies or excised liver tissue should take ~5–10 d to develop (Fig. 4d, right) and should be passaged when the plate is approaching 80% confluency.
▲ CRITICAL STEP CO lines should always express the biliary markers CK19, CK7, Sox9 and GGT (Fig. 6a,b) and display ALP and GGT activity (Fig. 6c,d, respectively). Established CO lines should be composed of a <99% pure population of $CK19^+/CK7^+$ cells (Fig. 6e). After approximately passage 2, CO lines derived from different tissues of origin or through different derivation methods will appear morphologically identical (Supplementary Fig. 4a).
? TROUBLESHOOTING

Cell culture: changing medium for maintenance of CO lines ● Timing Variable, depending on cell line; hands-on time is 20 min every 48 h

▲ CRITICAL Once primary cholangiocytes have been isolated and plated as described above, culture conditions for all CO lines are the same, and the following procedural steps for CO maintenance (Steps 15–30) apply equally to all CO lines, regardless of tissue of origin or derivation method. Equally, the characterization data shown in Fig. 6 are representative of CO lines derived from all tissue types or derivation methods.
▲ CRITICAL Change the medium approximately every 48 h.

11 Prepare 1 ml of William's E+ medium per well, supplemented with 500 ng/ml R-spondin, 50 ng/ml EGF and 100 ng/ml DKK-1, for each well of a 24-well plate. In addition, 50 ng/ml HGF and 2 µM FSK can be added optionally for slow-growing lines requiring >5–7 d between passages.
? TROUBLESHOOTING

12 Carefully aspirate the old medium from the well.
▲ CRITICAL STEP Tilt the plate when aspirating and aspirate from the edge of the well to avoid disrupting the Matrigel dome.

13 Add the new medium to all the wells, using a 5- or 10-ml pipette.
14 Continue to culture cells.
▲ CRITICAL STEP When adding medium, tilt the plate and hold the pipette against the side of the well to avoid disrupting the Matrigel dome. Add the medium slowly.

Passaging of CO lines for maintenance ● Timing 95 min

15 CO lines should be passaged approximately once every 5 d. However, the optimal time for passaging should be decided on basis of the confluency of the organoids; therefore, the cells should be examined daily (Fig. 5b, image 1).
▲ CRITICAL STEP Allowing the wells to become too confluent may lead to the collapse of organoids and subsequent cell death (Supplementary Fig. 4b, image 2).
16 Remove the medium and add 500 µl of cell recovery solution to each well. The pipette should be aimed at the center of the Matrigel dome and the cell recovery solution should be ejected forcefully to disrupt the surface of the dome.
17 Mechanically dissociate the remaining Matrigel dome by scraping with a p1000 pipette (Fig. 5a, image 1).
▲ CRITICAL STEP Ensure that the whole surface of the well has been scraped to remove as many cells as possible.
18 Transfer the cells from each well to a 15-ml centrifuge tube.
19 Wash each well with 500 µl of cell recovery solution. (Optional) The same 500 µl can be carried across to each of the wells at this step to minimize the volume of cell recovery solution required for the washes.
20 Incubate the cells on ice at 4 °C for 30 min to fully dissolve the Matrigel.
21 Centrifuge at 444*g* for 4 min at room temperature.
? TROUBLESHOOTING
22 Aspirate the supernatant.
23 If appropriate, use this wash step to split the cell pellet into multiple fractions.
▲ CRITICAL STEP We recommend splitting the pellet appropriately to allow the generation of a single plate of organoids from a single pellet fraction. This is important in order to avoid prolonged use of the Matrigel master mix in the following steps. This can lead to Matrigel solidification and gravitation of larger cell clumps to the bottom of the mix, compromising uniform distribution of cells and seeding density.
▲ CRITICAL STEP CO pellets can typically be split at a ratio between 1:4 and 1:6, depending on the number of wells in the initial plate and their confluency (Fig. 5a). For reference, Fig. 5b, image 4 depicts a representative pellet for plating nine CO wells (~4.0 $\times 10^5$ cells), obtained after a 1:4 split.
24 Resuspend in William's E+ medium, mixing well and using the following formula to calculate the minimum volume of medium required:

$$\text{Volume of medium to add (ml)} = \text{Number of pellets to be made after splitting}$$

For example, for a 1:4 split, resuspend in 4 ml of medium.
25 Divide the cell suspension among multiple 15-ml centrifuge tubes, adding 1 ml per tube (e.g., for a 1:4 split, share the 4-ml volume equally among four 15-ml centrifuge tubes).
26 Centrifuge at 444*g* for 4 min at room temperature.
27 (Optional) Cryopreserve CO pellets at this point, if necessary, by resuspending each in 1 ml of CellBanker 2, transferring to a 2-ml cryovial and freezing immediately at −80 °C.
▲ CRITICAL STEP For long-term cryopreservation, COs should be stored in a liquid nitrogen cryobank.
▲ CRITICAL STEP Cryovials should be transferred immediately to dry ice after removal from liquid nitrogen storage, to prevent uncontrolled thawing. CO cryovials should be thawed in a 37 °C water bath, and the cells should be transferred immediately to prewarmed William's E+ medium supplemented with 10 µM Y27632 and centrifuged at 444*g* for 4 min at room temperature. Thawed cells can then be plated as described in Steps 3–10.
■ PAUSE POINT Cryopreserved COs can be stored for short-term storage (<6 weeks) at −80 °C, but long-term storage at this temperature will affect the viability and overall health of the line. COs can be stored in a liquid nitrogen cryobank for an extended duration (>10 years), provided the temperature is not permitted to rise above −130 °C.

28 Resuspend the pellet in a volume of 3× supplemented William's E+ medium (supplemented with 1.5 µg/ml R-spondin, 150 ng/ml EGF, 30 µM (3 µl/ml) Y27632 and 300 ng/ml DKK-1) as described in Step 5. See the '3× supplemented William's E+ solution' in the 'Reagent setup' section for instructions on how to prepare this solution and how to determine the appropriate volume to add.
▲ **CRITICAL STEP** The number of plated wells of COs depends on the size of the resulting cell pellet. For example, a pellet of ~4.0 × 10^5 cells (Fig. 5b, image 4) should be plated in nine wells.

29 Use a p200 pipette to mechanically dissociate the pellet to break up the organoids. This should typically be done ~30–50 times, although the exact number will vary according to the starting size of the organoids.
▲ **CRITICAL STEP** Organoids must be dissociated into small clumps of ~10–20 cells to allow cysts to reform after splitting (Fig. 5b, image 5). Mechanical dissociation should be done slowly to avoid damaging the cells.
▲ **CRITICAL STEP** Organoid breaking must be carried out with a p200 pipette, even if the volume of 3× William's E+ medium required exceeds 200 µl. In that case, add the initial 200 µl and break the organoids as described in this step before adding the remaining volume of the medium.
? TROUBLESHOOTING

30 Plate the organoids onto a preheated 24-well tissue culture plate as described in Steps 3–10.
▲ **CRITICAL STEP** Organoids should reform from small clumps into organoids 24–48 h after plating (Fig. 5b, image 7(ii); enlarged image in Supplementary Fig. 2, image 2). Organoids should proliferate rapidly and should reach ~80% confluence 5 d after plating.
? TROUBLESHOOTING

Preparation of 5 mg/ml collagen gel before generation of densified collagen scaffolds

● **Timing 10 min**

▲ **CRITICAL** Densified collagen scaffolds can be prepared to yield a sheet or tubular form. The sheet form produces a structure that has a well-defined thickness and density, and yields highly reproducible scaffolds, owing to the controlled nature of the process, whereas the collagen tube method is more technically challenging.

▲ **CRITICAL** To produce a collagen gel, first mix a collagen gel precursor solution. This neutralizes the pH of the stock collagen solution and raises the ionic content, which induces the collagen fibrils to form a gel. Here, we produce two collagen sheets by preparing 2.5 ml of collagen precursor solution, which is prepared to a final collagen concentration of 5 mg/ml. 1 ml of this volume is sufficient to produce a collagen scaffold of a reproducible thickness (~750 µm), using the recommended specimen tubes. The quantities in parentheses represent the volumes required for a final volume of 2.5 ml, which is enough for two collagen sheets.

▲ **CRITICAL** All equipment and reagents must be sterilized before use, and the following steps must take place in a class II biological safety cabinet under aseptic conditions.

31 Transfer 10× Medium 199 at a 10% (vol/vol) final volume to a sterile 50-ml tube (0.25 ml).

32 Calculate the volume of stock collagen solution required to yield a final collagen concentration of 5 mg/ml (1.25 ml). This is calculated by the following formula:

$$\text{Volume stock collagen (ml)} = \frac{5\,(\text{mg/ml})}{\text{Stock collagen concentration (mg/ml)}} \times \text{Precursor solution final volume (ml)}$$

33 Add sterile 1 M NaOH solution to the precursor solution at 2.5% (vol/vol) the volume of stock collagen solution to be added (31 µl).

34 Add sterile 7.5% (wt/vol) sodium bicarbonate solution to the precursor solution at 3% (vol/vol) the final volume (75 µl).
▲ **CRITICAL STEP** This volume makes up a constituent volume of the collagen gel precursor solution and so must be accurate, or the concentration of collagen after gelation will vary.

35 Using a 1-ml syringe, transfer stock collagen solution, at the precalculated volume, to the precursor solution (1.25 ml).
▲ **CRITICAL STEP** The stock collagen solution will be viscous because of its high concentration; use a syringe rather than a pipette to transfer the collagen accurately.
? TROUBLESHOOTING

36 Shake the collagen precursor solution vigorously until it develops a uniform color.
? TROUBLESHOOTING

37 Calculate the remaining volume of cell medium to be added to the precursor solution to reach the required final volume (0.894 ml) and transfer it to the Falcon tube containing the precursor solution.

38 Centrifuge the collagen precursor solution at 200*g* for 1 min at 4 °C to remove air bubbles and then return the liquid to the bottom of the Falcon tube.

Generation of densified collagen scaffolds

39 Generate collagen scaffolds either as flat sheets (option A) or as tubes (Fig. 1c; option B). If using commercially produced PGA scaffolds, proceed to the next step.

(A) **Fabrication of densified collagen sheets** ● **Timing 1–2 h**

▲ **CRITICAL** Larger-sized densified collagen sheets are possible with larger (flat-bottom) containers (e.g., a 24-well plate). To produce collagen sheets of the same thickness, the collagen precursor solution should be poured into the container such that the height of the solution is 25 mm.

(i) Using a 1-ml syringe and 18-gauge needle, transfer the 5 mg/ml collagen precursor solution to a specimen tube until the height of the solution is 25 mm (Fig. 7b, image 1). Repeat as necessary.

▲ **CRITICAL STEP** Avoid inserting air bubbles into the mixture. Add collagen solution slowly.

(ii) Gel the collagen solution by placing the specimen tube in a 37 °C incubator for 30 min.

▲ **CRITICAL STEP** To maintain sterility, transfer the specimen tube within an upside down 15-ml Falcon tube.

? TROUBLESHOOTING

(iii) Tightly roll three sheets of absorbent paper towels into a cylinder roughly 5 mm in diameter and secure it with autoclave tape.

(iv) Using scissors, cut the paper cylinder to 25 mm in length. Flatten the end by pushing the cylinder against a sterile surface (i.e., a 10-cm plate). Autoclave both the paper cylinder and a nylon membrane.

▲ **CRITICAL STEP** The paper cylinder must have a flat edge in order to contact suitably and thus dry the collagen gel evenly.

(v) Using scissors, cut a piece of nylon membrane into a round piece of a slightly smaller diameter than that of the specimen tube.

(vi) Return the specimen tube to the class II biological safety cabinet. Carefully place the nylon membrane on top of the gel and then place the paper towel wadding into the specimen tube, on top of the membrane (Fig. 7b, image 2(i)).

(vii) Apply very light finger pressure to the top of the wadding so as to make good contact with the gel and then leave the gel to densify for ~1 h (Fig. 7b, images 1–3(i)).

? TROUBLESHOOTING

(viii) Monitor the densification process every 5–10 min to ensure that the wadding is in contact with the gel, and occasionally apply light pressure to keep the wadding in place.

▲ **CRITICAL STEP** Applying too much pressure will rip the top surface of the gel.

? TROUBLESHOOTING

(ix) The densification is terminated when the paper towel has almost reached the bottom of the specimen tube and no water can be further removed (Fig. 7b, image 3(ii)). Once this has occurred, remove the paper wadding; the collagen gel and nylon membrane should be adhered to the wadding.

? TROUBLESHOOTING

(x) Using tweezers, carefully grip the edge of the collagen sheet and peel it away from the paper wadding.

(xi) The nylon membrane is likely to remain attached to the collagen sheet. By gripping the nylon sheet with tweezers, peel this away from the collagen sheet (Fig. 7b, image 4).

▲ **CRITICAL STEP** Avoid ripping the collagen sheet by gently peeling it away from the nylon membrane.

? TROUBLESHOOTING

(xii) Wash the scaffold in William's E+ medium in a six-well plate to remove the pink coloration.

(xiii) For storage, place the densified collagen sheet in fresh William's E+ medium or PBS in a six-well plate or another appropriate container (Fig. 7b, image 5). Seal the plate with Parafilm and store it at 4 °C. Otherwise, proceed to the next step.

■ PAUSE POINT The densified collagen sheet can be stored at 4 °C for up to 3 months before seeding.

(xiv) Warm the collagen sheet to 37 °C before cell seeding, by placing it in an incubator. Cells can be seeded onto the surface of the collagen sheet at this point and cultured for several months as described in the subsequent steps.

(B) **Fabrication of densified collagen tubes** ● Timing ~5–26 h

(i) Using a 1-ml pipette, transfer the precursor solution to the densification chamber until the chamber is full (~1.5 ml; Fig. 8c, image 1).

▲ CRITICAL STEP Avoid inserting air bubbles into the mixture. Add collagen solution slowly.

(ii) Gel the collagen solution by placing the densification chamber in a 37 °C incubator for 30–60 min.

? TROUBLESHOOTING

(iii) To form a collagen tube, it is necessary to dislodge the collagen gel from the top of the funnel to encourage the gel surface to drop. To do this, use a sterile pair of tweezers under a sterile class II biological safety cabinet to gently peel the collagen gel away from the walls of the chamber (Fig. 8c, image 2).

(iv) Loosen the screws attaching the base to the funnel.

(v) Return the densification chamber to the incubator. Monitor the chamber regularly for 30 min until the level of the collagen gel drops to the top of the metallic wire (Fig. 8c, image 3).

▲ CRITICAL STEP The top end of the metallic wire, embedded in the collagen, will prevent the gel surface from dropping further. Water will continue to be removed through evaporation around the sides of the funnel to yield a tubular structure.

▲ CRITICAL STEP There should be a visible gap between the collagen gel and the edges of the funnel.

? TROUBLESHOOTING

(vi) Monitor the densification chamber in the incubator for a further 4–24 h to allow for evaporation of the water phase of the gel (Fig. 8b, panel 4).

▲ CRITICAL STEP It is important to monitor the collagen gel and prevent the tube from over-drying, on the basis of the humidity conditions of the incubator.

(vii) Continue the process until the vast majority of water has evaporated. The collagen scaffold should consist of a dense and thin cylindrical component around a wire core, with a larger region near the top of the funnel (Fig. 8c, image 4).

? TROUBLESHOOTING

(viii) Transfer 4 ml of William's E+ medium to a six-well plate. Use a sterile pair of tweezers to grip the top of the collagen tube and slowly pull it upward over the end of the metallic wire (Fig. 8c, image 5).

▲ CRITICAL STEP Be careful not to damage the collagen tube with the tweezers or the end of the metallic wire.

? TROUBLESHOOTING

(ix) Place the collagen tube in a six-well plate containing William's E+ medium for storage. The pink coloration will disappear from the collagen tube over several hours (Fig. 8d, images 1 and 2).

(x) Before surgical implantation, it is necessary to trim away the excess collagen sheet and cut a suitable length of tube for the experiment. Place the tube under a dissecting microscope and use a surgical scalpel to cleanly trim any excess collagen (Fig. 8d, image 3).

(xi) Determine a suitable length of collagen tube along the scaffold. Pick a region that is cylindrical in nature (likely the middle section). Use a surgical scalpel to cleanly cut across the tube to yield the required length for the particular application (Fig. 8d, image 4).

▲ CRITICAL STEP Trimming the tube is a particularly difficult step, probably requiring the assistance of an experienced surgeon. Be extremely careful not to cut into the lumen of the tube. Doing so will result in leakages when the tube is perfused.

(xii) Observe the patent lumen under phase contrast with an inverted microscope (Fig. 8d, image 5).

(xiii) Transfer the densified collagen tube to the six-well plate.

(xiv) Store the collagen tube in William's E+ medium in the incubator until ready. The surfaces of the tubes can be further seeded with cells at this point.

■ PAUSE POINT Unseeded collagen tubes can be stored in William's E+ medium or PBS at 4 °C for up to 3 months.

Seeding COs onto scaffolds

40 To seed COs onto densified collagen sheets, see option A. To seed COs onto densified collagen tubes, see option B. For seeding COs onto PGA scaffolds, which are available commercially (see 'Materials' section), see option C (Fig. 1d).

▲ **CRITICAL** The use of an optimal CO line is essential for scaffold seeding. Suboptimal lines will result in reduced cell attachment, proliferation and long-term viability. All CO lines should express the biliary markers CK19, CK7, Sox9 and GGT (Fig. 6a,b) and display ALP and GGT activity (Fig. 6c,d). Healthy CO lines should require passaging every 5 d (Fig. 5b, image 1). CO lines that fail to meet these criteria should not be considered for scaffold seeding. See the 'Troubleshooting' section for Steps 10, 11, 29 and 30 for guidance on how to improve the quality of a suboptimal CO line.

(A) **Seeding on densified collagen sheets** ● **Timing ~2 h 35 min–4 h**

▲ **CRITICAL** Collagen scaffolds must be of an optimal quality to be used for seeding. Batch-test the stock collagen solution used for collagen densification for cell attachment and proliferation and confirm that the densification process has completed fully (see 'Troubleshooting' section for Step 39A) and the scaffold has not dried out during storage to ensure the quality of the collagen scaffolds.

▲ **CRITICAL** For long-term storage, maintain the collagen scaffolds in PBS to prevent them from drying out.

(i) Remove the PBS and place the collagen scaffold in a dry 24-well tissue culture plate; then place it in an incubator for 30 min–1 h, or until the PBS has evaporated and residues on the surface are no longer visible.

▲ **CRITICAL STEP** Drying the scaffold before seeding is necessary, as the presence of excess liquid on the scaffold's surface may prevent cell attachment. This step is required both if the scaffold has been stored long term and if seeding takes place immediately after fabrication of the densified collagen scaffold.

▲ **CRITICAL STEP** Allowing the scaffold to dry for a prolonged period following evaporation of the medium/PBS may affect the collagen fiber micro-architecture.

(ii) Remove the organoids from the Matrigel domes using cell recovery solution and incubate them on ice for 30 min as described in Steps 16–26. An optimal seeding density of 1.5×10^6 cells/cm^2 has been observed to give confluent scaffolds over a short period of time; the number of wells required for the required surface area should be calculated using the following formula:

$$\text{Number of cells} = \text{Scaffold surface}\left(\text{cm}^2\right) \times 1.5 \times 10^6 \text{ cells/cm}^2$$

(iii) Aspirate the supernatant and resuspend the pellet in an adequate volume of William's E+ medium supplemented with 500 ng/ml R-spondin, 50 ng/ml EGF, 100 ng/ml DKK-1 and 10 μM Y27632.

▲ **CRITICAL STEP** For the seeding solution, a cell density of 5×10^4 cells/μl is recommended. For example, a pellet of 1×10^6 cells, equivalent to ~10 confluent wells, is resuspended in a volume of 20 μl. Once seeded on a scaffold surface of 0.65 cm^2, this should allow the cells to form a confluent layer in ~2 weeks' time, with slight variations depending on the organoid line.

(iv) Gently pipette up and down with a p20 pipette 30–40 times to mechanically dissociate the organoids into small clumps (~10–20 cells per clump) and obtain a homogeneous solution.

? TROUBLESHOOTING

(v) Seed the cells by directly pipetting this solution onto the scaffold's surface with a p10 pipette (Fig. 9b, images 3(i) and 3(ii)).

▲ **CRITICAL STEP** To achieve a homogeneous attachment, it is recommended to seed multiple 5-μl aliquots in different positions all over the scaffold surface.

? TROUBLESHOOTING

(vi) After seeding on collagen scaffolds, keep the plate in a 37 °C incubator for 1–2 h to allow the cells to attach to the scaffold.

▲ **CRITICAL STEP** Monitor the scaffolds every 30 min to avoid drying the cells out.

? TROUBLESHOOTING

(vii) Prepare 2 ml of William's E+ medium supplemented with 500 ng/ml R-spondin, 50 ng/ml EGF, 100 ng/ml DKK-1 and 10 μM Y27632 for each scaffold.

(viii) To add the medium, tilt the plate and slowly add the medium from the bottom of the well (Fig. 9b, image 5).

▲ CRITICAL STEP Medium must be added as slowly as possible, using a p1000 pipette. Care must be taken to avoid disrupting the scaffold when adding the medium.

? TROUBLESHOOTING

(ix) Culture the seeded scaffold for 4 d before the first medium change, in order to maximize cell attachment. After this period, replace the medium with 500 µl of William's E+ medium supplemented with 500 ng/ml R-spondin, 50 ng/ml EGF and 100 ng/ml DKK-1 every other day.

▲ CRITICAL STEP When the medium is changed, all previous medium must first be aspirated. Care must be taken to avoid disrupting the scaffold during medium aspiration.

▲ CRITICAL STEP COs will start growing and expanding on the scaffold after a first lag phase (lasting ~4–5 d after seeding); then confluency should be reached in ~2 weeks, according to the age of the cell line (Fig. 9d,e).

? TROUBLESHOOTING

(B) **Seeding onto the lumen of densified collagen tubes** ● Timing **2 h 30 min–3 h 30 min**

(i) Working under aseptic conditions, transfer the densified collagen tube onto a dry 10-cm plate.

(ii) Leave it to dry under a class II biological safety cabinet for approximately half an hour, or until almost all the residual PBS has evaporated.

▲ CRITICAL STEP Prepare the CO cell suspension as detailed in Step 40B(iii,iv)) during the waiting time described in Step 40B(ii).

(iii) Passage the organoids as described in Steps 16–26. The number of wells required for the desired tube area should be calculated using the following formula:

$$\text{Number of cells} = \text{Tube internal surface}\left(\text{cm}^2\right) \times 6.5 \times 10^6\ \text{cells/cm}^2$$

▲ CRITICAL STEP For the seeding solution, a cell density of 2.5×10^4 cells/µl is recommended. For example, a pellet of 6×10^5 cells, equivalent to ~6 confluent wells, is resuspended in a volume of 25 µl. Once seeded in the lumen of a tube with a 1.5-cm length and 250-µm diameter, a confluent layer of cells should form in ~4 weeks' time, with slight variations depending on the organoid line.

▲ CRITICAL STEP Seeding of the luminar surface of the densified collagen tubes requires a greater cell density than seeding of flat scaffolds, as a higher proportion of the cells are likely to be lost during the seeding process and so cells should be seeded in excess to guarantee adequate seeding of the whole tube area.

(iv) Resuspend the cells in 25 µl of William's E+ medium with 50 ng/ml EGF and 10 µM Y27632.

(v) Use a p20 pipette to carefully break the COs into small clumps (10–20 cells).

▲ CRITICAL STEP Failure to break the COs into small enough clumps (Supplementary Fig. 2, image 2) will result in the cells failing to form a confluent monolayer on the luminal surface of the tube.

? TROUBLESHOOTING

(vi) Using a 34-gauge Hamilton removable needle and a pair of fine forceps, cannulate the tube with the 34-gauge needle. For best results, this should be done under a dissecting microscope (Fig. 10b, image 2).

▲ CRITICAL STEP Cannulation of the tube should ideally be performed by an experienced surgeon. Improper attempts at cannulation can result in disruption of the construct wall beyond repair.

(vii) Use a p200 pipette to transfer the cell suspension to a 25- or 50-µl Hamilton syringe.

▲ CRITICAL STEP It is highly advisable to use Hamilton syringes, as recommended in the 'Equipment' list, or some other model of small-volume syringes with removable needles and no dead space. This is due to the very low volume of cell suspension required for seeding, which is smaller than the dead space in standard needles.

(viii) Slowly depress the plunger on the syringe to deposit the cell suspension in the lumen of the tube while simultaneously removing the needle from the tube in order to distribute the cells evenly along the tube lumen (Fig. 10b, image 3).

? TROUBLESHOOTING

(ix) Incubate the freshly seeded tube in a covered 10-cm plate at 37 °C without medium for up to an hour to allow cell attachment.
? TROUBLESHOOTING

(x) Transfer the tube to a six-well plate.

(xi) Prepare 2 ml of William's E+ medium supplemented with 500 ng/ml R-spondin, 50 ng/ml EGF, 100 ng/ml DKK-1 and 10 μM Y27632.

(xii) Tilt the plate and use a p1000 pipette to add the medium slowly to the side of the well until the tube is covered.
▲ CRITICAL STEP Medium must be added as slowly and carefully as possible, to avoid disruption of the newly attached cells. Care must be taken to avoid touching the tube with the pipette.
? TROUBLESHOOTING

(xiii) Culture the seeded tube for 4 d before the first medium change, in order to maximize cell attachment. After this period, replace the medium with 2 ml of William's E+ medium supplemented with 500 ng/ml R-spondin, 50 ng/ml EGF and 100 ng/ml DKK-1 every 4 d in order to reduce the disruption caused by medium change.
▲ CRITICAL STEP When changing the medium, all previous medium must first be aspirated. Care must be taken to avoid disrupting the tube during medium aspiration.
▲ CRITICAL STEP Maintain the construct in culture. A confluent layer of cells should form in ~4 weeks, depending on the age of the cell line (Fig. 10c,d).
? TROUBLESHOOTING

(C) **Seeding on PGA scaffolds ● Timing 2 h 10 min–4 h 10 min**

(i) Place the PGA scaffold, with a thickness of 1 mm and density of 50 mg/cm^3, in 1 M NaOH for 10–30 s.

(ii) Sterilize the scaffold by immersion in 70% (vol/vol) EtOH for 30 min.

(iii) Air-dry the PGA scaffold in a six-well tissue culture plate under a sterile class II biological safety cabinet for a further 30 min (Fig. 9c, image 1).
▲ CRITICAL STEP Ensure that all traces of NaOH and EtOH are gone from the scaffold before beginning seeding. Improper drying can lead to cell death and failure to attach to the scaffold.

(iv) Remove the COs from organoid culture and prepare a suspension of small clumps as described in Step 40A(ii–iv).
▲ CRITICAL STEP Given the pore size of the electrospun PGA, it is important that the CO clumps be no smaller than 40–60 cells per clump, as small cell clumps will fall through the pores of the scaffold and not be retained.
? TROUBLESHOOTING

(v) Gently pipette up and down with a p20 pipette 10–20 times in order to obtain a homogeneous cell suspension with CO clumps of ~40–60 cells per clump.
? TROUBLESHOOTING

(vi) Seed the cells onto the PGA scaffold as described in Step 40A(v–x) (Fig. 9c, images 3(i) and 3(ii)).
? TROUBLESHOOTING

Characterization of COs

41 To analyze COs using IF, follow option A. To analyze COs by flow cytometry, follow option B. To extract RNA for qPCR, follow option C.

(A) **Immunofluorescence ● Timing ~3 d**

(i) Aspirate the William's E+ culture medium.

(ii) Add 1 ml of 4% (vol/vol) PFA per well.
▲ CRITICAL STEP PFA should be added gently to the side of the well so as to avoid disrupting the Matrigel dome.

(iii) Incubate at 4 °C for 20 min to fix the cells.
? TROUBLESHOOTING

(iv) Aspirate the PFA.
▲ CRITICAL STEP The PFA should be aspirated with a p1000 pipette to avoid disruption of the Matrigel dome.

(v) Wash twice in PBS. Each wash should take 10 min.
■ PAUSE POINT The CO plate can be sealed and kept at 4 °C for up to 4 weeks.

(vi) Prepare a solution of 10% (vol/vol) donkey serum and 0.1% (vol/vol) Triton X-100 in PBS.
? TROUBLESHOOTING

(vii) Add 1 ml of this solution to each organoid well and incubate the plate at room temperature for 1 h to block and permeabilize the COs.

? TROUBLESHOOTING

(viii) Dilute the primary antibodies in a solution of 1% (vol/vol) donkey serum and 0.1% (vol/vol) Triton X-100 in PBS.

(ix) Add 500 µl of primary antibody solution per CO well.

(x) Stain the COs overnight at 4 °C.

(xi) Wash the COs three times with 1% (vol/vol) donkey serum and 0.1% (vol/vol) Triton X-100 in PBS. Each wash should take 45 min.

(xii) Dilute the secondary antibodies in a solution of 1% (vol/vol) donkey serum and 0.1% (vol/vol) Triton X-100 in PBS.

(xiii) Add 500 µl of secondary antibody solution per CO well.

(xiv) Stain the COs overnight at 4 °C.

▲ **CRITICAL STEP** The CO plates should be wrapped in foil to prevent exposure of the secondary antibodies to light.

? TROUBLESHOOTING

(xv) Aspirate the secondary antibody solution.

(xvi) Prepare a 1:10,000 (vol/vol) solution of Hoechst 33258 in PBS.

(xvii) Incubate the COs in this Hoechst 33258 solution for 10 min at room temperature.

? TROUBLESHOOTING

(xviii) Aspirate the Hoechst 33258 solution.

(xix) Wash the COs three times with PBS. Each wash should take 45 min.

(xx) Add a final 1 ml of PBS per CO well and image the COs immediately or store the plate at 4 °C until ready for analysis.

■ **PAUSE POINT** The plates can be stored at 4 °C for up to 3 months, provided the stained wells have an adequate covering of PBS and the plates are properly sealed.

(xxi) Image using a confocal microscope. All of our IF images (Figs. 6a and 11a,c,e) were acquired using a Zeiss LSM 700 confocal microscope. ImageJ 1.51h software (Wayne Rasband, NIHR; http://Imagej.nih.gov/ij) was used for image processing such as merging of different channels.

(B) **Flow cytometry** ● **Timing 5.5 h**

(i) *Preparation of a single-cell suspension*. Passage the organoids as described in Steps 16–24.

(ii) Resuspend the pellet in 1 ml of William's E+ medium and centrifuge at 444*g* for 4 min at room temperature.

(iii) Prepare a solution of Accutase (prewarmed to 37 °C) with 4 mg/ml DNase I and 10 µM Y27632.

▲ **CRITICAL STEP** Omission of DNase I and Y27632 can lead to cell clumping and greatly reduced viability.

(iv) Aspirate the supernatant and resuspend the pellet in 1 ml of Accutase solution.

(v) Incubate the cells at 37 °C for up to 5 min to produce a single-cell suspension.

▲ **CRITICAL STEP** Examine the cells under a microscope halfway through to check the progress of the dissociation

? TROUBLESHOOTING

(vi) Add 1 ml of William's E+ medium or 1% (wt/vol) BSA in PBS with 4 mg/ml DNase I and 10 µM Y27632 to the cell suspension.

(vii) Centrifuge the cells at 444*g* for 4 min at room temperature.

(viii) Resuspend the pellet in 1 ml of William's E+ medium or 1% (wt/vol) BSA in PBS with 4 mg/ml DNase I and 10 µM Y27632.

(ix) Filter through a 40-µm filter.

▲ **CRITICAL** If performing flow cytometry on a live cell population, skip Step 40B(x–xv) and go directly to Step 40B(xvi–xxix) (staining of a single-cell suspension for flow cytometry).

? TROUBLESHOOTING

(x) Centrifuge the cells at 444*g* for 4 min at room temperature.

(xi) Resuspend the pellet in 1 ml of 4% (vol/vol) PFA.

(xii) Incubate the cells at 4 °C for 15 min to fix the cells.

(xiii) Add 1 ml of 1% (wt/vol) BSA in PBS.
(xiv) Centrifuge the cells at 444*g* for 4 min at room temperature.
(xv) Resuspend the pellet in 1 ml of 1% (wt/vol) BSA in PBS.
▲ **CRITICAL STEP** Cells should be handled very carefully after fixation to avoid damage. Pellets should be resuspended by flicking of the centrifuge tube (as opposed to pipetting), and all pipetting should be done slowly.
■ **PAUSE POINT** After fixation, cells can be stored at 4 °C for up to 2 d.
(xvi) *Staining a single-cell suspension for flow cytometry*. If staining for cell-surface markers only, prepare a 1:20 dilution of FcR block in 1% (wt/vol) BSA in PBS.
(xvii) If staining for intracellular markers, prepare a 1:20 dilution of FcR block in 1% (wt/vol) BSA in PBS with 0.1% Triton X-100 (vol/vol).
(xviii) Centrifuge the cells at 444*g* for 4 min at room temperature and resuspend the pellet in 200 µl of diluted FcR block.
(xix) Incubate at room temperature for 30 min.
(xx) Prepare a master mix of all antibodies (if using conjugated antibodies) or all primary antibodies (if using separate primary and secondary antibodies) in 1% (wt/vol) BSA in PBS.
▲ **CRITICAL STEP** An aliquot of the cell suspension (at least 1×10^5 cells) should be used as an unstained control. If using separate primary and secondary antibodies, another aliquot must be used for a secondary-only control. Both aliquots should be kept at 4 °C until required.
(xxi) Centrifuge the cells at 444*g* for 4 min at room temperature.
(xxii) Resuspend the pellet in 200 µl of master mix solution.
(xxiii) If using conjugated antibodies, incubate at 4 °C for half an hour. If using primary antibodies, incubate at room temperature for an hour.
(xxiv) If using conjugated antibodies, wash the cells three times in 1% (wt/vol) BSA in PBS and filter through a 40-µm filter before analyzing the sample on the flow cytometer.
(xxv) If using unconjugated antibodies, wash the cells three times in 1% (wt/vol) BSA in PBS. Each wash should take 5 min.
(xxvi) Prepare a solution of all secondary antibodies in 1% (wt/vol) BSA in PBS.
(xxvii) Resuspend the cells in 200 µl of secondary antibody solution and incubate at room temperature for 1 h.
▲ **CRITICAL STEP** The secondary-only control should also be stained at this point.
▲ **CRITICAL STEP** The cells should be kept in the dark to prevent exposure of the secondary antibody to light.
(xxviii) Wash the cells three times in 1% (wt/vol) BSA in PBS. Each wash should take 5 min.
(xxix) Resuspend the cells in 200 µl of 1% (wt/vol) BSA in PBS and filter through a 40-µm filter before analyzing the sample on a flow cytometer. All our flow cytometric analyses were performed on a FACS Cyan flow cytometer and analyzed using FlowJo v.10.4.2.

(C) **RNA extraction** ● **Timing ~2 h**
(i) If isolating RNA from an established CO line, first remove COs from organoid culture as described in Steps 16–25. If isolating RNA from a suspension of primary cells, go straight to Step 40C(ii).
(ii) Centrifuge the cells at 444*g* for 4 min at room temperature.
(iii) Aspirate the supernatant and resuspend the pellet in 350 µl of RNA lysis buffer.
▲ **CRITICAL STEP** Ensure that the lysed cell suspension is fully homogenized.
(iv) Transfer the lysed cell suspension to a prelabeled 1.5-ml Eppendorf tube and store the tube immediately at −80 °C.
▲ **CRITICAL STEP** A delay in transferring the lysed sample to −80 °C storage can result in degradation of RNA quality.
■ **PAUSE POINT** Samples in RNA lysis buffer can be stored at −80 °C for >1 year until needed.
(v) Thaw the samples on ice.
(vi) Use the GenElute Mammalian Total RNA Miniprep Kit to extract RNA from the samples according to the manufacturer's instructions.

Troubleshooting

Troubleshooting advice can be found in Table 1.

Table 1 | Troubleshooting table

Step	Problem	Possible reason	Solution
2A(iii)	Very few or no cells are collected after mechanical dissociation	Cell detachment during PBS washes	Reduce the number of washes If the tissue has been in cold storage solution for longer than 2–4 h, consider omitting the wash step. Aspirate any excess bile with a p1000 pipette instead Centrifuge the PBS to collect the cells detached during the washes
2A(ix, xii)	Pellet contains too much debris	Forceful scraping of the tissue can mechanically dissociate part of the fibrous tissue, as well as biliary epithelia	Scrape the tissue very gently and avoid scraping the same area of tissue more than twice Where possible, remove large debris with a p1000 pipette before centrifugation
2A(x)	Cells do not form a pellet in Step 2A(x) after mechanical dissociation	Inadequate wash	Increase the number of PBS washes before mechanical dissociation
		Remnants of bile and/or debris in the cell suspension	Ensure that the tissue is adequately washed before you start mechanical dissociation Use a p1000 pipette to remove large pieces of debris before transferring the cells to a 50-ml centrifuge tube
	Cells are lost during the wash steps	Washing was done in PBS or medium with inadequate protein content	Use only complete William's E+ medium during the wash steps or 1% (wt/vol) BSA in PBS
2A(xviii), 2B(v)	Organoids do not form following plating	Poor cell viability (PCV) due to tissue drying during the dissection steps	Dissect the tissue as quickly as possible and submerge it in medium as soon as dissection is complete
		PCV due to stress of mechanical dissociation	Avoid vigorous scraping of the tissue resulting in cell death Avoid vigorous washes and pipetting resulting in increased cell stress and/or death
		PCV due to prolonged cold storage	Process the tissue as soon as possible after surgical excision
		PCV due to lack of necessary cytokines in the medium	Ensure that the medium contains 150 ng/ml EGF and 10 μM Y27632 at every stage
		PCV due to poor quality of tissue culture medium and reagents (Matrigel or cytokines)	Batch-test Matrigel and medium components Always store Matrigel and cytokines at −80 °C Avoid repeat freeze–thaw cycles of cytokines and do not use Matrigel that has undergone more than two freeze–thaw cycles
2C(viii), 2D (xxvii)	Organoids do not form once the tissue is plated	PCV due to tissue drying during the dissection steps	Complete the dissection step as quickly as possible
		PCV due to stress of mechanical dissociation	Ensure that the dissected liver pieces are as small as possible so they can fit into the tip of a p1000 pipette without difficulty
		PCV due to prolonged cold storage	Process the tissue as soon as possible after surgical excision
		PCV due to lack of necessary cytokines in the medium	Ensure that the medium contains 150 ng/ml EGF and 10 μM Y27632 at every stage
		PCV due to poor quality of tissue culture medium and reagents (Matrigel or cytokines)	Batch-test Matrigel and medium components
2D(v)	Poor viability of cells before EpCAM sorting	Prolonged enzymatic dissociation	Examine the cells every 10 min during the dissociation. Ensure that the dissociation is stopped as soon as a single-cell suspension is obtained and the majority of liver cells have been released from the extracellular matrix (Supplementary Fig. 2b, image 4)
		Vigorous pipetting to dissociate cell clumps, resulting in cell death	Dissociate cell clumps gently. Prolong enzymatic digestion if vigorous pipetting is required
		Prolonged cold storage	Process the tissue as soon as possible after surgical excision
2D(v, vii)	Cells clumping during or after dissociation to a single-cell suspension	DNA fragments in the suspension originating from non-viable cells cause cholangiocytes to clump	Monitor the cells closely during dissociation. If cells show signs of clumping, increase the concentration of DNase I by 30%

Table continued

Table 1 (continued)

Step	Problem	Possible reason	Solution
			Following filtering, the cells should be resuspended in 1% (wt/vol) BSA in PBS supplemented with 4 mg/ml DNase I and 10 μM Y27632
2D(xv)	Substantial loss of cells after single-cell dissociation	Cell adhesion to the surfaces of the centrifuge tube during centrifugation or MACS sorting	Resuspend cells in sterile 1% (wt/vol) BSA in PBS with 4 mg/ml DNase I and 10 μM Y27632 Prime centrifuge tubes with 1% (wt/vol) BSA in PBS before use
2D(xxiv)	Blockages during the MACS sorting	Cell clumps remain in the cell suspension	Filter the sample immediately before running on the MACS cell sorter
6	Matrigel does not form a dome but attaches to the side of the well during plating	Remnants of solidified Matrigel blocking the pipette tip and preventing uniform dispensation of the gel	Change pipette tip
8, 30	Cells attach to the bottom of the plate	Delay in inverting the plate after plating of the cells	Ensure that the plates are adequately prewarmed
		Delay in Matrigel solidification due to low plate starting temperature, allowing cell clumps to gravitate to the bottom of the plate	Ensure plating occurs on a plate heater to allow the Matrigel to solidify as quickly as possible. Keep the plates inverted for 30 min in a 37 °C incubator
10, 11	Cells form small spheres lacking a lumen after plating	Overly dense initial plating, preventing organoid expansion	Passage the cells earlier than 5 d and plate at a reduced density Add 2 μM FSK to the medium
21	Matrigel remnants are present in the pellet following the incubation with cell recovery solution	Incubation time was too short	Ensure that the cells have been incubated for the full 30 min in cell recovery solution and that the volume of ice is adequate to keep the cells at 4 °C
10, 11, 29	Cells demonstrate signs of stress, such as thickening of organoid walls, organoid collapse and reduced organoid proliferation. Cell death is observed for several days after passaging/consistently over several passages	Events during passaging could be causing stress to the cells: dissociating the organoids too vigorously during Step 29 or prolonged duration of passaging, stressing the cells by delaying return to optimal culture conditions	Avoid vigorous dissociation during passaging and minimize delays during passaging
		Suboptimal batch of Matrigel	Batch-test new lots of Matrigel
		Suboptimal quality of the cytokine medium components used	Store all stock solutions at 4 °C and do not use stock solutions made more than 3 months earlier. Where applicable, do not use stock solutions beyond their expiry date. Store all cytokines at −80 °C
		Mycoplasma contamination	Test organoid cultures for Mycoplasma contamination
		Delay in passaging the cells (Supplementary Fig. 4b)	Passage COs when 80% confluent with no signs of organoid collapse, typically every 5 d. Plates should be observed daily to determine the optimum time for passaging
		Overly dense plating, preventing organoid proliferation (Supplementary Fig. 4b)	Passage the cells earlier than the typical 5 d and ensure that the cells are plated more sparsely at the next passage
		Additional cytokines needed	Increase the working concentration of EGF used during maintenance to up to 100 ng/ml
			Add FSK at a 2 μM working concentration (0.2 μl/ml of a 10-mM stock)
			Add HGF at a 50 ng/ml working concentration
35	Stock collagen solution is highly viscous upon arrival	If the stock collagen solution is stored at temperatures < 2 °C, it can appear to have gelled	Warm the stock collagen solution to room temperature until the collagen solution is liquid. Once liquid, store at 4 °C
36, 39A(ii)	Collagen precursor solution solidifies in the mixing tube.	Solution mixing occurs too slowly	Before starting, cool all the reagents to 4 °C
		The room temperature is too high	Mix the solution in an ice bath
39A(vii, viii)	Collagen gel densification stops prematurely	The absorbent paper wadding has poor contact with the collagen gel and so cannot remove water effectively	Remove the paper wadding from the specimen tube and flatten the end in contact with the collagen gel. Once sufficiently flat, return it to densification chamber

Table continued

Table 1 (continued)

Step	Problem	Possible reason	Solution
		As the paper wadding absorbs water, it expands and becomes wedged in the specimen tube, preventing further densification	Gently remove the paper wadding from the specimen tube and replace it with a fresh roll with a slightly reduced diameter
39A(ix)	Following densification steps and removal of paper wadding, the specimen tube is empty	Collagen solution has been prematurely absorbed into the paper wadding before gelation	Repeat the process and extend the time for collagen gelation from 30 min to 1 h Test gelation by carefully pressing the metal spatula against the top surface. Only add paper wadding once you are sure that the collagen has gelled
39A(xi)	Collagen sheet was not attached to paper wadding on its final removal	After the removal of the wadding, the collagen sheet remains at the bottom of the specimen tube	The scaffold can be removed carefully with a pair of tweezers or by some PBS flushed into the specimen tube
	Once removed from the densification chamber, the lower part of the scaffold retains a gel-like structure	Densification has been stopped prematurely, causing the lower part of the collagen sheet to retain a higher water content	Return the scaffold to the densification chamber and continue the densification process with fresh paper wadding
39B(ii)	Before collagen gelation, the level of the collagen solution has dropped	The collagen precursor solution is leaking out of the bottom of the funnel of the densification chamber	Keep the chamber upright and carefully tighten the screws such that the base is firmly attached to the funnel. Add an extra volume of collagen precursor solution until the funnel is once again full
	The level of the collagen gel has dropped below the top of the metallic wire	The volume of collagen above the wire was unable to stop the collagen gel from dropping below the wire	Use scissors to remove a couple of millimeters of length from the top of the metallic wire. Repeat the collagen gelling process
39B(v)	The level of the collagen gel has not dropped to the top of the metallic wire	The paper towels at the base are not in sufficient contact with the gel and so water is not being drawn out	Repeat the process. When loosening the screws, do not displace the base away from the funnel, thereby keeping the paper towels in contact with the bottom of the collagen gel
39B(v, vii, viii)	Collagen gel has not densified after 24 h	There has been insufficient evaporation of water from the collagen gel to form a tube	Use sterile tweezers to repeat the process of peeling the collagen gel from the chamber walls. One should observe a 1- to 2-mm spacing between the collagen gel and funnel walls. Continue densifying until a tube forms The humidity of the incubator may be high and so an insufficient volume of water has evaporated from the collagen gel. Continue step 39B(vii), monitoring the evaporative process, until a collagen tube forms
40A(iv, v, vi, viii, ix), 40B(v, viii, ix), 40C(v, vi)	Low cell attachment immediately after seeding	Reduced incubation time, preventing cell attachment	After seeding, increase the duration of the incubation step a further 30 min
		Cell detachment during medium change	Add medium very carefully. Tilt the plate and hold the pipette against the side of the well to avoid disrupting the Matrigel dome. Add the medium slowly, using a p1000 pipette
		Low cell number. Optimal cell number and attachment potential may vary between lines	Optimize the seeding density for each CO line
		Prolonged incubation, leading to cell death and drying	Monitor the scaffolds closely after seeding and before addition of medium. Check the scaffolds every 30 min to ensure that the seeding solution has not evaporated
		Small clump size, leading to loss of cells through the pores of the PGA scaffold	Optimize the clump size when seeding PGA scaffolds
		Single cells or very small clumps floating in the seeding solution and preventing attachment	Pipette more slowly and for fewer times when breaking the COs into small clumps
		Remnants of EtOH or NaOH in PGA scaffolds, leading to cell death in PGA scaffolds	Increase the drying time to ensure that all traces of NaOH and EtOH are gone (PGA scaffolds only)
		Excessive breaking of the CO clumps, reducing cell viability	Use a p200 pipette instead of a p20 to break the CO clumps Pipette more slowly when breaking the CO clumps

Table continued

Table 1 (continued)

Step	Problem	Possible reason	Solution
40A(v), 40C(vi)	Immediately after seeding, the cell suspension overspills from the scaffold	The seeding volume is too big	Immediately retrieve the spilled solution and seed it again onto the scaffold
		The seeding has occurred too close to the edge	Reduce the total volume of cell suspension used during seeding
40B(v)	CO clumps form organoid-like 3D structures rather than a monolayer	CO clumps were not dissociated to a sufficiently small size	Break clumps further, using a p10 pipette if necessary
40B(viii)	Cell suspension overflows from the construct lumen during seeding	Rapid addition of the cell suspension with inadequate needle withdrawal	Dispense cells slowly, simultaneously withdrawing the needle from the tube lumen
40A(ix), 40B(xiii), 40C(vi)	Low cell density on the scaffold	The cells may have been seeded too sparsely	Increase the cell density Allow a longer time for the cells to reach confluency
40A(x), 40B(xii), 40C(vii)	Poor cell survival and/or expansion on the scaffold	Cells are washed away during medium change	Increase the amount of medium to 1 ml and change it very carefully every 4 d
		Y27632 was not added to the medium	Ensure that fresh Y27632 is added to the medium when seeding
		Suboptimal CO line	All CO lines should express the biliary markers CK19, CK7, Sox9 and GGT (Fig. 6a,b) and display ALP and GGT activity (Fig. 6c,d). Healthy CO lines should be proliferating at a rate requiring passaging every 5 d (Fig. 5b, image 1). Do not attempt scaffold seeding with a CO line that does not meet these criteria. See the Troubleshooting advice for Steps 10, 11 and 29 for recommendations on how to improve the quality of a suboptimal CO line
		Suboptimal collagen batch for collagen scaffolds	Batch-test all new lots of collagen solution (collagen scaffolds only)
		Suboptimal quality of cytokines, medium components or collagen stock	Store all stock solutions at 4 °C and do not use stock solutions made more than 3 months previously. Where applicable, do not use stock solutions beyond their expiry date. Store all cytokines at −80 °C
		Remnants of EtOH or NaOH in PGA scaffolds, leading to cell death in PGA scaffolds	Increase the drying time (70 min) to ensure that all traces of NaOH and EtOH are gone (PGA scaffolds only)
		Prolonged incubation, leading to cell death and drying	Monitor the scaffolds closely after seeding and before addition of medium; check the scaffolds every 30 min to ensure that they have not dried out
41A(iii)	Staining appears weak or non-specific	The 4% (vol/vol) PFA may have degraded	Store 4% (vol/vol) PFA at 4 °C and do not use it for longer than 1 month
		Samples may have been fixed for too long	Reduce fixation time. Do not attempt to fix too many samples at one time, to avoid accidental over-fixation
41A(vi)	Nuclear and intracellular staining is poor	The cells are not properly permeabilized, preventing adequate penetration of the antibody	Increase the concentration of Triton X-100, e.g., 0.3% (vol/vol) Triton X-100 or 0.5% (vol/vol) Triton X-100
41A(vii, xiv)	High levels of non-specific and background staining	Blocking time may have been too short	Increase blocking time, e.g., to 1 h
		Secondary antibody incubation may have been too long	Incubate secondary antibodies for 1 h at room temperature instead of overnight at 4 °C
41A(xvii)	DAPI staining is unclear	Incubation with DAPI may not have been long enough	Increase incubation with DAPI to 20 or 30 min
41B(v)	COs do not dissociate into a single-cell suspension	Cell clumping and/or poor viability	Increase the concentration of DNase I in the Accutase solution Ensure that all pipetting is done as slowly and carefully as possible
		CO clumps are not breaking up into single cells during the 5-min incubation period	Ensure that the Accutase solution is prewarmed Prolong incubation (e.g., 7–10 min)
41B(ix)	Single-cell suspension forms clumps	Concentration of DNase I is too low	Increase the concentration of DNase I, e.g., to 6 mg/ml

Timing

The timings below are estimates based on the approximate time required for a researcher with experience in this protocol to complete each of the steps. When attempting this protocol for the first time, researchers may find that aspects of the Procedure take longer to complete.
Step 1, tissue collection: 1–8 h
Step 2A, derivation of ECOs from deceased organ donors: 1 h 20 min–1 h 50 min
Step 2A(i–viii), washing, dissecting and scraping the tissue: 20–30 min
Step 2A(ix–xv), wash steps and optional red blood cell lysis: 20–40 min
Step 2A(xvi–xviii), organoid plating: 40 min
Step 2B, derivation of ECOs through ERCP brushings: 30 min
Step 2C(i and ii), tissue dissection: 10–20 min
Step 2C(iii–vi), washing and plating preparation: 10–15 min
Step 2C(vii and viii), plating: 10 min
Step 2D(i–iii), preparing the tissue for digestion: 10 min
Step 2D(iv–vii), digestion and filtering: ~1 h
Step 2D(viii–xvi), red cell lysis, washing and cell counting: 20–30 min
Step 2D(xvii–xxvii), MACS sorting and plating: ~1 h
Steps 3–10, plating of primary cholangiocytes in organoid format: 10–40 min
Steps 11–14, changing medium for maintenance of CO lines: variable, depending on cell line; hands-on time is 20 min every 48 h
Steps 15–21, removal of organoids from Matrigel: 40 min
Steps 22–26, washing and splitting the pellet: 10 min
Steps 28–30, plating the cells: 45 min
Steps 31–38, preparation of 5 mg/ml collagen gel: 10 min
Step 39A(i–vi), preparation of the densification chamber: ~45 min
Step 39A(vii–ix), collagen densification: 1 h
Step 39A(x–xiv), removal and storage of the densified collagen scaffold: ~10 min
Step 39B(i and ii), loading chamber with collagen and gelation: 40 min–1 h
Step 39B(iii–vii), collagen densification: 4–24 h
Step 39B(viii–xiv), removal and storage of the densified collagen tube: ~30 min
Step 40A(i), drying of the collagen scaffold: 30 min–1 h
Step 40A(ii–iv), preparation of the COs for seeding: 45 min
Step 40A(v), scaffold seeding: 15 min
Step 40A(vi), waiting step before medium addition: 1–2 h
Step 40A(vii–ix), medium addition: 5 min
Step 40B(i and ii), drying of collagen tube: 30 min–1 h
Step 40B(iii–v), preparation of the COs for seeding: 45 min
Step 40B(vi–viii), tube cannulation and cell seeding: 30 min
Step 40B(ix), cell attachment: 30 min–1 h
Step 40B(x–xiii), addition of medium: 15 min
Step 40C(i–iii), preparation of the PGA scaffold: ~1 h
Step 40C(iv and v), preparation of CO suspension: 40 min
Step 40C(vi), seeding of the PGA scaffold, waiting, and medium addition: ~1.5–2.5 h
Step 41A(i–v), organoid fixation: 40 min
Step 41A(vi–ix), blocking and primary antibody addition: ~90 min
Step 41A(x), primary antibody staining: overnight
Step 41A(xi–xiii), washing and secondary antibody addition: ~2 h 30 min
Step 41A(xiv–xv), secondary antibody staining: overnight
Step 41A(xvi–xxi), washing and nuclear staining: ~2 h 40 min
Step 41B(i–x), preparation of a single-cell suspension: 60 min
Step 41B(xi–xv), fixation: 30 min
Step 41B(xvi–xix), blocking: 45 min
Step 41B(xx–xxiv), staining with conjugated antibodies: 45 min
Step 41B(xxv–xxix), staining with separate primary and secondary antibodies: 2 h 30 min
Step 41C(i and ii), cell lifting: 40 min
Step 41C(iii and iv), RNA lysis: 10 min
Step 41C(v and vi), RNA extraction: 1 h

Anticipated results

We describe a protocol for the isolation of primary biliary epithelial cells from a variety of clinical samples, their propagation as COs and the generation of bioengineered biliary tissue by seeding of these organoids on PGA or densified collagen scaffolds. Our cholangiocyte isolation methods (ERCP, mechanical scraping, EPCAM sorting) result in a >95% pure ($CK7^+/CK19^+$) population of isolated cholangiocytes (Figs. 2e, 3d and 4e). Furthermore, 95% of plated samples derived from excised bile ducts (when appropriately flushed of bile after excision) and 100% of samples derived from gallbladders, liver biopsies and ERCP brushings yield robust CO lines within 5 d of initial plating (Supplementary Table 1). CO lines can be derived from $EpCAM^+$ liver samples with an approximate efficiency of 66% (Supplementary Table 1). Although it is important to derive lines from fresh, highly viable primary tissue to ensure the most reliable results, robust, highly proliferative CO lines can also be derived from poor-quality samples with low cell numbers (Supplementary Fig. 5). CO lines can subsequently be passaged approximately every 5 d and can typically be split in a 1:4–1:6 ratio for further expansion, analysis or cryopreservation.

The resulting organoids consist of a near-homogeneous (>99%) population of cholangiocytes (Fig. 6e). They express biliary markers such as CK19, CK7, Sox9 and GGT (Fig. 6a) at levels comparable to those of primary tissue (Fig. 6b) in the absence of hepatic markers such as albumin (Fig. 6a). Furthermore, CO lines exhibit key cholangiocyte functions, such as ALP and GGT activity (Fig. 6c,d). COs also display functional secretory capacity, as measured by the luminal secretion of rhodamine 123 (see Fig. 2a–c in ref. [4]) and bile acid transport, as measured by export of the fluorescently labeled bile acid CLF (see Fig. 2d–f in ref. [4]). In addition, COs respond appropriately to hormonal signals such as secretin and somatostatin (see Fig. 2i,j in ref. [4]). For further validation, COs can be transplanted under the kidney capsule of immunocompromised mice, where they form tubular structures retaining expression of biliary markers such as CK7 and CK19 and are capable of long-term survival (see Supplementary Fig. 7 in ref. [4]).

COs can be seeded onto both densified collagen and PGA scaffolds to form bioengineered biliary tissue. In addition, COs can be seeded onto the lumen of tubular densified collagen scaffolds (Fig. 11e). The efficiency of cell attachment following seeding is variable among CO lines. However, following attachment, the cells demonstrate a unique potential to expand and fully populate the scaffold. Therefore, it is always possible to generate confluent constructs by varying how long the scaffolds are maintained in culture. The resulting tissue expresses key cholangiocyte markers such as CK19 and CK7 (Fig. 11a,c,e) and exhibits biliary function such as GGT activity (Fig. 11b,d,f). These constructs can be used to successfully reconstruct or repair the biliary tree of immunocompromised mice (see Figs. 4 and 6 in ref. [4]) while retaining the expression of biliary markers and function following transplantation (see Figs. 4 and 6 in ref. [4]).

Reporting Summary

Further information on research design is available in the Nature Research Reporting Summary linked to this article.

Data availability

The authors declare that the main data supporting this study are available within the article. Additional data are available from the corresponding authors upon request.

References

1. Park, S. M. The crucial role of cholangiocytes in cholangiopathies. *Gut Liver* **6**, 295–304 (2012).
2. Lazaridis, K. N. & LaRusso, N. F. The cholangiopathies. *Mayo Clin. Proc.* **90**, 791–800 (2015).
3. Murray, K. F. & Carithers, R. L. AASLD practice guidelines: evaluation of the patient for liver transplantation. *Hepatology* **41**, 1407–1432 (2005).
4. Sampaziotis, F. et al. Reconstruction of the mouse extrahepatic biliary tree using primary human extrahepatic cholangiocyte organoids. *Nat. Med.* **23**, 954–963 (2017).
5. Sampaziotis, F. et al. Cholangiocytes derived from human induced pluripotent stem cells for disease modeling and drug validation. *Nat. Biotechnol.* **33**, 845–852 (2015).
6. Sampaziotis, F. et al. Directed differentiation of human induced pluripotent stem cells into functional cholangiocyte-like cells. *Nat. Protoc.* **12**, 814–827 (2017).
7. Lugli, N. et al. R-spondin 1 and noggin facilitate expansion of resident stem cells from non-damaged gallbladders. *EMBO Rep.* **17**, 769–779 (2016).

8. Sato, T. et al. Long-term expansion of epithelial organoids from human colon, adenoma, adenocarcinoma, and Barrett's epithelium. *Gastroenterology* **141**, 1762–1772 (2011).
9. Huch, M. et al. In vitro expansion of single Lgr5^{+} liver stem cells induced by Wnt-driven regeneration. *Nature* **494**, 247 (2013).
10. Kessler, M. et al. The Notch and Wnt pathways regulate stemness and differentiation in human fallopian tube organoids. *Nat. Commun.* **6**, 8989 (2015).
11. Huch, M. et al. Long-term culture of genome-stable bipotent stem cells from adult human liver. *Cell* **160**, 299–312 (2015).
12. Karthaus, W. R. et al. Identification of multipotent luminal progenitor cells in human prostate organoid cultures. *Cell* **159**, 163–175 (2014).
13. Barker, N. et al. Lgr5^{+ve} stem cells drive self-renewal in the stomach and build long-lived gastric units in vitro. *Cell Stem Cell* **6**, 25–36 (2010).
14. Koo, B.-K. & Clevers, H. Stem cells marked by the R-spondin receptor LGR5. *Gastroenterology* **147**, 289–302 (2014).
15. Glinka, A. et al. Dickkopf-1 is a member of a new family of secreted proteins and functions in head induction. *Nature* **391**, 357 (1998).
16. Fedi, P. et al. Isolation and biochemical characterization of the human Dkk-1 homologue, a novel inhibitor of mammalian Wnt signaling. *J. Biol. Chem.* **274**, 19465–19472 (1999).
17. Bafico, A., Liu, G., Yaniv, A., Gazit, A. & Aaronson, S. A. Novel mechanism of Wnt signalling inhibition mediated by Dickkopf-1 interaction with LRP6/arrow. *Nat. Cell Biol.* **3**, 683 (2001).
18. Cui, S., Capecci, L. M. & Matthews, R. P. Disruption of planar cell polarity activity leads to developmental biliary defects. *Dev. Biol.* **351**, 229–241 (2011).
19. Strazzabosco, M. & Fabris, L. Development of the bile ducts: essentials for the clinical hepatologist. *J. Hepatol.* **56**, 1159–1170 (2012).
20. Place, E. S., George, J. H., Williams, C. K. & Stevens, M. M. Synthetic polymer scaffolds for tissue engineering. *Chem. Soc. Rev.* **38**, 1139–1151 (2009).
21. Dhandayuthapani, B., Yoshida, Y., Maekawa, T. & Kumar, D. S. Polymeric scaffolds in tissue engineering application: a review. *Int. J. Polym. Sci.* **2011**, 290602 (2011).
22. O'Brien, F. J. Biomaterials & scaffolds for tissue engineering. *Mater. Today* **14**, 88–95 (2011).
23. Lutolf, M. P. & Hubbell, J. A. Synthetic biomaterials as instructive extracellular microenvironments for morphogenesis in tissue engineering. *Nat. Biotechnol.* **23**, 47 (2005).
24. Cheung, H.-Y., Lau, K.-T., Lu, T.-P. & Hui, D. A critical review on polymer-based bio-engineered materials for scaffold development. *Compos. Part B Eng.* **38**, 291–300 (2007).
25. Kehoe, S., Zhang, X. F. & Boyd, D. FDA approved guidance conduits and wraps for peripheral nerve injury: a review of materials and efficacy. *Injury* **43**, 553–557 (2012).
26. Frisch, S. & Francis, H. Disruption of epithelial cell-matrix interactions induces apoptosis. *J. Cell Biol.* **124**, 619–626 (1994).
27. Zeugolis, D. I., Paul, R. G. & Attenburrow, G. Engineering extruded collagen fibers for biomedical applications. *J. Appl. Polym. Sci.* **108**, 2886–2894 (2008).
28. Abou Neel, E. A., Cheema, U., Knowles, J. C., Brown, R. A. & Nazhat, S. N. Use of multiple unconfined compression for control of collagen gel scaffold density and mechanical properties. *Soft Matter* **2**, 986–992 (2006).
29. Landi, F. et al. Endoscopic treatment of anastomotic biliary stricture after adult deceased donor liver transplantation with multiple plastic stents versus self-expandable metal stents: a systematic review and meta-analysis. *Transpl. Int.* **31**, 131–151 (2018).
30. Seehofer, D., Eurich, D., Veltzke-Schlieker, W. & Neuhaus, P. Biliary complications after liver transplantation: old problems and new challenges. *Am. J. Transpl.* **13**, 253–265 (2013).
31. Cellon. BioFELT scaffolds from BMS. *Cellon* http://www.cellon.lu/biofelt-scaffold.html (2019).
32. Justin, A. W., Saeb-Parsy, K., Markaki, A. E., Vallier, L. & Sampaziotis, F. Advances in the generation of bioengineered bile ducts. *Biochim. Biophys. Acta Mol. Basis Dis.* **1864**, 1532–1538 (2018).
33. Zhang, L. & Hui, L. Bile ducts regenerated. *Nature* **547**, 171 (2017).
34. Thomas, H. Bioengineering the common bile duct. *Nat. Rev. Gastroenterol. Hepatol.* **14**, 504 (2017).
35. Günther, C., Brevini, T., Sampaziotis, F. & Neurath, M. F. What gastroenterologists and hepatologists should know about organoids in 2019. *Dig. Liver Dis.* https://doi.org/10.1016/j.dld.2019.02.020 (2019).
36. Huch, M. et al. Unlimited in vitro expansion of adult bi-potent pancreas progenitors through the Lgr5/R-spondin axis. *EMBO J.* **32**, 2708–2721 (2013).
37. Cho, W. K., Mennone, A. & Boyer, J. L. Isolation of functional polarized bile duct units from mouse liver. *Am. J. Physiol. Gastrointest. Liver Physiol.* **280**, G241–G246 (2001).
38. Demetris, A. J. et al. Isolation and primary cultures of human intrahepatic bile ductular epithelium. *In Vitro Cell. Dev. Biol.* **24**, 464–470 (1988).
39. Auth, M. K. et al. Morphogenesis of primary human biliary epithelial cells: induction in high-density culture or by coculture with autologous human hepatocytes. *Hepatology* **33**, 519–529 (2001).
40. Ogawa, M. et al. Directed differentiation of cholangiocytes from human pluripotent stem cells. *Nat. Biotechnol.* **33**, 853 (2015).
41. De Assuncao, T. M. et al. Development and characterization of human induced pluripotent stem cell-derived cholangiocytes. *Lab. Investig.* **95**, 684–696 (2015).
42. Gjorevski, N. et al. Designer matrices for intestinal stem cell and organoid culture. *Nature* **539**, 560 (2016).

43. Petrowsky, H. & Clavien, P.-A. in *Transplantation of the Liver* 3rd edn. (eds Busuttil, R. W. & Klintmalm, G. B. G.) 582–599 (W.B. Saunders, 2015).
44. Badylak, S. F. The extracellular matrix as a scaffold for tissue reconstruction. *Semin. Cell Dev. Biol.* **13**, 377–383 (2002).
45. Dong, C. & Lv, Y. Application of collagen scaffold in tissue engineering: recent advances and new perspectives. *Polymers* **8**, 42 (2016).
46. Glowacki, J. & Mizuno, S. Collagen scaffolds for tissue engineering. *Biopolymers* **89**, 338–344 (2008).
47. Drury, J. L. & Mooney, D. J. Hydrogels for tissue engineering: scaffold design variables and applications. *Polymers* **24**, 4337–4351 (2003).
48. Brown, R. A., Wiseman, M., Chuo, C.-B., Cheema, U. & Nazhat, S. N. Ultrarapid engineering of biomimetic materials and tissues: fabrication of nano- and microstructures by plastic compression. *Adv. Funct. Mater.* **15**, 1762–1770 (2005).
49. Gieseck, R. L. 3rd et al. Maturation of induced pluripotent stem cell derived hepatocytes by 3D-culture. *PLoS One* **9**, e86372 (2014).

Acknowledgements

We acknowledge the Cambridge Biorepository for Translational Medicine for the provision of human tissue used in the study and thank N. Georgakopoulos and B. Bareham for their roles in collecting and distributing this tissue. We also thank W.G. Bernard and L. Gambardella for their help and advice with regard to the fixation and staining of tubular bioengineered biliary constructs. O.C.T. was supported by an MRC-Sackler Doctoral Training Partnership. F.S. was supported by an Addenbrooke's Charitable Trust Grant, an Academy of Medical Sciences Clinical Lecturer Starter Grant (SGL019/1071) and an NIHR Clinical Lectureship. A.W.J. and A.E.M. acknowledge support from EPSRC (EP/R511675/1 and EP/N509620/1) and the Isaac Newton Trust. T.B. was supported by an EASL PhD Juan Rodes Studentship. The L.V. lab is funded by the ERC Proof of Concept grant Relieve-Chol, by the ERC advanced grant New-Chol, the Cambridge University Hospitals National Institute for Health Research Biomedical Research Centre and the core support grant from the Wellcome Trust and Medical Research Council of the Wellcome–Medical Research Council Cambridge Stem Cell Institute. A.W.J., F.S., L.V., A.E.M. and K.S.-P. gratefully acknowledge support from the Rosetrees Trust (REAG/240 and NMZG/233). A.K.F. and E.M. were supported by funds from the Norwegian PSC Research Center.

Author contributions

O.C.T.: manuscript writing and editing, coordination of study, execution of experiments and data acquisition, validation of the CO culture protocol, design and production of figures, final approval of the manuscript. A.W.J.: manuscript writing and editing, design, concept, development and validation of the collagen densification protocol, final approval of the manuscript. T.B.: manuscript writing and editing, collection of data, validation of the CO culture, collagen densification and scaffold seeding protocols. S.E.C.: production of schematics for Figs. 1, 2, 3, 4, 5, 7, 8, 9 and 10 and validation of the collagen densification protocol. K.T.M.: execution of experiments and data acquisition. A.K.F.: development and validation of the CO and ERCP brushing collection protocols. H.Z.: validation of CO culture and data acquisition. E.M.: critical revision of the manuscript, validation of the CO protocols. K.S.-P.: design and concept of the study, development of the protocol, critical revision and final approval of the manuscript. A.E.M.: design and concept of the collagen densification protocol, critical revision and final approval of the manuscript. L.V.: design and concept of the study, critical revision and final approval of the manuscript. F.S.: design and concept of the study, development and validation of the protocol, manuscript writing and editing, critical revision and final approval of the manuscript. O.C.T., A.W.J., and T.B. contributed equally to this work.

Competing interests

L.V. is a founder and shareholder of DefiniGEN. L.V., F.S. and K.S.-P. are founders and shareholders of Bilitech. The remaining authors declare no competing interests.

Additional information

Supplementary information is available for this paper at https://doi.org/10.1038/s41596-019-0168-0.

Reprints and permissions information is available at www.nature.com/reprints.

Correspondence and requests for materials should be addressed to L.V. or F.S.

Publisher's note: Springer Nature remains neutral with regard to jurisdictional claims in published maps and institutional affiliations.

Received: 11 June 2018; Accepted: 19 March 2019;
Published online: 20 May 2019

Related links
Key references using this protocol
Sampaziotis, F. et al. *Nat. Med.* **23**, 954–963 (2017): https://doi.org/10.1038/nm.4360
Sampaziotis, F. et al. *Nat. Biotechnol.* **33**, 845–852 (2015): https://doi.org/10.1038/nbt.3275
Sampaziotis, F. et al. *Nat. Protoc.* **12**, 814–827 (2017): https://doi.org/10.1038/nprot.2017.011

nature research

Corresponding author(s): Dr Fotios Sampaziotis, Dr Ludovic Vallier

Reporting Summary

Nature Research wishes to improve the reproducibility of the work that we publish. This form provides structure for consistency and transparency in reporting. For further information on Nature Research policies, see Authors & Referees and the Editorial Policy Checklist.

Statistical parameters

When statistical analyses are reported, confirm that the following items are present in the relevant location (e.g. figure legend, table legend, main text, or Methods section).

n/a	Confirmed	
☐	☒	The exact sample size (*n*) for each experimental group/condition, given as a discrete number and unit of measurement
☐	☒	An indication of whether measurements were taken from distinct samples or whether the same sample was measured repeatedly
☐	☒	The statistical test(s) used AND whether they are one- or two-sided *Only common tests should be described solely by name; describe more complex techniques in the Methods section.*
☐	☒	A description of all covariates tested
☐	☒	A description of any assumptions or corrections, such as tests of normality and adjustment for multiple comparisons
☐	☒	A full description of the statistics including central tendency (e.g. means) or other basic estimates (e.g. regression coefficient) AND variation (e.g. standard deviation) or associated estimates of uncertainty (e.g. confidence intervals)
☐	☒	For null hypothesis testing, the test statistic (e.g. *F*, *t*, *r*) with confidence intervals, effect sizes, degrees of freedom and *P* value noted *Give P values as exact values whenever suitable.*
☒	☐	For Bayesian analysis, information on the choice of priors and Markov chain Monte Carlo settings
☒	☐	For hierarchical and complex designs, identification of the appropriate level for tests and full reporting of outcomes
☒	☐	Estimates of effect sizes (e.g. Cohen's *d*, Pearson's *r*), indicating how they were calculated
☐	☒	Clearly defined error bars *State explicitly what error bars represent (e.g. SD, SE, CI)*

Our web collection on statistics for biologists may be useful.

Software and code

Policy information about availability of computer code

Data collection	N/A
Data analysis	N/A

For manuscripts utilizing custom algorithms or software that are central to the research but not yet described in published literature, software must be made available to editors/reviewers upon request. We strongly encourage code deposition in a community repository (e.g. GitHub). See the Nature Research guidelines for submitting code & software for further information.

Data

Policy information about availability of data

All manuscripts must include a data availability statement. This statement should provide the following information, where applicable:

- Accession codes, unique identifiers, or web links for publicly available datasets
- A list of figures that have associated raw data
- A description of any restrictions on data availability

The authors declare that the main data supporting this study are available within the article. Extra data are available from the corresponding authors upon request.

Field-specific reporting

Please select the best fit for your research. If you are not sure, read the appropriate sections before making your selection.

☒ Life sciences ☐ Behavioural & social sciences ☐ Ecological, evolutionary & environmental sciences

For a reference copy of the document with all sections, see nature.com/authors/policies/ReportingSummary-flat.pdf

Life sciences study design

All studies must disclose on these points even when the disclosure is negative.

Sample size	No sample size calculations were performed. Sample sizes were chosen based on previous experience with the assays in the lab.
Data exclusions	No data were excluded from the analyses
Replication	All experimental findings described in this article are consistent with the findings described in Sampaziotis et al; Reconstruction of the mouse extrahepatic biliary tree using primary human extrahepatic cholangiocyte organoids; Nat Med. (2017) Aug;23(8):954-963
Randomization	Randomization was not applicable to this study as all comparisons were performed between different populations of cells (organoids vs mouse embryonic feeder controls), rather than a baseline population that was treated or manipulated in different ways. However, within each population, samples for analysis were chosen randomly and all analyses are representative.
Blinding	Blinding was not required for the analyses performed in this study as all experimental data were collected with the aim of characterizing and validating the systems described in the protocol. Where groups of cells were compared, blinding was not possible as the identity of the cells was apparent to an experienced researcher based on their morphology.

Reporting for specific materials, systems and methods

Materials & experimental systems

n/a	Involved in the study
☐	☒ Unique biological materials
☐	☒ Antibodies
☐	☒ Eukaryotic cell lines
☒	☐ Palaeontology
☒	☐ Animals and other organisms
☒	☐ Human research participants

Methods

n/a	Involved in the study
☒	☐ ChIP-seq
☐	☒ Flow cytometry
☒	☐ MRI-based neuroimaging

Unique biological materials

Policy information about availability of materials

Obtaining unique materials	CO lines were generated from primary human tissue from deceased organ donors following deceased donor organ transplantation. Anonymised donor details for all CO lines are available in supplementary table 1. CO lines are available upon request.

Antibodies

Antibodies used	Supplementary table 2 contains a full list of antibodies used, with suppliers' names, catalogue numbers, clone, and dilutions used in the study
Validation	Antibody validation and relevant citations are shown on the manufacturer's website for all antibodies used

Eukaryotic cell lines

Policy information about cell lines

Cell line source(s)	Human biliary tissue from deceased organ donors. All human tissue was obtained with full ethical approval (REC reference

Cell line source(s)	numbers: 12/EE/0253, NRES Committee East of England, Cambridge Central and 15/EE/0152 NRES Committee East of England, Cambridge South) and informed consent from the donors' families.
Authentication	CO lines were authenticated by matching their karyotype to the sex of the donor
Mycoplasma contamination	All lines were tested regularly for mycoplasma contamination and were found to be negative
Commonly misidentified lines (See ICLAC register)	N/A

Flow Cytometry

Plots

Confirm that:

☒ The axis labels state the marker and fluorochrome used (e.g. CD4-FITC).

☒ The axis scales are clearly visible. Include numbers along axes only for bottom left plot of group (a 'group' is an analysis of identical markers).

☒ All plots are contour plots with outliers or pseudocolor plots.

☒ A numerical value for number of cells or percentage (with statistics) is provided.

Methodology

Sample preparation	Cells were isolated from primary biliary tissue (figures 2, 3 and 4) or from established CO lines (figure 6). Cells were treated with accutase for 5 minutes, fixed in 4% PFA for 20 minutes and then stained with first primary and then secondary antibodies, each for 1 hour at room temperature. A detailed description of the protocol used for flow cytometry preparation can be found in Step 41, section B.
Instrument	FACS Cyan (Beckman Coulter)
Software	FlowJo 10.4.2
Cell population abundance	Relevant populations were determined by positive expression of Cytokeratin 7 and cytokeratin 19. All flow cytometry samples had a purity of > 95% (CK7+/CK19+).
Gating strategy	The gating strategy is described in supplementary figure 4

☒ Tick this box to confirm that a figure exemplifying the gating strategy is provided in the Supplementary Information.